

**Synthetic, electrochemical and structural
aspects of β -diketonato and carboxylate
complexes of aluminium**

*A dissertation submitted in accordance with the requirements for
the degree*

Magister Scientiae

in the

Department of Chemistry

Faculty of Natural and Agricultural Sciences

at the

University of the Free State

by

Hendrik Jacobus Gericke

Supervisor

Prof. J.C. Swarts

Acknowledgements

I would hereby like to thank my supervisor, Prof. J.C. Swarts, for all his invaluable advice, inspirational ideas, infinite patience and continuing innovative ideas throughout my studies.

I would like to thank Dr. J. Conradie and Dr. F. Muller especially for assistance with computational chemistry and crystallography respectively, and Dr. F. Prinsloo (Sasol) for his insight and direction. I would also like to thank SASOL for funding this research.

Thank you to all the members of the Physical Chemistry Group (2008) for your support and friendship.

Finally, I am, as always, grateful for the support and guidance of my family and our Heavenly Father for His infinite grace.

Abstract

A series of ferrocene-containing *tris*- β -diketonato aluminium(III) complexes of the form $\text{Al}(\text{FcCOCHCOR})_3$ ($\text{R} = \text{CF}_3, \text{CH}_3, \text{C}_6\text{H}_5, \text{Fc}$ with $\text{Fc} = \text{ferrocenyl}$) were synthesized and subjected to structural and electrochemical investigations. ^1H NMR-spectroscopy distinguished between the *mer* and *fac* isomers of $(\text{FcCOCHCOPh})_3$ and $\text{Al}(\text{FcCOCHCOCH}_3)_3$. $\text{Al}(\text{FcCOCHCOCF}_3)_3$ existed only as the *mer*-isomer. A single crystal X-ray crystallographic determination of the structure of $\text{Al}(\text{FcCOCHCOCF}_3)_3$ confirmed the existence of the *mer*-isomer ($Z = 4$, space group $P2_12_12_1$). All Fc/Fc^+ electrochemical couples of $\text{Al}(\text{FcCOCHCOR})_3$ could be resolved cyclic voltammetrically. For $\text{R} = \text{Fc}$, formal reduction potentials of the ferrocenyl group were found to be $E^{\circ'} = 33, 123, 304, 432, 583$ and 741 mV versus free ferrocene respectively. A cytotoxic study showed that aluminium(III) has an inhibiting effect on the cytotoxicity of ferrocene-containing β -diketones.

Aluminium formate and acetate were synthesized from $\gamma\text{-Al}_2\text{O}_3$ as aluminium source and the carboxylate bonding modes identified by FTIR. Dodecanoato and octadecanoato alumoxane as well as aluminium dodecanoate, pentadecanoate, octadecanoate and ferrocenoate were synthesized from the corresponding potassium carboxylate salts and aluminium *tris*-isopropoxide. All complexes were characterized by FTIR and elemental analysis. It was difficult but not impossible to synthesize polymeric aluminium carboxylates with a 1:3 ratio of aluminium:carboxylic acid. It was found that the mode of carboxylate coordination to aluminium may be predicted by FTIR analyses. The difference in C=O stretching frequencies, $\Delta\nu = \nu_{\text{antisymmetric}} - \nu_{\text{symmetric}} > 200 \text{ cm}^{-1}$ indicate monodentate coordination. If $80 < \Delta\nu < 120$ the bonding mode is bridging, while $60 < \Delta\nu < 70$ indicate bidentate coordination. Asymmetric bidentate or monodentate coordination modes occur when $160 < \Delta\nu < 190 \text{ cm}^{-1}$.

Key words: Aluminium, β -diketone, ferrocene, electrochemistry, cyclic voltammetry, aluminium carboxylate.

Opsomming

'n Reeks ferroseen-bevattende *tris*- β -diketonato aluminium(III) komplekse van vorm $\text{Al}(\text{FcCOCHCOR})_3$ ($\text{R} = \text{CF}_3, \text{CH}_3, \text{C}_6\text{H}_5, \text{Fc}$ waar $\text{Fc} = \text{ferroseniel}$) is gesintetiseer en onderwerp aan strukturele en elektrochemiese ondersoek. ^1H KMR-spektroskopie het tussen die *mer*- en *fac*-isomere van $\text{Al}(\text{FcCOCHCOPh})_3$ and $\text{Al}(\text{FcCOCHCOCH}_3)_3$ onderskei, terwyl $\text{Al}(\text{FcCOCHCOCF}_3)_3$ slegs as die *mer*-isomeer bestaan. 'n Enkel-kristal X-straal-kristallografie bepaling van die struktuur van $\text{Al}(\text{FcCOCHCOCF}_3)_3$ ($Z = 4$, ruimtegroep = $P2_12_12_1$) het die bestaan van die *mer*-isomeer bevestig. Met behulp van sikliese voltammetrie kon tussen alle Fc/Fc^+ -koppels van $\text{Al}(\text{FcCOCHCOR})_3$ onderskei word. Die formele reduksiepotensiale van die ses koppels van die $\text{R} = \text{Fc}$ kompleks was as $E^{\circ} = 33, 123, 304, 432, 583$ en 741 mV versus vry ferroseen bepaal. Sitotoksiese studies het getoon dat aluminium(III) 'n inhiberende effek op die sitotoksiteit van ferroseen-bevattende β -diketone het.

Aluminiumformaat en -asetaat is vanuit $\gamma\text{-Al}_2\text{O}_3$ as aluminiumbron gesintetiseer en die karbosilaat bindingsmodes met FTIR geïdentifiseer. Dodekanoato- en oktadekanoato-alumoksane, asook aluminiumdodekanoaat, -pentadekanoaat, -oktadekanoaat en -ferrosenoaat is vanuit die ooreenstemmende kalium karboksilaatsoute en aluminium *tris*-isopropoksied as aluminiumbron gesintetiseer. Alle komplekse is deur FTIR en elementalanalise gekarakteriseer. Dit is gevind dat dit moeilik maar nie onmoontlik is om polimeriese aluminiumkarboksilate met 'n 1:3 verhouding van aluminium:karboksiesuur te sintetiseer nie. Dit is gevind dat die manier van karboksilaatkoördinerings aan aluminium deur FTIR metings voorspel kan word. Die verskil in $\text{C}=\text{O}$ strekkingsfrekwensies, $\Delta\nu = \nu_{\text{antisimmetries}} - \nu_{\text{simmetries}} > 200 \text{ cm}^{-1}$ dui op monodentate koördinerings. Indien $80 < \Delta\nu < 125$ is die bindingstipe bruggend, terwyl $60 < \Delta\nu < 70$ op bidentate koördinerings dui. Asimmetriese bidentate of monodentate koördinerings vind plaas as $160 < \Delta\nu < 190 \text{ cm}^{-1}$.

Slutelwoorde: Aluminium, β -diketone, ferroseen, elektrochemie, sikliese voltammetrie, aluminiumkarboksilaat.

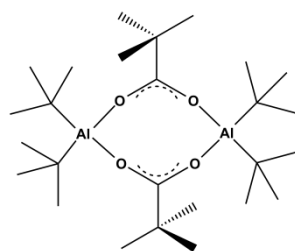
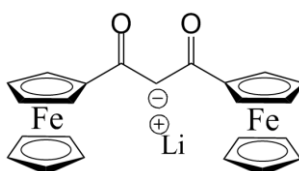
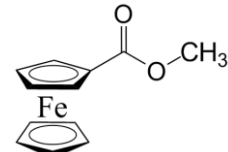
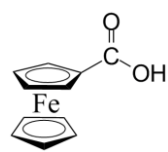
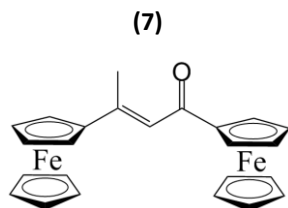
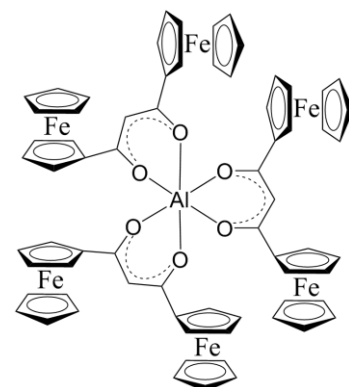
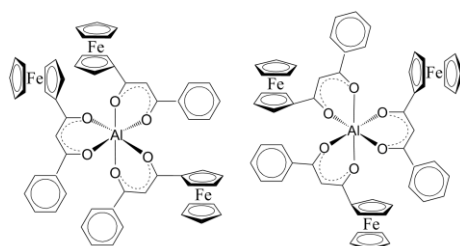
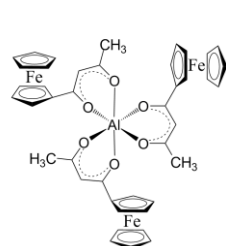
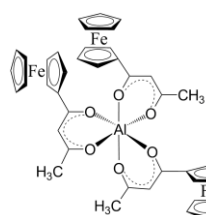
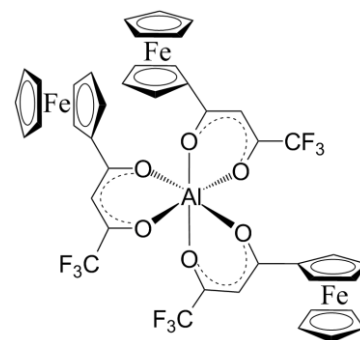
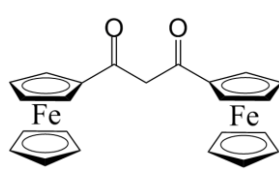
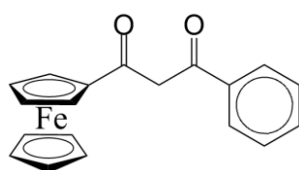
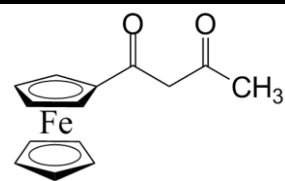
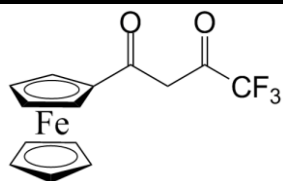
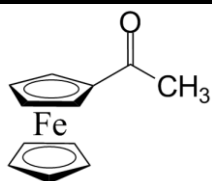
Table of Contents

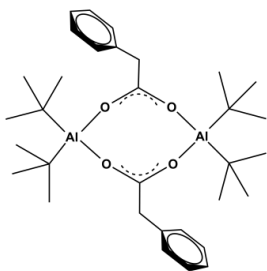
CHAPTER 1 : INTRODUCTION	8
<hr/>	
CHAPTER 2 : LITERATURE SURVEY	12
<hr/>	
2.1. Introduction	12
2.2. β-diketones	12
2.2.1. Synthesis of ferrocene-containing β -diketones	12
2.2.2. Solution behaviour of ferrocene-containing β -diketones	14
2.2.3. β -diketonato bonding to metals	17
2.2.4. Aluminium β -diketonato complexes	20
2.2.5. Medical applications of aluminium compounds and ferrocene-containing β -diketonato complexes	28
2.3. Carboxylates	30
2.3.1. Carboxylic acid bonding to metals	30
2.3.2. Aluminium carboxylates	37
2.4. Electrochemistry	52
2.5. Concluding remarks	56
<hr/>	
CHAPTER 3 : RESULTS AND DISCUSSION	62
<hr/>	
3.1. Introduction	62
3.2. Synthesis	63
3.2.1. Ferrocene-containing β -diketones	63
3.2.2. β -diketonato complexes of aluminium(III)	67
3.2.3. Solution Stereochemistry	71
3.2.4. Single crystal x-ray structure of $\text{Al}(\text{FcCOCHCOCF}_3)_3$	74

3.2.5. Electrochemistry of aluminium β -diketonato complexes	80
3.2.6. The cytotoxicity of ferrocene-containing β -diketonato complexes of aluminium(III)	105
3.3. Aluminium Carboxylates	109
3.3.1. Introduction	109
3.3.2. FTIR characterisation of monocarboxylic acids	110
3.3.3. Computational investigation of aluminium carboxylates	115
3.3.4. Synthesis and characterisation of aluminium carboxylates	129
3.3.5. Conclusion	156
CHAPTER 4 : EXPERIMENTAL	161
<hr/>	
4.1. Introduction	161
4.2. Materials	161
4.3. Spectroscopic measurements	161
4.4. Synthesis and characterisation of β-diketones and β-diketonato aluminium(III) complexes	162
4.4.1. Methylferrocenoate, (12) [Scheme 3.1, p. 61]	162
4.4.2. β -diketones	163
4.4.3. Aluminium β -diketonato complexes	167
4.4.4. Aluminium carboxylate complexes	173
4.5. Electrochemistry	181
4.6. Single crystal X-ray crystallography of $Al(FcCOCHCOF_3)_3$	182
4.7. Cytotoxic determinations	183
4.7.1. Sample preparation	183
4.7.2. Cell cultures	184
CHAPTER 5 : SUMMARY AND FUTURE PERSPECTIVES	185
<hr/>	

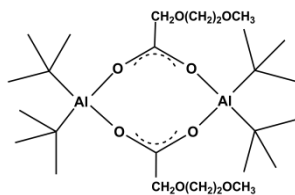
5.1. Introduction	185
5.2. Summary of results	185
5.3. Future prospects	188
APPENDIX	190
<hr/>	
NMR spectra	190
Infrared spectra	193
Crystallographic data for Al(FcCOHCOF₃)₃	197
<hr/>	

List of structures

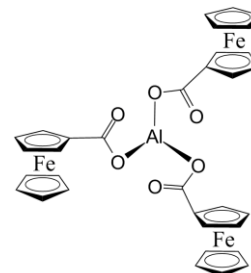




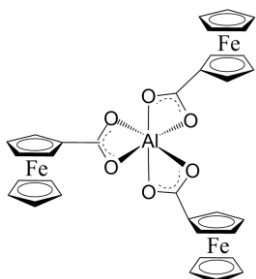
(16)



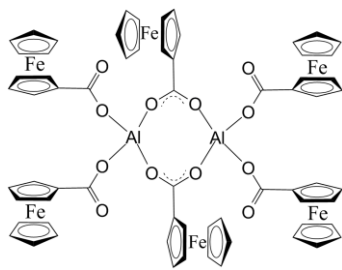
(17)



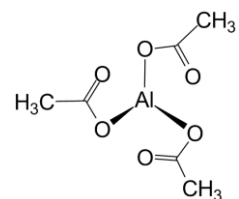
(18)



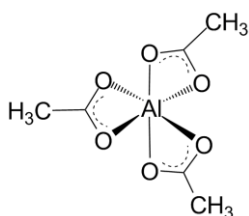
(19)



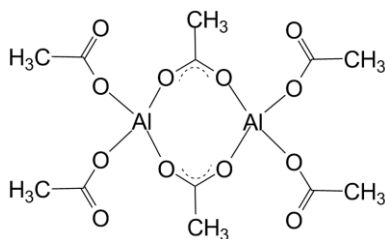
(20)



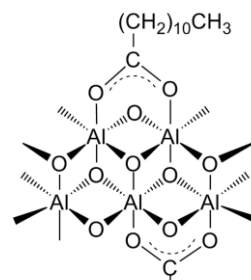
(21)



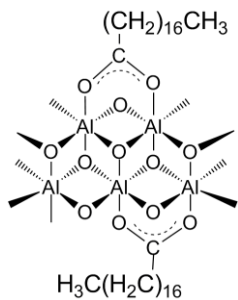
(22)



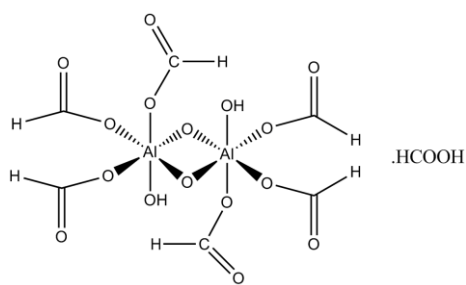
(23)



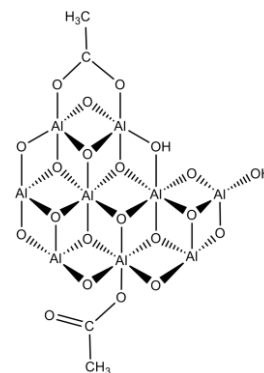
(24)



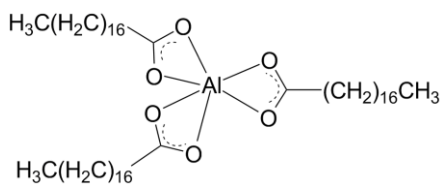
(25)



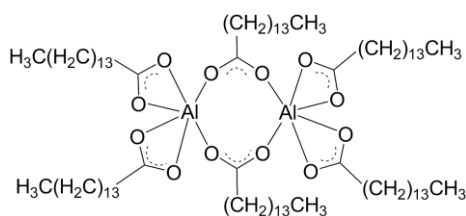
(26)



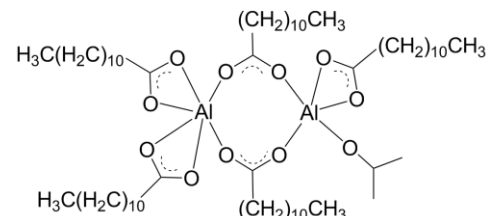
(27)



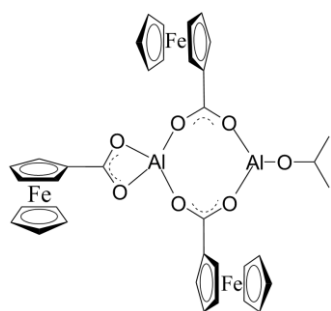
(28)



(29)



(30)



(31)

Abbreviations

LDA	:	Lithium diisopropylamide
Bipy	:	Bipyridine
Fc	:	Ferrocene, Ferrocenyl
CV	:	Cyclic voltammetry
SW	:	Osteryoung Square wave voltammetry
Et	:	Ethyl (CH_2CH_3)
O ⁱ Pr	:	Isopropoxide ($\text{OCH}(\text{CH}_3)_2$)
Ph	:	Phenyl (C_5H_5)
acac	:	Acetylacetonato
cod	:	Cyclo-octadiene

Chapter 1 : Introduction

Aluminium oxide is well known as the stationary phase during column chromatography. It has also been used as solid support for various reactions including dehydrogenation,¹ reactions with formic and acetic acid,² selective oxidation of alcohols to carbonyl compounds using iodobenzene diacetate,³ and aziridination and cyclopropanation reactions using copper nanoparticles.⁴ In a review by Rajadurai,⁵ pathways towards decarboxylation of carboxylic acids to give ketones were described. In this review, the influence of transition metal oxides was especially highlighted on these reactions. No mention was made of Al₂O₃ in this review. Recognising this limitation the author focused his research attention on the fundamentals of oxygenated aluminium complexes including β-diketonates and carboxylates.

The commercial applications of aluminium carboxylates are vast.⁶ Most frequently, applications fall into four categories.

- i. They are used as finishing agents for waterproofing of cloth and mordants in textile dying.
- ii. Pharmaceutical applications rely on antiseptic, astringent and basic properties of aluminium carboxylates.⁷
- iii. The gelling properties of aluminium carboxylates of longer-chained carboxylic acids find applications in the manufacture of cosmetics and coatings.
- iv. A more recent application is the usage of aluminium carboxylates as precursor to aluminium oxide in the production of ceramics.⁸

Most aluminium carboxylates exhibit low solubility. Characterisation of aluminium carboxylates is difficult because suitable solid state characterisation methods for these amorphous materials are limited.⁹ The bonding mode of carboxylic acids to aluminium is still disputed in literature and gives rise to the need for a qualitative technique to distinguish between different bonding modes.¹⁰ Especially bidentate chelation of carboxylates to the cationic trivalent aluminium centre lack conclusive easy identification as this bonding mode gives rise to unstable four-membered pseudo-aromatic rings because of weak orbital overlapping, **Figure 1.1**.

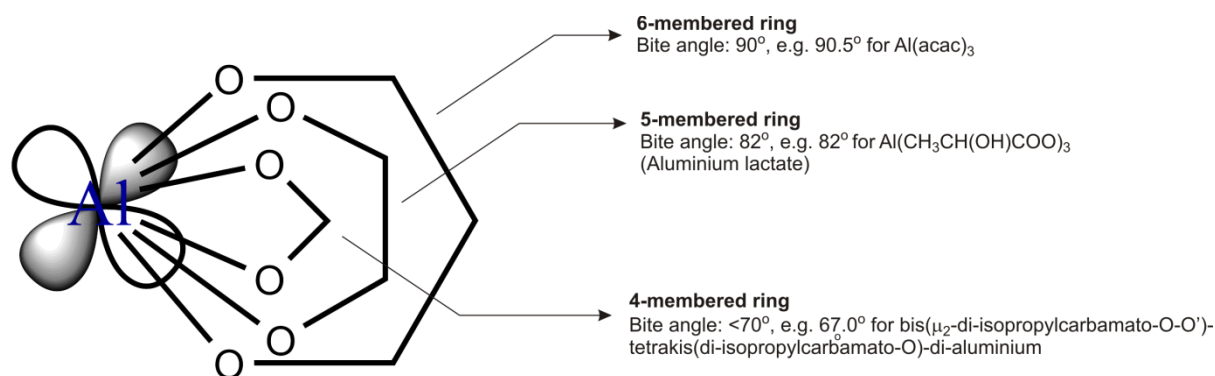


Figure 1.1: Orbital overlap of octahedral aluminium(III) in 4-, 5- and 6-membered pseudo-aromatic chelate rings. The ideal O-Al-O bite angle would be 90° . This is found in 6-membered pseudo-aromatic coordination systems like $\text{Al}(\text{acac})_3$, showing a bite angle of 90.5° .^{11, 12} Five-membered pseudo-aromatic coordination systems were shown to have bite angles of ca. 82.1° , for example in $\text{Al}(\text{CH}_3\text{CH}(\text{OH})\text{COO})_3$.¹³ Four-membered pseudo-aromatic coordination systems are very rare and very unstable, as this coordination mode has bite angles of less than 70° , e.g. $\text{bis}(\mu_2\text{-di-isopropylcarbamato-O-O}')\text{-tetrakis}(\text{di-isopropylcarbamato-O})\text{-di-aluminium}$.¹⁴

β -diketones give access to a class of coordination complexes that is stable, simple to synthesise and easy to characterise. Stability arises from effective ligand and metal centre bonding orbitals in six-membered pseudo-aromatic chelate rings, **Figure 1.1**. A study of stable aluminium β -diketonato complexes would assist greatly in probing the general behaviour of aluminium-oxygen complexes, not least because of the higher stability of the

six-membered β -diketonato complexes, but also because it would aid in identification of the preferred bonding mode of carboxylate-type ligands in aluminium complexes. Ferrocene-containing β -diketonato-complexes were found to be effective drugs against certain types of cancer cells, also showing favourable selectivity to cancer versus normal cells.¹⁵ Given that aluminium has a degree of biotoxicity, a preliminary investigation into the anti-cancer activity of ferrocene-containing aluminium β -diketonato complexes will elucidate possible biomedical applications of this new class of compounds. Ferrocene-containing β -diketones are redox active. Multiple ferrocenyl moieties coordinate to the same metal centre will highlight the ability of that metal centre to allow electronic communication of differently charged redox active ligands via the central coordinating metal.¹⁶

Against the given background the following goals were set for this research project:

1. The synthesis and characterisation of ferrocene-containing β -diketonato aluminium(III) compounds to act as models of stable six-membered pseudo-aromatic ring complexes of aluminium.
2. Determination of the three dimensional geometry of the complexes of goal 1 utilising single crystal x-ray diffraction and various spectroscopic techniques.
3. The investigation of electrochemical properties of β -diketonato aluminium(III) compounds utilising cyclic voltammetry, square wave voltammetry and linear sweep voltammetry and to quantify any thorough-bond or through-space communication between differently charged ferrocenyl moieties facilitated by aluminium(III) .
4. Evaluation of the cytotoxicity of ferrocene-containing β -diketonato aluminium(III) compounds.

5. The synthesis of various types of aluminium carboxylato compounds, including aluminium tricarboxylates, carboxylato-alumoxanes and ferrocene-containing aluminium carboxylates.
6. To develop FTIR techniques to quantitatively distinguish between different bonding modes in aluminium carboxylato complexes.

¹ K. Schlögl and H. Egger, *Monatshefte Für Chemie*, 376, **94** (1963).

² R. Narayanan and R. M. Laine, *J. Mater. Chem.*, 2097, **10** (2000).

³ R. S. Varma, R. K. Saini and R. Dahiya, *J. Chem. Research*, 120, (1998).

⁴ M. L. Kantam, V. S. Jaya, M. J. Lakshmi, B. R. Reddy, B. M. Choudary and S. K. Bhargava, *Cat. Commun.*, 1968, **8** (2007).

⁵ S. Rajadurai, *Catal. Rev. Sci. Eng.*, 385, **36** (1994).

⁶ G. H. Warner in *Kirk-Othmer Encyclopaedia of chemical technology 3rd edition*, John Wiley and Sons, 1978, pp. 202-209.

⁷ T. Salifoglou in *Metallotherapeutic Drugs and Metal-based Diagnostic Agents*; eds. M. Gielen and E. R. T. Tiekink, John Wiley & Sons, Hoboken USA, 2005, pp. 65 – 82.

⁸ R. Narayanan and R. M. Laine, *J. Mater. Chem.*, 2097, **10** (2000).

⁹ R. C. Mehrotra and A. K. Rai, *Polyhedron*, 1967, **10** (1991).

¹⁰ C. C. Landry, N. Pappé, M.R. Manson, A. W. Apblett, A. N. Tyler, A. N. Macinnes and A. R. Barron, *J. Mater. Chem.*, 331, **5** (1995).

¹¹ L. S. von Chrzanowski, M. Lutz and A. L. Spek, *Acta Cryst.*, m3318, **E62** (2006).

¹² L. S. von Chrzanowski, M. Lutz and A. L. Spek, *Acta Cryst.*, m129, **C63** (2007).

¹³ G. G. Bombi, B. Corain, A. A. Sheikh-Osman and G. C. Valle, *Inorg. Chim. Acta*, 79, **171** (1990).; B. Corain, B. Longato, A. A. Sheikh-Osman, G. G. Bombi and C. Maccà, *J. Chem. Soc. Dalton Trans.*, 169, (1992).

¹⁴ D. B. Dell'Amico, F. Calderazzo, M. Dell'Innocenti, B. Guldenpfennig, S. Lanelli, G. Peilizzi, P. Robino, *Gazz. Chim. Ital.*, 283, **123** (1993).

¹⁵ W. C. du Plessis, T. G. Vosloo and J. C. Swarts, *J. Chem. Soc., Dalton Trans.*, 2507, (1998).

¹⁶ H. J. Gericke, N. L. Barnard, L. Erasmus, J. C. Swarts, M. J. Cook and M. A. S. Aquino, Submitted *Inorg. Chim. Acta.*, 2008.

Chapter 2 : Literature survey

2.1. Introduction

In this chapter, because of research goals 1 – 6 (Chapter 1), the content is organised to present synthetic strategies surrounding β -diketones as ligands, their coordination to metals (for this study Al is important) and medical aspects. The electrochemical properties of ferrocene-containing β -diketones and some metal complexes thereof are then reviewed with regard to goal 3. In the section thereafter, carboxylato complexes are focussed on. In particular, with reference to goals 5 and 6, the synthesis and infrared characteristics of known aluminium carboxylato complexes are reviewed in detail.

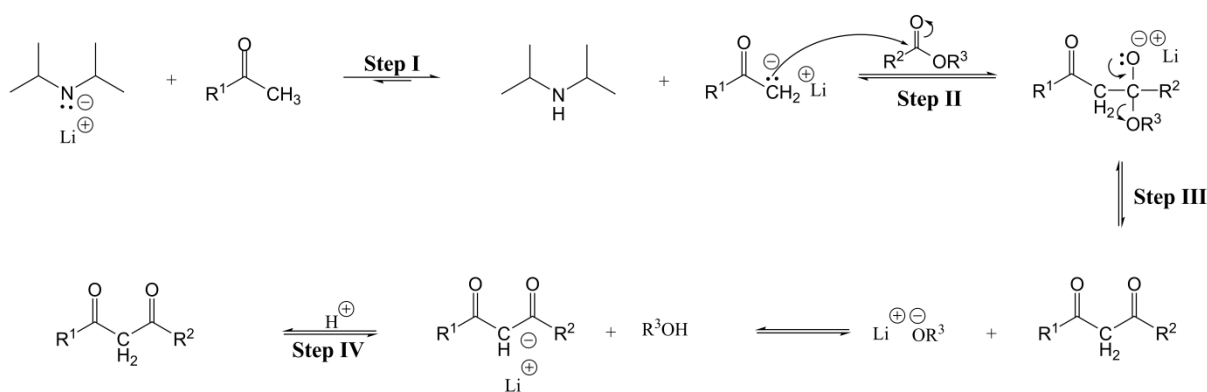
2.2. β -diketones

2.2.1. Synthesis of ferrocene-containing β -diketones

With respect to the first goal set in this research project, the synthesis of ferrocene-containing β -diketones, some β -diketone bonding modes in metal complexes and the general coordination chemistry of aluminium β -diketonato complexes in particular, are important. Generally, β -diketones are synthesised by a Claisen condensation of a ketone with an appropriate ester, acid anhydride or an acid chloride. The mechanism of a Claisen condensation involves the abstraction of an α -hydrogen atom from the ketone to form a carbanion. The carbanion then attacks the ester, acid anhydride or acid chloride to form the β -diketone.¹ Upon using acetylferrocene (**1**) as the ketone, the electron-donating properties of the ferrocenyl-group lower the acidity of the methyl protons.² This necessitates the use of

a strong base to abstract the α -hydrogen atom from the ketone. The bases most often used in the synthesis of ferrocene-containing β -diketones are potassium or sodium amide in liquid ammonia³, alkoxides, including sodium methoxide⁴ and sterically hindered bases, like lithium diisopropylamide (LDA)⁵. Du Plessis *et al.* reported an effective adaptation of Cullen and co-workers⁵ method to a one-pot procedure using lithium diisopropylamide as base. This method led to both higher yields and faster reactions. The mechanism of a Claisen condensation of a ketone with an ester using lithium diisopropylamide as base is shown in

Scheme 2.1.



Scheme 2.1: The mechanism of the Claisen condensation of a ketone with an ester using lithium diisopropylamide as basic initiator.

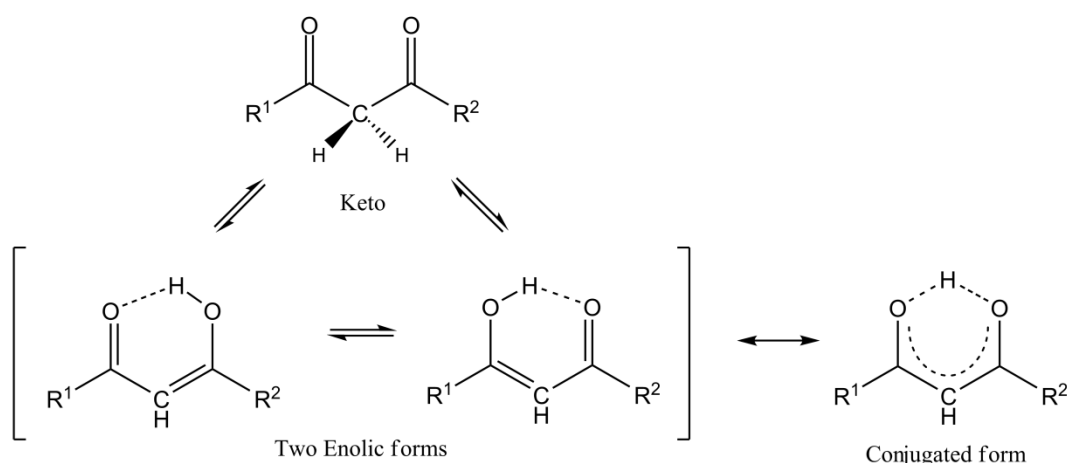
The condensation with esters is proposed to involve a three-step ionic mechanism. In the first step an α -hydrogen atom is removed from the ketone by lithium diisopropylamide. This forms the lithium salt (carbanion) of the ketone and diisopropylamine. The second step, step II in **Scheme 2.1**, involves the addition of the carbanion to the carbonyl carbon of the ester. In the third step, an alkoxide is liberated in favour of the reconstitution of the carbonyl group. Due to the low pK_a values of β -diketones (e.g. pK_a of $CH_3COCH_2COCH_3$ is 8.95²) the lithium alkoxide in step III is strong enough to deprotonate the β -diketone and

thus the latter is isolated as the lithium salt during the reaction. The β -diketone is then regenerated by acidification during step IV.

Self aldol condensation, an unwanted side reaction, which also occurs in Claisen condensation reactions, is minimized by ensuring the added base is not the limiting reagent in the reaction.

2.2.2. Solution behaviour of ferrocene-containing β -diketones

Different tautomers of β -diketones react with metals at different rates and the properties of the enol and keto isomers can differ substantially.⁶ It is thus important to review keto-enol tautomerisation of β -diketones in detail as this relates directly to goal 1. In solution, β -diketones exist as mixtures of keto and enol forms, which are related by a 1, 3 hydrogen shift.⁷ Asymmetric β -diketones can have two different enolic forms as shown in **Scheme 2.2**.⁸⁻⁹



Scheme 2.2: The keto-enol tautomerism of asymmetric β -diketones, with one keto and two possible enolic forms. The conjugate form on the right represents a pseudo-aromatic ring.

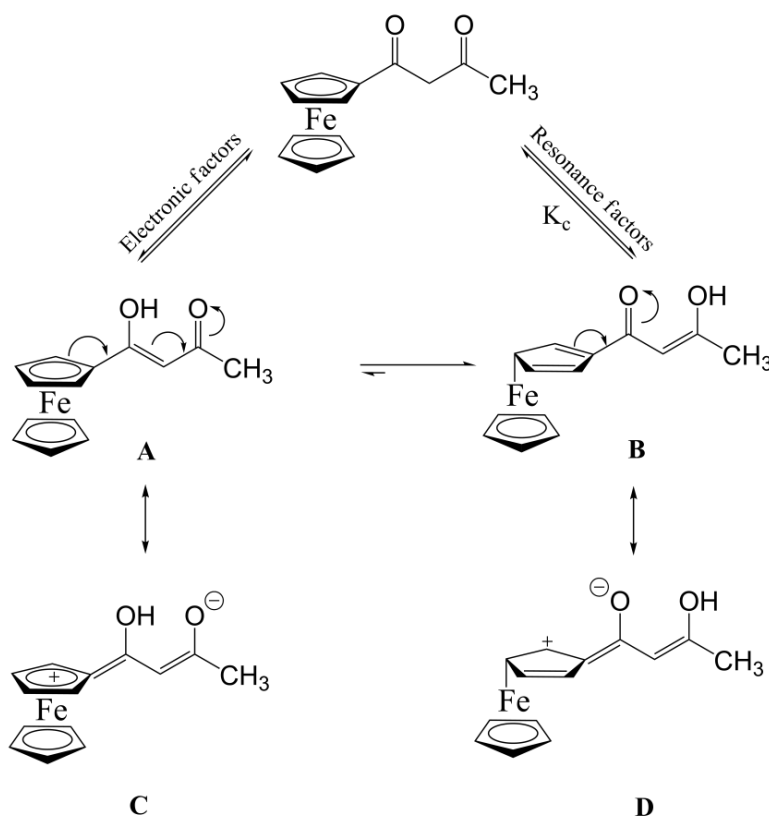
The enolic forms are stabilized by π -electron conjugation and an intramolecular hydrogen bond.¹⁰ Various factors determine which of the three forms of the β -diketone will be dominant in solution and have been studied by various authors using a variety of techniques ranging from spectroscopic to theoretical methods.⁸

Among these factors, the substituents R^1 and R^2 on the β -diketone play a significant role in deciding which tautomer will exist predominantly. In a calculation-based investigation, Kwon and Moon⁹ reported that a substituent attached to one of the carbonyl carbons is more likely to stabilise the enol form toward that carbonyl. This implies the hydroxyl group of the enol form will be located on the substituted carbon. The enol stabilisation effect of the substituent increases in the order (lowest) $C(CH_3)_3 < CH_3 < C_6H_5 < CF_3$ (highest). Aromatic and electron-withdrawing substituents on the carbonyl carbons tend to favour the enolic tautomers,¹¹ whilst sterically bulky substituents forces the keto-enol equilibrium to the keto side.¹² Furthermore, enolisation is usually observed toward the substituent with the lowest electronegativity.²

The preferred tautomer is also influenced by the solvent used. Reeves⁸ demonstrated that pyrrole forms a hydrogen bond with the carbonyls of acetyl acetone leading to the enolic form being preferred. Triethylamine forms a hydrogen bond with the hydroxyl proton of the enolic form of acetylacetone, thus leading to the enolic form being preferred. The concentration of the β -diketone in solution also influences the keto-enol equilibrium. Higher concentrations of the β -diketone favour the enolic form.¹³

More recently, Du Plessis *et al.* defined electronic and resonance factors as two different driving forces that determine the preferred enolic form as well as the keto-enol equilibrium position of ferrocene-containing β -diketones. Due to excellent conjugation of aromatic

ferrocenyl groups with the carbonyl groups of β -diketones, $\text{FcCOCH}_2\text{COCH}_3$ has at least the two enolic forms shown in **Scheme 2.3**. Crystallography and NMR spectroscopy indicated **B** in **Scheme 2.3** as the dominating enolic form, even though electronically enolisation was expected to occur toward the ferrocenyl moiety since the group electronegativity of the ferrocenyl group ($\chi_{\text{Fc}} = 1.87$) is lower than that of the methyl group ($\chi_{\text{CH}_3} = 2.34$). The reason for this observation is that canonical forms like **D** lead to better stabilisation of the enolic form **B** compared to canonical form **C** stabilising **A**.



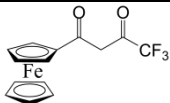
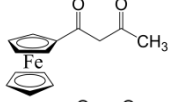
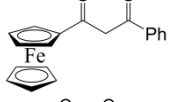
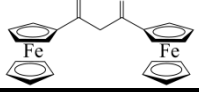
Scheme 2.3: Resonance and electronic factors determine both the keto-enol equilibrium position as well as which enolic tautomer dominates. (Adapted from W. C. du Plessis, T. G. Vosloo and J. C. Swarts, *J. Chem. Soc., Dalton. Trans.*, 2507, (1998).)

In a further study by Du Plessis and co-workers¹⁴ it was shown that the conversion kinetics from the keto tautomer to the preferred enol tautomer is slow ($\text{FcCOCH}_2\text{COCH}_3$ has half-life

of 173 minutes for keto to enol conversion). It was also found that the keto form of the ferrocene-containing β -diketones dominates directly after isolation (because the lithium salt of the β -diketone exists almost exclusively as the keto isomer, see **Scheme 2.1**, p. 13) from basic aqueous solutions. It is important to note that the enolic form is the only stable isomer for ferrocene-containing β -diketones in the solid state.

Since the methine protons of β -diketones are acidic it is relevant to tabulate the solution parameters of ferrocene-containing β -diketones in **Table 2.1**.

Table 2.1: pK_a' values and % enol tautomer of various ferrocene-containing β -diketones and the electronegativity of substituents according to the Gordy scale (Adapted from W. C. du Plessis, W. L. Davis, S. J. Cronje and J. C. Swarts, *Inorg. Chim. Acta*, 97, **314** (2001).).

β -diketone	χ_R	pK_a' ^(a)	% enol ^(b)
	3.01	6.53(3)	97
	2.34	10.01(2)	78
	2.21	10.41(2)	91
	1.87	13.1(1)	67

(a) : At 21°C, $\mu = 0.1 \text{ mol.dm}^{-3}$ (NaClO_4)

(b) : In CDCl_3 at 298 K

2.2.3. β -diketonato bonding to metals

Both the methine protons in the keto form and the hydroxyl proton in the enol form of the β -diketones are acidic. The removal of these protons generate 1,3-diketonato anions

(Figure 2.1), which can coordinate to a wide array of metals. Diketonato anions occur extensively as a chelating species.

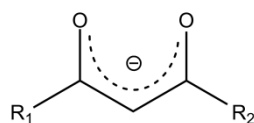


Figure 2.1: A 1,3-diketonato anion formed by deprotonation of a β -diketone.

Various coordination modes of β -diketonato anions to metals are possible. A list of the bonding modes encountered most often is given in **Table 2.2**. The largest collection of metal β -diketonato complexes exhibit κ^2 -O,O' oxygen-bonded chelation. Complexes having this coordination mode are frequently planar with similar C-C, C-O and M-O distances. β -diketonato anions form stable six-membered pseudo-aromatic rings so readily, that even alkali metal complexes can be isolated, e.g. $\text{Rb}_2[(\text{CF}_3\text{COCHCOCF}_3)_3\text{Na}]$.¹⁵

Table 2.2: The different bonding modes of β -diketone ligands to metals (Adapted from A. R. Siedle in *Comprehensive Coordination Chemistry*; eds. G. Wilkinson, R. D. Gillard and J. A. McCleverty, Pergamon Press, Oxford, 1987, vol. 2, pp. 365-412.).

Type of coordination	Representation	Example	Ref
κ^2 -O,O' chelation		$\text{Pd}(\text{F}_3\text{CCOCHCOCF}_3)_2$	16
Semi-chelation		$\text{Pd}\{\text{Ph}_2\text{PC}_2\text{H}_4\text{P}(\text{Ph})\text{C}_2\text{H}_4\text{PPh}_2\}\{\text{F}_3\text{CCOCHCOCF}_3\}^+$	17
κ -O Monodentate oxygen coordination		$\text{Pd}(4\text{-ClC}_5\text{H}_4\text{N})_4(\text{F}_3\text{CCOCHCOCF}_3)$	18

$\eta^2 + \sigma$ -bonded		$\text{Pd}(\text{CH}_2\text{COCHCHCH}_3)(\text{Cl})(\text{PPh}_3)$	19
σ -bonded		$\text{Pd}(\text{bipy})(\text{Cl})(\text{C}-\text{CH}_2\text{COCHCOCH}_3)$	19
Carbon-bonded σ		$\text{Pt}(\text{C}-\text{CH}_3\text{COCHCOCH}_3)(\text{O},\text{O}-\text{CH}_3\text{COCHCOCH}_3) (-1)$	20
Tridentate (O, O, C)		$[\text{Pt}(\text{C},\text{O},\text{O}-\text{C}_3\text{H}_7\text{COCHCOCH}_3)(\text{CH}_3)_3]_2$	21
η^1 -C, κ -O diketonato dianions		$\text{Pt}(\text{C},\text{O}-\text{CH}_2\text{COCHCOCF}_3)(\text{PPh}_3)_2$	22
Bridging		$[\text{Na}_3(\text{C}_5\text{H}_7\text{O}_2)_3(\text{C}_5\text{H}_5\text{N})]_n$	23

Bonding modes other than chelation occur less frequently, since these bonding modes lack the stability supplied by pseudo-aromatic ring formation. The bonding modes of β -diketonato anions are not limited to the examples given in **Table 2.2** and can often occur as a combination of the different bonding modes.

An example of this is illustrated clearly by a complex prepared by Patra and co-workers.²⁴ The complex incorporates simultaneous κ^2 -O,O-chelation and carbon-bonded bridging acetylacetonato ligands and is shown in **Figure 2.2**.

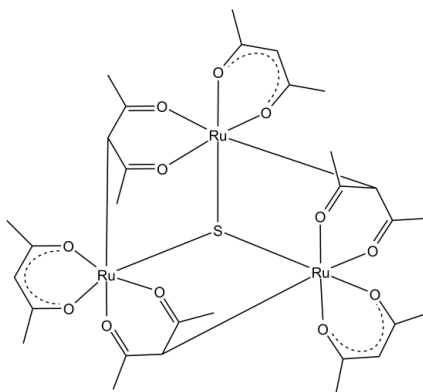


Figure 2.2: A μ_3 -sulfido bridged mixed-valent triruthenium complex prepared by Patra and co-workers showing κ^2 -O,O'- and σ -C-bonded bridging acetylacetonato ligands. (From S. Patra, B. Mondal, B. Sarkar, M. Niemeyer and G. K. Lahiri, *Inorg. Chem.*, 1322, **42** (2003).)

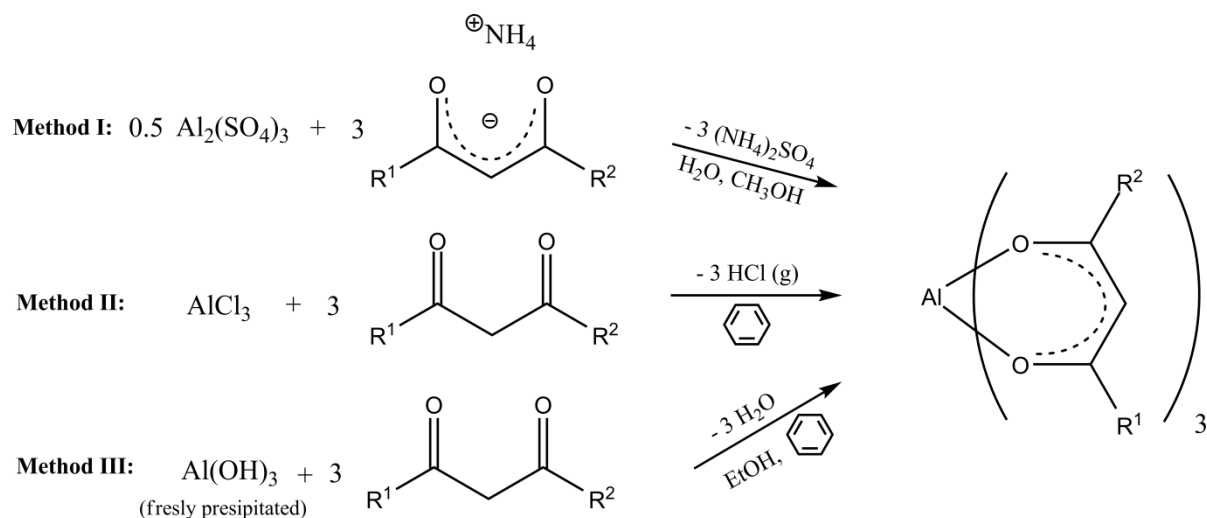
2.2.4. Aluminium β -diketonato complexes

In this section the synthesis, structural properties and reactions of aluminium β -diketonato complexes will be reviewed. This part of chapter 2 relates directly to achieving goal 1. The chemistry of aluminium β -diketonato complexes is also dominated by κ^2 -O,O'-oxygen-bonded chelation and no examples of monodentate, bridging or neutral coordination could be found in literature.²⁵

2.2.4.1. The synthesis of β -diketonato aluminium(III) complexes

The first β -diketonato aluminium(III) complex was tris(acetylacetonato) aluminium(III).²⁶ Tris(β -diketonato) aluminium(III) complexes have been synthesised via a variety of routes as shown in **Scheme 2.4**. Method I is applied most frequently, which involves dissolution of the β -diketone in aqueous ammonia (if the ligand is water soluble) or a mixture of aqueous ammonia and methanol.²⁷ Aqueous ammonia removes the methane proton from the β -

diketone and forms the ammonium salt. This is due to the acidity of the methine protons of β -diketones as discussed in section 2.2.2. The ammonium salt is then reacted with aluminium sulphate. The product precipitates to drive the reaction to completion. Method I has also been applied in the synthesis of tris(ferrocenyl-1,3-butanedionate) aluminium(III) by Zanello *et al.*²⁸ This complex, $[(\text{FcCOCHCOCH}_3)_3\text{Al}]$ is the only known ferrocene-containing β -diketonato aluminium(III) complex.



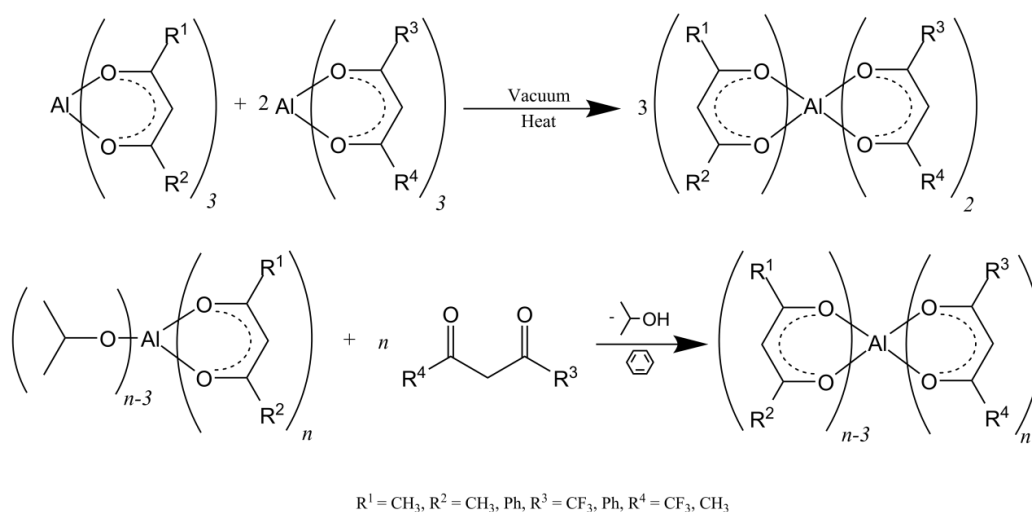
Scheme 2.4: Three methods commonly used to synthesise tris(β -diketonato) aluminium(III) complexes. (Adapted from R.C. Mehrotra and A.K. Rai, *Polyhedron*, 1967, **10** (1991).)

Method II involves refluxing the β -diketone with aluminium chloride in benzene, with the reaction being driven to completion by the removal of gaseous HCl.²⁹ In method III Mehrotra and Rai demonstrated that the tris(β -diketonato) aluminium(III) complex can be synthesised from freshly precipitated aluminium hydroxide.²⁵ This reaction thus illustrates that β -diketones is acidic enough to attack freshly precipitated aluminium hydroxide.

The aqueous chemistry of aluminium is complex, due to the existence of many hydrolysis species.³⁰ Tomany and co-workers performed an investigation on the kinetics and

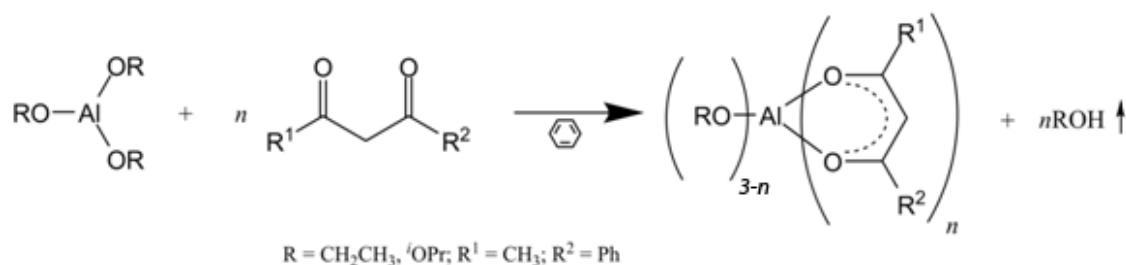
mechanism of the reactions of aluminium(III) with acetylacetonate, trifluoro acetylacetonate and heptane-3,5-dione at low pH (2.5 - 3.5).³¹ In this investigation aluminium is suggested to react with the β -diketones via two pathways. In the first pathway $[\text{Al}(\text{H}_2\text{O})_6]^{3+}$ reacts with the enol tautomer of the β -diketone ($k_E = 1.7(\pm 1.3) \times 10^{-2} \text{ dm}^3 \text{ mol}^{-1} \text{ s}^{-1}$ for acetylacetonate) and is acid-independent. The second pathway is second-order inverse acid-dependant and indicates that $[\text{Al}(\text{H}_2\text{O})_5(\text{OH})]^{2+}$ reacts with the enolate ions of the β -diketones ($k_E = 4.32 (\pm 0.18) \times 10^6 \text{ dm}^3 \text{ mol}^{-1} \text{ s}^{-1}$ for acetylacetonate anion). This indicates that $[\text{Al}(\text{H}_2\text{O})_6]^{3+}$ has low reactivity towards the enol tautomer of acetylacetonate and the low ability of aluminium(III) to abstract a methine proton from acetylacetonate and other β -diketones.

Mixed β -diketonato aluminium(III) complexes of the type $\text{Al}(\text{R}^1\text{COCHCOR}^2)_n(\text{R}^3\text{COCHCOR}^4)_{3-n}$ are also known in literature.^{25, 32} Preparation of these complexes relies on the interchange of ligands. **Scheme 2.5** shows two reactions commonly used to prepare mixed β -diketonato aluminium(III) complexes. The second reaction uses milder conditions and is driven to completion by the liberation of isopropanol, but this reaction requires a mixed alkoxy β -diketonate as starting material.



Scheme 2.5: The synthesis of mixed β -diketonato aluminium(III) complexes of the type $\text{Al}(\text{R}^1\text{COCHCOR}^2)_n(\text{R}^3\text{COCHCOR}^4)_{3-n}$ by means of ligand exchange reactions.

Mixed alkoxy β -diketonato aluminium(III) complexes of the type $\text{Al}(\text{R}^1\text{COCHCOR}^2)_n(\text{OR}^3)_{3-n}$ are synthesised directly from an aluminium alkoxide and the β -diketone (**Scheme 2.6**).^{25, 33} A driving force of the reaction is the azeotropic removal of the alcohol with benzene. It is also interesting to note that the alkoxide groups are significantly more reactive than the β -diketonato ligands. Another reason why the β -diketonato ligands displace the alkoxide is that bidentate ligands (β -diketonates) form stronger bonds with the coordinating metal than monodentate (alkoxide) ligands.



Scheme 2.6: The synthesis of mixed alkoxy β -diketonato aluminium(III) complexes from aluminium alkoxides.³³

Other mixed ligand variants include mixed chloride β -diketonato or β -ketoester derivatives, mixed ligand complexes of the form $\text{Al}(\beta\text{-diketonato})_{3-n}(\text{L})_n$ ($\text{L} = 8\text{-hydroxyquinoline}$), mixed siloxide β -diketonato complexes and numerous β -diketonato bimetallic aluminium derivatives with bridging alkoxide groups.³³

In an investigation on the heat of formation of aluminium acetylacetonate by Hill and Irving³⁴, it was found that the heat of formation in the gaseous phase was $-1668.78 \text{ kJ mol}^{-1}$. The aluminium-oxygen bond energy at 25°C was found to be 276 kJ mol^{-1} .

2.2.4.2. The structural properties of β -diketonato aluminium(III) complexes

The first tris(β -diketonato) aluminium(III) complex to be characterised by X-ray crystallography was tris(acetylacetonato)aluminium(III).²⁵ Like most tris(β -diketonato) aluminium(III) complexes, $\text{Al}(\text{acac})_3$ is monomeric and octahedral. Initial crystallographic investigations revealed two allotropic modifications of $\text{Al}(\text{acac})_3$, namely the α - and β -polymorphs.³⁵ The α -polymorph has a monoclinic crystal lattice (space group $P2_1/c$), whilst the β -polymorph has an orthorhombic crystal lattice (space group $Pbca$). McClelland³⁶ reported the crystal structure of γ -tris(acetylacetonato) aluminium(III) in 1975 with the spacegroup $Pna2_1$. Recently von Chrzanowski and co-workers³⁷ redetermined the structure at 110 K. Four molecules are present within the crystal structure as shown in **Figure 2.3**. Molecule 1 (Al1) has approximately C_2 symmetry, whilst molecule 2 to 4 approximate D_3 symmetry.

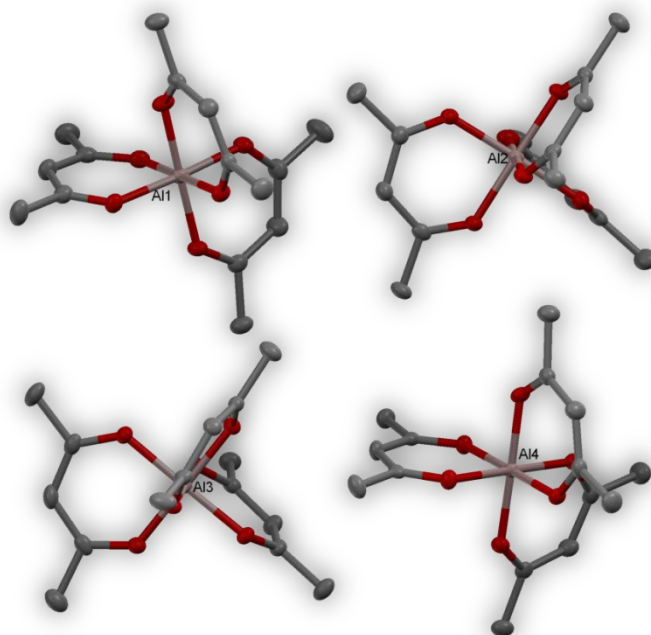


Figure 2.3: The crystal structure of γ -tris(acetylacetonato)aluminium(III) consisting of four independent molecules. (From L. S. von Chrzanowski, M. Lutz and A. L. Spek, *Acta Cryst.*, m3318, **E62** (2006).)

It should also be noted that the α - and γ -polymorphs can occur in the same crystallization batch. In a further investigation by von Chrzanowski and co-workers³⁸ on α -tris(acetylacetonato) aluminium(III) a new δ -polymorph was discovered at 110 K. A phase transition of the α - to the δ - polymorph occurs between 150 and 110 K. The spacegroup of the δ -polymorph remains $P2_1/c$. Three molecules occur in the asymmetric unit of the δ -polymorph, all showing approximately D_3 symmetry. One of the three molecules is shown in **Figure 2.4**.

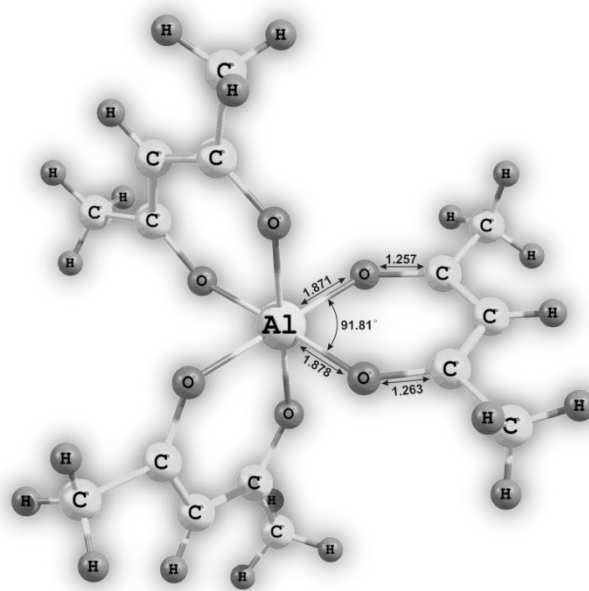


Figure 2.4: The crystal structure of δ -tris(acetylacetonato) aluminium(III). (From L. S. von Chrzanowski, M. Lutz and A. L. Spek, *Acta Cryst.*, m129, **C63** (2007).)

All the tris-(acetylacetonato) aluminium(III) molecules of the different polymorphs show similar Al-O bonding distances ranging between 1.871 Å for the δ -polymorph to 1.890 Å for the γ -polymorph. The O-Al-O bonding angles range from 90.19° to 90.81° , which is ideal for the orbital overlap in an octahedral structure. The crystal structure of a mixed alkoxide β -diketonato aluminium(III) complex, $[\text{Al}(\text{O}^i\text{Pr})_2(\text{acac})]_3$, shows this complex exists as a trinuclear aluminium cluster (**Figure 2.5**). It has β -diketonato O-Al-O bonding angles of ca.

88.1° and isopropoxide O-Al-O bonding angles of between 74.4° and 83.3°. The β -diketonato Al-O bond lengths are similar to the bonding lengths in $\text{Al}(\text{acac})_3$. Al-O β Pr bonding lengths are slightly longer than the Al- β -diketonato bonds, indicating weaker bond strengths, greater flexibility and the possibility of smaller O-Al-O bonding angles. Other examples of mixed alkoxide β -diketonato aluminium(III) crystal structures include $[\text{Al}(\text{O}^i\text{Pr})(\text{Et}_2\text{acac})_2]_2$ ³⁹ and $[\text{Al}(\text{OSeMe}_3)_2(\text{acac})]_2$ ⁴⁰.

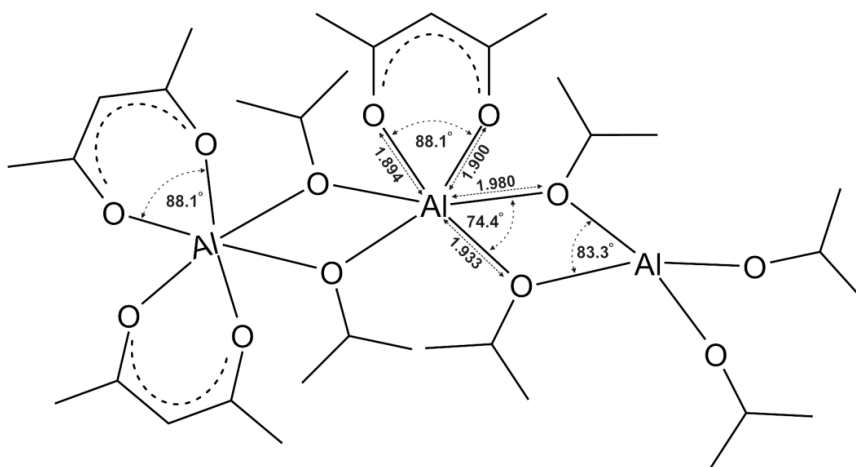


Figure 2.5: The structure of $[\text{Al}(\text{O}^i\text{Pr})_2(\text{acac})_3]_3$ showed this complex to exist as a four-membered aluminium-oxygen heterocycle with smaller O-Al-O bonding angles than in the $[\text{Al}(\text{acac})_3]$ complex. (From J. H. Wengrovius, M. F. Garbauskas, E. A. Williams, R. C. Going, P. E. Donahue and J. F. Smith, *J. Am. Chem. Soc.*, 983, **108** (1986).)

Unsymmetrical tris(β -diketonato) complexes of aluminium and other metals also exhibit *mer*- and *fac*-geometrical isomerism.^{41, 42} This has been shown by a ¹H NMR study for tris(1-ferrocenyl-1,3-butanedionate) aluminium(III) synthesized by Zanello and co-workers, **Figure 2.6**.²⁸ A ratio of 2:3 for *fac*:*mer* was observed, showing that the symmetrically arranged *fac*-isomer occurs in lower concentration than the unsymmetrical *mer*-isomer.

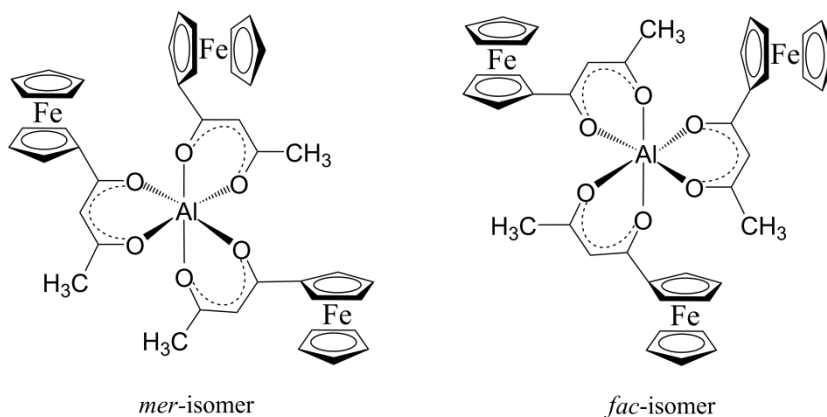


Figure 2.6: *Mer* and *fac* geometrical isomers of tris(1-ferrocenyl-1,3-butanedionate) aluminium(III) (From P. Zanello, F. F. de Bianai, C. Glidewell, J. Koenig and S. J. Marsh, *Polyhedron*, 1795, **18** (1998).)

2.2.4.3. Reactions of β -diketonato aluminium(III) complexes

β -diketonato complexes of metals can undergo various reactions.⁷ These reactions include substitution at the methine carbon, hydrolysis or solvolysis⁴³, displacement reactions, ligand exchange reactions and rearrangement reactions. Of these different reactions, displacement reactions are prevalent in mixed β -diketonato and alkoxide complexes, where the alkoxide ligands are more labile than the β -diketonato.³³ This type of reaction was illustrated in **Scheme 2.5** (previous section, p. 22) in the synthesis of mixed β -diketonato aluminium complexes. Ligand exchange reactions, where one β -diketonato ligand is exchanged for another, are also observed in β -diketonato aluminium complexes and also used in the synthesis of mixed β -diketonato aluminium complexes. Another example of a ligand exchange reaction is the reaction of $\text{Al}(\text{acac})_3$ with $\text{Al}(\text{CF}_3\text{COCHCOCF}_3)_3$ to produce $\text{Al}(\text{acac})_2(\text{CF}_3\text{COCHCOCF}_3)$ and $\text{Al}(\text{acac})(\text{CF}_3\text{COCHCOCF}_3)_2$. In chlorobenzene at 25 °C an equilibrium constant of 3.34×10^4 is observed for this reaction.⁴⁴ Aluminium β -diketonato complexes can also undergo rearrangement reactions.

Intramolecular stereoisomerization of $\text{Al}(\text{iPrCOCHCOiPr})_3$ and $\text{Al}(\text{iPrCOCHCOiPr})(\text{CF}_3\text{COCHCOCF}_3)_2$ was observed by Pickering and co-workers.⁴⁵ The proposed mechanism for stereoisomerization is a rhombic twist mechanism for alkyl or aryl substituted β -diketonato complexes and a bond-breaking mechanism via a five-coordinate square pyramidal intermediate.

2.2.5. Medical applications of aluminium compounds and ferrocene-containing β -diketonato complexes

Investigating the medical applications and impacts of aluminium compounds and ferrocene-containing β -diketonato complexes directly relate to goal 4 – the evaluation of ferrocene-containing β -diketonato complexes of aluminium as anti-cancer agents. Some medical applications of aluminium compounds will be described to illustrate their medical viability, followed by examples of ferrocene-containing complexes that show anti-cancer activity.

Aluminium compounds are frequently used in metallopharmaceutical applications.⁴⁶ Aluminium hydroxide, aluminium phosphate and alum ($\text{KAl}(\text{SO}_4)_2 \cdot 12\text{H}_2\text{O}$) are frequently used as adjuvants (compounds that possess the ability to bind to a specific antigen) in immunisation therapies. Aluminium hydroxide and aluminium glycinate ($\text{Al}(\text{NH}_2\text{CH}_2\text{COO})(\text{OH})_2$) are frequently used as antacids, functioning both to neutralize stomach acid and to facilitate healing of ulcers.

Aluminium hydroxide is also used as a phosphate binder in patients with renal disease, whilst aluminium acetate mono basic ($\text{Al}(\text{O}_2\text{CCH}_3)_2(\text{OH})$) is frequently used as a topical

antiseptic and an astringent. Aluminium compounds can also assist in regulation of lipid metabolism.

However, cationic aluminium compounds have no known biological function in humans and can disrupt a range of metabolic activities and processes in cells. Accordingly Berend and co-workers⁴⁷ concluded that aluminium is a potent neurotoxin. In a review on the effects of aluminium on iron metabolism in mammalian cells, Oshiro⁴⁸ identified two pathways of aluminium uptake in cells: receptor-mediated endocytosis and transferrin-independent iron uptake systems. Aluminium was also found to bind directly to a cellular iron sensor. Programmed cell death (apoptosis) pathways in brain cells are induced by aluminium and thus aluminium may be linked to Alzheimer's disease.

Anitha and Rao⁴⁹ found that trivalent aluminium shows great affinity for phosphate groups of DNA. Biological ligands are typically oxygen, phosphates and carboxylates, all of which bind readily to aluminium. Binding sites in DNA include heterocyclic nitrogen atoms, carbonyls and phosphate oxygens. Accordingly it was reported that aluminium forms several Al-DNA complexes with DNA, which depend on aluminium concentration and pH.

These examples thus clearly indicate the ability of aluminium to alter cell metabolism and even induce cell death, serving as motivation for anti-cancer testing of aluminium compounds.

Metal β -diketonato complexes, like $[\text{Rh}(\text{acac})(\text{cod})]$, are known to be active against various types of cancer cells.⁵⁰ Ferrocenium salts as well as ferrocene-containing complexes, like ferrocene-containing diruthenium tetracarboxylates, also show anti-cancer cells activity.⁵¹

2.3. Carboxylates

This section is concerned with carboxylic acids as ligands and the aluminium complexes thereof. Bonding modes of carboxylates to metals will be examined, followed by the synthesis and characterisation of aluminium carboxylates, which relates to goal 4. The infrared characterisation of carboxylates and aluminium carboxylates will be examined in detail as this is relevant to reaching goal 5.

2.3.1. Carboxylic acid bonding to metals

The summary on the different bonding modes of carboxylic acids to metals were obtained from a review by C. Oldham⁵².

2.3.1.1. Monocarboxylates

Usually carboxylic acids behave as mono-negative oxygen donors, leading to ionic bonding between the carboxylic acid and the metal. Coordination is also observed and occurs via the oxygen atoms. Three types of oxygen atom coordination have been observed, namely monodentate, bidentate chelating and bridging coordination. The bridging mode of coordination is observed in five variants. **Table 2.3** summarizes the different bonding modes.

Table 2.3: Tabulation of the different bonding modes of monocarboxylic acids. (Adapted from C. Oldham in *Comprehensive Coordination Chemistry*; eds. G. Wilkinson, R. D. Gillard and J. A. McCleverty, Pergamon Press, Oxford, 1987, vol. 2, pp. 435-459.)

Type of coordination	Representation	Example	Ref.
Ionic		HCOO ⁻ Na ⁺	53
Monodentate		B(O ₂ CMe) ₂ (acac)	54
Bidentate chelating		Zn(O ₂ CMe) ₂ ·2H ₂ O	55
Bridging modes			
Syn-syn		[Cr(O ₂ CMe) ₂ H ₂ O] ₂	56, 57
Anti-anti		Cu(O ₂ CH) ₂ ·4H ₂ O	58
Anti-syn		Cu(O ₂ CH) ₂ ·4H ₂ O	59
Tridentate		Cu(O ₂ CMe)	60
Monoatomic (μ-oxo)		[Cu(O ₂ CMe)L ₂] L = salicylaldehyde derivative	61

X-ray diffraction techniques are the preferred method to identify the bonding mode present in a complex. Other viable techniques include IR and NMR spectroscopy. Due to the low symmetry of the carboxylate group (C_{2v}) coordination to a metal does not significantly lower the symmetry. In infrared spectroscopy of carboxylates, the C-O stretching frequencies are the most prominent. To differentiate between bonding modes the separation of the symmetric and antisymmetric stretching frequencies are compared to that of a known carboxylic ionic salt. During monodentate coordination in carboxylates, the two C-O bonds

are no longer equivalent like those in the anion and furthermore one metal-oxygen distance is substantially shorter than the next shortest metal-oxygen distance. This inequivalence of the two carbon-oxygen bonds is used in detection of this bonding mode using infrared spectroscopy. The *ca.* 1600 cm^{-1} band of the free acid anion is shifted to higher energy (higher cm^{-1} value) during monodentate coordination. According to Oldham, this should also lead to an increase in the separation (Δ) between the symmetric ($\nu_{sym}(\text{CO})$) and antisymmetric ($\nu_{asym}(\text{CO})$) stretching frequencies relative to that of the free ion. For monodentate acetate systems $\nu_{sym}(\text{CO})$ is expected at *ca.* 1680 cm^{-1} and $\nu_{asym}(\text{CO})$ usually occurs at *ca.* 1420 cm^{-1} , thus producing $\Delta\nu = 260 \text{ cm}^{-1}$. In the free acetate ion $\Delta\nu$ is 164 cm^{-1} , generally a $\Delta\nu \geq 200 \text{ cm}^{-1}$ is indicative of monodentate coordination.⁵² However this technique is prone to error in cases where the two C-O bonds are approximately equal in length, and different results are likely if the coordination metal varies with charge, e.g. Ca^{2+} , Al^{3+} , Ti^{4+} , Cr^{6+} , etc. This research program addressed the possibility of using Δ -values to establish binding modes in particular for Al^{3+} .

In general though, chelating coordination is less common than monodentate coordination. In both symmetrical chelation and bridging coordination the two C-O bonds remain equivalent as in the case of the free ion. In a chelating system the OCO angle (115°) is usually smaller than that of the bridging coordination mode (125°).⁵² The ring strain induced by this smaller OCO angle translates into chelating coordination occurring far less (if at all) than bridging coordination. The exception is when the metal is divalent; like Ca^{2+} . The equivalence of the two C-O bonds have lead to infrared spectroscopy not being frequently used to differentiate between chelating and bridging bonding modes. However, smaller $\Delta\nu$'s are observed for chelating and bridging coordination than for ionic bonding. In turn, smaller values of $\Delta\nu$ are observed for chelating than for bridging coordination. The difference

between $\Delta\nu$'s have, however, not been used to distinguish between the bridging and chelating bonding modes.

When considering bridging systems, systems with *syn-syn* coordination are the most common. Two common structures in this class are the paddlewheel and triangular carboxylates shown in **Figure 2.7**. The *anti-anti* and *anti-syn* bridging modes occur mostly in polymeric carboxylate complexes. The *monatomic* and *tridentate* carboxylate bridges between two metals occur frequently in alkoxide chemistry. Of all the carboxylate ligands it is noteworthy to mention that the formate ligand is very versatile in its bridging capability. Bridging carboxylate configuration according to literature, is often only recognized by crystallographic structural determinations.

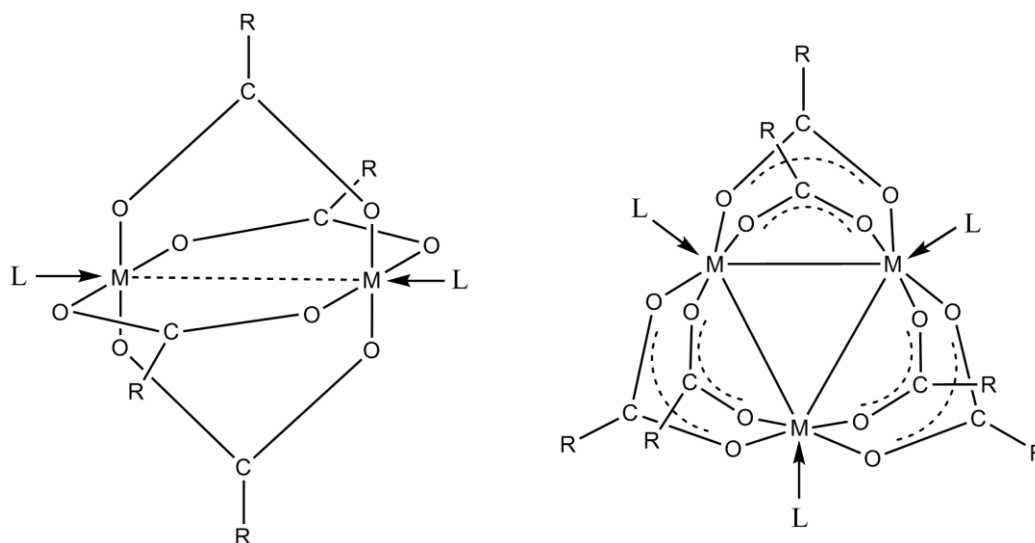


Figure 2.7. Common structures showing the *syn-syn* bridging coordination mode. The paddlewheel carboxylates (left, $M = \text{Cu, Mo, Cr, Re}$)⁶² and the triangular carboxylates (right, $M = \text{Cr, V}$)⁶³.

As mentioned earlier, for the bridging coordination mode, the two C-O bond lengths are equivalent and this should increase the difficulty to distinguish between chelating and

bridging using vibrational spectroscopy. However, for the acetate systems a value for $\Delta\nu$ smaller than 105 cm^{-1} could indicate chelation rather than bridging.

A final coordination mode arises when acetic acid is σ -bonded to a transition metal (Pd, Mo, Fe) via the methylene group of the acid, giving $\text{M-CH}_2\text{COOH}$.⁷ This coordination mode is however less likely for longer-chained carboxylic acids.

2.3.1.2. Dicarboxylates

Difunctionalised carboxylic acids are often chelating ligands. Two modes of chelation are observed as listed in **Table 2.4**. Monodentate coordination occurs less frequently but is still possible. Of the different types of chelation, $\kappa^2\text{-O,O'}$ -chelation leading to five-membered rings occurs more frequently. Perhaps the most notable of all the ligands forming five-membered rings is oxalic acid, having numerous examples in literature. Chelation involving the coordination of the CO_2^- group, leading to four-membered rings, occurs with longer chained dicarboxylic acids. Steric strain produced by four-membered rings lead to the strong tendency of dicarboxylic acids to form chelate rings with more than four atoms. Indeed oxalic acid displays this behaviour, forming five-membered rings during coordination. Six-membered rings are preferred by malonic acid leading to chelation. Thus it is important to note that steric strain plays a significant role in determining which type of coordination will be achieved and that five- and six-membered rings are preferred above four-membered rings.

Table 2.4: Monodentate and chelating coordination modes of dicarboxylic acids to metals. (Adapted from C. Oldham in *Comprehensive Coordination Chemistry*; eds. G. Wilkinson, R. D. Gillard and J. A. McCleverty, Pergamon Press, Oxford, 1987, vol. 2, pp. 435-459.)

Type of coordination	Representation	Example	Ref.
Monodentate		$[\text{Co}(\text{en})_2\text{X}(\text{ox})]^a$ X = halogen	64
$\kappa^2\text{-O,O'}$ four-membered ring		$\text{Ca}(\text{ox})(\text{H}_2\text{O})_2^b$	65
Chelating $\kappa^2\text{-O,O'}$ five-membered ring		$[\text{Co}(\text{ox})\text{N}_4]$	66

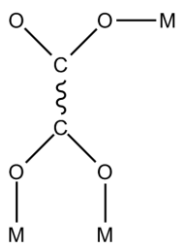
a: en = ethylene diamine, ox = oxalate ($\text{C}_2\text{O}_4^{2-}$)

Dicarboxylic acids also exhibit various bridging bonding modes, some of which are illustrated in **Table 2.5**. Bidentate bridging involves coordination of two of the oxygen atoms of the dicarboxylic acid. The *trans*-coordination mode has been observed for dimethyl oxalate ($\text{Me}_2\text{C}_2\text{O}_4$), whilst *cis*-bridging occurs in $[(\text{NH}_3)(\text{H}_2\text{O})\text{Co}(\text{C}_2\text{O}_4)\text{Co}(\text{NH}_3)_5]^{4+}$ and *syn-syn* bridging is seen in some cobalt(III) amine complexes.

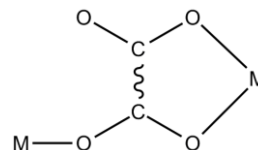
Table 2.5: Bridging modes of dicarboxylic acids. (Adapted from C. Oldham in *Comprehensive Coordination Chemistry*; eds. G. Wilkinson, R. D. Gillard and J. A. McCleverty, Pergamon Press, Oxford, 1987, vol. 2, pp. 435-459.)

Bridging Mode	Type	Illustration
	Bidentate	
<i>syn-syn</i> , ref. 67	<i>Cis</i> , ref. 68	<i>trans</i> , ref. 69

Tridentate

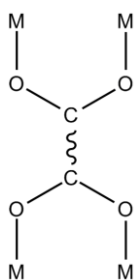


monodentate + *syn-syn*, ref. 70

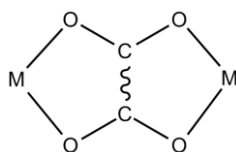


monodentate + κ^2 -*O,O'* chelated, ref. 71

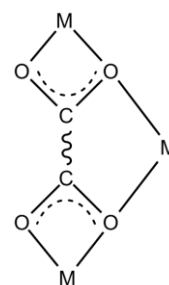
Tetradentate



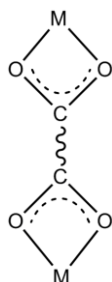
two-(*syn-syn*), ref. 72



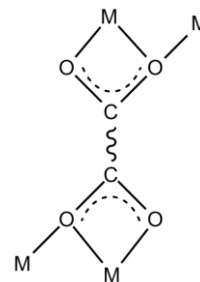
two-(κ^2 -*O,O'*-chelation), ref. 73



two-(κ^2 -*O,O'*-chelation) giving 4-membered rings + κ^2 -*O,O'*-chelation, ref. 74



two-(κ^2 -*O,O'*-chelation) giving 4-membered rings, ref. 75



two-(κ^2 -*O,O'*-chelation + monoatomic), ref. 76

Tridentate bridging involves coordination of three of the oxygen atoms. Examples include $\text{Sc}(\text{OH})(\text{C}_3\text{H}_2\text{O}_4) \cdot 2\text{H}_2\text{O}$ ⁷¹ for monodentate + κ^2 -*O,O'*-chelation and $\{[(\text{NH}_3)_3\text{Co}]_2(\text{NH}_3)_5\text{Co}(\text{OH})(\text{C}_2\text{O}_4)\}^{5+}$ ⁷⁰ for monodentate + *syn-syn* bridging. Tetradentate bridging, involving the coordination of four of the oxygen atoms of a dicarboxylic acid, is by far the abundant bridging form. Of the tetradentate bridging modes two-(κ^2 -*O,O'*-chelation) occurs most frequently. Typical examples of two-(η^n chelation) include $[(\text{py}_4\text{Ru})_2(\text{C}_2\text{O}_4)]^{2+}$ and $[(\text{triammine Cu})_2(\text{C}_2\text{O}_4)]^{2-}$.⁷³ Malonate complexes of europium, $\text{Eu}_2(\text{mal})_3 \cdot 8\text{H}_2\text{O}$, and

cadmium, $\text{Cd}(\text{mal})\cdot\text{H}_2\text{O}$, show two- $(\kappa^2\text{-O,O'-chelation})^{74} + \kappa^2\text{-O,O'-chelation}$, leading to one six- and two four-membered rings being formed. The last two bridging modes in **Table 2.5** are observed in the malonate complex $\text{Nd}(\text{C}_3\text{H}_2\text{O}_4)_3\cdot 8\text{H}_2\text{O}^{75}$ and in the oxalate complex $[\{(\text{NH}_3)_3\text{Co}\}_4(\mu\text{-OH})_4(\mu\text{-C}_2\text{O}_4)]^{6+}{}^{76}$.

2.3.2. Aluminium carboxylates

2.3.2.1. Introduction

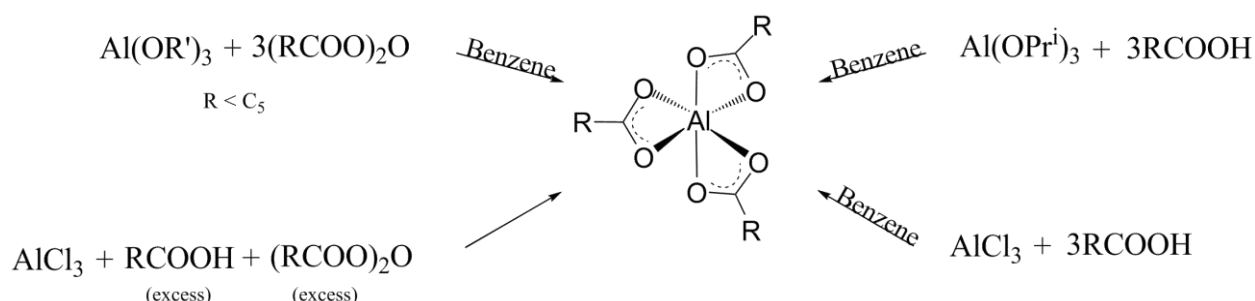
In this section, close attention will also be paid to the synthesis of aluminium complexes of monocarboxylic acids and the FTIR characterisation of these complexes as to facilitate reaching both goals 4 and 5. Aluminium carboxylates can normally be derived from aluminium hydroxide, $\text{Al}(\text{OH})_3$, by replacement of the hydroxyl groups. A monocarboxylic acid like formic acid can lead to three types of aluminium formate: dibasic aluminium formate, $(\text{HO})_2\text{Al}(\text{OOCH})$ – observe the two hydroxy groups coordinated to Al – monobasic aluminium formate, $(\text{HO})\text{Al}(\text{OOCH})_2$, and aluminium triformate, $\text{Al}(\text{OOCH})_3$.

Commercial applications of aluminium carboxylates include the use as finishing agents for waterproofing cloth and as mordants in textile dyeing.⁷⁷ The antiseptic, astringent and basic properties of aluminium carboxylates lead to various applications in pharmaceutical preparations. Since the higher molecular weight aluminium carboxylates have gelling properties, they find application in the manufacture of both cosmetics and coatings.

2.3.2.2. Synthesis

In a review on aluminium alkoxide, β -diketonato complexes and carboxylates, Mehrotra and Rai⁷⁸ describe several synthetic approaches to aluminium tricarboxylates. Refluxing aluminium isopropoxide with an excess carboxylic acid in benzene produces an aluminium tricarboxylate and isopropanol which, together with liberated water, is fractionated off azeotropically with benzene (bp. 69.3 °C⁷⁹). Aluminium tricarboxylates of short chain-length (acetate, propionate and butyrate) can be prepared by refluxing an aluminium alkoxide and three equivalents of acid anhydride in benzene. Another approach is to employ anhydrous aluminium chloride, an excess of the particular acid anhydride and an excess of the carboxylic acid, however carboxylates of higher chain length could not be synthesized in this manner. Aluminium tricarboxylates as well as aluminium chloride carboxylates, $AlCl_{3-x}(OOCR)_x$, have also been synthesized by refluxing anhydrous aluminium trichloride and the appropriate carboxylic acid in benzene, until the evolution of hydrochloric acid ceased. Gilmour and co-workers also synthesised aluminium tristearate using anhydrous pyridine as solvent.⁸⁰ The different synthetic methods are summarized in

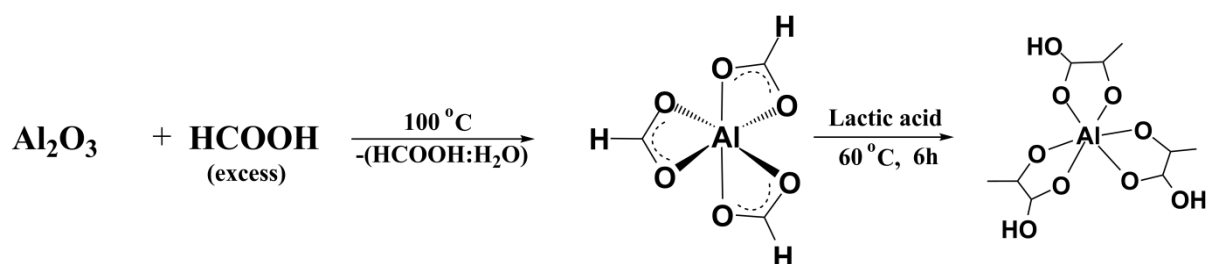
Scheme 2.7.



Scheme 2.7: Four synthetic approaches to aluminium tricarboxylates. The above structure is idealised.

The author wish to inject a word of caution here. His own research to be described in Chapter 3 showed it is exceedingly difficult to obtain the aluminium tricarboxylates in **Scheme 2.7**. This research program has shown that many publications reporting tricarboxylato aluminium(III) complexes may actually have obtained some bridged form of aluminium, similar to a range of compounds known as alumoxanes.

More recently Narayanan and Laine¹⁶ reported that aluminium formates can be synthesized directly from aluminium hydroxide. Gibbsite, boehmite and Al_2O_3 were used as aluminium sources and reacted with formic acid to produce aluminium formate. Water that formed during the reaction was removed by distilling of a water-formic acid azeotrope (bp. 107.3 °C⁷⁹) that was formed. Gibbsite derived aluminium formate was then utilized to synthesize aluminium lactate by heating the formate in lactic acid. X-ray crystallography revealed that Al(III) is surrounded by three lactate ligands arranged in an octahedral fashion. Each lactate ligand is bound to aluminium via the oxygen of the carboxylate group and the α -hydroxy oxygen. The hydroxy proton is retained and a five-membered ring is formed with aluminium.⁸¹



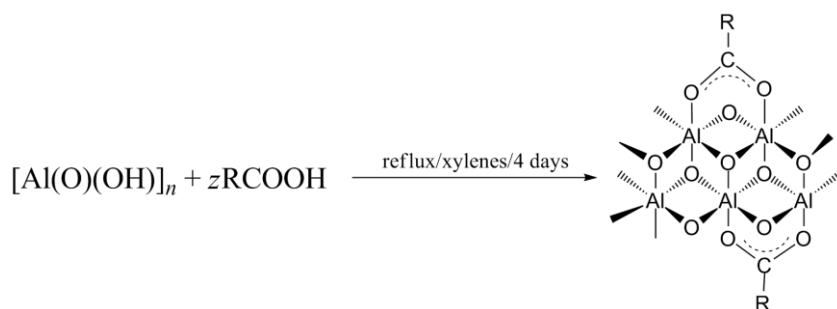
Scheme 2.8: The synthesis of aluminium formate directly from aluminium hydroxide and formic acid. The above tricarboxylate structure is idealised.

According to Mehrotra and Rai⁷⁸, aluminium carboxylates are highly susceptible to hydrolysis. Thus in each of the synthetic methods in **Scheme 2.7**, the reaction is either performed in benzene which forms an azeotrope with water or the alcohol that formed and

is easily removed, or the reaction is performed with the acid anhydride, which reacts with any water present. The lower aluminium carboxylates like formates, acetates and propionates are soluble in common organic solvents and they are hydrolysed when exposed to water. However, solubility increases with hydrocarbon chain length.

Ferrocene-containing aluminium carboxylates were prepared by Okada and Nakajima⁸² by reacting ferrocene-containing dicarboxylic acids with aluminium chloride. The acids included 1,1'-bis(3-carboxypropanoyl) ferrocene, 1,1'-bis(5-carboxypentaoyl) ferrocene and 1,1'-bis(9-carboxynonaoyl) ferrocene.

Another class of aluminium carboxylate compounds that can be obtained directly from an aluminium hydroxide source, boehmite, is carboxylato-alumoxanes. Barron and co-workers^{83,84, 85} report that boehmite reacts with carboxylic acids to form carboxylato-alumoxanes, having a boehmite-like core and carboxylate groups bound in a bridging fashion on the surface of an alumoxane particle. The general synthetic strategy involved refluxing boehmite and the appropriate acid in xylenes for four days. For the acetate and propionate alumoxanes, acetic acid and propionic acid was respectively refluxed with boehmite for four days (**Scheme 2.9**). This is similar to the synthesis of aluminium formate, but water is not removed from the reaction, thus leading to the boehmite core being retained.



Scheme 2.9: The synthesis of carboxylato-alumoxanes from boehmite. R = (CH₂)_nCH₃, n = 0 – 11.

The characteristics of carboxylato-alumoxanes differ significantly from aluminium tricarboxylates. Lower order carboxylato-alumoxanes are insoluble, whilst carboxylato-alumoxanes with higher chain length are only insoluble in common organic solvents. They are however soluble in pyridine and DMF at higher temperatures.

With respect to this study, it proved almost impossible to synthesise chelated aluminium tricarboxylates. Invariable, in the presence of only trace amounts of moisture, carboxylato-alumoxanes dominate, see Chapter 3.

2.3.2.3. Bonding, structural aspects and characterisation

In this section the bonding of carboxylic acids to aluminium will be examined, accompanied by FTIR and structural data. Five- and six-membered ring-complexes of aluminium will also be considered. Three bonding modes of carboxylic acids to aluminium frequently are implied in discussions on aluminium carboxylates, **Figure 2.8**.

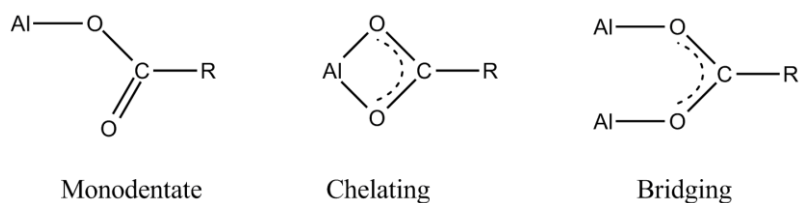


Figure 2.8. The three bonding modes of monocarboxylic acids to aluminium which are frequently encountered or considered in the aluminium carboxylate chemistry.

In an investigation on dialkylaluminium carboxylates, Bethley and co-workers⁸⁵ indicated by means of *ab initio* calculations the relative energy differences between the different bonding modes of carboxylic acids encountered in these complexes, shown in **Figure 2.9**.

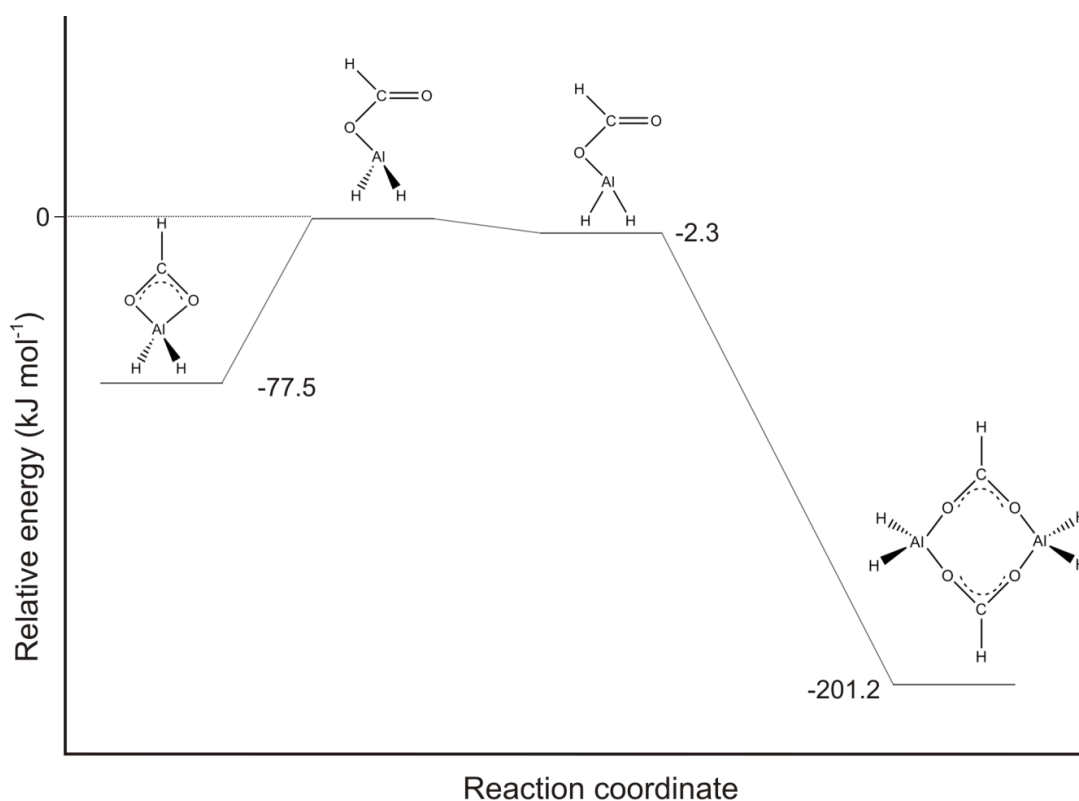


Figure 2.9: The calculated relative energy diagram for dialkyl aluminium carboxylate compounds. Calculations were at the MP2/3-21G(*) level. The relative energy differences are given in kJ mol^{-1} . (From C. E. Bethley, C. L. Aitken, C. J. Harlan, Y. Koide, S. G. Bott and A. R. Barron, *Organometallics*, 329, **16** (1997).)

Results of this investigation indicate that bridging coordination is by far the most stable for aluminium followed by chelation and monodentate coordination. Bethley and co-workers also concluded that $\Delta G = -77.5 \text{ kJ mol}^{-1}$ stabilisation provided by chelation is insignificant when compared to the enthalpy (ΔH) of -407 kJ mol^{-1} for the conversion reaction of the monodentate species into the dimeric bridged species. Furthermore, the Al-O bond strength is 512 kJ mol^{-1} . They concluded that isolation of the chelating carboxylate may only be possible in the absence of an external Lewis base and if the carboxylate substituents may be large enough to prohibit dimerisation because of steric hinderance. It is also important to note the calculated O-C-O bonding angles of 114.1° for chelation, 124.2 and 124.4° for

monodentate coordination and 123.4° for the bridging mode. Thus chelation shows significantly smaller O-C-O bonding angles. Calculated O-Al-O bonding angles are 67.84° for chelation and 109.8° for bridging coordination, both deviating by about 20° from the 90° observed for β -diketonato complexes of aluminium. From this research, Bethley and co-workers calculated that bridging coordination is much favoured over the chelation mode. The author's own research, discussed in Chapter 3, shows dimerisation is not the only competing structure for the chelated complex. Carboxylato-alumoxane formation also lowers the probability of detecting a chelated aluminium carboxylate.

Very few crystallographic examples of monodentate coordination of monocarboxylic acids to aluminium could be found in literature.^{86, 87, 88, 89} Two aluminium carboxylates that show monodentate coordination of a carboxylic acid to aluminium are given in **Figure 2.10**. Acetoxy-((R,R)-N,N'-bis(3,5-di-*t*-butylsalicylidene)-1,2-cyclohexanediamine-N,N',O,O') aluminium(III)⁸⁹ (structure I in **Figure 2.10**) has an R-factor of 5.26, which is high in comparison to modern crystallographic determinations with R-factors less than 1.5. This complex has an Al-O bond distance of 1.768 Å for the monocarboxylate ligand. The O-C-O angle of the monocarboxylate is 124.09° . Tetramethylammonium acetato-trimethyl aluminium(III)⁸⁶ (structure II in **Figure 2.10**) shows an Al-O bond distance of 1.833 Å, an O-C-O angle of 117.05° and has an R-factor of 9.20, which is significantly higher than the R-factors of 1.5 or better for modern crystallographic determinations. In these aluminium complexes of monocarboxylic acids a larger ligand or ligands block the coordination sites on aluminium, allowing for only monodentate coordination of the carboxylic acid.⁸⁶⁻⁸⁹ Another example of monodentate bonding occurs in an aluminium porphyrin isolated by Davidson and co-workers⁹⁰, where benzoic acid is coordinated to aluminium in a monodentate fashion.

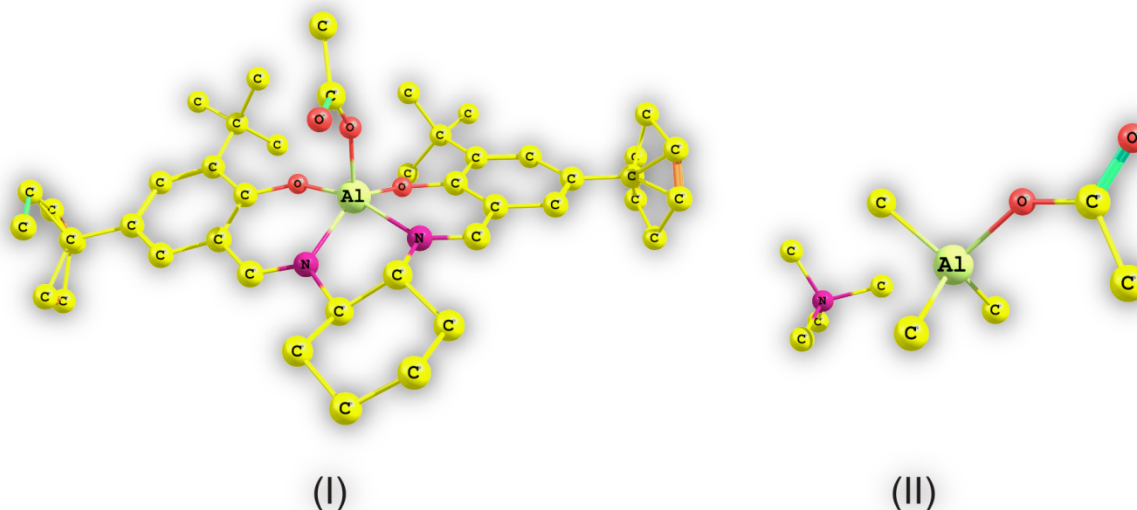


Figure 2.10: The crystal structures of Acetoxy-((R,R)-N,N'-bis(3,5-di-*t*-butylsalicylidene)-1,2-cyclohexanediamine-*N,N',O,O'*) aluminium(III)⁸⁹ (Structure I) and Tetramethylammonium acetato-trimethyl aluminium(III)⁸⁶ (Structure II), both showing monodentate coordination of a carboxylic acid to aluminium.

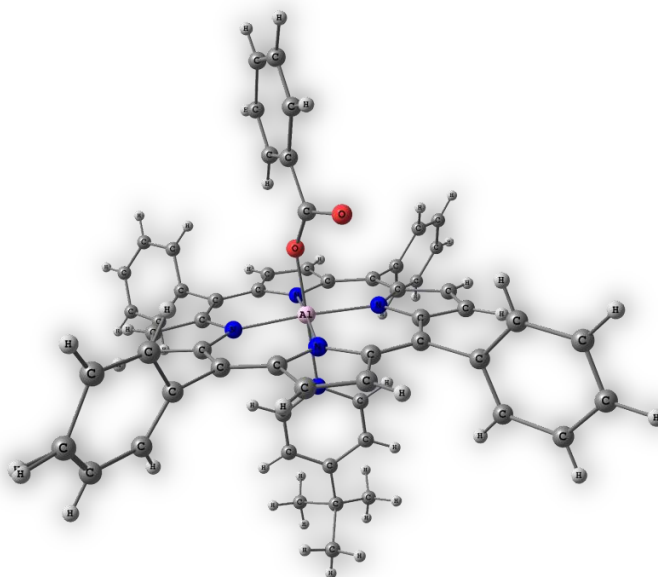
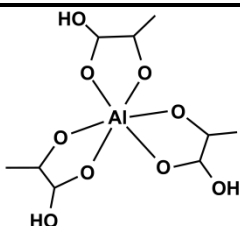
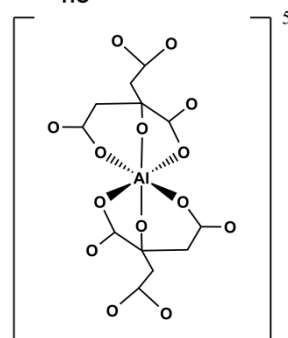
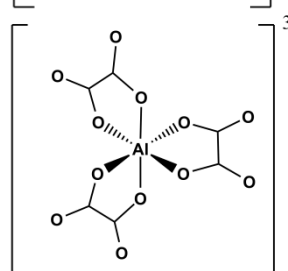
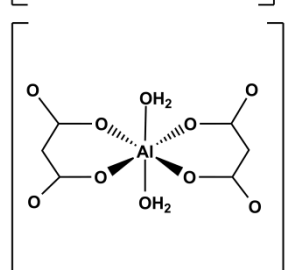


Figure 2.11: The crystal structure of a porphyrin showing monodentate coordination of benzoic acid to aluminium(III).

Numerous examples of dicarboxylic and tricarboxylic acids showing monodentate coordination for every individual carboxylato functional group (even through the full ligand may be polydentate), are known. A number of these complexes are shown in **Table 2.6**.

Table 2.6: The Al-O bond distances and O-Al-O bonding angles of dicarboxylic and tricarboxylic acid complexes of aluminium showing monodentate coordination.

Structure	Al-O distance (Å)	O-Al-O angle (°)	Ref
(A) 	1.856(4)-1.908(4)	82.1(1)-96.9(1)	91 92
(B) 	1.836(1)-1.959(1)	85.56(6)-94.47(6)	93, 94, 95
(C) 	1.876(3)-1.908(4)	83.1(2)-100.1(2)	96, 97, 98, 99
(D) 	1.862(2)-1.902(2)	86.3(1)-93.1(1)	97, 100, 101

A = Aluminium lactate, $\text{Al}(\text{CH}_3\text{CH}(\text{OH})\text{COO})_3$

B = Aluminium citrate, $(\text{NH}_4)_5[\text{Al}(\text{C}_6\text{H}_4\text{O}_7)_2] \cdot 2\text{H}_2\text{O}$

C = Aluminium oxalate, $\text{K}_3[\text{Al}(\text{C}_2\text{O}_4)_3]$

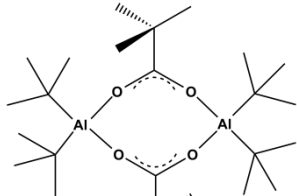
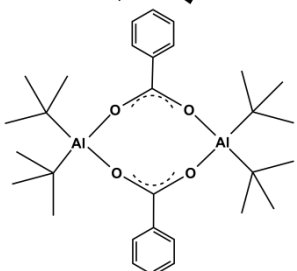
D = Aluminium malonate, $\text{K}[\text{Al}(\text{C}_3\text{H}_2\text{O}_4)_2(\text{H}_2\text{O})_2] \cdot 2\text{H}_2\text{O}$

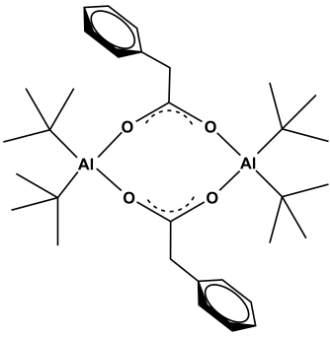
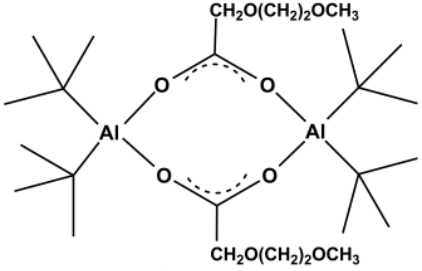
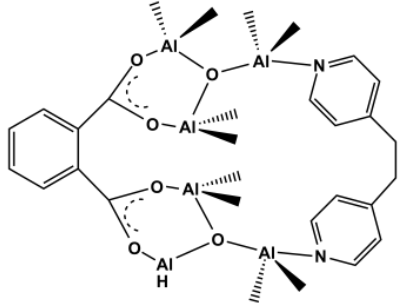
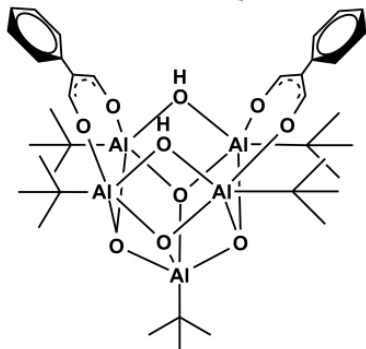
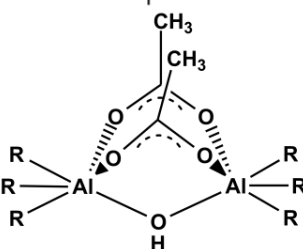
Since many aluminium carboxylates exhibit low solubility, various complexes exist that cannot be characterised by NMR or crystallographically. An example of this may be found in the research of Alexander and co-workers¹⁰² who investigated the interaction of poly(acrylic acid) and propionic acid with pseudo boehmite (AlOOH). Poly(acrylic acid) and propionic

acid showed monodentate bonding to AlOOH with $\Delta\nu(\text{CO})$ values of 270 and 240 cm^{-1} respectively. XPS (X-ray photon spectroscopy) analyses of these compounds were however inconclusive due to the carboxylate oxygen peaks being overshadowed by the oxygen peak contributions of AlOOH. Narayanan and Laine synthesised aluminium triformate directly from gibbsite exhibiting a $\Delta\nu(\text{CO})$ value of 230 cm^{-1} .¹⁰³ This Δ -value is indicative of the probable existence of monodentate coordination of monocarboxylic acids to aluminium.

Aluminium carboxylate complexes showing bridging coordination are numerous in literature. A summary of a series of structures showing this coordination mode is given in **Table 2.7**. Due to the numerous Al-O environments it is often difficult to assign the symmetric and antisymmetric carbonyl stretching frequencies and it is also obvious that more than one symmetric and asymmetric frequency pair is possible in complicated structures. It is however clear that, apart from a few extreme examples, $\Delta\nu(\text{CO})$ is generally greater than 100 cm^{-1} and smaller than 200 cm^{-1} .

Table 2.7: The Al-O bond distances and O-Al-O bonding angles of bridging carboxylate complexes of aluminium.

	Structure	Al-O distance (Å)	O-Al-O angle (°)	Ref
A		1.809(3)	107.6(1)	85
B		1.809(3)-1.811(3)	107.8(1)	85

C		1.806(4)-1.810(4)	106.5(2)	85
D		1.767(7)-1.837(6)	103.1(3)-105.5(3)	85
E		1.801(2)-1.809(2)	117.69(11)- 119.09(10)	104, 105
F		1.820(3)-2.086(4)	75.6(2)-109.4(2)	84
G		1.850(8)-1.980(7)	86.4(4)-114.8(4)	106

R = C₂H₅CO₂CH₃

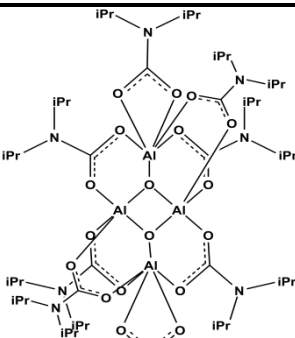
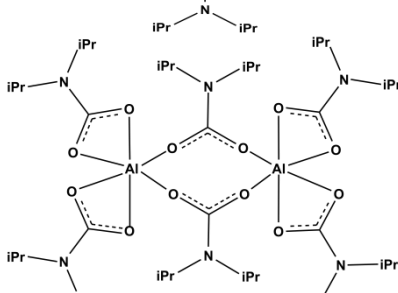
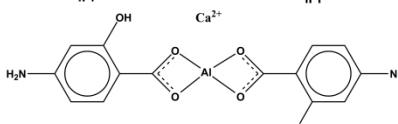
All the structures in **Table 2.7** have been confirmed crystallographically. The average Al-O bond distances range between 1.801 to 1.837 Å, however distances up to 2.086 Å can be observed for the more extreme examples (F). Apart from these exceptions, the Al-O bond

distances are shorter for the bridging mode than for the monodentate coordination mode and the distances observed for β -diketonato complexes of aluminium, indicating stronger bonds and increased stability. The O-Al-O bonding angles for the bridging coordination ($86.4^\circ - 119.09^\circ$) mode are larger than those observed for monodentate coordination ($82.1^\circ - 100.1^\circ$) and β -diketonato chelation ($90.19^\circ - 90.81^\circ$).

There are only three crystal structures for bidentate chelation of monocarboxylic acids to aluminium in literature.^{107 - 109} The compounds having bidentate chelation of carboxylic acids to aluminium are shown in **Table 2.8**. The Al-O bond distances are between 1.868 and 2.035 Å, which is longer than Al-O bond distances for bridging coordination (1.823 – 1.935 Å). The O-Al-O bonding angles for bidentate chelation are between 66.99° and 67.76° . This is substantially smaller than the bonding angles observed for bridging coordination ($86.4^\circ - 119.09^\circ$) and β -diketonato coordination ($90.19^\circ - 90.81^\circ$). These small bonding angles are again an indication of the instability of bidentate carboxylato aluminium compounds. It is also important to note that all the carboxylic acids having bidentate coordination have electron donating functionalities.

For compounds A and B, in **Table 2.8**, the electron donation arises from nitrogen atoms substituted with isopropyl groups. For compound C, the benzene ring is substituted with a hydroxyl group in the ortho position and amine in the para position. Both of these substituents have lone electron pairs which can be delocalised into the benzene ring, creating an electron donating ring. Electron donation is thus required to stabilise bidentate coordination of carboxylic acids to aluminium.

Table 2.8: The Al-O bond distances and O-Al-O bonding angles of bidentate carboxylate complexes of aluminium.

Structure	Al-O distance (Å)	O-Al-O angle (°)	R-Factor	Ref
	1.934 – 1.964 ^a 1.823 – 1.935 ^b	67.69 – 67.71	6.40	107
	1.868 – 2.035 ^a 1.821 ^b	66.99 – 67.76	4.44	108
	-	-	-	109

iPr = isopropyl, a = bidentate bonding, b = bridging coordination

Several authors suggested bidentate chelation. Leger and co-workers synthesised and characterised several di- and tricarboxylates of aluminium using long chained monocarboxylic acids.¹¹⁰ In aluminium, IR trilaurate carbonyl stretching frequencies was observed at 1639 cm⁻¹ and 1580 cm⁻¹, respectively assigned to bidentate chelation and bridging coordination. In aluminium dilaurate, carbonyl stretching frequencies at 1607 cm⁻¹ was assigned to bidentate chelation and the frequency at 1580 cm⁻¹ was assigned to bridging coordination. No symmetric and antisymmetric carbonyl stretching assignments were made. There is however a stretching band at approximately 1470 cm⁻¹. Based on the results from the present research program, as discussed in Chapter 3, it became apparent

that the assignment of carboxylato binding modes is probably incorrect. Monodentate and bridging carboxylate coordination are more likely to be present in these complexes.

The final structural aspect to be considered in this literature survey is the effect of ring size on the stability and rate of formation on aluminium carboxylates. When considering the rate of ligand promoted dissolution of $\delta\text{-Al}_2\text{O}_3$ in **Figure 2.12**, it is clear that five- and six-membered rings are formed more readily and at faster rates than seven-membered rings or monodentate complexes.^{111, 112, 113}

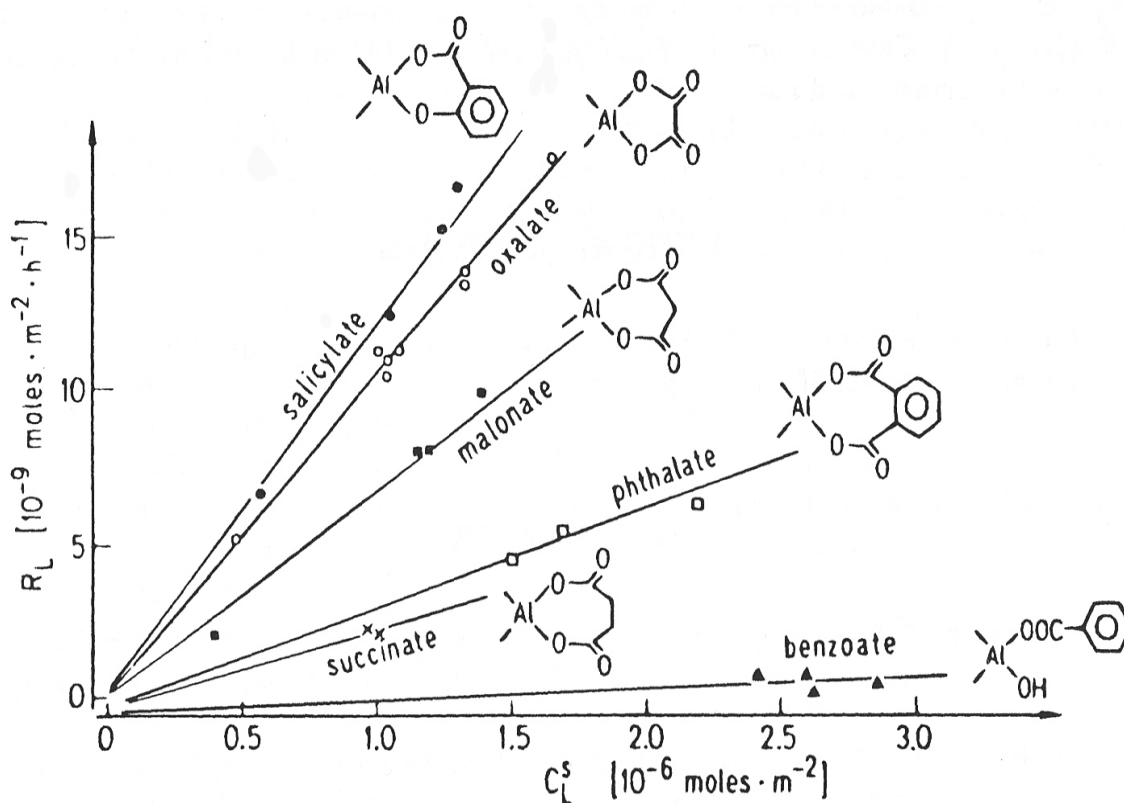
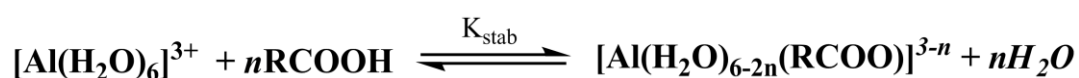
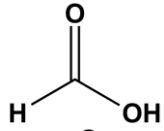
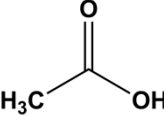
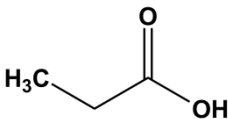
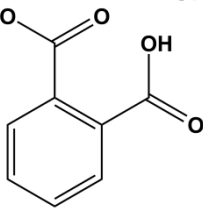
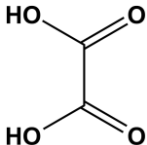


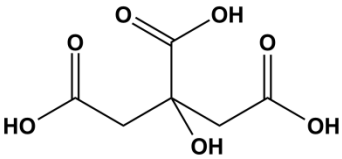
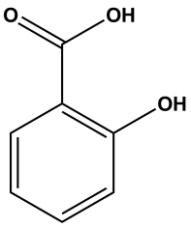
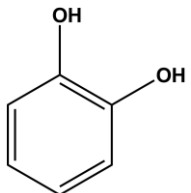
Figure 2.12: The rate of ligand-promoted dissolution of $\delta\text{-Al}_2\text{O}_3$ versus the concentration of the ligands. (From S. Goldberg, J. A. Davis and J. D. Hem in *The Environmental Chemistry of Aluminium 2nd edition*; eds. G. Sposito, Lewis Publishers, Florida, 1996, pp. 317; W. Stumm, B. Wehrli and E. Wieland, *Croatica Chem. Acta*, 249, **60** (1987); G. Furrer, W. Stumm, *Geochim. Cosmochim. Acta*, 1947, **50** (1986).).

It is, however, difficult to distinguish between preference for five- or six-membered rings, which is probably related to the similar and near ideal O-Al-O bonding angles (ca. 90°) shown by these complexes (Table 2.6). The stability constants of several aluminium carboxylates are shown in Table 2.9.¹¹⁴ Low stability constants are observed for short chained monocarboxylic acids, whilst the highest values are exhibited by five- and six-membered ring-complexes. This then indicates the preference for five- and six-membered ring-complexes in the reaction of aluminium with carboxylic acids, α- or β-dicarboxylates and α-hydroxy carboxylates.

Table 2.9: Stability constants of Al³⁺ complexes with a number of organic acids. (From G. F. Vance, F. J. Stevenson and F. J. Sikora in *The Environmental Chemistry of Aluminium 2nd edition*; eds. G. Sposito, Lewis Publishers, Florida, 1996, pp. 192.)



Acid	Name	No of ligands	pK _{stab}	Ionic strength
	Formic acid	1	1.36	1.0
	Acetic acid	1 2	1.51 3.76	1.0 0.3
	Propionic acid	1	1.69	1.0
	Phthalic acid	1 2	3.18 6.32	0.1 0.1
	Oxalic acid	1 2 3	6.10 11.09 15.12	1.0 1.0 1.0

	Citric acid	1	8.32	0.25
	Salicylic acid	1	12.9	0.1
		2	23.2	0.1
		3	29.8	0.1
	Catechol	1	16.3	0.1
		2	29.3	0.1
		3	37.6	0.1

2.4. Electrochemistry

In this final section a very brief overview will be given on electrochemical techniques, which relate to the electrochemical characterisation of ferrocene-containing β -diketonato complexes of aluminium (Goal 2). Electrochemical techniques have been the subject of various reviews in literature, giving the necessary background for application to a variety of systems.^{115, 116, 117} A few critical concepts will be highlighted from these reviews.

Cyclic voltammetry experiments are performed by cycling the potential of the working electrode, immersed in a solution containing the analyte and electrolyte, versus a reference electrode and measuring the current flow between the working electrode and an auxiliary electrode. The working electrode is frequently either a platinum or glassy-carbon electrode. Glassy carbon is preferred for ferrocene compounds. The reference electrode depends on the experimental conditions used. Two frequently used reference electrodes are the calomel electrode and the silver chloride electrode. The cyclic voltammogram then consists

of an oxidation and a reduction peak, which depends on the compound being analysed. The most important parameters in cyclic voltammetry are:

- i. The peak anodic potential (E_{pa}), the peak cathodic potential (E_{pc}),
- ii. the peak anodic and cathodic currents (i_{pa} and i_{pc}),
- iii. the half-wave potential ($E_{1/2}$)
- iv. the formal reduction potential $E^{0'}$ and
- v. the peak potential separation (ΔE_p).

The formal reduction potential $E^{0'}$ is defined in equation (2-1). The equation for half-wave potential is shown in equation (2-2), where $E^{0'}$ is the formal reduction potential and D_R and D_O are the diffusion coefficients of the reduced and oxidized forms of the complex being analysed, n the number of electrons involved in the reactions. The peak potential separation is simply the difference between the peak anodic and cathodic potentials. Theoretically, reversible electrochemical processes must show, $\Delta E_p = 59/n$ mV, with n the amount of electrons involved in the redox couple. However, experimentally, reversible electrochemical behaviour is still assigned for processes showing ΔE_p values up to 90 mV. Values larger than 90 are regarded to indicate quasi-reversible processes, while values larger than 180 mV imply electrochemical irreversible (slow electron transfer between substrate and electrode) processes.

$$E^{0'} = \frac{E_{pa} + E_{pc}}{2} \quad (2-1)$$

$$E_{1/2} = E^{0'} + \left(\frac{RT}{nF}\right) \ln\left(\frac{D_R}{D_O}\right)^{1/2} \quad (2-2)$$

$$\Delta E_p = E_{pa} - E_{pc} \quad (2-3)$$

$$i_p = (2.69 \times 10^5)n^{3/2}AD^{1/2}Cv^{1/2} \quad (2-4)$$

The peak current is represented by equation (2-4), where n is the number of electrons involved in the reaction, A is the electrode area in cm^2 , D is the diffusion coefficient ($\text{cm}^2.\text{s}^{-1}$), C is the concentration ($\text{mol}.\text{cm}^{-3}$) and v is the scan rate ($\text{V}.\text{s}^{-1}$). For reversible electrochemical behaviour, the ratio i_{pa}/i_{pc} should approach unity.

Ferrocene shows reversible electrochemical behaviour and is often used as internal standard in electrochemical experiments. Ferrocene can undergo a one electron oxidation to form the ferrocenium ion, $[\text{Cp}_2\text{Fe}^{3+}]$, which can be reduced back to ferrocene, $[\text{Cp}_2\text{Fe}^{2+}]$.

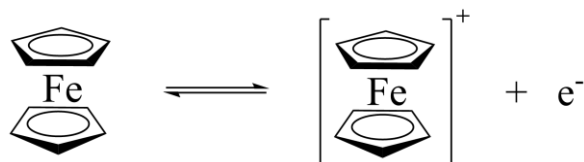


Figure 2.13: The electrochemistry of ferrocene.

In Osteryoung square wave voltammetry (SW), the potential over the working electrode is modulated as an increasing and decreasing square wave function in a step-like fashion. This gives better peak separation in closely overlapped reduction or oxidation signals. In linear sweep voltammetry (LSV) the potential over the working electrode is slowly increased, whilst steps in the current are proportional to the number of electrons transferred.

Superior results in electrochemistry are obtained when using a non-coordinating solvent such as dichloromethane. Acetonitrile is also frequently encountered in electrochemical studies, but it possesses the ability to coordinate to positively charged or electrophilic species. Coordination can lead to additional reduction or oxidation peaks being observed, as well as reduced electrochemical reversible behaviour. A final consideration in electrochemical experimentation is the choice of a suitable non-coordinating supporting electrolyte. Tetrabutylammonium hexafluorophosphate is frequently used as supporting electrolyte,

however, the PF_6^- anion still possesses the ability to coordinate or associate with electrophilic systems to form ion pairs, $\text{M}^+\dots\text{PF}_6^-$. The salt, tetrabutylammonium tetrakis(pentafluorophenyl)borate $[\text{NBu}_4]^+[\text{B}(\text{C}_6\text{F}_5)_4]^-$, given in **Figure 2.14**, shows almost no coordination to or ion pair formation with negatively or positively charged species.

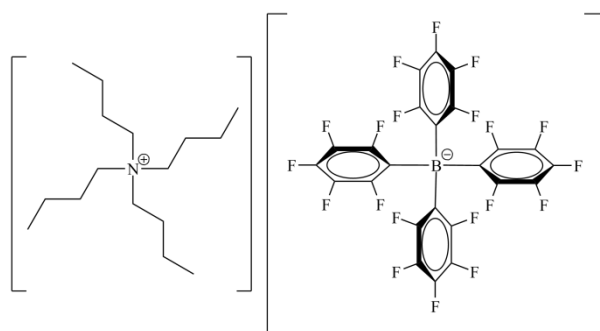


Figure 2.14: Tetrabutylammonium tetrakis(pentafluorophenyl)borate, $[\text{NBu}_4]^+[\text{B}(\text{C}_6\text{F}_5)_4]^-$, is frequently used as non-coordinating supporting electrolyte in electrochemical experiments.

The only known ferrocene-containing β -diketonato aluminium complex, $\text{Al}(\text{CH}_3\text{COCHCOFc})_3$, was isolated by Zanello and co-workers.²⁸ The electrochemistry of this compound in CH_2Cl_2 / 0.2 M NBu_4PF_6 showed a single broad ($\Delta E_p > 100$ mV) ferrocenyl-related oxidation and reduction signal. No resolution between redox processes of different ferrocenyl groups of various metal complexes (**Table 2.10**) was observed in this study, **Figure 2.15**.

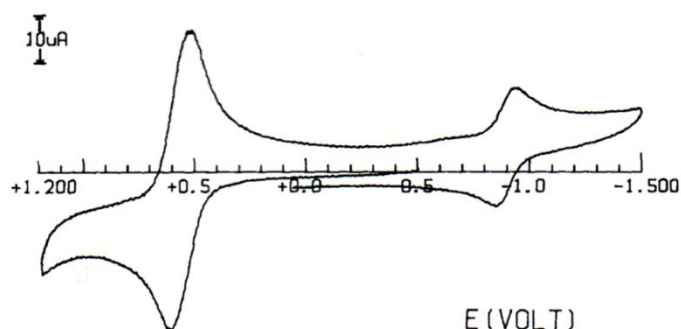


Figure 2.15: The Cyclic voltammogram of $[(\text{H}_3\text{CCOCHCOFc})_3\text{Fe}]$ using a platinum working electrode on a CH_2Cl_2 solution containing $0.8 \times 10^{-3} \text{ mol dm}^{-3}$ of $[(\text{H}_3\text{CCOCHCOFc})_3\text{Fe}]$ and 0.2 mol dm^{-3} $[\text{NBu}_4]^+[\text{PF}_6]^-$ at a scan rate of 200 mV s^{-1} . (From P. Zanello, F.F. de Biani, C. Glidewell, J. Koenig and S.J. Marsh, *Polyhedron*, 1998, **17**, 1795.)

Table 2.10: The electrochemical parameters for the redox processes exhibited by the β -diketonato complexes examined by Zanello and co-workers using CH_2Cl_2 as solvent and $[\text{NBu}_4]^+[\text{PF}_6]^-$ as supporting electrolyte. (From P. Zanello, F.F. de Biani, C. Glidewell, J. Koenig and S.J. Marsh, *Polyhedron*, 1998, **17**, 1795.)

Complex	Ferrocene-centered oxidation			Metal-centered reduction		
	E° (mV)	ΔE_p (mV)	n^a	E° (mV)	ΔE_p (mV)	n^a
$\text{H}_3\text{CCOCHCOFc}$	0.64	88	1	-	-	-
$(\text{H}_3\text{CCOCHCOFc})_3\text{Al}$	0.58	114	3	-	-	-
$(\text{H}_3\text{CCOCHCOFc})_3\text{Cr}$	0.58	90	3	-	-	-
$(\text{H}_3\text{CCOCHCOFc})_3\text{Mn}$	0.59	130	3	-0.36	370	1
$(\text{H}_3\text{CCOCHCOFc})_3\text{Fe}$	0.58	118	3	-0.88	92	1
$(\text{H}_3\text{CCOCHCOFc})_2\text{Co}$	0.59	122	2	-0.90	110	1
$(\text{H}_3\text{CCOCHCOFc})_2\text{Ni}$	0.58	166	2	-0.88	74	1
$(\text{H}_3\text{CCOCHCOFc})_2\text{Cu}$	0.56	70	2	-1.28	-	-
Fc	0.39	80	1	-	-	-

a: Number of electrons involved in the redox reaction.

Zanello and co-workers used CH_2Cl_2 as solvent and $[\text{NBu}_4]^+[\text{PF}_6]^-$ as supporting electrolyte.

The current study, according to goal 3, investigated the electrochemistry of several new ferrocene-containing β -diketonato aluminium complexes as well as the aluminium complex studied by Zanello, utilising CH_2Cl_2 as solvent and $[\text{NBu}_4]^+[\text{B}(\text{C}_6\text{F}_5)_4]^-$ as supporting electrolyte, with the specific aim to detect and quantify any intramolecular electrostatic communications as a function of formal reduction potentials and group electronegativity.

2.5. Concluding remarks

Having highlighted much of the existing literature and newest published research results relating to aluminium β -diketonato and aluminium carboxylato complexes, the author can now proceed to discuss his own research results with respect to β -diketonato and carboxylato aluminium complexes.

- ¹ M. B. Smith and J. March in *March's Advanced Organic Chemistry: Reactions, Mechanisms, and Structure*; John Wiley and Sons, New York, 2001, 5th edition, pp. 569 – 573.
- ² W. C. du Plessis, T. G. Vosloo and J. C. Swarts, *J. Chem. Soc., Dalton Trans.*, 2507, (1998).
- ³ C. R. Hauser and C. E. Cain, *J. Org. Chem.*, 1142, **23** (1958).
- ⁴ V. Winmayr, *Naturwissenschaften*, 311, **45** (1958).
- ⁵ W. R. Cullen, S.J. Rettig and E.B. Wickenheiser, *J. Mol. Catal.*, 251, **66** (1991).
- ⁶ M. R. Jaffe, D. P. Fay, M. Cefola and N. Sutin, *J. Am. Chem. Soc., Dalton Trans.*, 2657, (1983).
- ⁷ A. R. Siedle in *Comprehensive Coordination Chemistry*; eds. G. Wilkinson, R. D. Gillard and J. A. McCleverty, Pergamon Press, Oxford, 1987, vol. 2, pp. 365-412.
- ⁸ L. W. Reeves, *Can. J. Chem.*, 1351, **35** (1957).
- ⁹ S. Moon and Y. Kwon, *Magn. Reson. Chem.*, 89, **39** (2001).
- ¹⁰ T. H. Lowry and K. S. Richardson in *Mechanism and Theory in Organic Chemistry*; eds. J. A. Woods, C. J. Dempster and B. Goldberg, Harper and Row Publishers, New York, 1976, pp. 450 -451.
- ¹¹ J. D. Park, H. A. Brown and J. R. Lacher, *J. Am. Chem. Soc.*, 4753, **75** (1953).
- ¹² G. Klose, P. H. Thomas, E. Uhlemann and J. Marki, *Tetrahedron*, 2695, **22** (1966).
- ¹³ A. Yogev and Y. Mazur, *J. Org. Chem.*, 2162, **32** (1967).
- ¹⁴ W. C. du Plessis, W. L. Davis, S. J. Cronje and J. C. Swarts, *Inorg. Chim. Acta*, 97, **314** (2001).
- ¹⁵ D. E. Fenton, C. Nave, and M. R. Truter, *J. Chem. Soc., Dalton Trans.*, 2188, (1973).
- ¹⁶ G. J. Bullen, R. Mason and P. Pauling, *Inorg. Chem.*, 246, **4** (1965).
- ¹⁷ A. R. Siedle, R. A. Newmark and L. H. Pignolet, *J. Am. Chem. Soc.*, 4947, **103** (1981).
- ¹⁸ A. R. Siedle, and L. H. Pignolet, *Inorg. Chem.*, 135, **21** (1982).
- ¹⁹ Z. Kanda, Y. Nakamura and S. Kawaguchi, *Inorg. Chem.*, 910, **17** (1978).
- ²⁰ R. Mason, G. B. Robertson and P. J. Pauling, *J. Chem. Soc. (A)*, 485, (1969).
- ²¹ R. N. Hargreaves and M. R. Truter, *J. Chem. Soc. (A)*, 2282, (1969).
- ²² S. Okeya, Y. Nakamura, S. Kawaguchi and T. Hinomoto, *Inorg. Chem.*, 1576, **20** (1981).
- ²³ L. Salmon, P. Thuéry and M. Ephritikhine, *Acta Cryst.*, m1250, **E62** (2006).
- ²⁴ S. Patra, B. Mondal, B. Sarkar, M. Niemeyer and G. K. Lahiri, *Inorg. Chem.*, 1322, **42** (2003).
- ²⁵ R.C. Mehrotra and A.K. Rai, *Polyhedron*, 1967, **10** (1991).
- ²⁶ M. J. Taylor in *Comprehensive Coordination Chemistry*; eds. G. Wilkinson, R. D. Gillard and J. A. McCleverty, Pergamon Press, Oxford, 1987, vol. 3, pp. 105 – 152.
- ²⁷ V. Kohler, *Am. Chem. J.*, 355, **24** (1902).
- ²⁸ P. Zanello, F. F. de Bianai, C. Glidewell, J. Koenig and S. J. Marsh, *Polyhedron*, 1795, **18** (1998).
- ²⁹ G. T. Morgan and H. D. K. Drew, *J. Chem. Soc.*, 1058, **119** (1921).

- ³⁰ D. K. Nordstrom and H. M. May in *The Environmental Chemistry of Aluminium 2nd edition*; eds. G. Sposito, Lewis Publishers, Florida, 1996, pp. 39 – 80.
- ³¹ C. T. Tomany, M. J. Hynes and T. Schmidt, *Int. J. Chem. Kinet.*, 257, **30** (1998).
- ³² J. J. Fortman and R. E. Sievers, *Inorg. Chem.*, 2022, **6** (1967).
- ³³ D.C. Bradley, R.C. Mehrotra, I.P. Rothwell and A. Singh in *Alkoxo and Aryloxo Derivatives of Metals*; eds. D.C. Bradley, Academic Press, New York, 2001, pp. 117 – 119.
- ³⁴ J. O. Hill and J. Irving, *J. Chem. Soc. (A)*, 971, (1966).
- ³⁵ W. T. Astbury and T. M. Gilbert, *Proc. R. Soc. London. Ser. A*, 448, **112** (1926).
- ³⁶ B. W. McClelland, *Acta Cryst.*, 2496, **B31** (1975).
- ³⁷ L. S. von Chrzanowski, M. Lutz and A. L. Spek, *Acta Cryst.*, m3318, **E62** (2006).
- ³⁸ L. S. von Chrzanowski, M. Lutz and A. L. Spek, *Acta Cryst.*, m129, **C63** (2007).
- ³⁹ J. H. Wengrovius, M. F. Garbaskas, E. A. Williams, R. C. Going, P. E. Donahue and J. F. Smith, *J. Am. Chem. Soc.*, 983, **108** (1986).
- ⁴⁰ M. F. Garbaskas, J. H. Wengrovius, R. C. Going and J. S. Kasper, *Acta Cryst.*, 1536, **C40** (1984).
- ⁴¹ R. C. Fay and T. S. Pepper, *J. Am. Chem. Soc.*, 2303, **84** (1962).
- ⁴² R. C. Fay and T. S. Pepper, *J. Am. Chem. Soc.*, 500, **85** (1963).
- ⁴³ R. G. Linck and R. E. Sievers, *Inorg. Chem.*, 806, **5** (1966).
- ⁴⁴ J. Fortman and R. E. Sievers, *Inorg. Chem.*, 2022, **6** (1067).
- ⁴⁵ M. Pickering, B. Jurado and C. S. Springer, *J. Am. Chem. Soc.*, 4503, **98** (1976).
- ⁴⁶ T. Salifoglou in *Metallotherapeutic Drugs and Metal-based Diagnostic Agents*; eds. M. Gielen and E. R. T. Tiekink, John Wiley & Sons, Hoboken USA, 2005, pp. 65 – 82.
- ⁴⁷ K. Berend, G. B. van der Voet and F. A. De Wolff in *Group 13 Chemistry II: Biological Aspects of Aluminium (Structure and Bonding)*; eds. H. W. Roesky and D. A. Atwood, Springer, Berlin, 2002, pp. 1 – 51.
- ⁴⁸ S. Oshiro in *Group 13 Chemistry II: Biological Aspects of Aluminium (Structure and Bonding)*; eds. H. W. Roesky and D. A. Atwood, Springer, Berlin, 2002, pp. 59 – 74.
- ⁴⁹ S. Anitha and K. S. J. Rao in *Group 13 Chemistry II: Biological Aspects of Aluminium (Structure and Bonding)*; eds. H. W. Roesky and D. A. Atwood, Springer, Berlin, 2002, pp. 79 – 96.
- ⁵⁰ G. Sava, S. Zorzet, L. Pressin, G. Mestroni, G. Zassinovich and A. Bontempi, *Inorg. Chem. Acta*, 69, **86** (1978).
- ⁵¹ C. E. J. van Rensburg, E. Kreft, J. C. Swarts, S. R. Dalrymple, D. M. MacDonald, M. W. Cooke and M. A. S. Aquino, *Anticancer Res.*, 889, **22** (2002).
- ⁵² C. Oldham in *Comprehensive Coordination Chemistry*; eds. G. Wilkinson, R. D. Gillard and J. A. McCleverty, Pergamon Press, Oxford, 1987, vol. 2, pp. 435-459.
- ⁵³ W. H. Zacharaisen, *J. Am. Chem. Soc.*, 1011, **62** (1940).
- ⁵⁴ F. A. Cotton and W. H. Ilesley, *Inorg. Chem.*, 300, **21** (1981).
- ⁵⁵ J. N. van Niekerk, F. R. L. Schoening and J. H. Talbot, *Acta Crystallogr.*, 720, **6** (1953).
- ⁵⁶ J. N. van Niekerk, F. R. L. Schoening and J. F. de Wet, *Acta Crystallogr.*, 501, **6** (1953).
- ⁵⁷ T. Allman, R. C. Goel, N. K. Jha and A. L. Beauchamp, *Inorg. Chem.*, 914, **23** (1984).

- ⁵⁸ R. Kiriyaama, H. Ibamoto and K. Matsuo, *Acta Crystallogr.*, 482, **7** (1954).
- ⁵⁹ G. A. Barclay and C. H. L. Kennard, *J. Chem. Soc.*, 3289, (1961).
- ⁶⁰ R. D. Mounts, T. Ogura and Q. Fernando, *Inorg. Chem.*, 802, **13** (1974).
- ⁶¹ A. M. Greenaway, C. J. O'Connor, J. W. Overman and E. Sinn, *Inorg. Chem.*, 1508, **20** (1981).
- ⁶² V. M. Rao, D. N. Sathyanarayana and M. Manohar, *J. Chem. Soc. Dalton Trans.*, 253, (1978).; T. Behling, G. Wilkinson, T. A. Stephenson, D. A. Tocher and M. D. Walkinshaw, *J. Chem. Soc. Dalton Trans.*, 2109, (1983).; M. Inoue and M. Kubo, *Inorg. Chem.*, 2310, **9** (1970).
- ⁶³ B. J. Allin, and P. Thornton, *Inorg. Nucl. Chem. Lett.*, 449, **9** (1973).; E. B. Boyer and S. D. Robinson, *Coord. Chem. Rev.*, 109, **50** (1983).
- ⁶⁴ S. C. Chan and M. C. Choi, *J. Inorg. Chem.*, 1949, **38** (1976).
- ⁶⁵ A. Karipides, J. Ault and A. T. Reed, *Inorg. Chem.*, 3299, **16** (1977).
- ⁶⁶ S. Yano, S. Yaba, M. Ajioka and S. Yoshikawa, *Inorg. Chem.*, 2414, **18** (1979).
- ⁶⁷ K. L. Scott, M. Green and A. G. Sykes, *J. Chem. Soc. (A)*, 3651, (1971).
- ⁶⁸ K. L. Scott, K. Wieghardt and A. G. Sykes, *Inorg. Chem.*, 6655, **12** (1973).
- ⁶⁹ M. W. Dougill and G. A. Jefferey, *Acta Crystallogr.*, 831, **6** (1953).
- ⁷⁰ E. Hansson, *Acta Chem. Scand.*, 2841, **27** (1973).
- ⁷¹ K. Wieghardt, *Z. Anorg. Allg. Chem.*, 142, **381** (1972).
- ⁷² F. Mazzi and G. Garavelli, *Period. Mineral.*, 269, **26** (1957).
- ⁷³ B. H. O'Connor and E. N. Maslen, *Acta Crystallogr.*, 824, **20** (1966).
- ⁷⁴ M. L. Post and J. Trotter, *J. Chem. Soc. Dalton Trans.*, 1922, (1974).
- ⁷⁵ H. Siebert and G. Tremmel, *Z. Anorg. Allg. Chem.*, 292, **390** (1972).
- ⁷⁶ E. Hansson, *Acta Chem. Scand.*, 2827, **27** (1973).
- ⁷⁷ G. H. Warner in *Kirk-Othmer Encyclopaedia of chemical technology 3rd edition Vol. 2*; eds. M. Grayson and D. Eckroth John Wiley and Sons, New York, 1978, pp. 202 – 209.
- ⁷⁸ R. C. Mehrotra and A. K. Rai, *Polyhedron*, 1967, **17** (1991).
- ⁷⁹ N. A. Lange and J. A. Dean in *Lange's Handbook of Chemistry*; McGraw-Hill, 1973, 10th edition, pp. 1496 – 1505.
- ⁸⁰ A. Gilmour, A. Jobling and S. M. Nelson, *J. Chem. Soc.*, 1972, (1956).
- ⁸¹ G. G. Bombi, B. Corain, A. A. Sheikh-Osman and G. C. Valle, *Inorg. Chim. Acta*, 79, **171** (1990).
- ⁸² Y. Okada and Y. Nakajima, *J. Oleo Sci.*, 655, **54** (2005).
- ⁸³ C. C. Landry, N. Pappé, M. R. Manson, A. W. Apblett, A. N. Tyler, A. N. Macinnes and A. R. Barron, *J. Mater. Chem.*, 331, **5** (1995).
- ⁸⁴ Y. Koide and A. R. Barron, *Organometallics*, 4026, **14** (1995).
- ⁸⁵ C. E. Bethley, C. L. Aitken, C. J. Harlan, Y. Koide, S. G. Bott and A. R. Barron, *Organometallics*, 329, **16** (1997).
- ⁸⁶ J. L. Atwood, W. E. Hunter and K. D. Crissinger, *J. Organomet. Chem.*, 403, **127** (1977).
- ⁸⁷ G. J. E. Davidson, L. H. Tong, P. R. Raithby and J. K. M. Sanders, *Chem. Commun.*, 3087, (2006).

- ⁸⁸ H. Hatop, M. Ferbinteanu, H. W. Roesky, F. Cimpoesu, M. Schiefer, H. G. Schmidt and M. Noltemeyer, *Inorg. Chem.*, 1022, **21** (2001).
- ⁸⁹ P. Chen, M. H. Chisholm, J. C. Gallucci, X. Zhang and Z. Zhou, *Inorg. Chem.*, 2588, **44** (2005).
- ⁹⁰ G. J. E. Davidson, L. H. Tong, P. R. Raithby and J. K. M. Sanders, *Chem. Commun.*, 2087, (2006).
- ⁹¹ G. G. Bombi, B. Corain, A. A. Sheikh-Osman and G. C. Valle, *Inorg. Chim. Acta*, 79, **171** (1990).
- ⁹² B. Corain, B. Longato, A. A. Sheikh-Osman, G. G. Bombi and C. Maccà, *J. Chem. Soc. Dalton Trans.*, 169, (1992).
- ⁹³ M. Matzapetakis, M. Kourgiantakis, M. Dakanali, C. P. Raptopoulou, A. Terzis, A. Lakatos, T. Kiss, I. Banyai, L. Iordanidis, T. Mavromoustakos and A. Salifoglou, *Inorg. Chem.*, 1734, **40** (2001).
- ⁹⁴ P. C. Hidber, T. J. Graule and L. J. Gauckler, *J. Am. Chem. Soc.*, 1857, **79** (1996).
- ⁹⁵ T. L. Feng, P. L. Gurian, M. D. Healy and A. R. Barron, *Inorg. Chem.*, 408, **29** (1990).
- ⁹⁶ M. K. Wang, J. L. White and S. L. Hem, *Clays Clay Min.*, 65, **31** (1983).
- ⁹⁷ A. Salifoglou, *Coord. Chem. Rev.*, 297, **228** (2002).
- ⁹⁸ N. Bulc, L. Golic and J. Sifatar, *Acta Cryst.*, 1829, **C40** (1984).
- ⁹⁹ L. Golic, I. Leban and N. Bulc, *Acta Cryst.*, 44, **C45** (1989).
- ¹⁰⁰ A. Tapparo, S. L. Heath, P. A. Jordan, G. R. Moore and A. K. Powell, *J. Chem. Soc. Dalton Trans.*, 1601, (1996).
- ¹⁰¹ S. B. Johnson, T. H. Yoon, B. D. Kocar and G. E. Brown, *Langmuir*, 4996, **20** (2004).
- ¹⁰² M. R. Alexander, G. Beamson, C. J. Blomfield, G. Leggett and T. M. Duc, *J. Electron. Spectrosc. Relat. Phenom.*, 19, **121** (2001).
- ¹⁰³ R. Narayanan and R.M. Laine, *J. Mater. Chem.*, 2097, **10** (2000).
- ¹⁰⁴ J. Lewinski, J. Zachara and I. Justyniak, *Inorg. Chem.*, 2575, **37** (1998).
- ¹⁰⁵ J. Lewinski, W. Bury, I. Justyniak and J. Lipkowski, *Angew. Chem. Int. Ed.*, 2872, **45** (2006).
- ¹⁰⁶ P. Sobota, M. O. Mustafa, J. Utko and T. Lis, *J. Chem. Soc. Dalton Trans.*, 1809, (1990).
- ¹⁰⁷ U. Abram, D. B. Dell'Amico, F. Calderazzo, S. Kaskel, L. Labella, F. Marchetti, R. Rovai, J. Strahle, *Chem. Commun.*, 1941, (1997).
- ¹⁰⁸ D. B. Dell'Amico, F. Calderazzo, M. Dell'Innocenti, B. Guldenpfennig, S. Lanelli, G. Peilizzi, P. Robino, *Gazz. Chim. Ital.*, 283, **123** (1993).
- ¹⁰⁹ Hayano and Imado, *Chem. Pharm. Bull.*, 772, **7** (1959).
- ¹¹⁰ A. E. Leger, R. L. Haines, C. E. Hubley, J. C. Hyde and H. Sheffer, *Can. J. Chem.*, 799, **35** (1957).
- ¹¹¹ S. Goldberg, J. A. Davis and J. D. Hem in *The Environmental Chemistry of Aluminium 2nd edition*; eds. G. Sposito, Lewis Publishers, Florida, 1996, pp. 271 – 331.
- ¹¹² W. Stumm, B. Wehrli and E. Wieland, *Croatica Chem. Acta*, 249, **60** (1987)
- ¹¹³ W. Stumm, *Geochim. Cosmochim. Acta*, 1947, **50** (1986).
- ¹¹⁴ G. F. Vance, F. J. Stevenson and F. J. Sikora in *The Environmental Chemistry of Aluminium 2nd edition*; eds. G. Sposito, Lewis Publishers, Florida, 1996, pp. 169 – 220.
- ¹¹⁵ P. T. Kissinger and W. R. Heineman, *J. Chem. Educ.*, 703, **60** (1983).
- ¹¹⁶ R. R. Gagné, C. A. Koval and G. C. Lisensky, *Inorg. Chem.*, 2855, **19** (1980).

¹¹⁷ D. H. Evans, K. M. O'Connell, R. A. Petersen and M. J. Kelley, *J. Chem. Educ.*, 291, **60** (1983).

Chapter 3 : Results and Discussion

3.1. Introduction

In this chapter, the research results of the author will be presented. Compounds that were synthesised and characterised include the following:

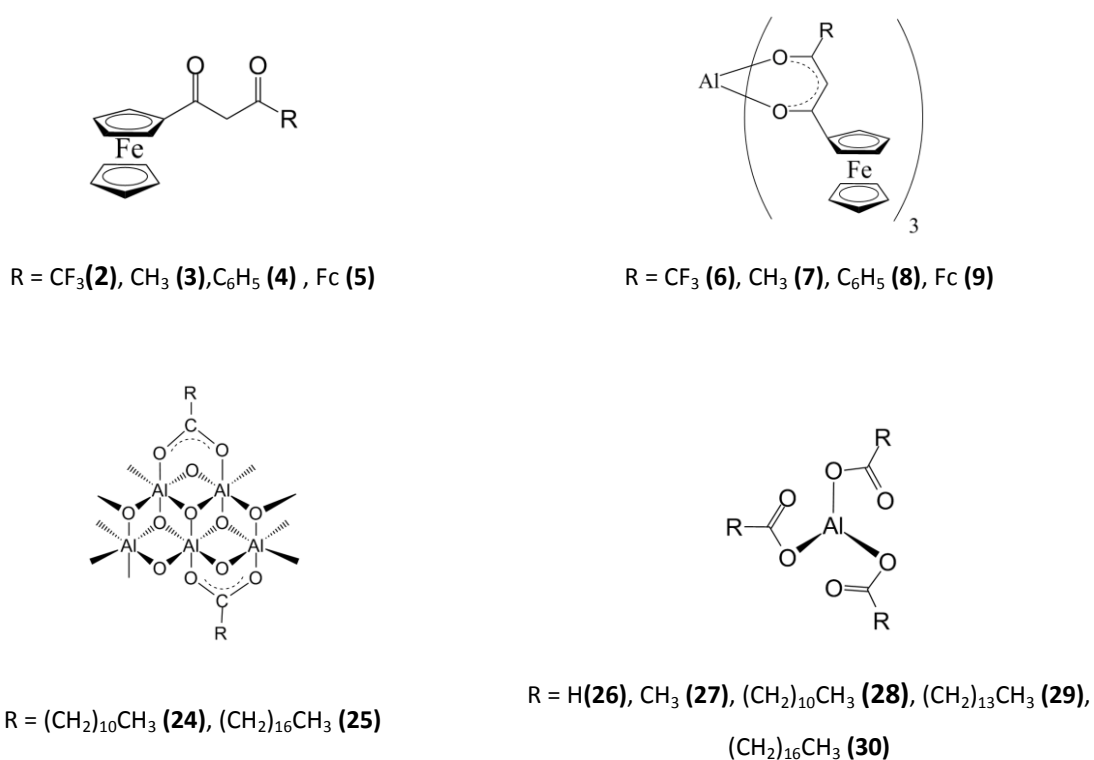


Figure 3.1. Structures of compounds synthesised during this research program. Structures (**24**) - (**30**) are idealised; they will be discussed in detail in the appropriate sections.

Firstly, the synthesis and characterization of one known and three new ferrocene-containing aluminium β -diketonates of the form $\text{Al}(\text{FcCOCHCOR})_3$ with $\text{R} = \text{CF}_3$, CH_3 , C_6H_5 or $\text{Fc} = \text{Fe}(\text{C}_5\text{H}_5)_2 =$ ferrocenyl are presented. The synthesis component of this research stems from goals 1 – 3, Chapter 1. The characterisation that will be presented include proton nuclear

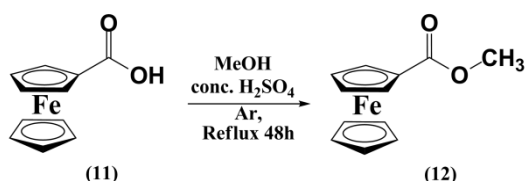
magnetic resonance (^1H), infrared spectroscopy, X-ray crystallography and electrochemical techniques such as cyclic voltammetry, linear sweep voltammetry and square wave voltammetry. The cytotoxic properties of the ferrocene-containing β -diketonato complexes of aluminium as per goal 4 (Chapter 1) will be presented next.

Secondly, according to goals 5 and 6, the synthesis and especially FTIR characterisation of aluminium carboxylates and carboxylato-alumoxanes will be discussed. Results from an exploratory quantum chemical computational study will expand this research compartment.

3.2. Synthesis and characterisation of β -diketones and β -diketonato aluminium(III) complexes

3.2.1. Ferrocene-containing β -diketones

The synthesis of 1,3-diferrocenylpropane-1,3-dione [$\text{FcCOCH}_2\text{COFc}$, **(5)**] required the preparation of methylferrocenoate **(12)** by the esterification of ferrocene carboxylic acid **(11)**. Solid yellow methylferrocenoate **(12)** was isolated in a yield of 75% after column chromatography.

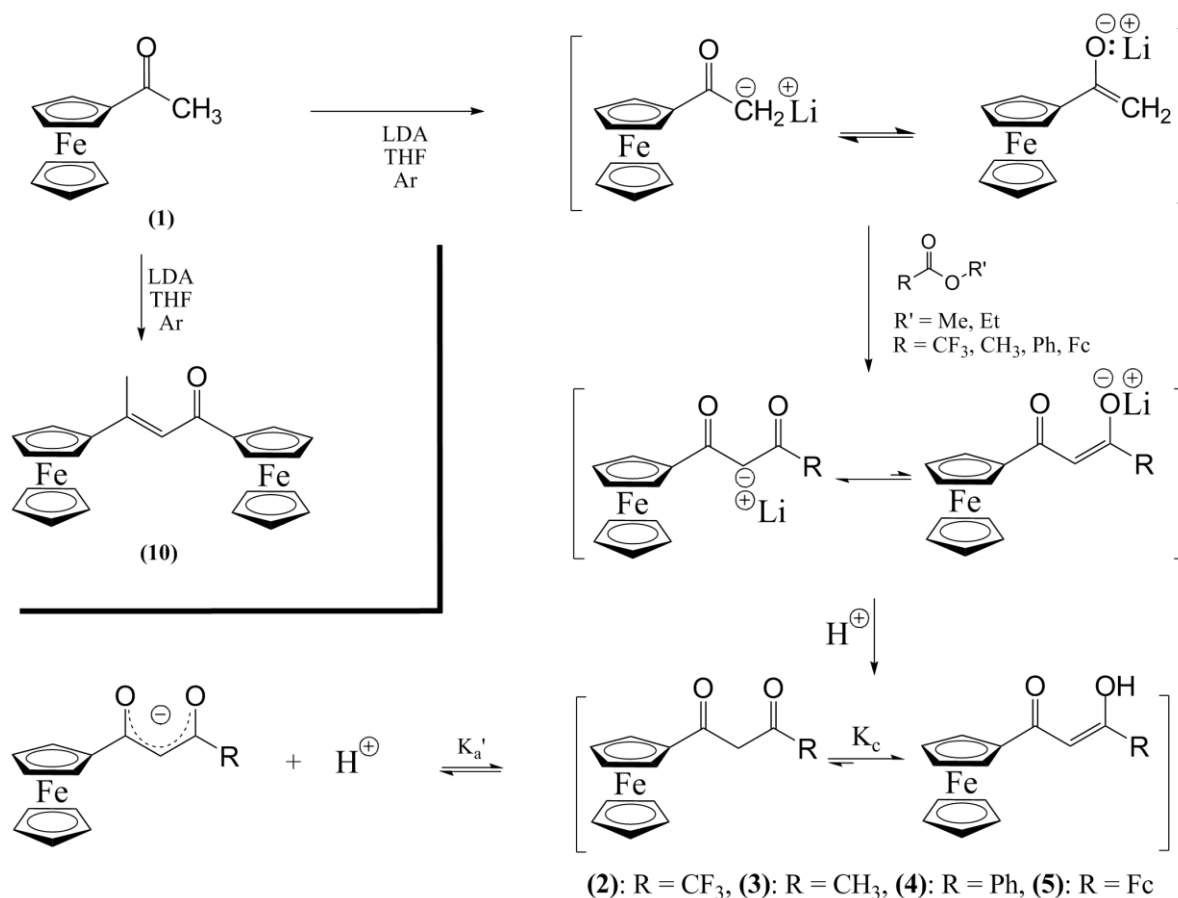


Scheme 3.1: The synthesis of methylferrocenoate.

As precursors to the synthesis of ferrocene-containing aluminium β -diketonates, four known ferrocene-containing β -diketones, $\text{FcCOCH}_2\text{COR}$ ($\text{R} = \text{CF}_3$ **(2)**, CH_3 **(3)**, C_6H_5 **(4)**, Fc **(5)**) were

prepared by Claisen condensation of acetylferrocene (**1**) and a suitable ester as shown in

Scheme 3.2.



Scheme 3.2: Claisen condensation of acetylferrocene (**1**) with appropriate esters ($\text{R}' = \text{Et}$ or Me) to give the desired ferrocene-containing β -diketones $\text{FcCOCH}_2\text{COR}$ ((**2**) - (**5**)). Self-aldol condensation of acetylferrocene (**1**) leads to the formation of the side product 1,3-diferrocenylbut-2-en-1-one (**10**).

The sterically hindered base, lithium diisopropylamide (LDA), was employed to remove a methyl proton from acetylferrocene (**1**) to produce the corresponding nucleophilic lithium salt, $(\text{FcCOCH}_2^-)\text{Li}^+$. The FcCOCH_2^- carbanion then attacks the carbonyl group of an appropriate ester and produces the corresponding lithium salts of the desired β -diketones. Previous research showed that $\text{Li}[\text{FcCOCHCOR}]$ exist mostly in the ketonate form, and not the enolate form, **Scheme 3.2**.¹ This salt is then protonated during workup to produce the desired ferrocene-containing β -diketones 4,4,4-trifluorobutane-1,3-dione [$\text{FcCOCH}_2\text{COCF}_3$,

(**2**), $pK_a' = 6.53$], 1-ferrocenylbutane-1,3-dione [$FcCOCH_2COCH_3$, (**3**), $pK_a' = 10.01$], 1-ferrocenyl-3-phenylpropane-1,3-dione [$FcCOCH_2COC_6H_5$, (**4**), $pK_a' = 10.41$] and 1,3-diferrocenylpropane-1,3-dione [$FcCOCH_2COFc$, (**5**), $pK_a' = 13.1$] in reasonable yield (**Table 3.1**, p. 65) after column chromatography. No general trend for the obtained yields could be identified, but the lower yield for (**3**) is thought to be due to trace amounts of moisture in the ethyl acetate used, despite drying over $CaCl_2$ and distillation.

Table 3.1. Yields obtained in the synthesis of ferrocene-containing β -diketones, $FcCOCH_2COR$.

R-Group	χ_R^a	$pK_a^{1,a}$	% enol ^b	% Yield
(2), R = CF_3	3.01	6.53(3)	97	30
(3), R = CH_3	2.34	10.01(2)	78	26
(4), R = C_6H_5	2.21	10.41(2)	91	31
(5), R = Fc	1.87	13.1(1)	67	29.5

^a Data from reference 2 in $CHCl_3$ at 293 K.

^b At equilibrium data from reference 2.

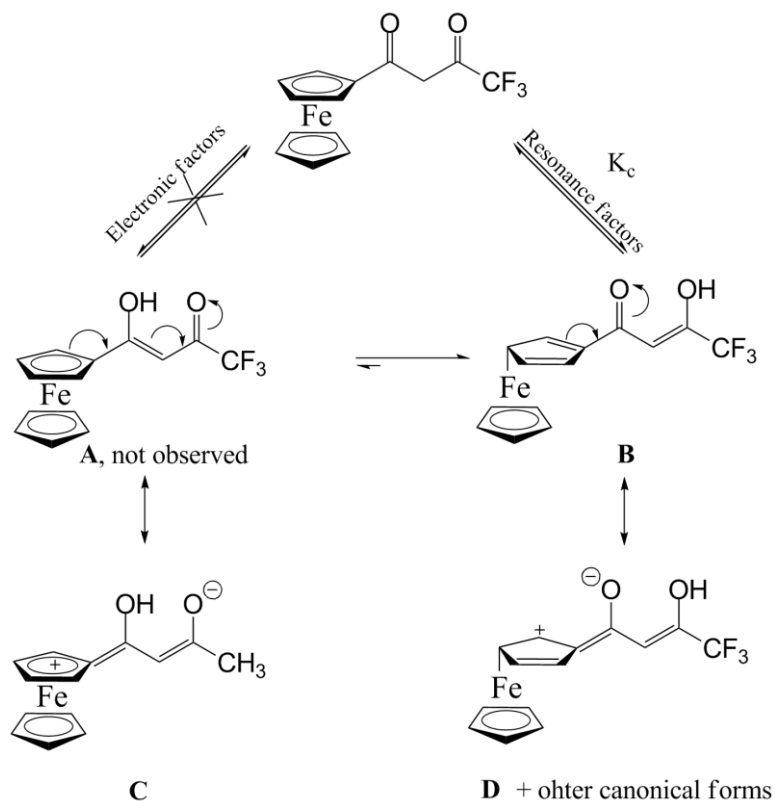
A slight excess of lithium diisopropylamide, dissolved in THF, was present during the Claisen condensation to ensure that the formation of the acetylferrocene lithium salt was complete. This minimized the self-aldol product condensation of acetylferrocene² which is 1,3-diferrocenylbut-2-en-1-one (**10**), **Scheme 3.2**. The time allowed for the formation of $FcCOCH_2Li^+$ was limited as a further measure to minimize self-aldol condensation. The presence of water leads to the conversion of lithium diisopropylamide into unreactive lithium hydroxide and diisopropylamine while oxygen converts lithium diisopropylamide to Li_2O , thus rigorous Schlenk conditions were adhered to. A key factor in the high yield isolation of β -diketones **2 – 5** is the amount of solvent (THF) used. If too much THF is used, $(FcCOCH_2^-)Li^+$ does not precipitate from the reaction mixture prior to ester addition and high yields of the aldol self condensation product, 1,3-diferrocenylbut-2-en-1-one (**10**), are

promoted. The formation of the lithium acetylferrocene salt is associated with an orange-red colour change of the reaction mixture. The lithium β -diketonato salt was visible as a maroon (for R = CF₃) to yellow (R = Fc) precipitate after completion of the reaction if the critical volume of THF is not exceeded. Column chromatography was not necessary to purify the β -diketones synthesised if the precipitated β -diketonato salt could be removed by filtration. Precipitation and purification is sometimes enhanced by ether addition because unreacted acetylferrocene, 1,3-diferrocenylbut-2-en-1-one (**10**) and other side products are soluble in ether while the β -diketonato salt is not. This does not work, however, if too much THF was originally used.

The β -diketone ligand exists in two dominant tautomeric forms that are in equilibrium with each other (**Scheme 3.2**). These forms are the keto and enol tautomers. In literature it is described that enolisation is generally away from the aromatic ferrocenyl group.² The equilibrium position of the lithium salts are very far to the left, i.e. the keto form (**Scheme 3.2**), while the equilibrium of the β -diketones (**2**) - (**5**) is 100% to the right (i.e. enol form) in the solid state. In solution, the enol form is still favoured, but the precise equilibrium position depends on the solvent and group electronegativity, χ_R , of each R group and temperature.

Du Plessis and co-workers² described two driving forces influencing the conversion between the keto and enol forms. These driving forces were labelled as electronic and resonance driving forces (**Scheme 3.3**). In **Scheme 3.3, A** should be favoured as the enol form of β -diketones 4,4,4-trifluorobutane-1,3-dione when electronic factors are considered. This is so because each R-substituent has a larger group electronegativity, χ_R , than the ferrocenyl group. This implies the carbonyl carbon atom adjacent to the ferrocenyl group is less

positive than the carbonyl carbon atom adjacent to the CF_3 (and other R groups). Consequently, from electronic considerations, it will be easier for the enolic form **A** to form than enol form **B**. However, canonical forms like **D** appear to have a bigger overall energy reducing effect on enol form **B** than canonical form, **C**, has on **A**, to the extent that **B** becomes the dominant enol isomer.

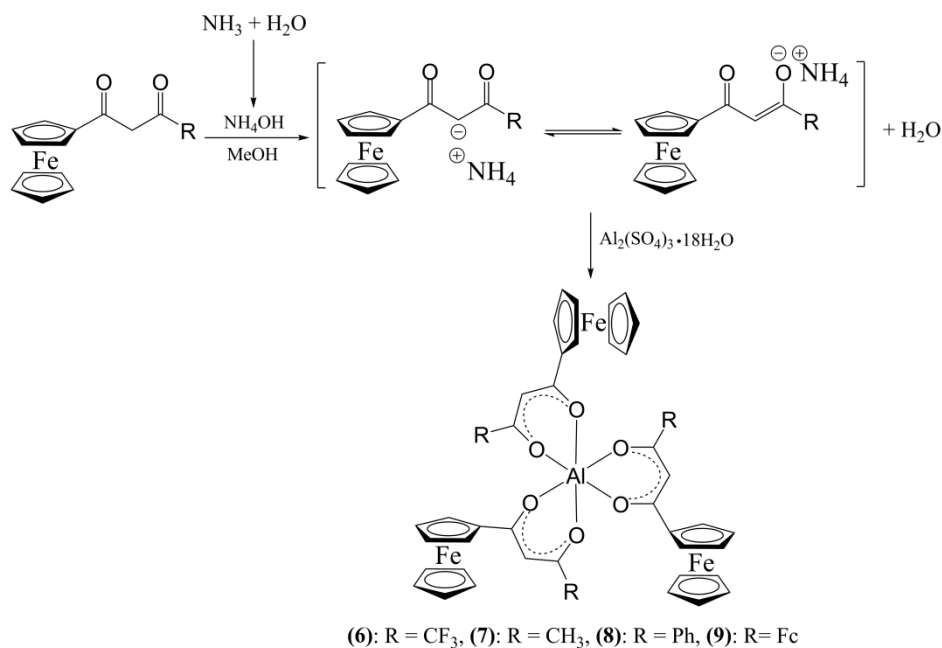


Scheme 3.3: Electronic and resonance considerations that may drive the keto-enol tautomerization.

3.2.2. β -diketonato complexes of aluminium(III)

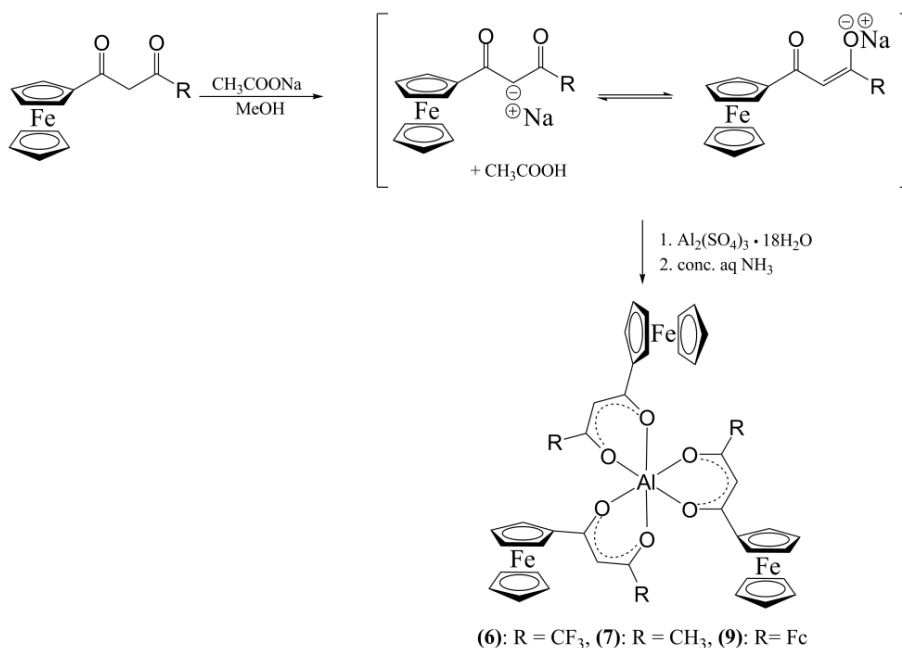
Three new $\text{Al}(\beta\text{-diketonato})_3$ complexes (**6**), (**8**) and (**9**), and one known $\text{Al}(\beta\text{-diketonato})_3$ complex (**7**) were synthesized by employing four different synthetic procedures. The first procedure was described by Zanello and co-workers³ for (**7**) and involves dissolving three equivalents of the β -diketone in methanol and concentrated aqueous ammonia and adding this solution to an aqueous solution of aluminium sulphate octadecahydrate, **Scheme 3.4**.

The quickly forming aluminium complex precipitates and is washed with water to remove any ammonia, ammonium sulphate and unreacted β -diketonato salts. Aqueous ammonia exists as an equilibrium between ammonia and ammonium hydroxide, **Scheme 3.4**. NH_3 first abstracts a proton from the free β -diketone. This results in an ammonium β -diketonato salt, which in turn reacts with aluminium to form the desired β -diketonato complex.



Scheme 3.4: Synthesis of $\text{Al}(\text{FcCOCHCOR})_3$, R = CF₃ (**6**), CH₃ (**7**), C₆H₅ (**8**) and Fc (**9**), complexes using concentrated aqueous ammonia in methanol.

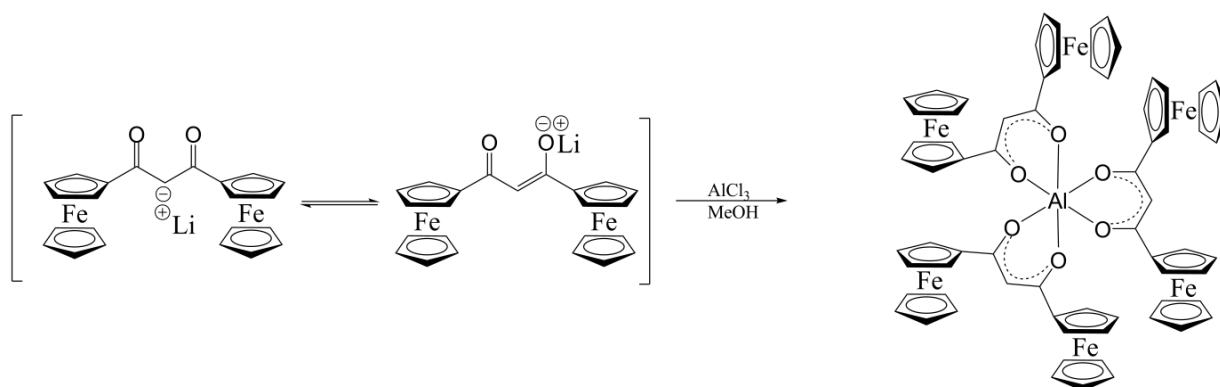
The second procedure that was used in this study involves dissolving the β -diketone in a methanol solution of sodium acetate. In general β -diketone chemistry, the acetate anion is often added to assist β -diketone complexation⁴ to metals. If the pK_a of the β -diketone is high enough, the acetate anion ($\text{pK}_b = 5.6 \times 10^{-8}$) can abstract a proton from the β -diketone. The resulting β -diketonato anion can then react with aluminium sulphate in water (**Scheme 3.5**). Aqueous ammonia was added to the reaction mixture after completion of the coordination reaction to effect product precipitation and neutralize any acetic acid that is formed during the reaction.



Scheme 3.5: Synthesis of Al(FcCOCHCOR)₃, R = CF₃ (**6**), CH₃ (**7**), Fc (**9**), complexes using sodium acetate in methanol.

The third and fourth procedures were only applied to the synthesis of (FcCOCHCOFc)₃Al (**9**).

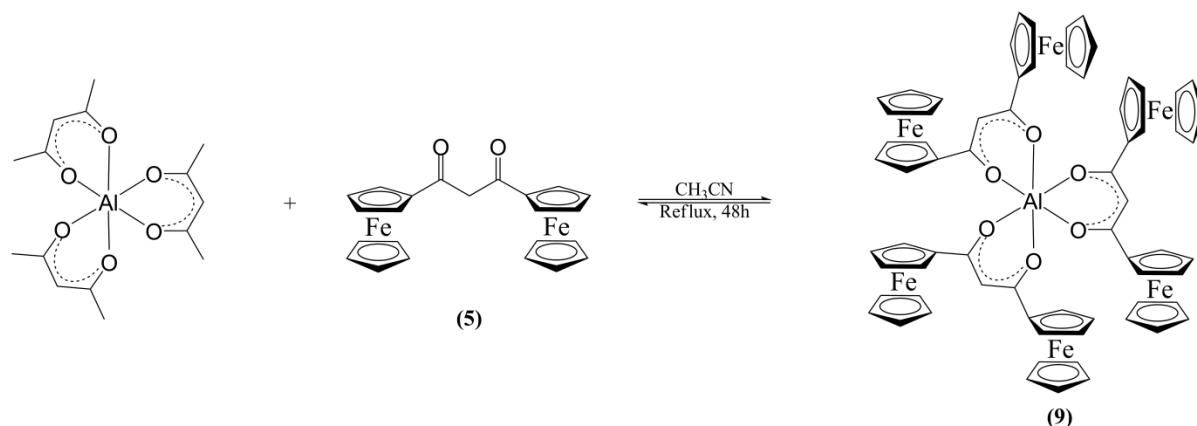
For method 3, aluminium trichloride dissolved in the minimum amount of water is reacted with 1,3-diferrocenylpropane-1,3-dionato lithium(I), [FcCOCHCOFc]⁻Li⁺ (**13**) in methanol (**Scheme 3.6**). The finely divided red precipitate that is formed is then centrifuged and washed with water and methanol.



Scheme 3.6: The synthesis of (FcCOCHCOFc)₃Al (**9**) from [FcCOCHCOFc]⁻Li⁺ (**13**).

The final synthetic approach used for the coordination of β-diketones to Al³⁺ was to reflux previously formed aluminium acetylacetonate and the β-diketone, 1,3-diferrocenylpropane-

1,3-dione [FcCOCH₂COFc, **(5)**], in acetonitrile for 48 hours (**Scheme 3.7**). This method involves the substitution of acetylacetonato groups by the desired β -diketone.



Scheme 3.7: The synthesis of $(\text{FcCOCHCOFc})_3\text{Al}$ (**9**) from aluminium acetylacetonate.

A comparison of the yields of the different synthetic procedures, see **Table 3.2** p. 70, indicates that concentrated aqueous ammonia in methanol is the most successful method.

Table 3.2. Percentage yields for the different methods of $\text{Al}(\beta\text{-diketonato})_3$ -synthesis applied.

B-diketone	Aluminium source	Method	Product	%Yield	
(2) , FcCOCH ₂ COCF ₃	$\text{Al}_2(\text{SO}_4)_3 \cdot 18\text{H}_2\text{O}$	[1] NH_3/MeOH	$\text{Al}(\text{FcCOCHCOCF}_3)_3$	32	
		[2] Na^+OAc		10	
(3) , FcCOCH ₂ COCH ₃	$\text{Al}_2(\text{SO}_4)_3 \cdot 18\text{H}_2\text{O}$	[1] NH_3/MeOH	$\text{Al}(\text{FcCOCHCOCH}_3)_3$	62	
		[2] Na^+OAc		<1	
(4) , FcCOCH ₂ COC ₆ H ₅	$\text{Al}_2(\text{SO}_4)_3 \cdot 18\text{H}_2\text{O}$	[1] NH_3/MeOH	$\text{Al}(\text{FcCOCHCOPh})_3$	50	
		[1] NH_3/MeOH		26	
(5) , FcCOCH ₂ COFc	$\text{Al}_2(\text{SO}_4)_3 \cdot 18\text{H}_2\text{O}$	[2] Na^+OAc	$\text{Al}(\text{FcCOCHCOFc})_3$	0	
	AlCl_3 (anhydrous)	[3] $\text{Li}^+[\text{FcCOCHCOFc}]^-$		23	
		$\text{Al}(\text{acac})_3$		[4] $\text{Al}(\text{acac})_3/\text{CH}_3\text{CN}$	7

Lower yields were obtained for the aqueous ammonia method during synthesis of **(5)** than compared to those obtained for **(2)**, **(3)** and **(4)**. The workup procedure was complicated by the formation of a white gel-like substance that is thought to be $\text{Al}(\text{OH})_3$ or other hydroxy

complexes of Al^{3+} . For this reason an excess of aluminium sulphate was employed during synthesis.

Large quantities of unreacted β -diketones were found when the sodium acetate method was employed. This suggested that sodium acetate might not effectively deprotonate the β -diketone ligands. Comparison of the four different methods used for $\text{Al}(\text{FcCOCHCOFc})_3$ synthesis shows the NH_3/MeOH method and the Li-salt method to give similar yields. Ligand exchange with $\text{Al}(\text{acac})_3$ proved less successful and it is proposed that the exchange of acetylacetonone with the more sterically demanding $\text{FcCOCH}_2\text{COFc}$ (**5**) is unfavourable.

3.2.3. Solution Stereochemistry

The formation of two isomers is possible for $\text{Al}(\text{FcCOCHCOFc}_3)_3$ (**6**), $\text{Al}(\text{FcCOCHCOCH}_3)_3$ (**7**) and $\text{Al}(\text{FcCOCHCOCH}_3)_3$ (**8**). For $\text{Al}(\text{FcCOCHCOFc})_3$ (**9**) only one isomer is possible. Zanello and co-workers³ identified the two isomers as the *mer*- and *fac*-isomers, in their study on the only previously known ferrocene-containing aluminium β -diketonato complex, $\text{Al}(\text{FcCOCHCOCH}_3)_3$ (**7**) (Figure 3.2).

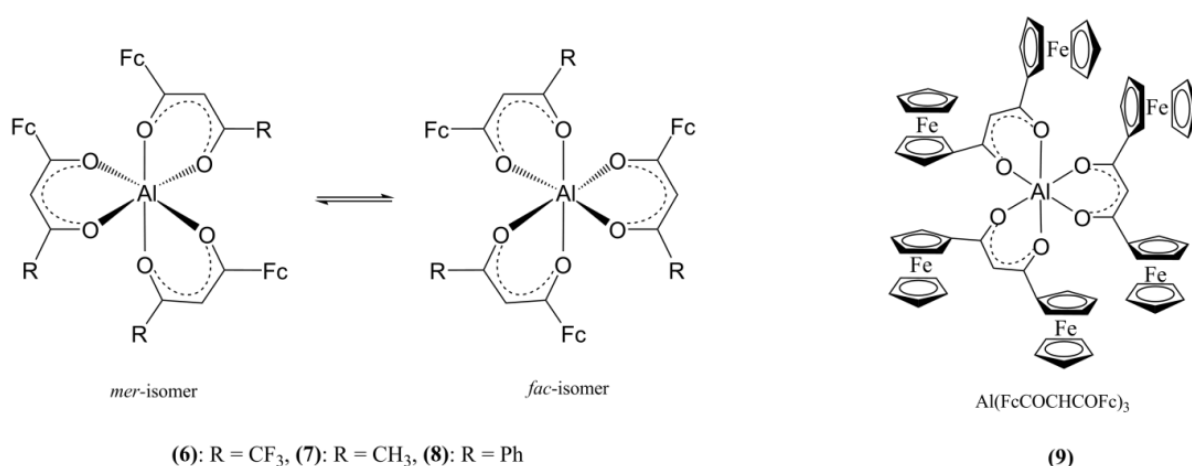


Figure 3.2: The two possible isomers for $\text{Al}(\text{FcCOCHCOR})_3$, R = CF_3 (**6**), CH_3 (**7**) and Ph (**8**), on the left, while $\text{Al}(\text{FcCOCHCOFc})_3$, (**9**), exists only as a single isomer and thus it is not labelled as *mer* or *fac*.

In the present study the ^1H NMR spectrum of a CDCl_3 solution of $\text{Al}(\text{FcCOCHCOCH}_3)_3$ (**Figure 3.3**) confirms Zanello's observation of the presence of both the *mer*- and *fac*-isomers in a ratio of 1.6:1. Three ^1H resonances of equal intensity for each of the CH_3 , COCHCO and C_5H_4 groups of the *mer*-isomer are observed. This is due to the inequality of these positions of the β -diketone side groups (Fc and R) in the *mer*-isomer.

A fourth resonance is observed in each of the regions of the different groups. This resonance corresponds to the *fac*-isomer. An unidentified NMR solvent impurity was observed in the CH_3 region at 2.20 ppm, integrating accidentally for three protons (**Figure 3.3**).

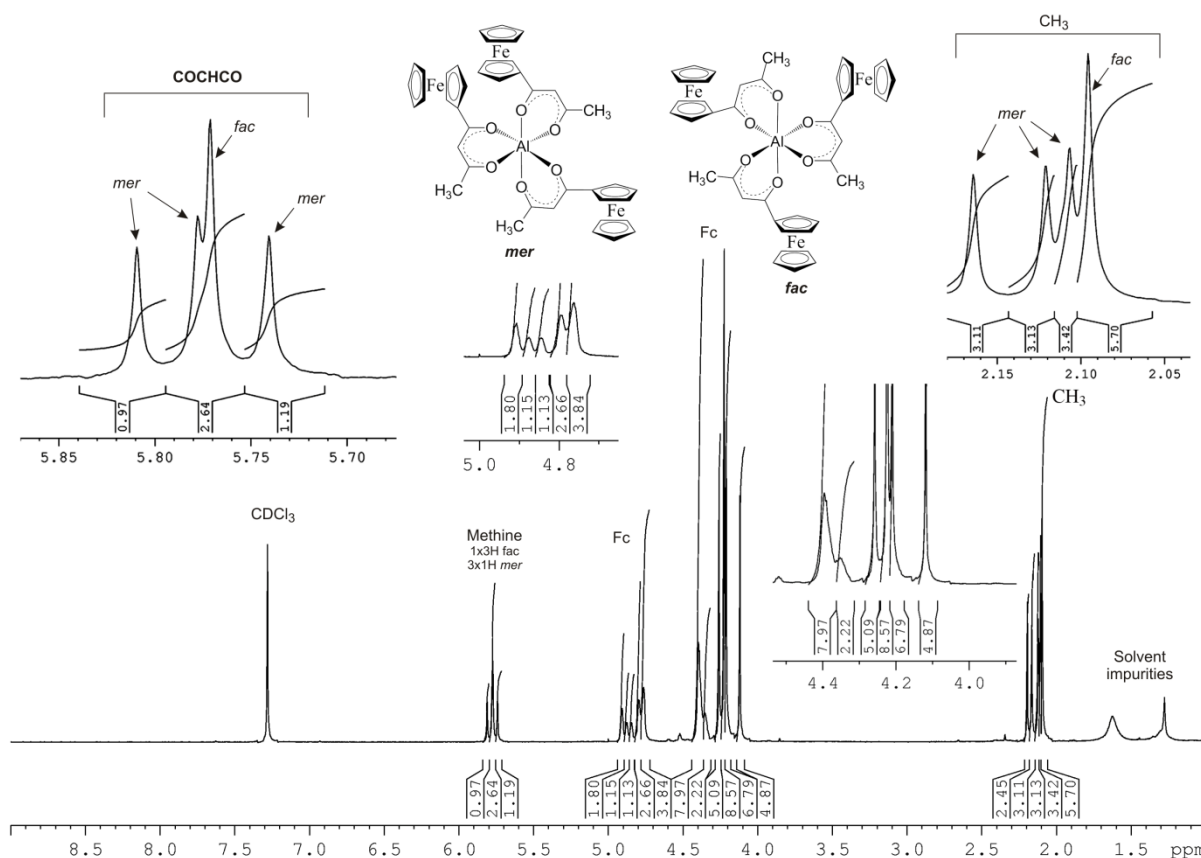


Figure 3.3: ^1H NMR of $\text{Al}(\text{FcCOCHCOCH}_3)_3$ (7) in CDCl_3 . *Mer*- and *fac*-isomers are labelled where assignments could be made unambiguously.

The ^1H NMR spectrum of $\text{Al}(\text{FcCOCHCOCF}_3)_3$ (**6**) (Figure 3.4) differs significantly from that of $\text{Al}(\text{FcCOCHCOCH}_3)_3$ (**7**) (Figure 3.3). Three resonance peaks of equal intensity are observed in the methine region at 6.1 ppm. The C_5H_5 protons of the ferrocenyl group are represented by two resonance peaks, one integrating for five protons and the other for ten protons. Similarly two groups of resonance peaks are encountered for the C_5H_4 protons of the ferrocenyl group each consisting of three closely overlapping triplet signals. This suggests that only one isomer, the *mer*-isomer is present in chloroform solutions for $\text{Al}(\text{FcCOCHCOCF}_3)_3$. The *fac*-isomer is not considered to be the specie present because the NMR peaks are constructed from three components, not one, as it should have been if the solution species present was the *fac*-isomer of $\text{Al}(\text{FcCOCHCOCF}_3)_3$.

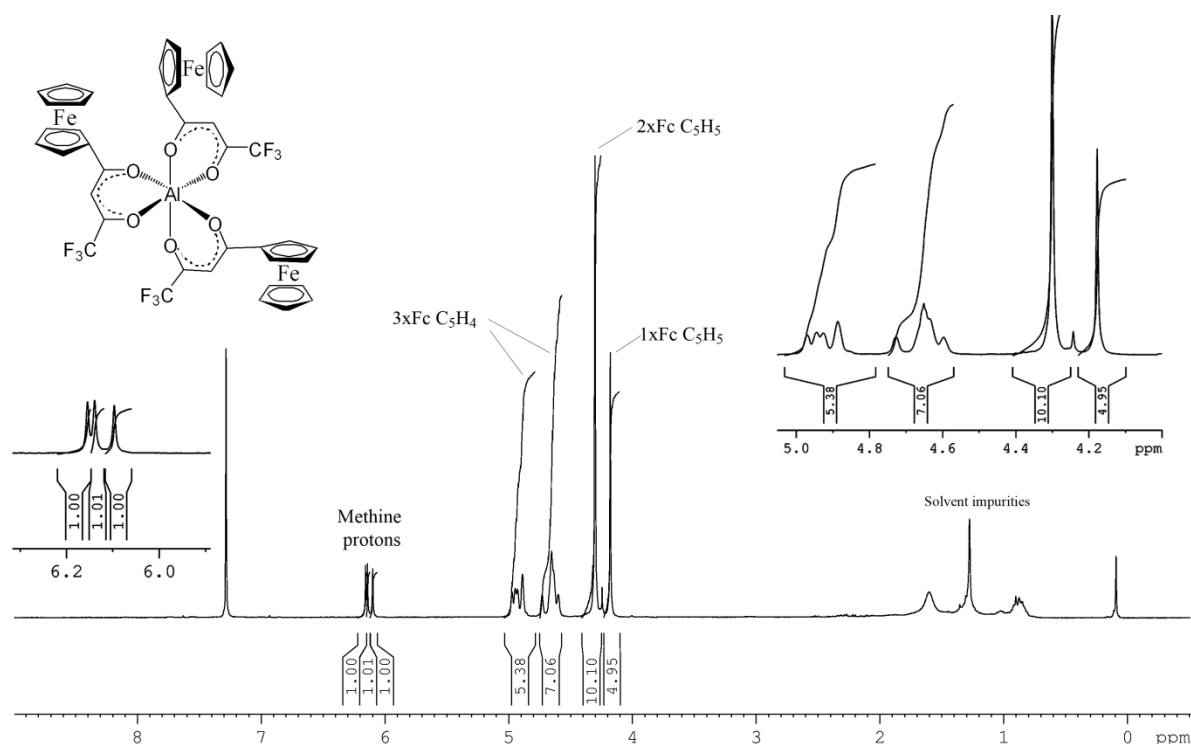


Figure 3.4: ^1H NMR of $\text{Al}(\text{FcCOCHCOCF}_3)_3$ (**6**) in CDCl_3 shows only the *mer*-isomer to be present.

The ^1H NMR of $\text{Al}(\text{FcCOCHCOPh})_3$ (**8**) shows three resonances in the methine region exhibiting a ratio of 2:1:1. Overlapping of two resonances can occur, leading to the

integration of the first resonance for twice the value of the others. This is consistent with the presence of the *mer*- and *fac*-isomers in solution.

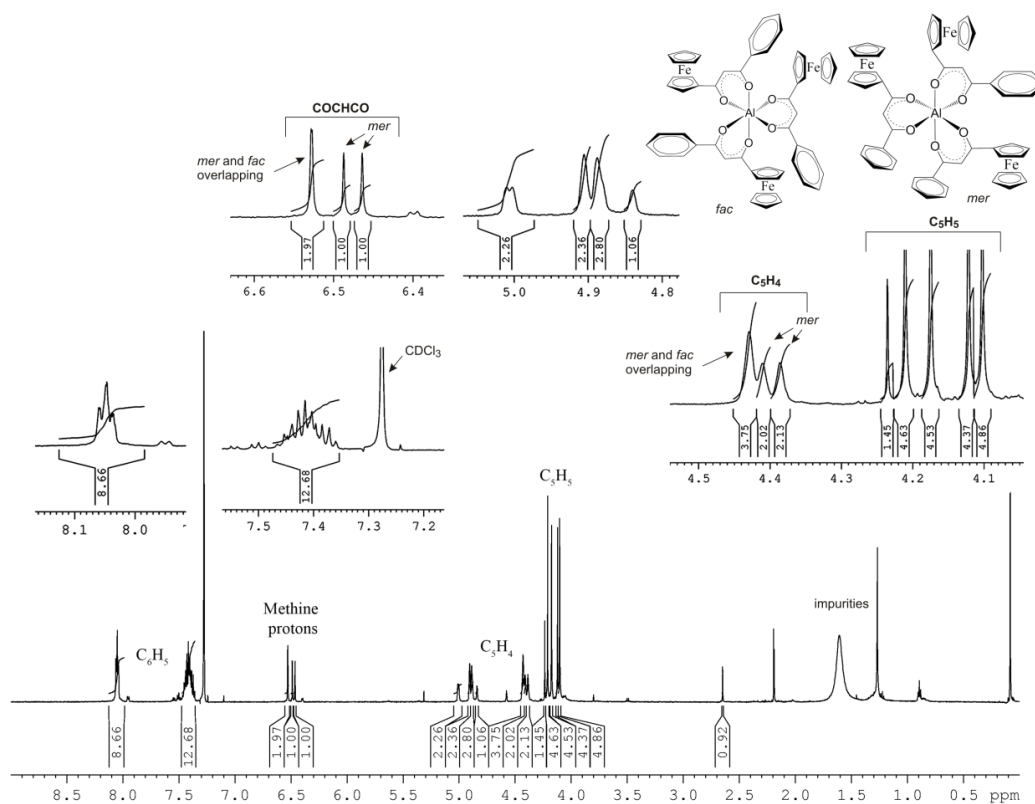


Figure 3.5: ^1H NMR of $\text{Al}(\text{FcCOCHCOPh})_3$ (**8**) in CDCl_3 showing *mer*- and *fac*-isomers.

The *mer*-isomer must produce three methine resonances of equal intensity, whilst the *fac*-isomer only produces one methine resonance overlapping with one of the *mer*-isomer methine protons. This indicates a 1:3 ratio of the *fac*-isomer to the *mer*-isomer.

At this point it is advantageous to record goal 1 (Chapter 1) of this research project has been achieved.

3.2.4. Single crystal x-ray structure of $\text{Al}(\text{FcCOCHCOF}_3)_3$

Attempts were made to obtain crystallographic quality crystals of complexes **6** – **9**, but only $\text{Al}(\text{FcCOCHCOF}_3)_3$ (**6**) gave crystals of sufficient quality to solve the structure by single

crystal X-ray diffraction. The structure determination was done, firstly, to establish the coordination mode (i.e. angles) around the Al centre. Secondly, for $\text{Al}(\text{FcCOCHCOCF}_3)_3$ (**6**), it provided the opportunity to prove that this complex exists in the *mer*-form as ^1H NMR analysis suggested. Other minor information that could be obtained includes determining whether the cyclopentadienyl rings of the ferrocenyl groups are in the staggered (D_{5d}) or eclipsed (D_{5h}) conformation, and the detection of any symmetric or asymmetric coordination (i.e. Al-O bond length comparisons) of each β -diketonato ligand. An evaluation of the β -diketonate bond lengths and Al-O bond lengths will also be useful to predict if, in principle, electronic communication between ferrocenyl and other β -diketonato substituents are possible in this complex.

$\text{Al}(\text{FcCOCHCOCF}_3)_3$ (**6**) crystallizes from acetone-hexane (1:1) to give an orthorhombic crystal system with $P2_12_12_1$ space group. The refinement parameters and crystal data are shown in **Table 3.3** and different views of the molecular structure of **6**, highlighting atom labelling, are shown in **Figure 3.6**.

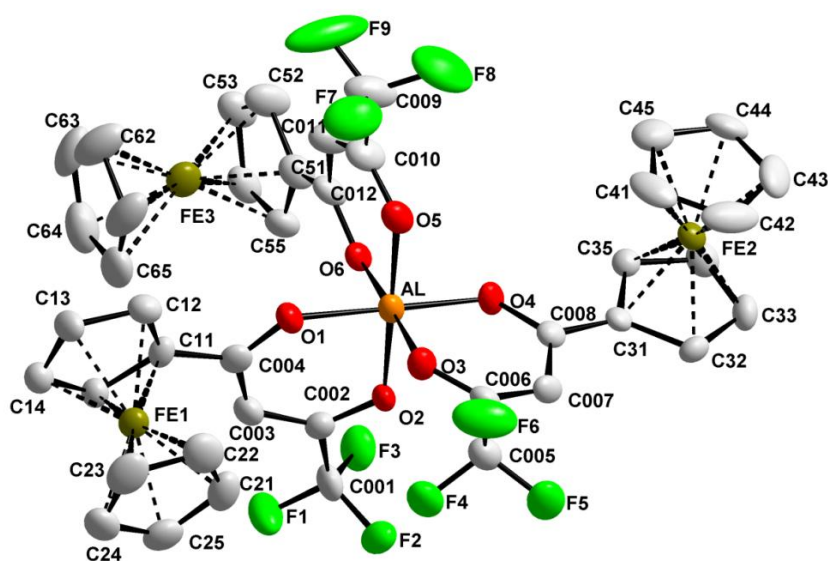


Figure 3.6: The molecular structure of $\text{Al}(\text{FcCOCHCOCF}_3)_3$ (**6**) showing atom labelling.

The structure is of high quality with a R-value of 0.0887. In comparison, some known aluminium carboxylate complexes (**Figure 2.10**, p. 44) showed R-values of up to 9.20. As predicted by ^1H NMR, $\text{Al}(\text{FcCOCHCOCF}_3)_3$ (**6**) was found to exist as the *mer*-isomer.

Table 3.3: Crystal data and structure refinement for $\text{Al}(\text{FcCOCHCOCF}_3)_3$ (**6**).

Parameter	Value	Parameter	Value
Empirical formula	$\text{C}_{42}\text{H}_{30}\text{AlF}_9\text{Fe}_3\text{O}_6$	Absorption coefficient / mm^{-1}	1.120
Molecular weight	996.19	θ range for data collection / $^\circ$	1.43 to 28.29
Crystal size / mm^3	0.57 x 0.09 x 0.06	Index ranges	$-13 \leq h \leq 13$, $-26 \leq k \leq 26$, $-26 \leq l \leq 27$
Temperature /K	100(2)	Reflections collected	40148
Wavelength / Å	0.71073	Independent reflections	10516 [R(int) = 0.0642]
Crystal system	Orthorhombic	Completeness to $\theta = 28.29^\circ$	99.9%
Space group	$P 2_1 2_1 2_1$	Max. and min. transmission	0.9358 and 0.5677
Unit cell dimensions / Å	a = 10.3997(9) b = 19.858(2) c = 20.508(2)	Refinement method	Full-matrix least-squares on F^2
Volume / Å^3	4235.2(7)	Data / restraints / parameters	10516 / 0 / 551
Z	4	Goodness-of-fit on F^2	0.983
Density (calculated) / Mg m^{-3}	1.562	Final R indices [$I > 2\sigma(I)$]	$R1 = 0.0587$, $wR2 = 0.1384$
F(000)	2008	R indices (all data)	$R1 = 0.0887$, $wR2 = 0.1501$
		Absolute structure parameter	0.035(17)
		Largest Diff. Peak and hole / $e \text{ Å}^{-3}$	1.565 and -0.535

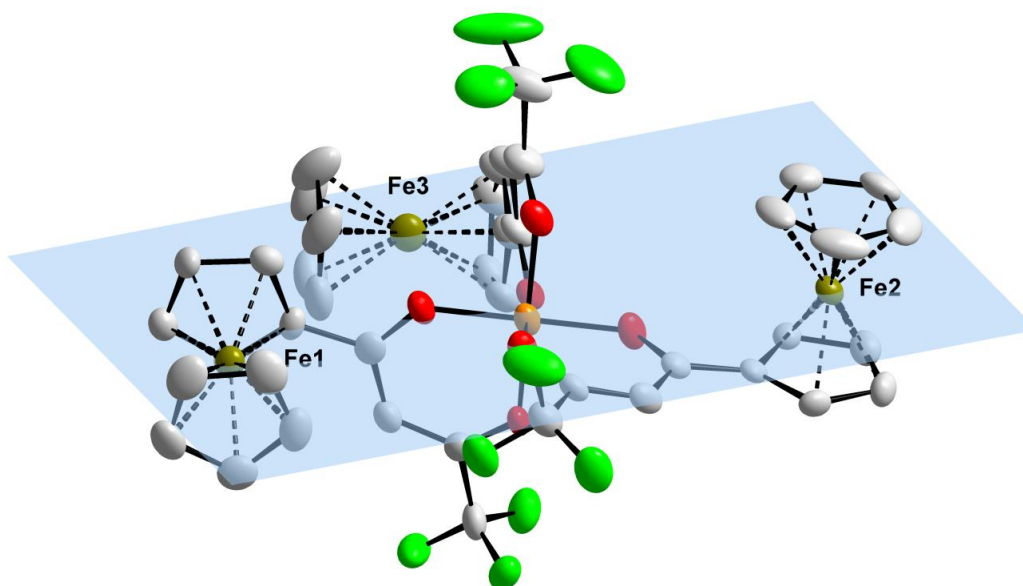


Figure 3.7: The molecular structure of $\text{Al}(\text{FcCOCHCOCF}_3)_3$ (**6**) showing the ferrocenyl-fragments centred on Fe(1) and Fe(3) are in the blue plane, whilst the ferrocenyl-fragment on Fe(2) is perpendicular to this plane.

The three β -diketonato fragments of **6** will be considered first (**Table 3.4**). The fragments are labelled according to the iron atoms of the ferrocenyl-moieties in **Figure 3.6**. It should be noted that typical C-C single bond lengths range from 1.38 (sp - sp : $-C\equiv C-C\equiv C-$) to 1.53 Å (sp^3 - sp^3 : $-C-C-$), whilst double bonds (C=C) range from 1.28 (sp - sp : $=C=C=$) to 1.32 Å (sp^2 - sp^2 : $-C=C-$).⁵ Furthermore, C-C bonds in compounds showing delocalization are expected to have distances that lie between the 1.48 Å of an sp^2 - sp^2 C-C single bond and the 1.32 Å of an sp^2 - sp^2 C=C double bond.⁶

Table 3.4: Comparison of bond lengths (Å) and angles of the β -diketonato fragments of $Al(FcCOCHCOCF_3)_3$ (**6**) and $FcCOCH_2COCF_3$. The β -diketonato fragments are labelled according to the iron atoms of the ferrocenyl-moieties in **Figure 3.6**. Bond lengths are examined from Fc to CF_3 .

Bonds	β -diketonato fragments of 6						Free $FcCOCH_2COCF_3^a$
	1		2		3		
	Bond length (Å)						
Fc-C(-O)	C(11)-C(004)	1.449(7)	C(31)-C(008)	1.424(6)	C(51)-C(012)	1.468(7)	1.448(6)
Fc-C-CH	C(003)-C(004)	1.406(7)	C(007)-C(008)	1.446(6)	C(011)-C(012)	1.411(7)	1.432(6)
CH-C-R	C(002)-C(003)	1.374(7)	C(006)-C(007)	1.342(7)	C(010)-C(011)	1.357(7)	1.345(6)
C-CF₃	C(001)-C(002)	1.517(7)	C(005)-C(006)	1.517(7)	C(009)-C(010)	1.526(8)	1.515(7)
C-O (FcCO)	C(004)-O(1)	1.271(6)	C(008)-O(4)	1.282(5)	C(012)-O(6)	1.274(6)	1.277(5)
C-O (CF₃CO)	C(002)-O(6)	1.286(6)	C(006)-O(3)	1.276(6)	C(010)-O(5)	1.289(6)	1.297(5)
Al-O^b	Al-O(1)	1.890(3)	Al-O(4)	1.868(3)	Al-O(6)	1.905(3)	-
Al-O	Al-O(2)	1.890(3)	Al-O(3)	1.868(3)	Al-O(5)	1.859(4)	-
	Bond angle (°)						
β-diketonate C-C-C		122.1(5)		122.0(4)		121.6(5)	120.0(4)

a: Crystallographic data of $FcCOCH_2COCF_3$ from W. C. Du Plessis, J. J. C. Erasmus, G. J. Lamprecht, J. Conradie, T. S. Cameron, M. A. S. Aquino and J. C. Swarts, *Can. J. Chem.*, 1999, **77**, 378.

b: Closest to the Fc group

All the C-C bonds in the β -diketonato ligand, except $C-CF_3$, have lengths (l) between 1.32 and 1.48 Å ($1.32 < l < 1.48$). The shortest bond is C(006)-C(007) (1.342(7) Å) and the longest is C(007)-C(008) (1.446(6) Å) both in fragment 2. Thus, C-C bonds in the β -diketonato backbone have delocalized character and in principle should be capable of conveying any electron-withdrawing and -donating effects between R and Fc β -diketonato side groups. The

difference between the two C-C bond lengths around the methine (CH) group in the backbone of the β -diketonato fragments, C(-O)-CH – C(-O) (**Table 3.4**), are 0.032, 0.104 and 0.054 Å for fragments 1, 2 and 3 respectively. Thus, ferrocenyl fragment 2 is decisively asymmetric, whilst fragments 1 and 3 are weakly asymmetric.

The free β -diketone (FcCOCHCOCF₃) is also asymmetric, with a difference of C-C-bonds around the CH (methine) group of 0.087 Å. In the free β -diketone enolisation occurs away from the ferrocenyl group, implying the larger C-(CH)-bond is closest to the ferrocenyl group.⁷ The same orientation is observed for all three ferrocenyl groups of **6**.

The average C-C bond distance in the ferrocenyl groups is 1.413 Å for the unsubstituted cyclopentadienyl rings and is 1.415 Å for substituted cyclopentadienyl rings. The longest bond is 1.445(9) Å (unsubstituted C_p ring of Fc3, i.e. the ferrocenyl group containing Fe(3)). The shortest bond is 1.359(6) Å (unsubstituted C_p ring of the ferrocenyl group containing Fe(1)). Delocalised bonding thus occurs throughout the ferrocenyl groups and electron withdrawing or donating effects may be transmitted through the β -diketonato backbone to and from the iron atoms.

Typical C=O bond lengths in β -diketones are 1.206 Å, whilst C-O bond lengths are 1.300 Å.⁷ For **6** all the C-O bonds lengths are between 1.206 and 1.300 Å, with the shortest being C(004)-O(1) with a length of 1.271(6) Å and the longest C(010)-O(5) with length 1.289(6) Å. The difference between the longest and shortest C-O bonds is 0.018 Å, whilst the difference between typical C=O and C-O bonds in β -diketones is 0.096 Å. It is clear that the C-O bonds encountered in **6** are much longer than typical C=O bonds and meaningfully shorter than C-O bonds and thus also show delocalised character. The β -diketonato fragments thus show

significant delocalisation and should be capable of facilitating through-bond electronic communication.

The aluminium atom in $\text{Al}(\text{FcCOCHCOCF}_3)_3$ (**6**) has an octahedral coordination sphere. The average Al-O bond length is 1.881 Å. The largest deviation from this average is 0.0245 Å for Al-O(6) which has a bond length of 1.905(3), whilst Al-O(5) has a bond length of 1.859(4) Å. Al-O(1) and Al-O(2) have equal bond lengths of 1.890(3) Å and so do Al-O(3) and Al-O(4) (1.868(3) Å). A crystal packing effect is the most probable reason for the inequality of Al-O(5) and Al-O(6) bond lengths. The difference between the largest (Al-O(6)) and smallest (Al-O(5)) Al-O bond lengths is 0.046 Å. The close agreement of all the Al-O bond lengths suggests that good electronic communication will be possible through the Al core of **6**. The capability of **6** to transmit electronic effects from one end of the molecule to the other was studied and quantified with the mathematical formulas in the electrochemical section of this study.

The average O-Al-O bond angle is 91.28° with the largest deviation from the average being 0.59° for O(5)-Al-O(6). These values are in close agreement with literature values^{8,9} for $\text{Al}(\text{acac})_3$. $\text{Al}(\text{acac})_3$ has Al-O bonding distances ranging between 1.871 Å for the δ -polymorph to 1.890 Å for the γ -polymorph and the O-Al-O bonding angles range from 90.19° to 90.81° . The large difference in electronegativity between the ferrocenyl group ($\chi_{\text{Fc}} = 1.87$) and the CF_3 group ($\chi_{\text{CF}_3} = 3.01$) leads to asymmetric β -diketonato ligands, showing shorter C-C bonds closer to the CF_3 group in the COCHCO fragments.

All three ferrocenyl groups were found to exist almost exclusively in the eclipsed form. The deviation from eclipsed form, as measured with the dihedral angles C(21)-centriod_{Cp ring}-centriod_{subst Cp ring}-C(11), C(41)-centriod_{Cp ring}-centriod_{subst Cp ring}-C(31) and C(61)-centriod_{Cp ring}-centriod_{subst Cp ring}-C(51), were 1.405(8)^o, 4.355(8)^o and 0.890(8)^o respectively. Bond angles in both the unsubstituted and substituted cyclopentadienyl rings averaged 108^o, the ideal theoretical value. The largest deviations from the average values were C(25)-C(21)-C(22) (+2.4^o) on a substituted C_p ring and C(12)-C(13)-C(14) (+2.0^o) on an unsubstituted C_p ring, both occurring in the cyclopentadienyl rings centred on Fe(1).

In conclusion, the crystal structure determination of **6** suggested that extensive electronic communication between the different ferrocenyl moieties would be possible due to the delocalised nature of the C-C backbone in the β-diketonato fragments and the almost equivalent C-O and Al-O bonds. The three β-diketonato ligands of **6**, like free FcCOCH₂COCF₃, exist to varying degrees as asymmetric fragments. Finally, **6** exists definitely in the *mer*-form as predicted by ¹H NMR.

3.2.5. Electrochemistry of aluminium β-diketonato complexes

3.2.5.1. Introduction

The electrochemistry of ferrocene containing β-diketones [(**2**) - (**5**)] has been reported in a previous study.⁷ In the present study, the electrochemistry of Al(FcCOCHCOR)₃, R = CF₃ (**6**), CH₃ (**7**), C₆H₅ (**8**) and Fc (**9**) is described. Cyclic voltammetry (CV), Osteryoung square wave voltammetry (SW) and linear sweep voltammetry (LSV) were performed to determine and quantify any intramolecular electronic communication that may exist between molecular

fragments of the synthesised aluminium β -diketonato complexes, $\text{Al}(\text{FcCOCHCOR})_3$, as outlined in goal 3 (Chapter 1). The effect of group electronegativity (χ_R) of the different β -diketonato R substituents on the formal redox potential ($E^{0'}$) was also investigated.

The only metallic redox active centre in the compounds studied was the iron centre of the ferrocenyl group. The oxidation state of iron changes reversibly between Fe(II) and Fe(III) in the ferrocene/ferrocenium couple, Fc/Fc^+ . Aluminium is not redox active. Redox couples can be classified as electrochemically reversible (theoretically characterised by $\Delta E_p = 59$ mV for a single electron process), quasi-reversible or irreversible. To allow for cell imperfections, in this study, $\Delta E_p < 90$ mV was still considered as representative of electrochemical reversible processes.¹⁰ ΔE_p values of between 90 and 150 ($90 < \Delta E_p < 150$) are taken as representative of quasi reversible electrochemical processes, while $\Delta E_p > 150$ are considered as representative of irreversible electrochemical processes. Peak cathodic potentials (E_{pc}), peak anodic potentials (E_{pa}) and formal redox potentials ($E^{0'}$) are reported versus free ferrocene, but were experimentally determined versus decamethyl ferrocene, Fc^* , to avoid overlap of the signals of the ferrocenyl groups in each complex with the signal of free ferrocene. Under the current experimental conditions $E^{0'}$ of Fc^* is -610 mV versus free Fc. Experiments were performed using an in-house constructed Ag/AgCl reference electrode immersed in an acetonitrile Luggin capillary bridged by a second capillary containing CH_2Cl_2 to minimize potential drift (over potentials). A key aspect of this study was the use of tetrabutylammonium tetrakis(pentafluorophenyl)borate, $[\text{NBu}_4][\text{B}(\text{C}_6\text{F}_5)_4]$, rather than tetrabutylammonium hexafluoro phosphate as electrolyte. All experiments were conducted at 25 °C using dichloromethane as solvent.

3.2.5.2. Ferrocene containing aluminium β -diketonato complexes

The main focus of this study was primarily on the behaviour of the ferrocenyl group of the β -diketonato ligands of the aluminium complexes, but β -diketone reduction can be observed at large negative potentials.

Cyclic voltammograms, linear sweep voltammograms and Osteryoung square wave voltammograms of $\text{Al}(\text{FcCOCHCOCH}_3)_3$ (**7**) are shown in **Figure 3.8** on p. 83, while electrochemical data that can be extracted from this is summarised in **Table 3.5** below.

Table 3.5: Electrochemical data of $\text{Al}(\text{FcCOCHCOCH}_3)_3$ (**7**). Peak anodic potentials, (E_{pa}) are referenced versus the free ferrocene couple, Fc/Fc^+ .

^a $v /$ mV/s	$E_{pa} /$ mV	$\Delta E_p /$ mV	$E^{\circ'} /$ mV	$i_{pa} /$ μA	i_{pc}/i_{pa}	$v /$ mV/s	$E_{pa} /$ mV	$\Delta E_p /$ mV	$E^{\circ'} /$ mV	$i_{pa} /$ μA	i_{pc}/i_{pa}
Fc*						Wave 1					
100	-585	68	-619	3.24	0.95	100	117	62	86	3.53	1.04
200	-579	74	-616	4.49	0.95	200	127	74	90	5.15	0.94
300	-579	78	-618	5.51	0.96	300	127	78	88	6.32	1.07
400	-578	80	-618	6.32	0.94	400	124	78	85	7.06	1.04
500	-574	87	-618	7.06	0.96	500	129	84	87	7.94	1.02
Wave 2						Wave 3					
100	235	66	202	3.53	0.92	100	325	64 ^b	293	3.53	0.92
200	231	74	194	5.29	0.83	200	329	72 ^b	293	5.44	0.86
300	247	86	204	6.18	0.95	300	333	78 ^b	294	6.47	0.98
400	251 ^b	94	204	6.76	0.96	400	336	82 ^b	295	7.06	0.98
500	253 ^b	96	205	8.09	0.91	500	339	88 ^b	295	8.82	0.97

(a) Symbols are as follows: v = scan rate, E_{pa} = peak anodic potential, E_{pc} = peak cathodic potential, $E^{\circ'}$ = formal reduction potential, i_{pa} = peak anodic current, i_{pc} = peak cathodic current and ΔE_p = difference in peak anodic and peak cathodic potentials.

(b) Estimated value due to low peak resolution.

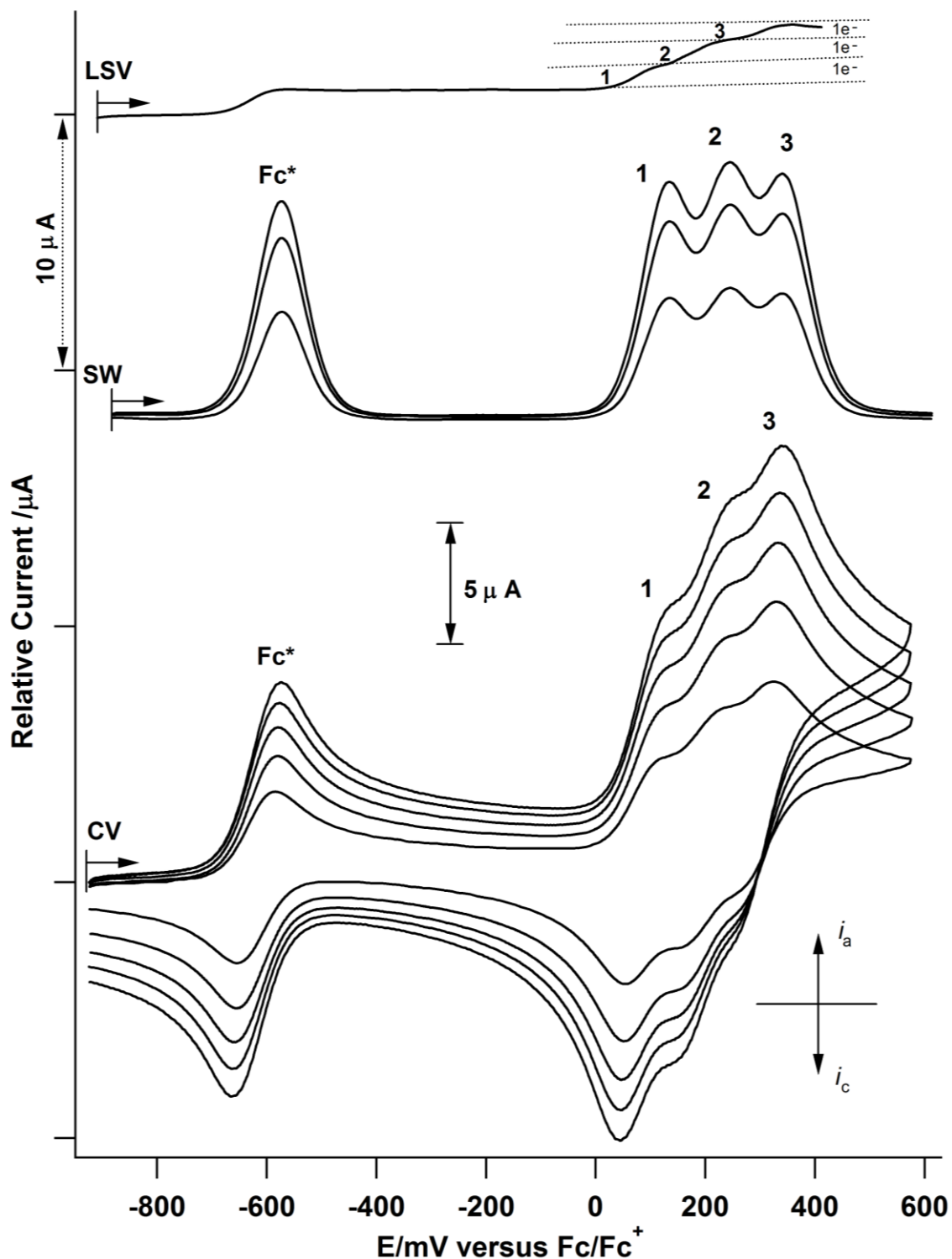
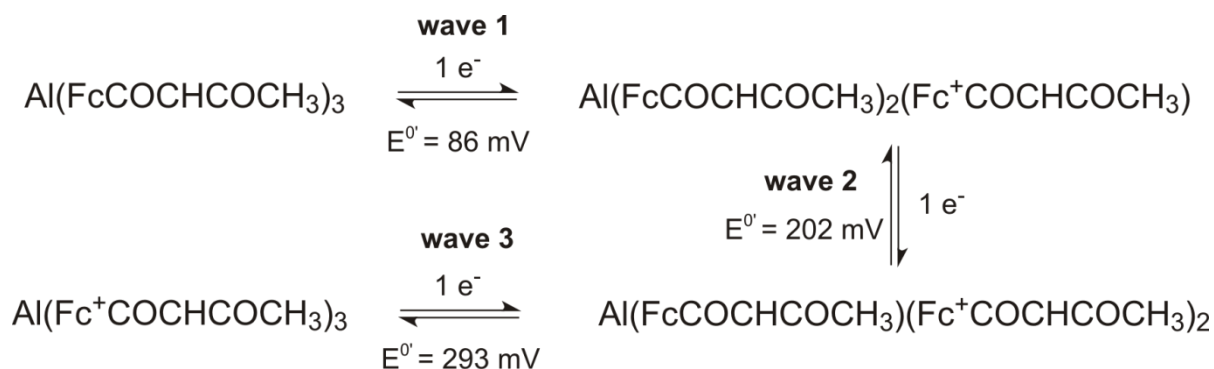


Figure 3.8: Linear sweep voltammogram (top), Osteryoung square wave voltammogram (middle) and cyclic voltammograms (bottom) of a 0.5 mmol dm^{-3} $\text{Al}(\text{FcCOCHCOCH}_3)_3$ (**7**) solution in $\text{CH}_2\text{Cl}_2/0.1 \text{ mol dm}^{-3}$ $[\text{NBu}_4][\text{B}(\text{C}_6\text{F}_5)_4]$ on a glassy carbon-working electrode at scan rates of 100, 200, 300, 400 and 500 mV/s for cyclic voltammograms and 1 mV/s for LSV. Osteryoung square wave voltammetry was performed at 5, 10 and 15 Hz. Decamethyl ferrocene (Fc^*) was used as internal standard. Fc^* has a potential of -610 mV versus Fc/Fc^+ . Arrows show the onset potential and scan direction.

Three ferrocene-related oxidation half reactions in the anodic CV sweep (the peaks pointing upward) and reduction half reactions in the cathodic CV sweep (the peaks pointing downward) were observed. The wave labelled 1 is associated with the oxidation of the ferrocenyl group of the first β -diketonato ligand of $\text{Al}(\text{FcCOCHCOCH}_3)_3$ (**7**), wave 2 represent ferrocenyl group oxidation of the second β -diketonato ligand and wave 3 is associated with ferrocene oxidation in the third ligand of $\text{Al}(\text{FcCOCHCOCH}_3)_3$. Each of the three ferrocene substituents showed reversible electrochemical behavior at slow scan rates because $\Delta E_p < 70$ mV were found. However, at higher scan rates the differences in peak potentials increased to almost 90 mV (**Table 3.3**). LSV confirmed three separate one-electron transfers for the oxidation of the three ferrocene substituents. The peak resolution of waves 1, 2 and 3 was increased by the application of Osteryoung square wave voltammetry from mere shoulders in the CV, to distinct separate peaks. The electrochemical processes associated with waves 1, 2 and 3 are summarised in **Scheme 3.8** below.



Scheme 3.8: The electrochemical processes associated with CV waves 1, 2 and 3 of $\text{Al}(\text{FcCOCHCOCH}_3)_3$ (**7**). E° values are given at a scan rate of 100 mV s^{-1} .

To put the observation of three electrochemical waves for **7** in perspective, it is important to note that in systems that allow electron delocalisation via through-space or via intramolecular through-bond conjugation, different formal reduction potentials (E°) can

frequently be detected for redox active groups in symmetrical complexes in which mixed valent intermediates are encountered.^{11, 12} In $\text{Al}(\text{FcCOCHCOCH}_3)_3$ (**7**) the ferrocenyl and ferrocenium groups are encountered as mixed-valent intermediates (see **Scheme 3.8**).

Zanello and co-workers³ have previously also investigated the electrochemistry of $\text{Al}(\text{FcCOCHCOCH}_3)_3$ (**7**) using NBu_4PF_6 as supporting electrolyte. They, however, only obtained a single, broad ferrocene related peak. Results from this lab showed resolution of closely overlapping peaks became worse if the concentration of the substrate was higher than 1 mM ($[\text{substrate}] > 1 \text{ mM}$).¹³ The compound studied that demonstrated this effect was $[\text{Ru}_2(\text{COO})_4]^+$. It is thus clear that by employing a low concentration (0.5 mmol) of the compound and by using $[\text{NBu}_4][\text{B}(\text{C}_6\text{F}_5)_4]$ as an electrolyte, resolution of closely overlapping multiple potential peaks can be enhanced. The advantageous effects in terms of enhanced peak resolutions was also observed before by Geiger¹⁴ in his studies on nickel thiofulvalene complexes and also by the Bloemfontein electrochemistry group in their studies on porphyrins¹⁰ and ruthenocene derivatives.¹³

From the ^1H NMR spectrum of $\text{Al}(\text{FcCOCHCOCH}_3)_3$ (**7**) it is clear that both the *mer*- and *fac*-isomers exist in appreciable quantities. However, it was impossible to distinguish between the two isomers electrochemically. This entirely expected result indicates that molecular geometry does not significantly influence the potential required to oxidise ferrocene, but bond delocalisation does transmit electron-donating or electron-withdrawing effects of molecular fragments to and from the ferrocenyl centres.

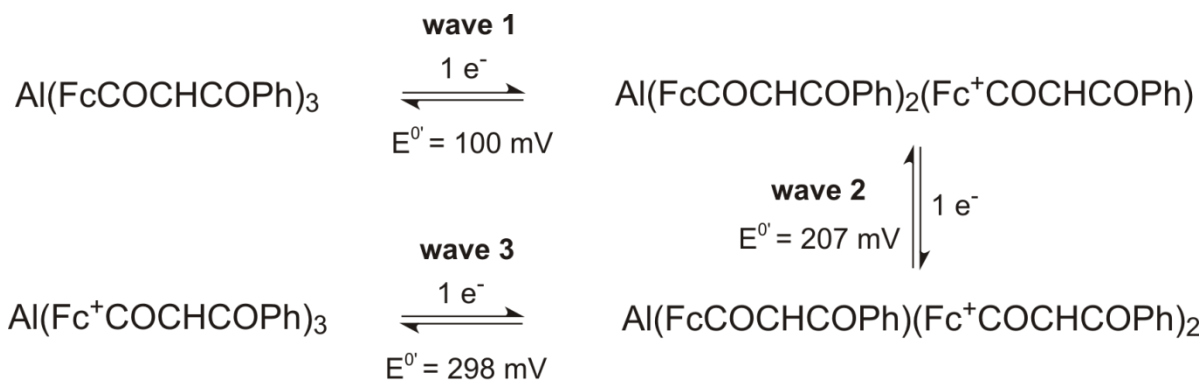
$\text{Al}(\text{FcCOCHCOPh})_3$ (**8**) (**Figure 3.9**) shows similar electrochemistry to that of $\text{Al}(\text{FcCOCHCOCH}_3)_3$ (**7**), also producing three electrochemically reversible ferrocene peaks in its voltammograms. Data is summarised in **Table 3.6**.

Table 3.6: Electrochemical data of Al(FcCOCHCOPh)₃ (**8**). Peak anodic potentials, (E_{pa}) are referenced versus the free ferrocene couple, Fc/Fc⁺.

^a v / mV/s	E_{pa} / mV	ΔE_p / mV	E^0 / mV	i_{pa} / μ A	i_{pc}/i_{pa}	v / mV/s	E_{pa} / mV	ΔE_p / mV	E^0 / mV	i_{pa} / μ A	i_{pc}/i_{pa}
Fc*						Peak 1					
100	-581	76	-619	6.5	0.98	100	131	62	100	1.94	1.17
200	-575	82	-616	9.4	0.97	200	139	70	104	3.06	1.00
300	-573	94	-620	11.5	0.99	300	131	70	96	4.03	0.92
400	-567	100	-617	12.7	0.99	400	141	80	101	4.84	0.90
500	-559	108	-613	14.4	0.98	500	147	84	105	5.65	0.91
Peak 2						Peak 3					
100	241	68	207	1.94	1.00	100	331	66 ^b	298	1.94	1.13
200	239	70	204	3.55	1.00	200	337	72 ^b	301	3.23	0.90
300	239	80	199	4.19	0.96	300	335	76 ^b	297	3.87	0.96
400	253	96	205	4.68	0.97	400	343	84 ^b	301	4.52	0.93
500	255	102	204	5.81	0.92	500	345	88 ^b	301	5.81	0.89

(a) Symbols are as follows: v = scan rate, E_{pa} = peak anodic potential, E_{pc} = peak cathodic potential, E^0 = formal reduction potential, i_{pa} = peak anodic current, i_{pc} = peak cathodic current and ΔE_p = difference in peak anodic and peak cathodic potentials.

(b) Estimated value due to low peak resolution.



Scheme 3.9: The electrochemical processes associated with CV waves 1, 2 and 3 of Al(FcCOCHCOPh)₃ (**8**). E^0 values are given at a scan rate of 100 mV s⁻¹.

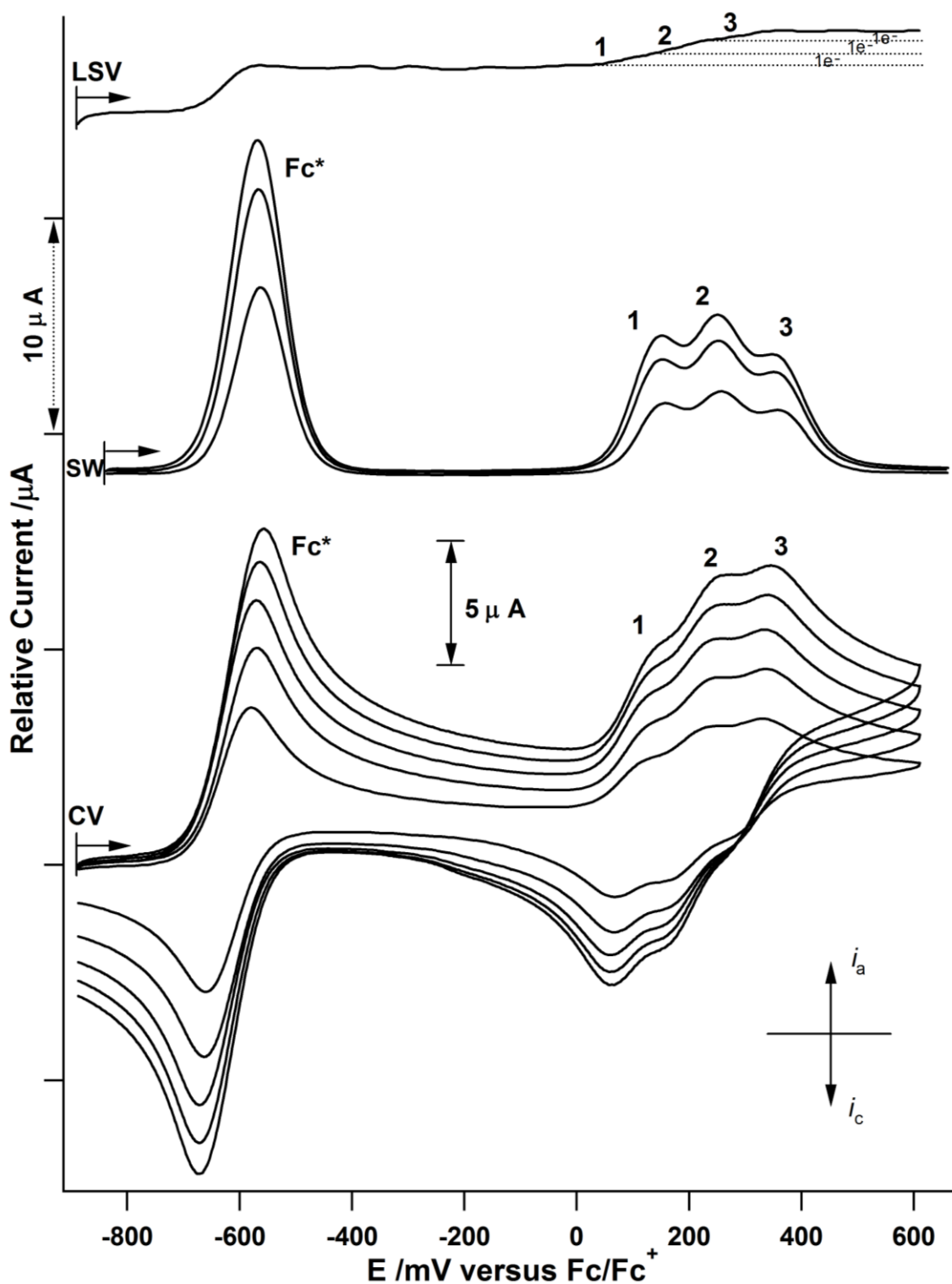


Figure 3.9: Linear sweep voltammogram (top), Osteryoung square wave voltammogram (middle) and cyclic voltammograms (bottom) of a 0.5 mmol dm^{-3} $\text{Al}(\text{FcCOCHCOPh})_3$ (**8**) solution in $\text{CH}_2\text{Cl}_2/0.1 \text{ mol dm}^{-3}$ $[\text{NBu}_4][\text{B}(\text{C}_6\text{F}_5)_4]$ on a glassy carbon-working electrode at scan rates of 100, 200, 300, 400 and 500 mV/s for cyclic voltammograms and 1 mV/s for LSV. Osteryoung square wave voltammetry was performed at 5, 10 and 15 Hz. Decamethyl ferrocene (Fc^*) was used as internal standard. Fc^* has a potential of -610 mV versus Fc/Fc^+ . Arrows show the onset potential and scan direction.

The electrochemistry of $\text{Al}(\text{FcCOCHCOCF}_3)_3$ (**6**) (Figure 3.10) differed from the other compounds. Data is summarised in Table 3.7 and Table 3.8.

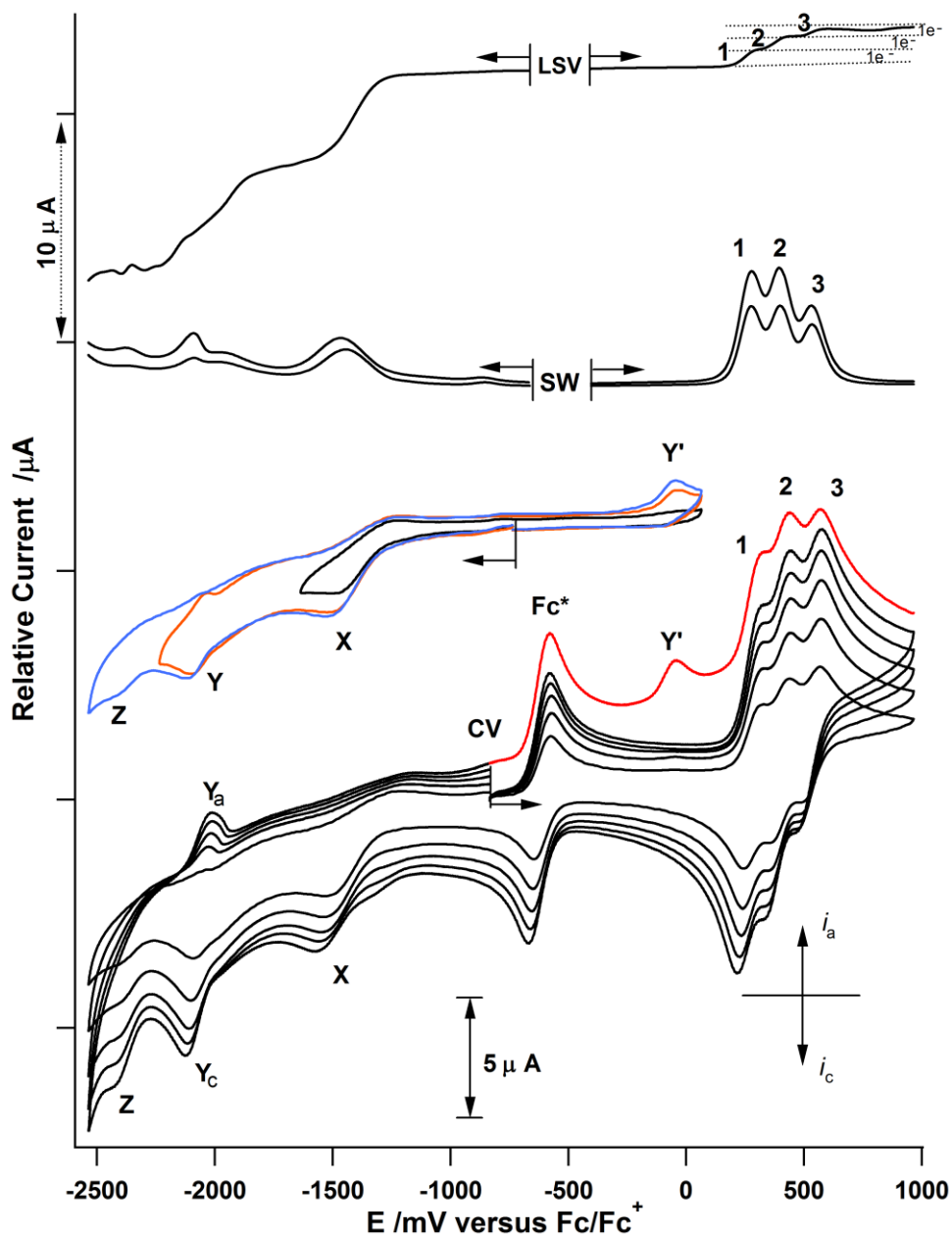


Figure 3.10: Linear sweep voltammogram (top), Osteryoung square wave voltammogram (middle) and cyclic voltammograms (bottom) of a 0.5 mmol dm^{-3} $\text{Al}(\text{FcCOCHCOCF}_3)_3$ (**6**) solution in $\text{CH}_2\text{Cl}_2/0.1 \text{ mol dm}^{-3}$ $[\text{NBu}_4][\text{B}(\text{C}_6\text{F}_5)_4]$ on a glassy carbon-working electrode at scan rates of 100, 200, 300, 400 and 500 mV/s for cyclic voltammograms and 1 mV/s for LSV. Osteryoung square wave voltammetry was performed at 5, 10 and 15 Hz. The CV's second from the bottom was scanned in a negative direction to cast more light on peaks X, Y, Z and Y' (scan rate = 100 mV/s). Decamethyl ferrocene (Fc^*) was used as internal standard. Fc^* has a potential of -610 mV versus Fc/Fc^+ . Arrows show the onset potential and scan direction.

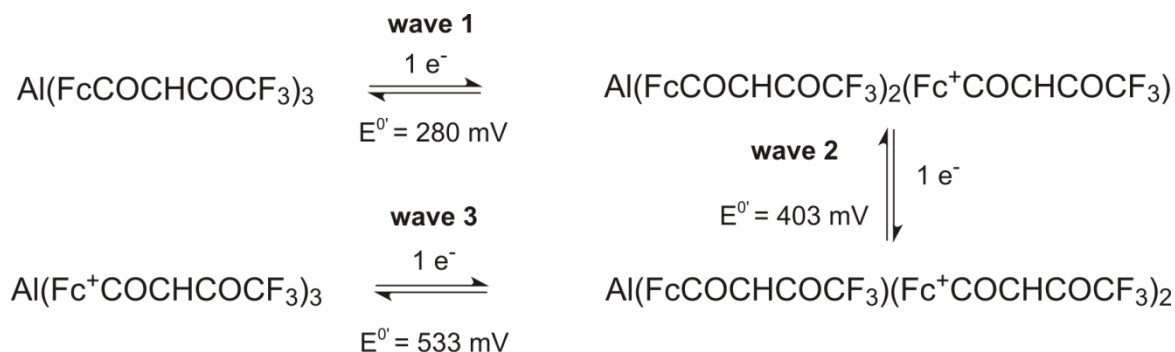
Table 3.7: Electrochemical data of $\text{Al}(\text{FcCOCHCOCF}_3)_3$ (**6**). Peak anodic potentials, (E_{pa}) are referenced versus the free ferrocene couple, Fc/Fc^+ .

^a $v /$ mV/s	$E_{pa} /$ mV	$\Delta E_p /$ mV	$E^{\circ} /$ mV	$i_{pa} /$ μA	i_{pc}/i_{pa} / mV	$v /$ mV/s	$E_{pa} /$ mV	$\Delta E_p /$ mV	$E^{\circ} /$ mV	$i_{pa} /$ μA	i_{pc}/i_{pa} / mV
Fc*						Peak 1					
100	-577	68	-611	2.9	0.94	100	313	66	280	3.1	1.11
200	-573	74	-610	4.0	0.92	200	319	78	280	4.5	1.07
300	-575	80	-615	4.8	0.93	300	320	85	278	3.7	1.57
400	-577	80	-617	5.8	0.94	400	317	86	274	6.5	1.00
500	-579	88	-623	6.8	0.95	500	315	88	271	7.6	0.98
Peak 2						Peak 3					
100	439	72	403	3.2	1.05	100	569	72	533	3.2	0.90
200	441	82	400	5.0	0.90	200	568	77	530	4.7	0.90
300	443	88	399	5.5	0.94	300	571	82	530	5.3	0.91
400	439	90 ^b	394	6.8	0.95	400	571	86	528	6.9	0.91
500	439	94 ^b	392	7.6	0.96	500	575	100b	525	8.1	0.96

(a) Symbols are as follows: v = scan rate, E_{pa} = peak anodic potential, E_{pc} = peak cathodic potential, E° = formal reduction potential, i_{pa} = peak anodic current, i_{pc} = peak cathodic current and ΔE_p = difference in peak anodic and peak cathodic potentials.

(b) Estimated value due to low peak resolution.

Upon scanning in a positive direction from the onset voltage of -800 mV, the CV of complex (**6**), $\text{Al}(\text{FcCOCHCOCF}_3)_3$, first shows the internal standard peaks labelled Fc^* , and then well resolved peaks 1, 2 and 3 which is associated with each of the three ferrocenyl groups. These three peaks represent sequential ferrocene oxidation according to the electrochemical scheme, **Scheme 3.10**, below.



Scheme 3.10: The electrochemical processes associated with waves 1, 2 and 3 of $\text{Al}(\text{FcCOCHCOCF}_3)_3$ (**6**). E° values are given at a scan rate of 100 mV s^{-1} .

However, if the CV scan is not stopped at the onset potential, but continued in a negative direction down to -2600 mV, three cathodic additional peaks, labelled X, Y_c and Z, are observed. On the return scan, scanning from -2600 to +1000 mV, anodic peak Y_a and Y' is observed. Y' was not detected during the first of the three cycles of this CV experiment. Potentials for these peaks are given in **Table 3.8**.

To focus a bit more on peaks X, Y_a , Z, Y_c and Y' , a second CV experiment was conducted in which the initial potential scanning direction was negative from the onset potential of -800 mV, **Figure 3.10**, second from the bottom. In this experiment, the two peaks (Y_a and Y') are still observed. In cycle two, i.e. scanning from -2600 to -100 mV in a positive direction the peak Y' was again detected. If the reversing potential, however, was not -2600 mV but -1700 mV, peaks Y_c and Z were cut off, only cathodic peak X was generated. When these potential limits were applied, peak Y' was not detected. If the reversing potential was changed to -2200 mV, peak Y_a was included in the cathodic process, and the new peak, Y' , was detected. This implies peak Y' is related to peak Y. It is thought that reductions X, Y and Z and the species associated with peak Y' are related to electron transfer processes associated with the aromatic β -diketonato core. It is likely that similar processes are possible for the other β -diketonato complexes, but since they were not detected, they appear to occur at negative potentials beyond that which the solvent window allows. The high electronegativity of the CF_3 groups must contribute to the reason why peaks X, Y_c and Z are observable for $Al(FcCOCHCOCF_3)_3$, **(6)**, but not $Al(FcCOCHCOCH_3)_3$, **(7)**, or $Al(FcCOCHCOPh)_3$, **(8)**. As previously stated, this investigation is geared towards the study of the metallocene moieties and therefore these processes are only noted, but full interpretation of the meaning is beyond the scope of this research project.

Table 3.8: Electrochemical data of $\text{Al}(\text{FcCOCHCOF}_3)_3$ (**6**) for electrochemical processes not in the ferrocene-region. Peak potentials are referenced versus the free ferrocene couple, Fc/Fc^+ .

ν /mV s ⁻¹	Peak Potential /mV				
	X	Y _a	Z	Y _c	Y'
100	-1503	-2093	-2411	-2029	-43
200	-1519	-2097	-2415	-2025	-41
300	-1523	-2103	-2418	-2015	-35
400	-1545	-2113	-2421	-2009	-39
500	-1553	-2119	-2431	-2011	-47

$\text{Al}(\text{FcCOCHCOFc})_3$, (**9**), exhibited low solubility in dichloromethane. A sufficient amount was, however, dissolved in dichloromethane to perform an electrochemical analysis (**Figure 3.11**, p. 92). The exact concentration of the solution is, however, not known as precipitation during the experiment indicated that much of the compound was simply suspended in solution. The resulting low effective concentration of dissolved $\text{Al}(\text{FcCOCHCOFc})_3$ (**9**) in the solvent probably contributed to the high peak resolution obtained during the experiments.

All six ferrocene oxidations and reductions are observed and could be resolved. The first oxidation appears as a shoulder on the CV of (**9**); however Osteryoung square wave voltammetry afforded extra resolution to confirm that all six ferrocene substituents can be observed electrochemically. Electrochemical data is summarised in **Table 3.9**, p. 93.

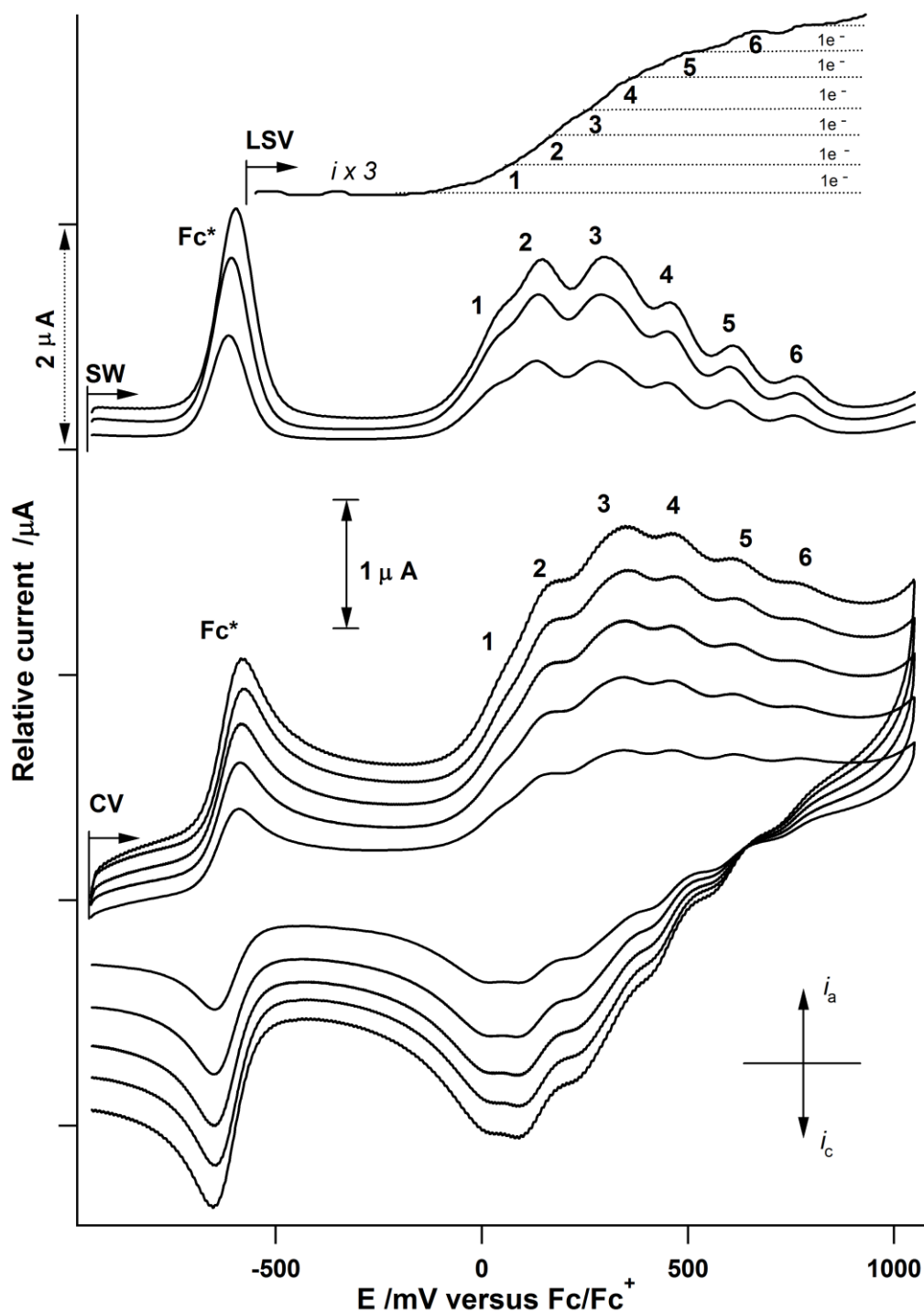


Figure 3.11: Linear sweep voltammogram (top), Osteryoung square wave voltammogram (middle) and cyclic voltammograms (bottom) of a $\text{Al}(\text{FcCOCHCOFc})_3$ (**9**) solution in $\text{CH}_2\text{Cl}_2/0.1 \text{ mol dm}^{-3}$ $[\text{NBu}_4][\text{B}(\text{C}_6\text{F}_5)_4]$ on a glassy carbon-working electrode at scan rates of 100, 200, 300, 400 and 500 mV/s for cyclic voltammograms and 1 mV/s for LSV. Osteryoung square wave voltammetry was performed at 5, 10 and 15 Hz. Decamethyl ferrocene (Fc^*) was used as internal standard. Fc^* has a potential of -610 mV versus Fc/Fc^+ . Arrows show the onset potential and scan direction. The current of the LSV experiment was scaled by a factor of 3 to afford better interpretation.

Table 3.9: Electrochemical data of Al(FcCOCHCOFc)₃ (**9**). Peak anodic potentials, (E_{pa}) are referenced versus the free ferrocene couple, Fc/Fc⁺.

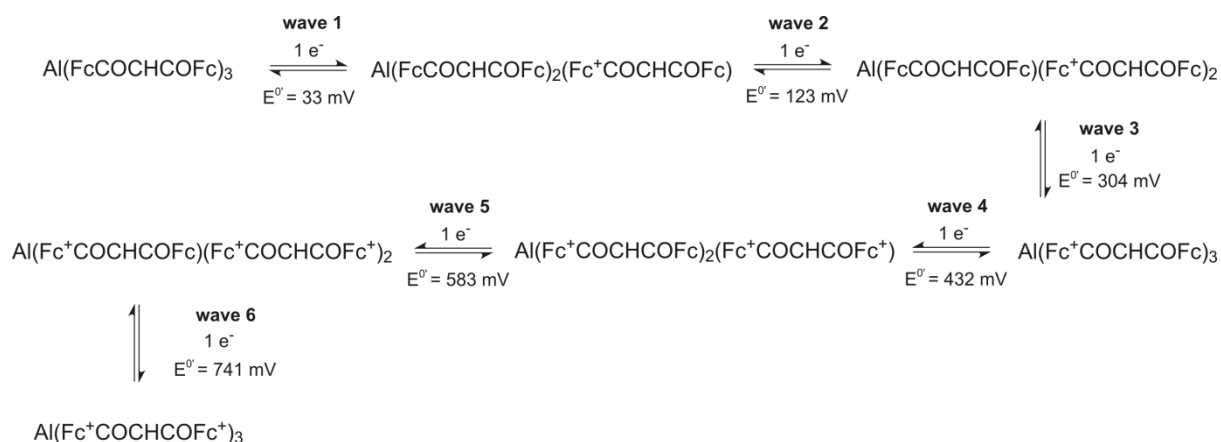
^a v / mV/s	E_{pa} / mV	ΔE_p / mV	$E^{o'}$ / mV	i_{pa} / μ A	i_{pc}/i_{pa} / mV	v / mV/s	E_{pa} / mV	ΔE_p / mV	$E^{o'}$ / mV	i_{pa} / μ A	i_{pc}/i_{pa} / mV
Fc*						Peak 1					
100	-590	58	-619	0.67	0.91	100	64 ^b	62	33	0.36	0.33
200	-586	60	-616	0.88	1.10	200	66 ^b	60	36	0.61	0.55
300	-584	64	-616	1.06	1.11	300	70 ^b	62	39	0.67	0.73
400	-578	68	-612	1.21	1.13	400	76 ^b	64	44	0.91	0.85
500	-580	72	-616	1.45	1.06	500	74 ^b	62	43	1.06	1.03
Peak 2						Peak 3					
100	154	62	123	0.39	1.08	100	340	72	304	0.45	1.07
200	162	70	127	0.70	1.04	200	340	88	296	0.76	1.08
300	166	72	130	1.06	0.91	300	346	92	300	0.97	0.94
400	172	78	133	1.33	0.91	400	348	96	300	1.21	0.98
500	168	76	130	1.45	-	500	350	98	301	1.36	0.98
Peak 4						Peak 5					
100	460	56	432	0.42	0.86	100	614	62	583	-	-
200	464	60	434	0.67	0.91	200	610	70	575	-	-
300	468	66	435	0.97	0.88	300	612	70	577	-	-
400	468	72	432	1.21	0.95	400	616	74	579	-	-
500	470	78	431	1.42	0.96	500	608	70	573	-	-
Peak 6											
100	770	58	741	-	-						
200	770	60	740	-	-						
300	754	64	722	-	-						
400	762	60	732	-	-						
500	772	68	738	-	-						

(a) Symbols are as follows: v = scan rate, E_{pa} = peak anodic potential, E_{pc} = peak cathodic potential, $E^{o'}$ = formal reduction potential, i_{pa} = peak anodic current, i_{pc} = peak cathodic current and ΔE_p = difference in peak anodic and peak cathodic potentials.

(b) Estimated value due to low peak resolution.

(-) Values not determined due to poor resolution.

If one assumes that oxidation of the ferrocenyl groups occur in a sequential way, the voltammograms depicted in **Figure 3.11** may be representative of the following electrochemical scheme:



Scheme 3.11: The electrochemical processes associated with waves 1 – 6 of $\text{Al}(\text{FcCOCHCOFc})_3$ (**9**). E° values are given at a scan rate of 100 mV s^{-1} .

Figure 3.12 provides the CV's of **6** – **9** as an array on top of each other for comparative purposes.

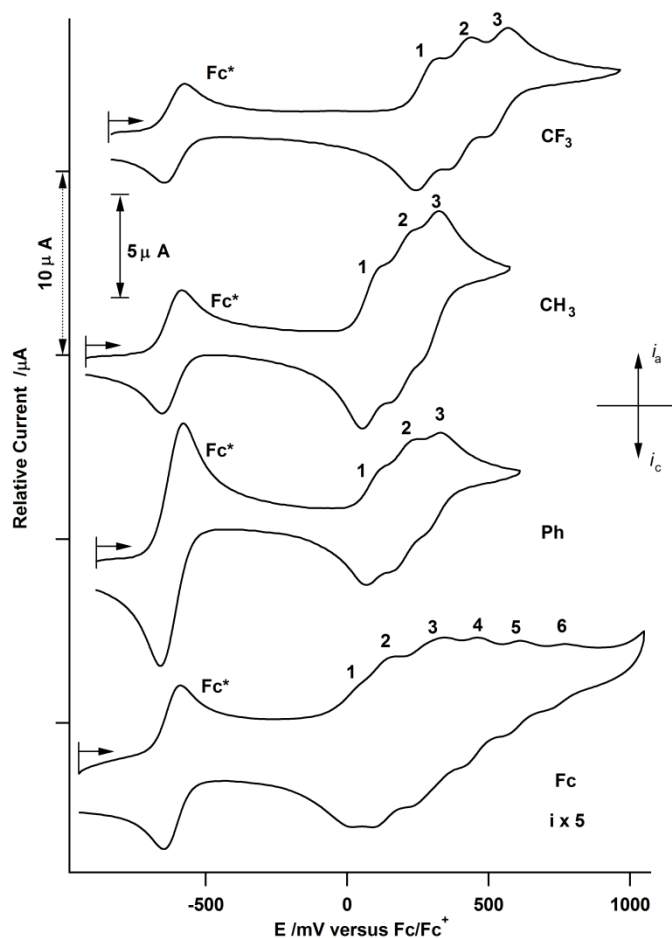
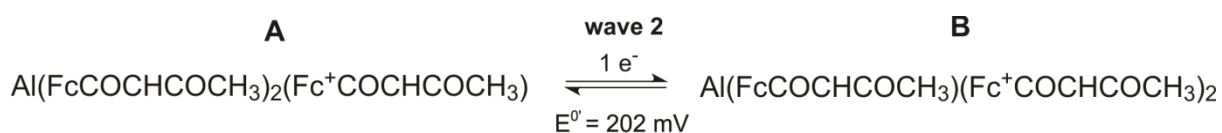


Figure 3.12: Cyclic voltammograms of $\text{Al}(\text{FcCOCHCOR})_3$ $R = \text{CF}_3$ (**6**), CH_3 (**7**), C_6H_5 (**8**) and Fc (**9**) performed at 100 mV/s . Due to the low solubility of $\text{Al}(\text{FcCOCHCOFc})_3$ its signal is scaled by a factor of 5 to allow better visual comparisons between **9** and the other complexes.

For **Figure 3.12** it is clear that $E^{0'}$ values for complexes **6 – 9** span over a huge potential range, from 33 to 738 mV. This can only happen if the electron density of the iron centres in each complex is effectively manipulated by the electron-withdrawing or electron-donating properties of each R-group in **6 – 9**. All other parts of the molecule remains constant (the same) for each compound and is then not the cause for the observed different potentials for all CV peaks. To explain and quantify the observed different potentials, use was made of the group electronegativities of the different R groups. The group electronegativity for each group is $\chi_{Fc} = 1.87$, $\chi_{CH_3} = 2.34$, $\chi_{Ph} = 2.21$, $\chi_{Fc^+} = 2.82$ and $\chi_{CF_3} = 3.01$.¹⁵ An increase in electronegativity of the substituents on the β -diketone ligand generally leads to a higher formal redox potential ($E^{0'}$) in a controlled way. This was well demonstrated on porphyrins (ref. 10). There the authors used the sum of the group electronegativity of the four meso substituents on porphyrins and found a linear relationship between $E^{0'}$ and $(\chi_{R^1} + \chi_{R^2} + \chi_{R^3} + \chi_{R^4})$.

This approach was used on complexes **6 – 9**, first on each complex individually and secondly, for all complexes unified in one relationship. Here the sum of the group electronegativities is always from six components in the tri-ligated complexes $Al(FcCOHCOCHCOR)_3$, i.e. from three ferrocenyl and three R-groups. To explain the approach that was used, consider peak 2 of $Al(FcCOHCOCHCOCH_3)_3$ (**7**) (**Figure 3.8**, p. 83). Peak 2 represents the couple:



The reduced form of the couple is labelled A, and the oxidised form is labelled B. For species A,

$$\sum \chi_R = 2(\chi_{Fc} + \chi_{CH_3}) + (\chi_{Fc^+} + \chi_{CH_3}) = 2(1.87 + 2.34) + (2.82 + 2.34) = 13.58.$$

Thus, a measure of the electron density on the ferrocenyl centre that is to be oxidised at wave 2 for $\text{Al}(\text{FcCOCHCOCH}_3)_3$ is $\sum \chi_R = 13.58$. The sum of electron density associated with the ferrocenyl group being oxidised, was calculated for all electron transfer processes of all the compounds in a similar manner. **Figure 3.13** shows this relationship first for each compound separately (top diagram) and then for all the compounds combined (bottom). Peaks 3, 4, 5 and 6 of $\text{Al}(\text{FcCOCHCOFc})_3$ (**9**) could not be used to fit the combined relationship in **Figure 3.13** (bottom) on p. 97.

In each individual complex a linear relationship between $E^{o'}$ and $\sum \chi_R$ is observed, indicating that greater potential is required to oxidise each successive ferrocene group. The equations predicting $E^{o'}$ from $\sum \chi_R$ for **6** – **9** were found to be:

- for $\text{Al}(\text{FcCOCHCOCF}_3)_3$ (**6**): $E^{o'} = 133.1 \sum \chi_R - 1670$,
- for $\text{Al}(\text{FcCOCHCOCH}_3)_3$ (**7**): $E^{o'} = 108.9 \sum \chi_R - 1285$,
- for $\text{Al}(\text{FcCOCHCOPh})_3$ (**8**): $E^{o'} = 104.2 \sum \chi_R - 1172$ and
- for $\text{Al}(\text{FcCOCHCOFc})_3$ (**9**): $E^{o'} = 151.8 \sum \chi_R - 1694$.

From the top graph in **Figure 3.13** it is clear that $\text{Al}(\text{FcCOCHCOFc})_3$ deviates from the general trend for all four compounds after more than two ferrocenyl groups are oxidised. The large increase in positive charges after two ferrocenyl groups in **9** is oxidised appears to require higher potentials to oxidise the remaining ferrocenyl groups in **this complex**. The equation of the line in the bottom of graph in **Figure 3.13**, is:

$$E^{o'} = 91.525 \sum \chi_R - 1019, \text{ with } R^2 = 0.960,$$

while the equation of the curve is:

$$E^{o'} = 6.313(\sum \chi_R)^2 - 83.53 \sum \chi_R + 179.2, \text{ with } R^2 = 0.972.$$

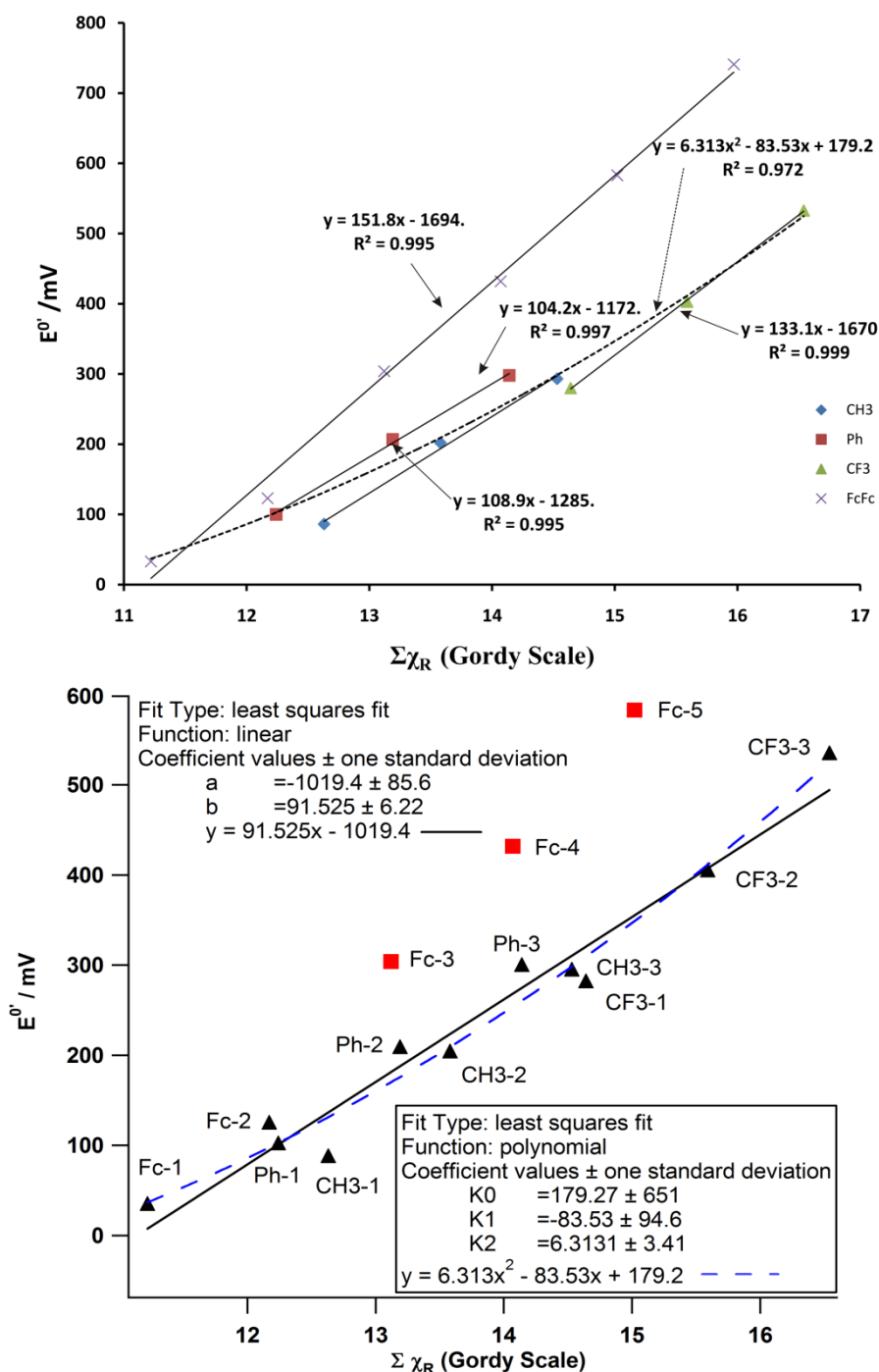


Figure 3.13: The relationship between the sum of the group electronegativities and the formal redox potentials, (a) top: for each compound individually, and (b) bottom: for all the compounds combined. The number following each substituent indicates which ferrocene group is being oxidized or reduced. In the bottom graph, points indicated by ■ were not used in the fitting program. These points represent redox processes 3, 4 and 5 (6 is not shown) of **9**.

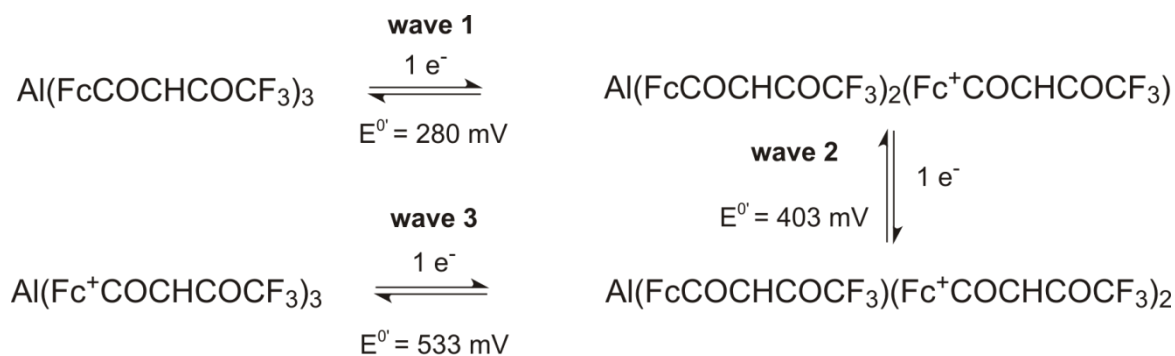
It is clear that the relationship between $E^{0'}$ and $\sum \chi_R$ is almost linear except if excessive charge plays a role (e.g. for **9**, peaks 3 – 6). Thus, it implies that electronic communication between ferrocenyl groups in **6** – **9** is very good.

To decide whether this communication is through-bond, i.e. relayed via the Al^{3+} core, or through-space, a few basic electrostatic calculations were performed on $Al(FcCOCHCOF_3)_3$. To establish a model capable of correlating the crystal structure of **6** with electrochemical communication during oxidation, various assumptions were made, whose verification lies beyond the scope of this research project. These assumptions are:

1. The solid state crystal structure of $Al(FcCOCHCOF_3)_3$ is assumed to be similar to the structure of this compound in solution.
2. It is also assumed that the oxidation of the ferrocenyl groups (Fc/Fc^+) in **6** does not appreciably change the molecular structure, including bond lengths and bond angles.
3. The only charged species in solution to play a role in this model is assumed to be the iron atoms of the ferrocenyl groups of **6**.
4. The iron atoms in the ferrocenyl groups are assumed to be point charges.

Assumption 1 is justified since the 1H NMR (solution) of **6** corresponds to the crystal structure (solid state) of **6**, both indicating the *mer*-isomer to be the only structure present in solution and solid state. It is, however, realised that the solid state structure and the structure in solution can differ, giving slightly different bond lengths and bond angles. The electrochemical experiments are performed in dichloromethane, which is non-coordinating, using tetrabutylammonium tetrakis(pentafluorophenyl)borate, $[NBu_4][B(C_6F_5)_4]$, which is also non-coordinating, as supporting electrolyte. There should then be very little interaction

between anions and cations from the electrolyte and the charged species involving complex **6** that is generated during the electrochemical experiments. This intuitively justifies assumption 3. $\text{Al}(\text{FcCOCHCOF}_3)_3$, (**6**), has three ferrocenyl-related couples, represented by waves 1, 2 and 3 in **Scheme 3.12**.



Scheme 3.12: The electrochemical processes associated with waves 1, 2 and 3 of $\text{Al}(\text{FcCOCHCOF}_3)_3$ (**6**). E° values are given at a scan rate of 100 mV s^{-1} .

In this model, only the oxidation of the ferrocenyl-groups in **6** will be focussed on. The effect of electric field (E) at an iron atom, due to the other two iron atoms, on the formal reduction potential will be examined. In classical Physics the electric field due to a point charge is given by: $E = \frac{1}{4\pi\epsilon_0} \frac{Q}{r^2} \hat{r}$, where Q is the charge of the particle, r is the distance from particle where the field is considered, \hat{r} the unit vector to the evaluation point and ϵ_0 is the permittivity constant ($\epsilon_0 = 8.54187817 \times 10^{-12} \text{ F m}^{-1}$). In order to correlate the electric field to the formal reduction potential (E°), it is first necessary to consider what constitutes E° . If no electronic communication occurred in **6**, then only one ferrocenyl-related peak would have been observed. The E° for such a peak would have been determined by the intrinsic components of the compound, i.e. the electronegativities of the various groups within the molecule other than the ferrocenyl groups. This will not change during any ferrocene-related electron transfer processes. Thus E° has an intrinsic part not determined or

influenced by electronic communication and will be labelled by E_{int} . E_{int} is thus not affected by a change in the charge during the oxidation of ferrocene to ferrocenium (Fc/Fc^+). Since communication is, however, observed it will have to be accounted for in the consideration of $E^{0'}$. It is then assumed that both through-bond and through-space communication can occur. To determine what effect these two types of communication have on $E^{0'}$, the distances between the different iron atoms from the crystal structure of **6** (**Figure 3.6**) will be considered.

The shortest through-bond distances between different Fe-atoms are given by:

$$\begin{aligned} Fe1 - Fe2 &= (Fe(1)-C(11)) + (C(11)-C(004)) + (C(004)-O(1)) + \\ &\quad (O(1)-Al) + (Al-O(4)) + (O(4)-C(008)) + \\ &\quad (C(008)-C(31)) + (C(31)-Fe(2)) \\ &= 13.204 \text{ \AA} \end{aligned}$$

$$\begin{aligned} Fe1 - Fe3 &= (Fe(1)-C(11)) + (C(11)-C(004)) + (C(004)-O(1)) + \\ &\quad (O(1)-Al) + (Al-O(6)) + (O(6)-C(012)) + \\ &\quad (C(012)-C(51)) + (C(51)-Fe(3)) \\ &= 13.276 \text{ \AA} \end{aligned}$$

$$\begin{aligned} Fe2 - Fe3 &= (Fe(2)-C(31)) + (C(31)-C(008)) + (C(008)-O(4)) + \\ &\quad (O(4)-Al) + (Al-O(6)) + (O(6)-C(012)) + \\ &\quad (C(012)-C(51)) + (C(51)-Fe(3)) \\ &= 13.280 \text{ \AA} \end{aligned}$$

The through-space distances are $Fe1 - Fe2 = 10.702 \text{ \AA}$, $Fe1 - Fe3 = 7.031 \text{ \AA}$ and $Fe2 - Fe3 = 9.484 \text{ \AA}$ as indicated in **Figure 3.14**. It is clear that the differences in through-bond distances are small, with a difference of 0.076 \AA between the longest and shortest, in comparison to the differences in through-space distances, where a difference of 3.671 \AA was observed

between the longest and shortest distances. For $\text{Al}(\text{FcCOCHCOCF}_3)_3$ it is thus safe to assume that the through-bond contribution to E^0 is independent of distance and that it is a constant for each electron removed during oxidation. Hence, the through-bond contribution to E^0 is labelled E_b .

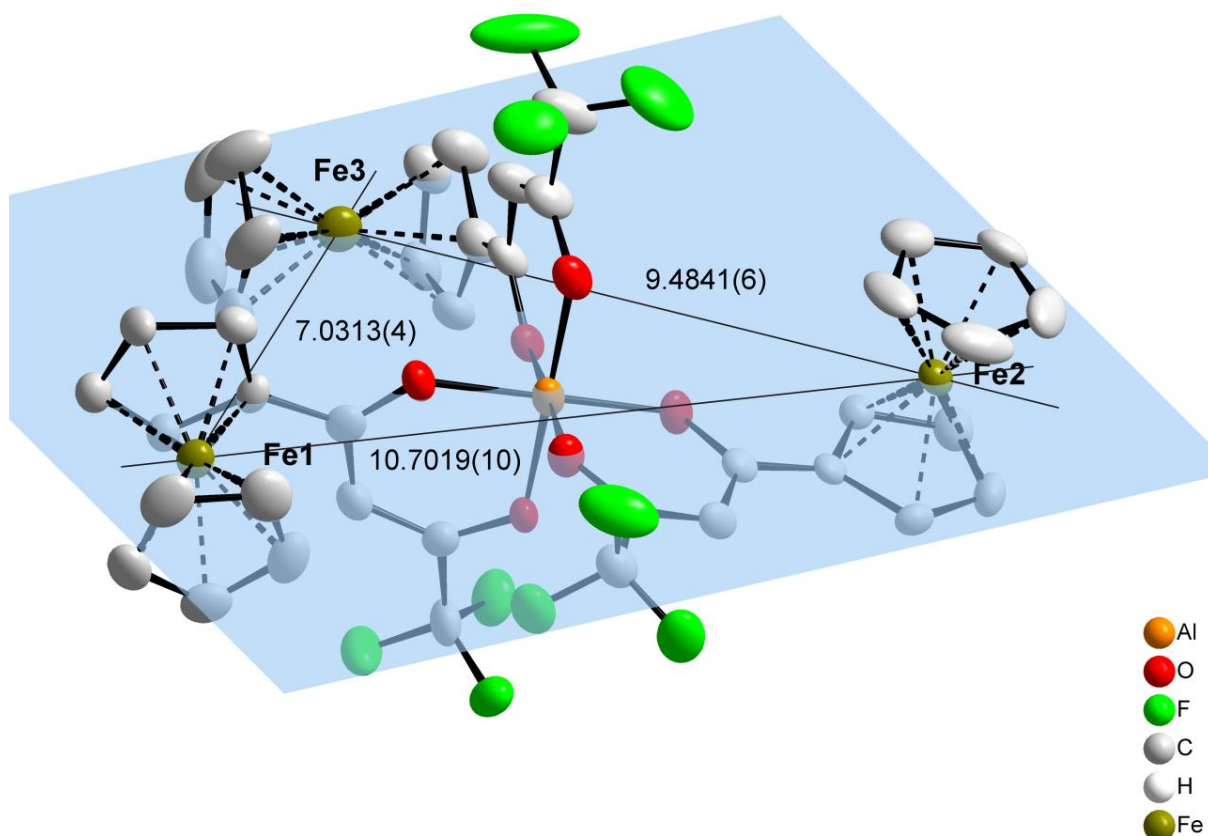


Figure 3.14: The crystal structure of $\text{Al}(\text{FcCOCHCOCF}_3)_3$ showing the through-space distances between the three iron atoms.

The through-space contribution to E^0 is assumed to be proportional to the net electric field at the iron atom being oxidised and is labelled E_s . E_s is defined as $E_s = kE$, where k is some constant to be determined and E is the net electric field. The oxidation of the three ferrocenyl groups in $\text{Al}(\text{FcCOCHCOCF}_3)_3$ can occur in six different orders. The oxidation is illustrated for the order [Fc3, Fc1, and Fc2] in **Figure 3.15**. The calculation process will be shown for this particular order.

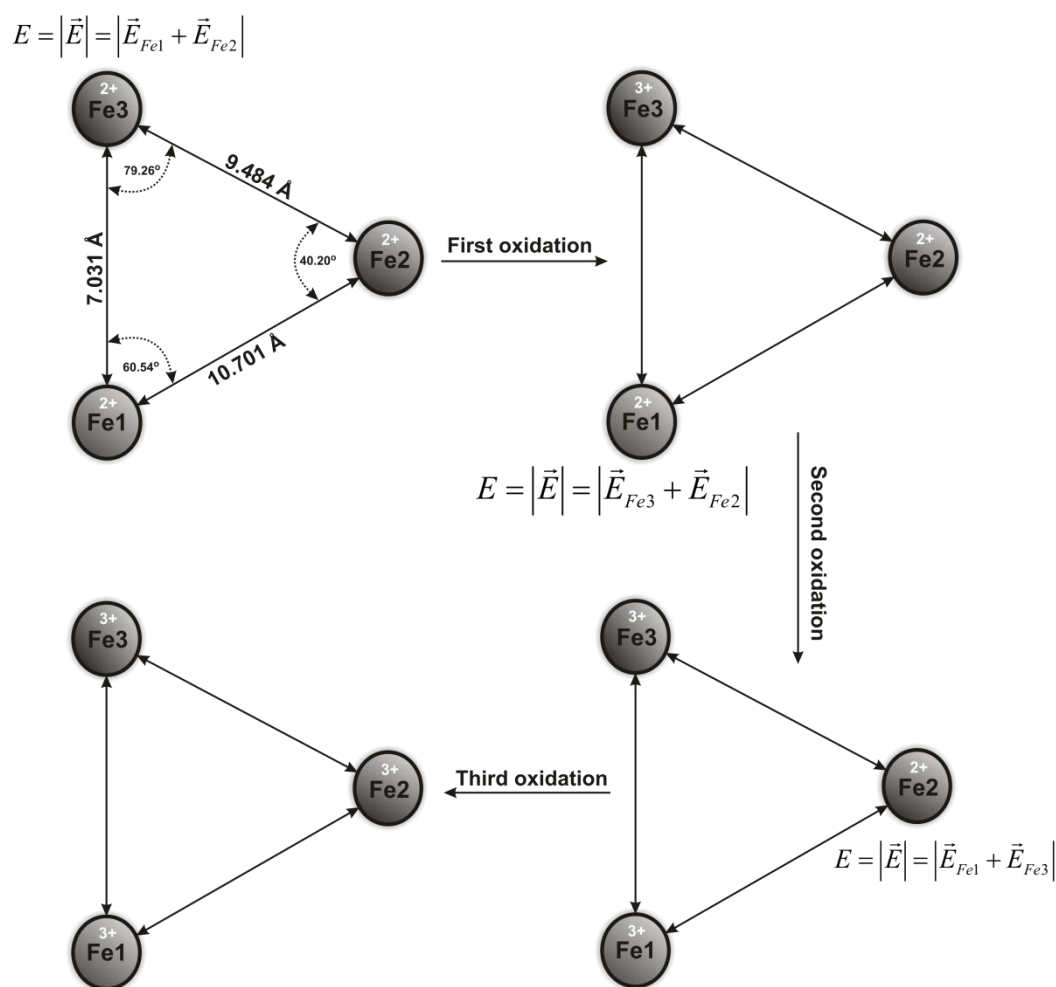


Figure 3.15: The oxidation of the three ferrocenyl groups of $\text{Al}(\text{FcCOCHCOCF}_3)_3$ in the order Fc3, Fc1 and then Fc2. The net electric field is indicated at the iron atom being oxidised in each step.

The equations relating formal reduction potential to electric field for each of the oxidations are given below.

$$\begin{aligned}
 E_{\text{wave1}}^{0'} &= E_s + E_{\text{int}} &= k |\vec{E}_{3,1,2}| + E_{\text{int}} \\
 E_{\text{wave2}}^{0'} &= E_s + E_{\text{int}} + E_b &= k |\vec{E}_{1,2,3^+}| + E_{\text{int}} + E_b \\
 E_{\text{wave3}}^{0'} &= E_s + E_{\text{int}} + 2E_b &= k |\vec{E}_{2,1^+,3^+}| + E_{\text{int}} + 2E_b
 \end{aligned}$$

In these equations, only the absolute value of the electric field at the point is considered, since the direction is not of importance. The first equation has no through-bond communication contribution to $E^{0'}$ since no oxidation has occurred yet and any through-

bond effects that may be present are already included in E_{int} , the intrinsic potential arising from the base compound. The first digit in the subscript of the electric field, e.g. 3 in $\vec{E}_{3,1,2}$, indicates at which ferrocenyl group the electric field is being considered. The second and third numbers in the subscript indicate which ferrocenyl group causes the electric field. Solving for k in these equations gives the equation below.

$$k = \frac{E_{\text{wave3}}^{0'} - 2E_{\text{wave2}}^{0'} + E_{\text{wave1}}^{0'}}{\left| \vec{E}_{2,1^+,3^+} \right| - 2 \left| \vec{E}_{1,2,3^+} \right| + \left| \vec{E}_{3,1,2} \right|} \quad (3.1)$$

Since the $E^{0'}$ values are known from electrochemical experiments, only the electric fields have to be calculated. The calculation of electric field is illustrated below.

$$\begin{aligned} \left| \vec{E}_{3,1,2} \right| &= \sqrt{\left| \vec{E}_{1,3} \right|^2 + \left| \vec{E}_{2,3} \right|^2} \\ &= \sqrt{\left| \frac{1}{4\pi\epsilon_0} \frac{(+2)e}{r_{1,3}^2} \right|^2 + \left| \frac{1}{4\pi\epsilon_0} \frac{(+2)e}{r_{2,3}^2} \right|^2} \\ &= \frac{2e}{4\pi\epsilon_0} \sqrt{\left(\frac{1}{r_{1,3}^2} \right)^2 + \left(\frac{1}{r_{2,3}^2} \right)^2} \end{aligned}$$

$$\begin{aligned} \left| \vec{E}_{1,2,3^+} \right| &= \sqrt{\left| \vec{E}_{1,3} \right|^2 + \left| \vec{E}_{1,2} \right|^2} \\ &= \sqrt{\left| \frac{1}{4\pi\epsilon_0} \frac{(+3)e}{r_{1,3}^2} \right|^2 + \left| \frac{1}{4\pi\epsilon_0} \frac{(+2)e}{r_{1,2}^2} \right|^2} \end{aligned}$$

$$\begin{aligned} \left| \vec{E}_{2,1^+,3^+} \right| &= \sqrt{\left| \vec{E}_{2,1} \right|^2 + \left| \vec{E}_{2,3} \right|^2} \\ &= \sqrt{\left| \frac{1}{4\pi\epsilon_0} \frac{(+3)e}{r_{1,2}^2} \right|^2 + \left| \frac{1}{4\pi\epsilon_0} \frac{(+3)e}{r_{2,3}^2} \right|^2} \\ &= \frac{3e}{4\pi\epsilon_0} \sqrt{\left(\frac{1}{r_{1,2}^2} \right)^2 + \left(\frac{1}{r_{2,3}^2} \right)^2} \end{aligned}$$

In the equations above r is the through-space distance between the iron atoms corresponding to the labels used and e is the charge of an electron. The calculations above were performed for the six different orders of oxidation. The values of all the constants and parameters are shown in **Table 3.10**.

Table 3.10: The calculated electrostatic parameters for the oxidation of $\text{Al}(\text{FcCOCHCOF}_3)_3$.

Order of oxidation	$E_{\text{first}} \times 10^{-9} / \text{N C}^{-1}$	$E_{\text{second}} \times 10^{-9} / \text{N C}^{-1}$	$E_{\text{third}} \times 10^{-9} / \text{N C}^{-1}$	$k \times 10^{-9} / \text{mV C N}^{-1}$	$E_s = kE / \text{mV}$			E_b / mV	$E_{\text{int}} / \text{mV}$
					E_{s1}	E_{s2}	E_{s3}		
A: Fc3 Fc1 Fc2	6.64	9.09	6.10	-1.289	-8.56	-11.7	-7.86	126	289
B: Fc3 Fc2 Fc1	6.64	5.42	9.51	1.315	8.74	7.12	12.51	125	271
C: Fc2 Fc1 Fc3	4.07	6.93	9.96	43.18	175	299	430	-0.8	104
D: Fc2 Fc3 Fc1	4.07	7.54	9.51	-4.633	-18.8	-35.0	-44.1	139	299
E: Fc1 Fc2 Fc3	6.34	4.94	9.96	1.090	6.91	5.39	10.86	125	273
F: Fc1 Fc3 Fc2	6.34	9.30	6.10	-1.136	-7.21	-10.57	-6.93	126	287

E = electric field at the iron atom being oxidised; k = constant relating electric field to potential; E_b = through-bond potential; E_{int} = intrinsic potential;

a = paths A, D and F is impossible because k cannot be negative, see discussion in text.

b = Path C is impossible because electron-withdrawing substituent cannot lower E^{O} as a negative E_b value imply.

Only some of the oxidation pathways (orders) produced valid values. Since the electrostatic effects created by more positive charges on the molecule after oxidation cannot decrease the formal reduction values – experimentally E^{O} increased successively for waves 1 through 5 – negative k values are not possible. This shows that pathways **A**, **D** and **F** are not possible. Pathway **C** shows a small negative value for the through-bond potential contribution. It cannot have a negative value as it is impossible for electron withdrawing substituents to lower the formal reduction potential. This leaves **B** and **E** as possible pathways. However, these pathways are nearly identical, each involving an initial oxidation

of one of the two ferrocenyl groups in the same plane (Fc1, Fc3), followed by the oxidation of Fc2, which is perpendicular to the plane and finally oxidising the remaining ferrocenyl group in the plane. This is expected from an electrostatic viewpoint since Fe1 and Fe3 are closest to one another.

The largest contribution to $E^{0'}$ by electrostatic considerations in one of the valid pathways (**B** or **E**) is $E_{s3} = 12.51$ mV for the third oxidation (Fc1) of pathway **B** (**Table 3.10**), which is significantly smaller than the through-bond contribution of 125 mV. This clearly indicates that the electronic communication between the ferrocenyl moieties of $\text{Al}(\text{FcCOCHCOF}_3)_3$, occurs primarily through bonds and not through space. This result may differ in other complexes where the distance between Fe-atoms may be much smaller than in $\text{Al}(\text{FcCOCHCOF}_3)_3$ because through-space interactions between charged species are inversely proportional to the distance between them.

This then concludes the electrochemical characterisation of the ferrocene-containing β -diketonato complexes of aluminium(III) and achieves goal 3 in Chapter 1. The extensive communication between the ferrocenyl groups of $\text{Al}(\text{FcCOCHCOF}_3)_3$ predicted by examination of the crystal structure thereof, was also proved and quantified.

3.2.6. The cytotoxicity of ferrocene-containing β -diketonato complexes of aluminium(III)

In fulfilment of goal 4 (Chapter 1), the four ferrocene-containing β -diketonato complexes of aluminium were subjected to cytotoxic studies to determine any potential anti-cancer activity. Unfortunately a saturated solution of $\text{Al}(\text{FcCOCHCOPh})_3$ (**8**) and $\text{Al}(\text{FcCOCHCOFc})_3$

(9) was still too diluted to register any cytotoxicity. The solubility of $\text{Al}(\text{FcCOCHCOCF}_3)_3$ (6) and $\text{Al}(\text{FcCOCHCOCH}_3)_3$ (7) was, however, sufficient for cytotoxic determinations. Human cervix epitheloid cancer cells, HeLa, were used for cytotoxic tests at a concentration of 500 cells well^{-1} . Since cisplatin (diamminodichloroplatinum(II)) is the most widely used metal-containing anti-cancer drug of all time, results of the present series of aluminium- and iron-containing drugs are benchmarked against it. The mean drug concentration from three experiments causing 50% cell growth inhibition, i.e. IC_{50} , is shown in Table 3.11 for a drug incubation period of 7 days. The IC_{50} value of $\text{Al}(\text{FcCOCHCOCF}_3)_3$ (6) was $10.6 \mu\text{mol dm}^{-3}$, indicating significant cytotoxic activity. $\text{Al}(\text{FcCOCHCOCH}_3)_3$ (7) was found to be much less active with $\text{IC}_{50} > 50 \mu\text{mol dm}^{-3}$. However, even 6 is still at least one order of magnitude less cytotoxic than cisplatin. The effect of an increased drug concentration on the cancer cell growth for cisplatin and $\text{Al}(\text{FcCOCHCOCF}_3)_3$ (6) is shown in Figure 3.16.

Table 3.11: Chemosensitivity for the complexes represented by IC_{50} ($\mu\text{mol dm}^{-3}$) after incubation for 7 days with HeLa cancer cell lines and lymphocytes (resting and stimulated), with cell concentrations of 500 cells well^{-1} . IC_{50} values of the free β -diketones were obtained from literature.

Complex	HeLa		Lymph (resting)		Lymph (stimulated)		Tumour specificity ^b
	IC_{50} / μM	\pm SEM	IC_{50} / μM	\pm SEM	IC_{50} / μM	\pm SEM	
$\text{Al}(\text{FcCOCHCOCF}_3)_3$ (6)	10.6	0.548	50	-	50	-	4.7
$\text{Al}(\text{FcCOCHCOCH}_3)_3$ (7)	>50	-	-	-	-	-	-
$\text{FcCOCH}_2\text{COCF}_3$ ^a	6.8	-	-	-	83.1	-	12.2
$\text{FcCOCH}_2\text{COCH}_3$ ^a	66.6	-	-	-	-	-	-
Cisplatin	0.9	0.1	30	11	21	13	25.3

a: Values from J. C. Swarts, T. G. Vosloo, S. J. Cronje, W. C. du Plessis, C. E. J. van Rensburg, E. Kreft and J. E. Van Lier, Submitted *Anticancer Res.*, 2008.

b: Tumour specificity = Lymph IC_{50} / HeLa IC_{50}

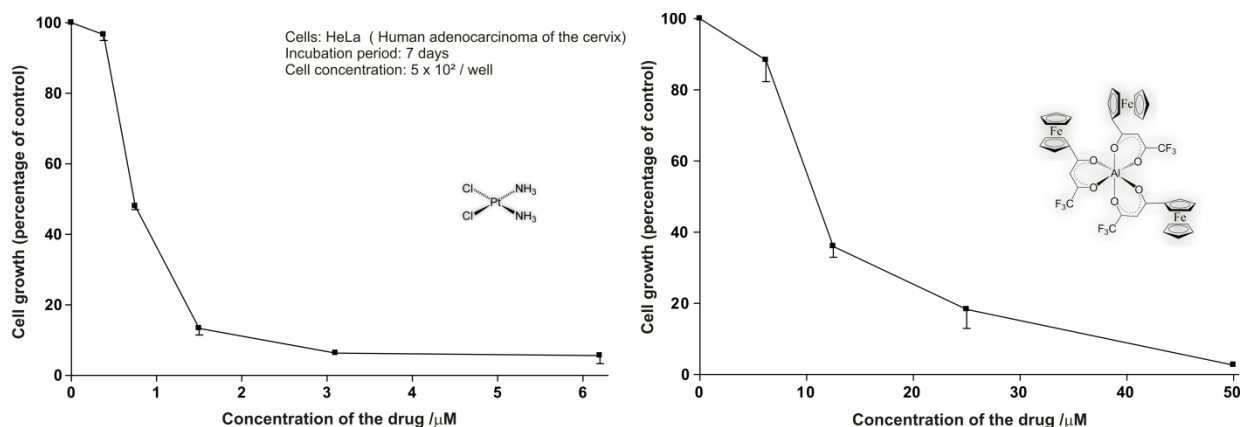


Figure 3.16: The effect of an increased drug concentration on the cancer cell growth for cisplatin (left) and $\text{Al}(\text{FcCOCHCOCF}_3)_3$ (**6**) (right).

The IC_{50} value of $\text{Al}(\text{FcCOCHCOCF}_3)_3$ (**6**) ($\text{IC}_{50} = 10.6 \mu\text{M}$) is also higher than the IC_{50} value of free FcCOCHCOCF_3 ($\text{IC}_{50} = 6.8 \mu\text{M}$) obtained from literature¹⁵ as shown in **Table 3.11**. It is important to realise that an effective cytotoxin for anti-cancer purposes should have high activity against cancer cells, whilst having low activity against stimulated lymphocytes. The tumour specificity for **6**, which was determined as $\text{Lymph IC}_{50} / \text{HeLa IC}_{50} = 50 / 10.6 = 4.7$, and is also lower than the specificity of cisplatin (25.3) and free FcCOCHCOCF_3 (12.2).

The percentage cell growth inhibition for $\text{Al}(\text{FcCOCHCOCF}_3)_3$ at $10 \mu\text{M}$ drug concentration is lower than the inhibition of free $\text{FcCOCH}_2\text{COCF}_3$ at both 10 and $30 \mu\text{M}$. If aluminium had a synergistic effect in $\text{Al}(\text{FcCOCHCOCF}_3)_3$, the cell growth inhibition would have been greater than three times the inhibition of free $\text{FcCOCH}_2\text{COCF}_3$. It is concluded that aluminium had an inhibiting effect on ferrocene-containing β -diketonato cytotoxicity. The Al complexes show far lower cell growth inhibition than a single equivalent of FcCOCHCOCF_3 , as shown in **Figure 3.17**.

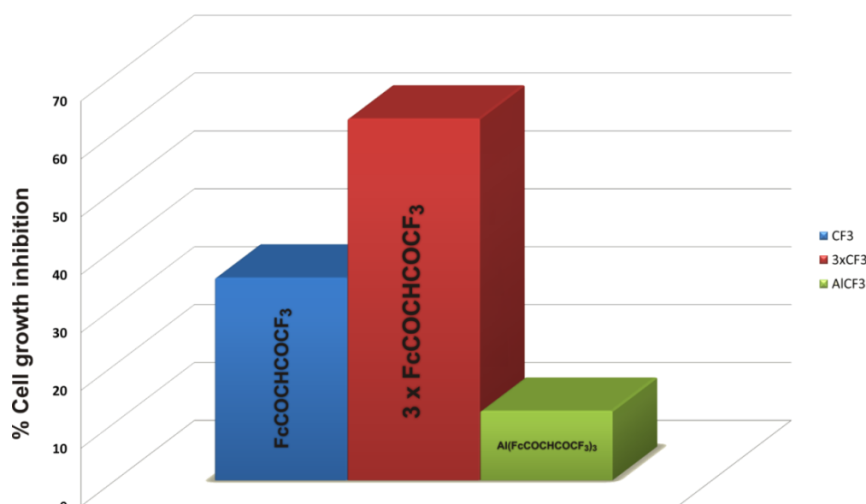


Figure 3.17: The comparison of percentage cell growth inhibition for free $\text{FcCOCH}_2\text{COCF}_3$ at concentrations of 10 μM (blue) and 30 μM (red) with $\text{Al}(\text{FcCOCHCOCF}_3)_3$ at 10 μM complex concentration. This gives an effective FcCOCHCOCF_3 concentration (green) of 30 μM . The low cell growth inhibition of $\text{Al}(\text{FcCOCHCF}_3)_3$ (green) compared to the free ligand clearly illustrate the inhibiting effect of aluminium on cytotoxicity.

Low solubility in biological media is a major drawback of the present series of aluminium complexes. Better solubility in aqueous-based biological media may be achieved by oxidising one or more of the ferrocenyl-moieties into the cationic (positively charged) ferrocenium species. It is concluded that the coordination of the β -diketones to aluminium has an inhibiting effect on the cytotoxicity of β -diketones and that β -diketonato complexes of aluminium are not suitable cytotoxins for anti-cancer treatment. Goal 4, to evaluate the cytotoxicity of ferrocene-containing β -diketonato aluminium(III) compounds, has now been completed.

3.2.7. Conclusion

This concludes the section on ferrocene-containing β -diketonato complexes of aluminium.

Goals 1 – 4, as defined in chapter 1, have now been addressed and achieved.

3.3. Aluminium Carboxylates

3.3.1. Introduction

In addition to ionic bonds, especially three types of coordination modes are considered possible for carboxylato complexes of aluminium, namely bidentate, monodentate and bridging coordination (**Figure 3.18**). The bidentate coordination mode of carboxylates can be divided into two categories, symmetric and asymmetric chelation. The existence of bidentate chelation of carboxylates of aluminium was confirmed in literature (Chapter 2, p. 49) and IR studies have been interpreted to indicate that aluminium tricarboxylates can exist in a bidentate coordination mode.¹⁶ Bridging coordination is however more abundant and appear to be more stable due to less ring strain. Its existence has also been confirmed by single crystal X-ray structure determination.¹⁷

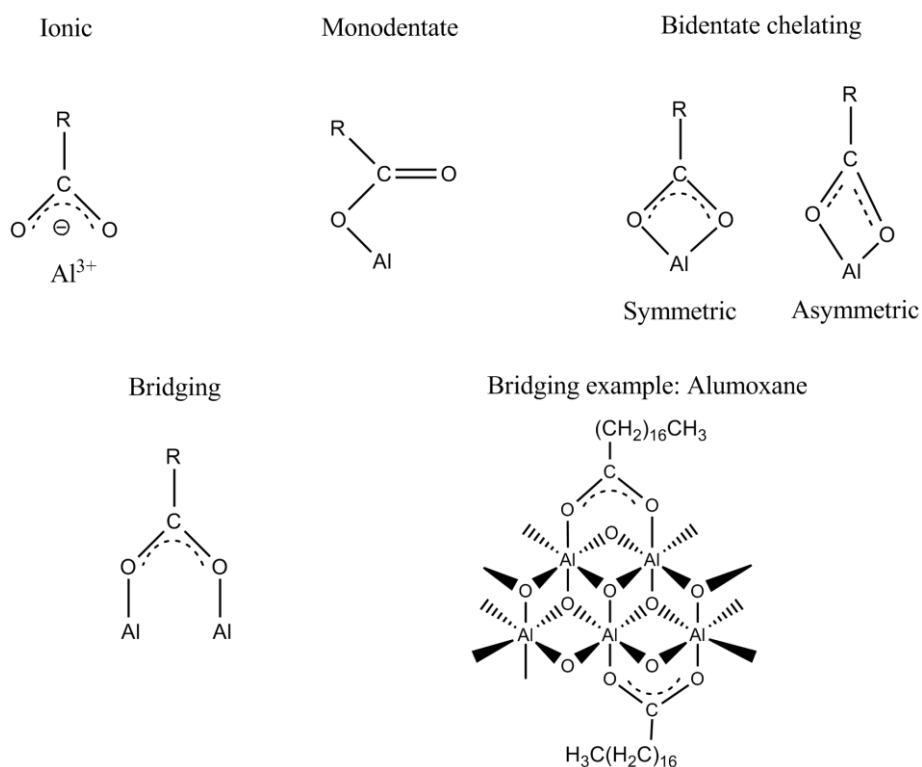


Figure 3.18: Important types of Al-coordination observed for the carboxylate group.

Due to low solubility of many aluminium carboxylate complexes, solution-based characterisation techniques like NMR are generally not useful. In contrast, solid state infrared spectroscopy is a quick and convenient method for characterising aluminium carboxylates. For structural determination of metal carboxylate complexes via infrared, there are three infrared stretching frequency bands of interest. The first two bands are the antisymmetric and symmetric carbonyl stretching bands, located between 1700 and 1400 cm^{-1} . The difference between these two bands ($\nu_{\text{symmetric}} - \nu_{\text{antisymmetric}}$) is defined as $\Delta\nu$. The third stretching band of importance is the metal-oxygen stretching band, occurring at ca. 980 cm^{-1} for aluminium. This study has as its goal to show how multiple peaks in this region can be used to distinguish between different types of metal-oxygen coordination bonds.

To achieve this, firstly, the infrared properties of monocarboxylic acids will be examined. Secondly, results from a preliminary computational investigation will be discussed as to establish some of the feasible coordination modes of carboxylic acids to aluminium. Finally, a series of aluminium carboxylates were synthesised and characterised by infrared spectroscopy (FTIR) and elemental analysis. Results will be used to predict the possible binding modes and structures of these compounds.

3.3.2. FTIR characterisation of monocarboxylic acids

For the intended synthesis of aluminium carboxylates a range of monocarboxylic acids were envisaged as ligands. The carbon chain length of acids varied from one, formic acid, to eighteen, stearic acid. Ferrocenoic acid was also used as a coordinating ligand. Since the infrared spectra of carboxylic acids and complexes thereof have been studied extensively in

literature, this technique was deemed suitable for their study.^{18,19} The infrared spectra of carboxylic acids have five frequency regions of interest.

- Normally, carboxylic acids show a strong, broad band for O-H stretching in the region $3300 - 2500 \text{ cm}^{-1}$. C-H stretching of alkyl and aromatic groups also occurs in this region, but usually as sharper, narrower signals. The broad O-H band is superimposed on the C-H stretching signals. The occurrence of carboxylic acids as hydrogen-bonded dimers leads to the O-H band being broad.
- The most important signal is the carbonyl stretching band (C=O). This band is usually very intense and occurs in the region ranging from $1760 - 1690 \text{ cm}^{-1}$ and changes here upon coordination will be used to determine the coordination mode later on in this chapter. The position of the carbonyl band depends on the type of carboxylic acid especially in terms of electron withdrawing or electron donating R-groups in RCOOH, as well as the presence of internal hydrogen bonding.
- C-O stretching is observed in the region $1320 - 1210 \text{ cm}^{-1}$.
- O-H bending occurs between $1440-1395 \text{ cm}^{-1}$ and $950 - 910 \text{ cm}^{-1}$. The $1440 - 1395 \text{ cm}^{-1}$ band may not be visible due to C-H bending bands also occurring in this region.

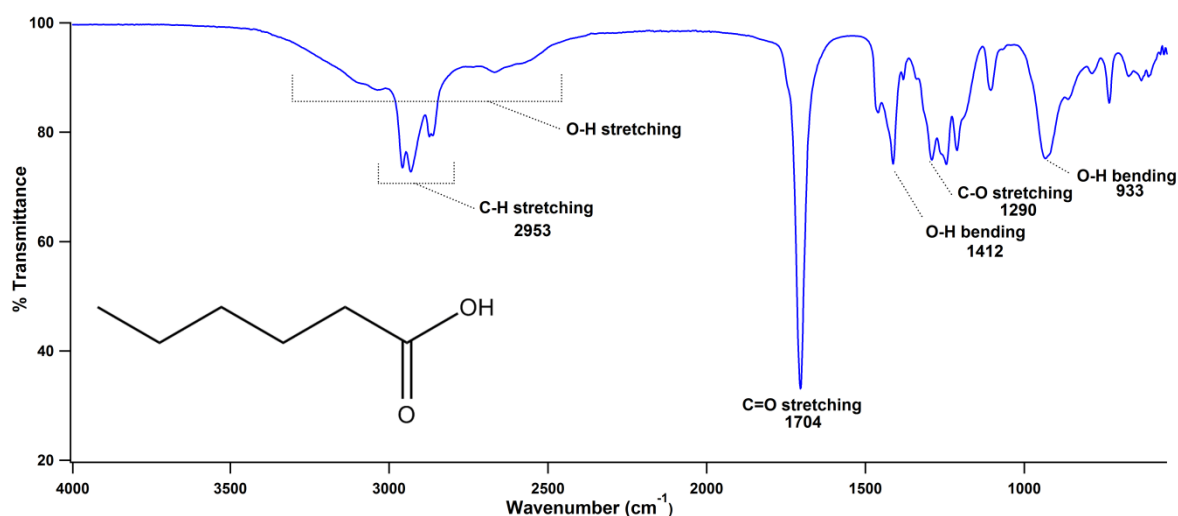


Figure 3.19: The infrared spectrum of hexanoic acid. Key bands are indicated.

The infrared spectra of a series (C_1 - C_{18}) of different commercial carboxylic acids were acquired and are shown in **Figure 3.20**. Three trends can be observed from the spectra. The first would be the increase in the intensity of the C-H stretching bands in the $3100 - 2700$ cm^{-1} region as the chain length increases, due to the increase in the amount of C-H bonds present in the longer carboxylic acids.

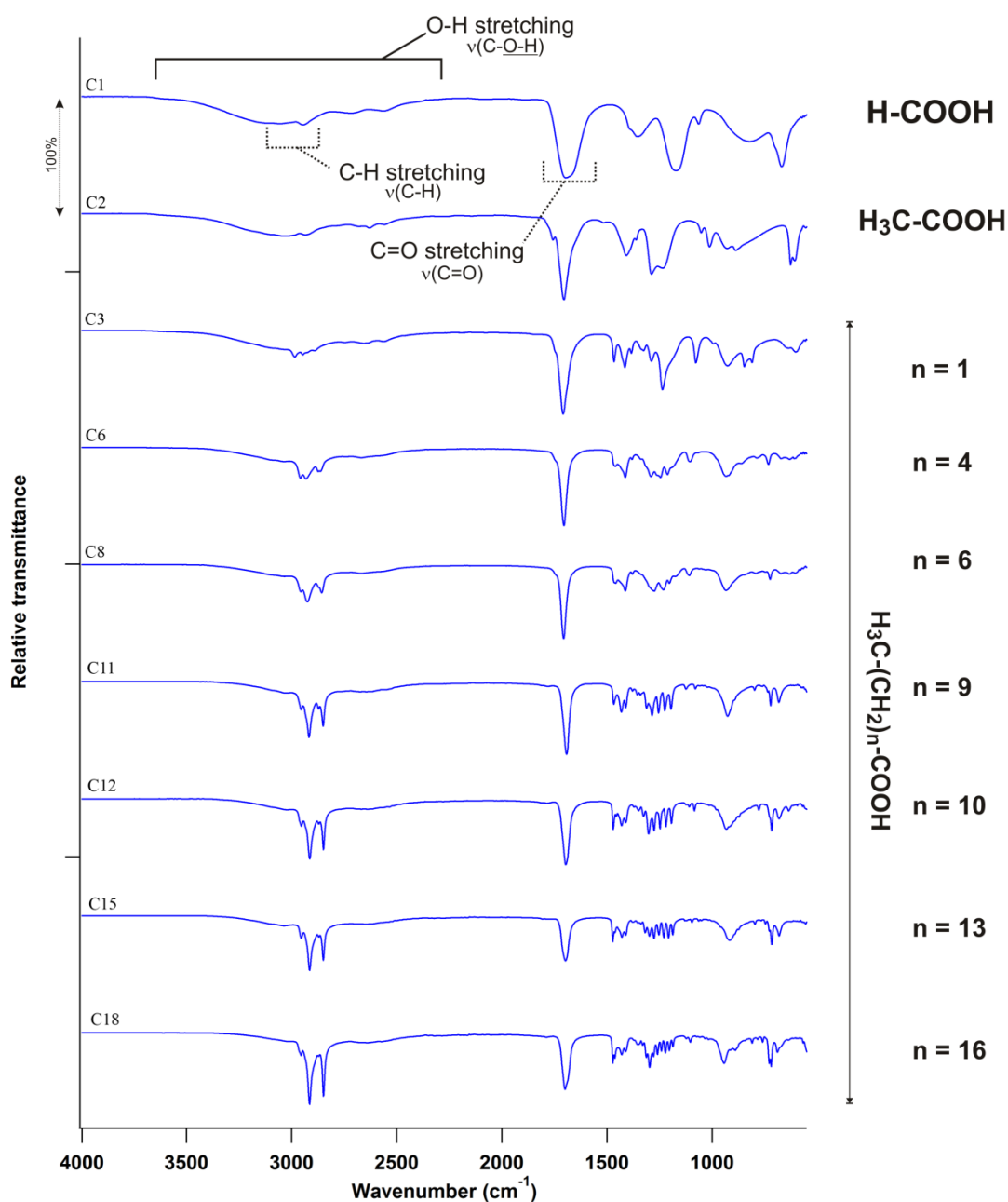


Figure 3.20: The infrared spectra of various commercial monocarboxylic acids, $\text{H}_3\text{C}(\text{CH}_2)_n\text{COOH}$.

Table 3.12: The infrared frequency bands of interest in carboxylic acids.

Acid	C-H stretching ^a (cm ⁻¹)	C=O stretching (cm ⁻¹)	C-O stretching (cm ⁻¹)	O-H bending (cm ⁻¹)
Formic (C1)	-	1696	1171	1354 820 ^b
Acetic (C2)	3039	1704	1234	1407 929
Propionic (C3)	2985	1708	1235	1414 926
Hexanoic (C6)	2931	1704	1291	1412 933
Octanoic (C8)	2925	1706	1275	1413 933
Undecanoic (C11)	2917	1692	1285	1431 925
Dodecanoic (C12)	2914	1696	1302	1430 931
Pentadecanoic (C15)	2914	1697	-	1428 916
Octadecanoic (C18)	2914	1699	1297	- 942

a: Middle of C-H stretching band is used for value.

b: Estimated value due to broad peak.

-: No value due to overlapping

The second trend is the numerical decrease in the C-H stretching frequencies (i.e. wavenumbers measured in cm⁻¹) with an increase in chain length (**Figure 3.21, Table 3.12**).

Thirdly, there is also an increase in numerical value of the C-O stretching frequency as the chain length increases (**Figure 3.22, Table 3.12**).

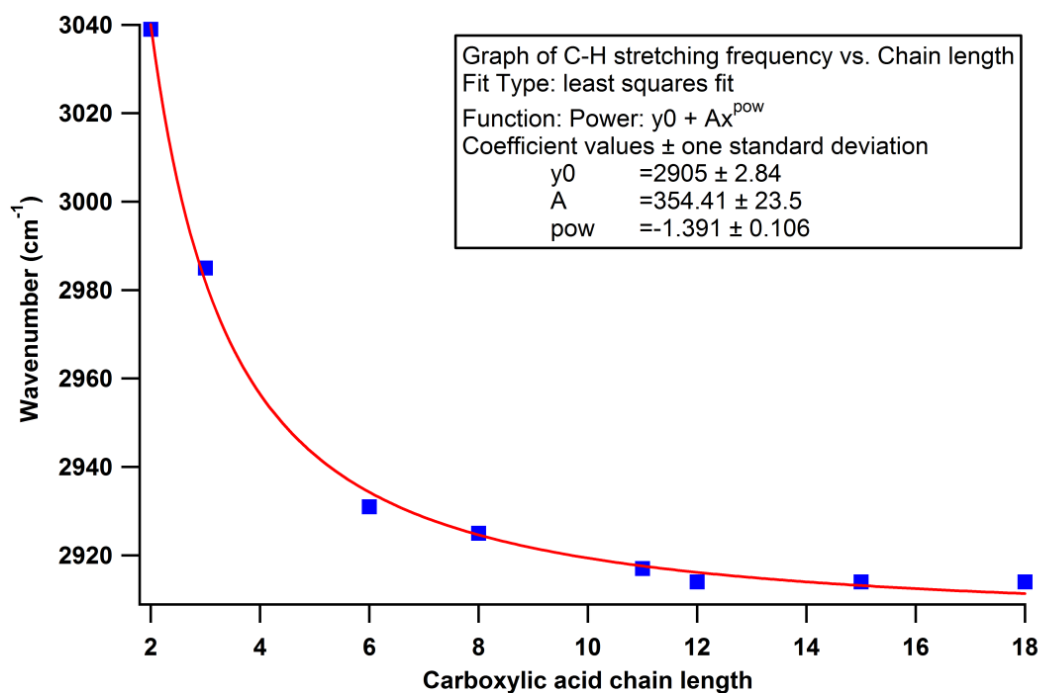


Figure 3.21: Graph of C-H stretching frequency versus carboxylic acid chain length. Data was fitted using a power function.

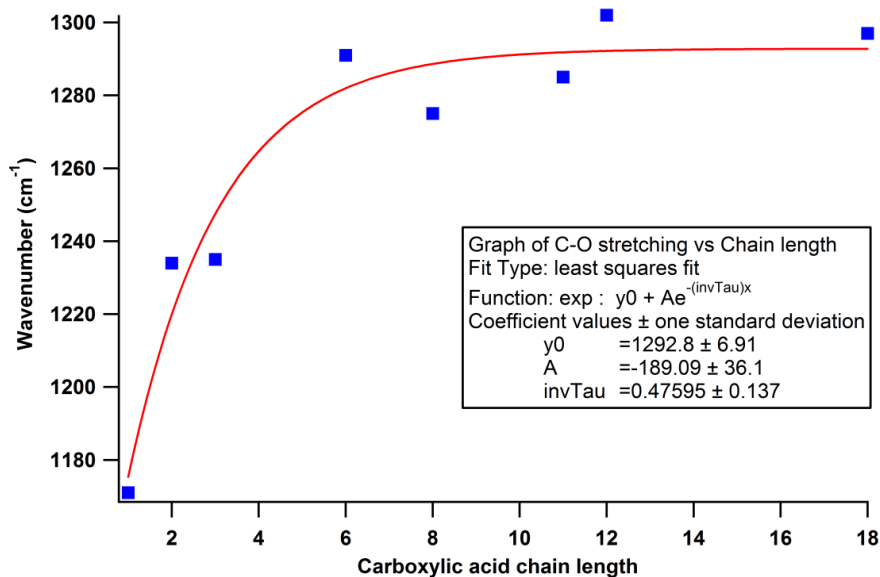


Figure 3.22: Graph of C-O stretching frequency versus carboxylic acid chain length. Data was fitted using an exponential function.

These trends are due to an increase in electron donation as the alkyl chain lengths increase. The effect does become less measurable at longer chain lengths, see **Figure 3.21**. The enhanced capacity of short chain acids over long chain acids to be involved in extended three-dimensional hydrogen bonding networks may also contribute to these observations.

The fitted equations in **Figure 3.21** and **Figure 3.22** can be used to determine the carboxylic acid chain length from C-H or C-O stretching frequencies. According to these fits,

$$\nu(C-H) = 2905 + 354n^{-1.391} \quad (3.2)$$

and

$$\nu(C-O) = 1293 - 189e^{-0.476n}, \quad (3.3)$$

where n is the number of C-atoms in the carboxylic acid with formula $H_3C-(CH_2)_xCOOH$, $n = x + 2$. Equation (3.2) is more accurate than equation (3.3) and it is more reliable for acids with chain lengths less than ten carbon atoms.

There is no marked difference in the C=O stretching bands of the carboxylic acids of various chain lengths and thus the C=O bands cannot be used to distinguish between the different

acids. The C=O bands will, however, change significantly upon coordination to aluminium(III) and the above data in **Table 3.12** can be used to determine whether coordination has occurred and if any uncoordinated acid is still present within a particular aluminium carboxylate complex.

3.3.3. Computational investigation of aluminium carboxylates

3.3.3.1. Introduction

An initial quantum chemical computational investigation was performed firstly to determine which bonding modes of carboxylic acids are feasible and secondly to identify the stable and preferred coordination spheres of aluminium carboxylates. The infrared spectra of aluminium carboxylates with different bonding modes was predicted by quantum chemical computations to aid in the assignment of the bonding modes deduced from infrared spectra of the aluminium carboxylates synthesised in the next section. The overall result of this research program may then be used to create a FTIR method to qualitatively distinguish between different bonding modes in aluminium carboxylate complexes, as per goal 6 in Chapter 1, and also to propose structures for the synthesised aluminium carboxylates.

3.3.3.2. Theoretical Approach

Density Functional Theory (DFT) calculations were carried out using the Amsterdam Density Functional 2007 (ADF) program system²⁰ with the PW91 (Perdew-Wang, 1991) exchange and correlation functional.²¹ To verify the performance of the PW91 functional, the OLYP²² (OPTX exchange functional combined with the Lee-Yang-Parr correlation functional^{23, 24})

GGA (Generalized Gradient Approximation) was also used for all the geometry optimizations. The TZP (Triple ζ polarized) all electron basis set, a fine mesh for numerical integration (5.5 for geometry optimizations and 6.0 for frequency calculations), a spin-restricted (gas-phase) formalism and full geometry optimization with tight convergence criteria as implemented in the ADF 2007 program, were used. The Gaussian full geometry optimization was done with tight convergence criteria as implemented in the Gaussian program package, version 03,²⁵ using the B3LYP²⁶ (B3 Becke 3-parameter exchange and Lee-Yang-Parr correlation) functional and the 6-311G(d,p) basis set for both exchange and correlation. The accuracy of the computational method was evaluated by comparing the root-mean-square deviations (RMSD's) between the optimized quantum mechanical determined molecular structures and experimentally determined crystal structures, using the non-hydrogen atoms in the molecule. RMSD values were calculated using the "RMS Compare Structures" utility in ChemCraft Version 1.5.²⁷ No symmetry limitations were imposed on the calculations.

3.3.3.3. Computational results and discussion

The reliability of the computational approach was confirmed by theoretically computing the structures of dialkylaluminium carboxylates $[(^t\text{Bu})_2\text{Al}(i\text{-O}_2\text{C}^t\text{Bu})]_2$ (**14**), $[(^t\text{Bu})_2\text{Al}(i\text{-O}_2\text{CPh})]_2$ (**15**), $[(^t\text{Bu})_2\text{Al}(i\text{-O}_2\text{CCH}_2\text{Ph})]_2$ (**16**) and $[(^t\text{Bu})_2\text{Al}(i\text{-O}_2\text{CCH}_2\text{-OCH}_2\text{CH}_2\text{OCH}_3)]_2$ (**17**) and comparing the calculated data with known single crystal X-ray diffraction structural data of the dialkylaluminium carboxylates as shown in **Table 3.13**.²⁸ The root-mean-square distances (RMSD) calculated for non-hydrogen atoms for the best three-dimensional superposition of calculated structures on experimental structures give a qualitative measurement of the accuracy of the ground state geometry of the calculated structures.

Table 3.13: Selected calculated and experimental bond lengths (Å) and angles (°) for the complexes (14) - (17).

Complex									
	(14)		(15)		(16)		(17)		
Program Method	ADF	ADF	ADF	ADF	ADF	ADF	ADF	ADF	
Functional	DFT	DFT	DFT	DFT	DFT	DFT	DFT	DFT	
Basis set	PW91	OLYP	PW91	OLYP	PW91	OLYP	PW91	OLYP	
	TZP	TZP	TZP	TZP	TZP	TZP	TZP	TZP	
Bond Length Range (Å)	X-Ray	Gaussian	X-Ray	Gaussian	X-Ray	Gaussian	X-Ray	Gaussian	
		B3LYP		B3LYP		B3LYP		B3LYP	
		6-311		6-311		6-311		6-311	
		G(d,p)		G(d,p)		G(d,p)		G(d,p)	
Al-O	1.809	1.852-1.878-1.878-1.884	1.809-1.811	1.852-1.873-1.873-1.876	1.806-1.809	1.861-1.886	1.767-1.835	1.842-1.901	1.853-1.889
Al-C	1.960	2.007-2.029-2.031	1.960-1.966	2.004-2.025-2.026	1.944-1.976	2.000-2.022-2.006	1.939-1.994	2.003-2.019-2.023	2.004
O-C	1.236	1.272-1.269-1.273	1.253-1.259	1.275-1.276	1.226-1.249	1.267-1.272	1.249-1.253	1.260-1.273	1.250-1.264
O-Al-O	107.70	109.65-107.4-108.54	107.80-107.81	109.55-1.873-1.876	106.52-106.52	108.12-105.91	105.49-105.53	103.88-103.66	102.21-102.22
O-Al-C	105.83-106.25	105.04-105.51-105.79	105.15-106.81	104.69-106.88	105.02-106.68	103.95-104.61	104.49-107.14	105.82-107.45	105.46-107.87
O-C-O	122.2	123.99-124.00	122.72-122.74	123.83-123.87	123.3	125.07-125.08	124.00-124.06	125.46-125.75	125.16-125.17
RMSD	-	0.08 0.11 0.28	-	0.08 0.14 0.38	-	0.10 0.19 0.41	-	0.12 0.18 0.37	

Excellent agreement between experimental and theoretical structures is obtained as reflected by the RMSD values (H excluded) of 0.08 - 0.19, depending on the functional used (**Table 3.13**). The smallest difference between calculated and experimental Al-O bond lengths was 0.043 Å (DFT PW91) in the structure of **(14)**. The largest difference concerning Al-O bonds was 0.104 Å (DFT OLYP) for **(17)**. All the computed Al-O bond lengths are slightly longer than the experimental bond lengths, with a difference of 2 – 6%.

From the above summarised structural comparisons it is clear that all theoretical calculations mostly repeated experimentally determined structural results at a 94% level and higher. As may further be seen in **Table 3.13** the methods that gave the smallest root mean square deviations from the crystal structures, and therefore the closest representation of experimental structural data, are the methods using the PW91 functional. Structural data computed with the ADF/PW91/TZP model for related compounds may be presented with an extrapolative equally high degree of accuracy.

As explained earlier, the reason for this study is to determine whether the coordination mode encountered in aluminium carboxylates is monodentate, bidentate or bridging. In a first approach towards this goal, the relative energy of the three ferrocene-containing aluminium carboxylates, **(18)**, **(19)** and **(20)** were calculated, as shown in **Figure 3.23**. These structures were identified as leading possible structures from literature searches.

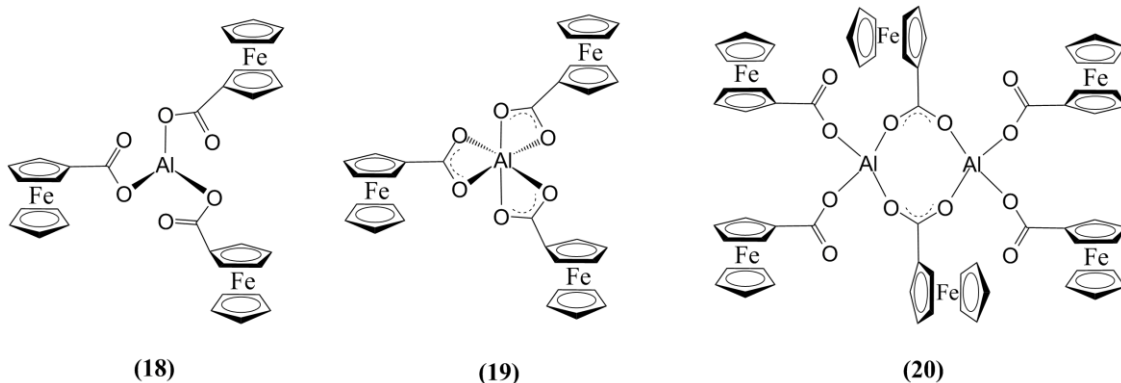


Figure 3.23: Complexes **(18)**, **(19)** and **(20)** that was studied computationally to determine the carboxylate coordination modes to aluminium.

All starting geometries for **(18)** gave as lowest energy geometry the geometry of **(19)**. No solution could be found with all three the carboxylate groups being monodentate. This suggests that most if not all speculated literature structures where Al-carboxylates are proposed as consisting of only three mono-coordinated ligands are probably wrong. Solutions were obtained where one or two of the carboxylate groups is monodentate as illustrated below (**Figure 3.24**), but these solutions were higher in energy than **(19)**.

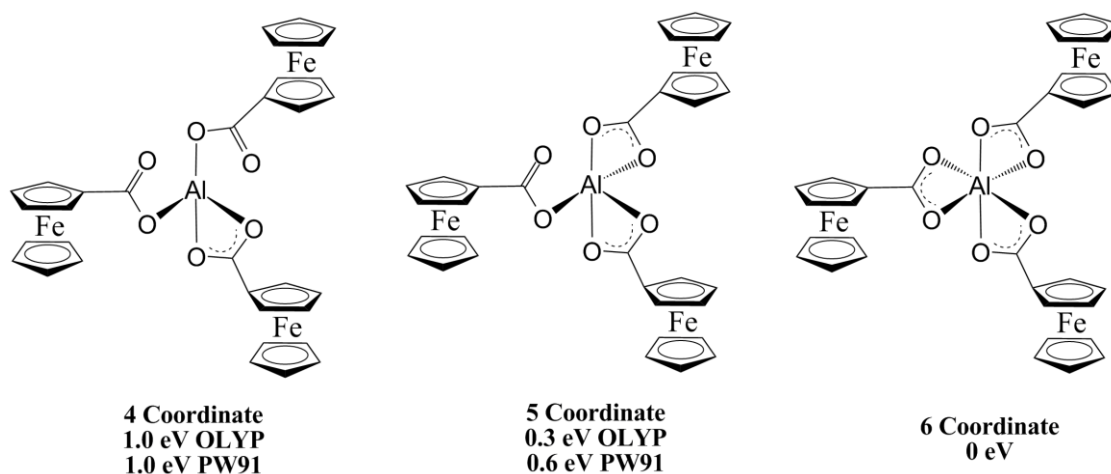


Figure 3.24: Computational solutions of **(18)** where one, two or three of the carboxylate groups is bidentate. The shown relative energies were manipulated from the computed values in such a way that the lowest energy compound, the one on the right has an energy of 0 eV. The energies associated with the other two complexes are much higher than the molecular energy of the structure on the right.

To determine the influence of the highly electron donating Fc group in complexes **(18)** and **(19)**, calculations were also done on related complexes **(21)** and **(22)** with the Fc group being replaced by CH₃ (**Figure 3.25**). In this case, however, no 3 or 4 coordinate solutions of **(21)** similar to those in **Figure 3.24** for the ferrocene-containing analogue could be obtained. Like for the ferrocene complex **(19)**, complex **(22)** also represented the minimum energy, structural solution. Calculation of complexes **(21)** and **(22)** in solution of water or chloroform were also performed to determine whether the solvent will stabilize the negative charge on the carboxylate oxygen which may lead to the 3 coordinated complex **(21)** and not complex **(22)** in solution. This, however, failed. Again only 5 and 6 coordinate solutions were obtained with the 6 coordinate complex **(22)** being *c.a.* 0.5 eV more stable than the 5-coordinate complex.

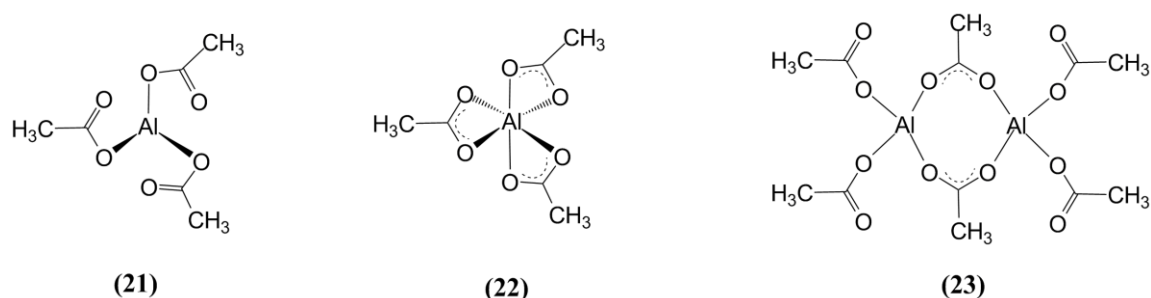


Figure 3.25: Aluminium triacetate compounds, analogous to the ferrocene-containing carboxylates investigated.

That aluminium carboxylates have a low propensity towards monocoordinations is supported by a search of all known crystal structures of aluminium carboxylates. A CSD²⁹ search for aluminium carboxylates showed only a few structures showing monodentate coordination of a carboxylic acid to aluminium as shown in **Figure 2.10**, p. 44. Most Al complexes were 6 or higher coordinated.

Since our calculations showed 5 or 6 coordinate aluminium carboxylates are possible, our attention was next focussed on dimeric structures having these coordination modes. The six coordination modes indicated below in **Figure 3.26**, show possible dimeric structures of the ferrocene complex, having the empirical formula $\text{Al}_2(\text{O}_2\text{CfC})_6$. The monomeric form of this empirical formula is, of course, $\text{Al}(\text{O}_2\text{CfC})_3$. Given the vast number of solutions, as well as the agreement between the results for the monomeric model where the Fc is replaced by CH_3 , calculations were first conducted for the equivalent methyl-containing complex to see which of the coordination modes could be possible for the dimeric complex **(23)** (**Figure 3.25**). No 4/4 (Al1/Al2) or 4/6 coordinate solutions (these coordination modes are defined for the ferrocene equivalent in **Figure 3.26**) could be found for the CH_3 -containing complex.

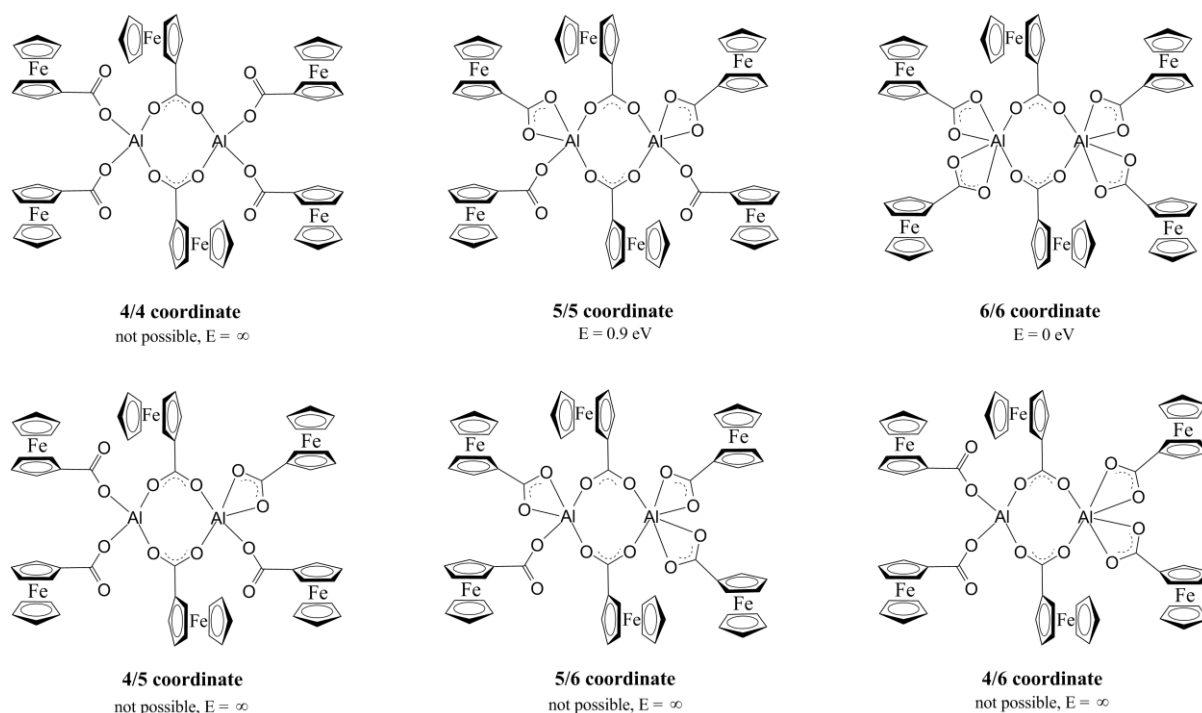


Figure 3.26: The different possible coordination modes of **(20)**.

The order of stability of the solutions for the Me-containing complex, (the lowest relative energy, given in brackets, corresponds to the most stable compound) are:

OLYP: Least stable – 4/5 and 5/5 coordinate (0.7 eV) < 5/6 coordinate (0.3 eV) < 6/6 coordinate (0 eV) – most stable.

PW91: Least stable – 5/5 coordinate (1.0 eV) < 5/6 coordinate (0.3 eV) < 6/6 coordinate (0 eV) - most stable.

That the 4/5, 5/5 and 5/6 coordinate solutions are real solutions and not local minima was confirmed by a frequency calculation. For the ferrocene-containing complex (**20**) only 5/5 and 6/6 coordinate solutions are obtained, implying the energies of the compounds showing the 4/4 or 4/5 coordination modes are infinite. Below is a presentation of the PW91 optimized 5/5 and 6/6 coordinate geometries of the dimeric ferrocene-containing complex (**20**). The 6/6 coordinate ferrocene-containing dimer is 0.9 eV (PW91) more stable than the 5/5 coordinate ferrocene-containing dimer.

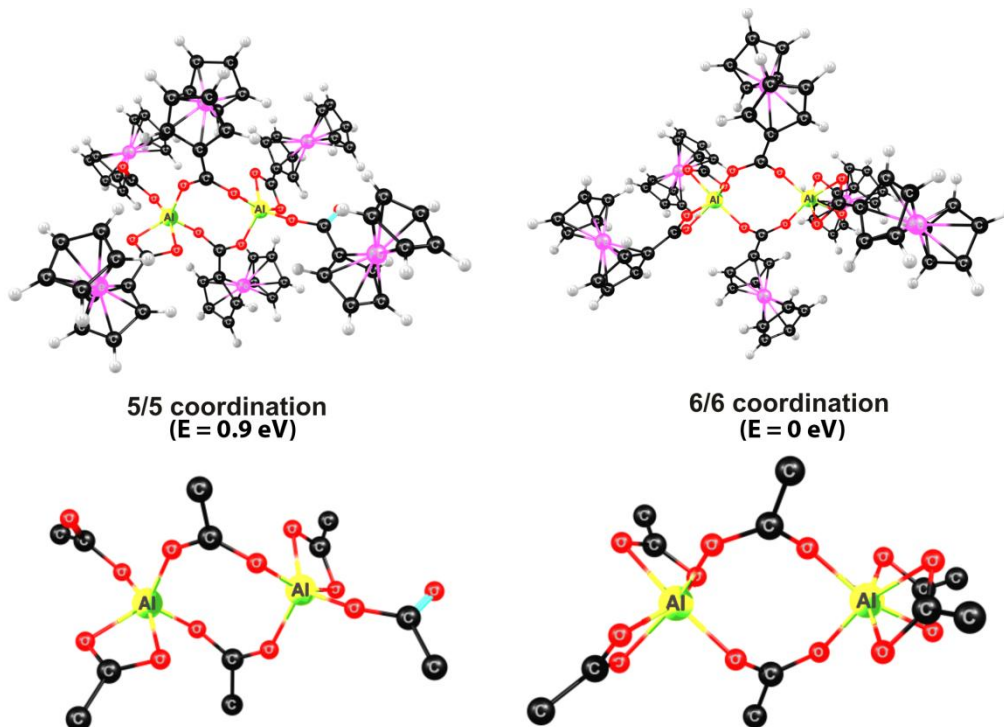


Figure 3.27: The 5/5 coordination ferrocene-containing dimer (top left) and the 6/6 coordination ferrocene dimer (top right). The Al-core structures for the two coordination modes are shown at the bottom respectively.

To compare the monomeric and dimeric structures, the total bonding energies were evaluated. In the evaluation of the CH₃-containing monomers *versus* CH₃-containing dimers, the dimer is less stable by 0.15 eV using the OLYP functional and more stable by 0.43 eV using the PW91 functional. For the ferrocene-containing monomers *versus* the ferrocene-containing dimers, the 6/6 coordinated dimer was more stable by 0.97 eV using the PW91 functional and 0.35 eV more stable using the OLYP functional.

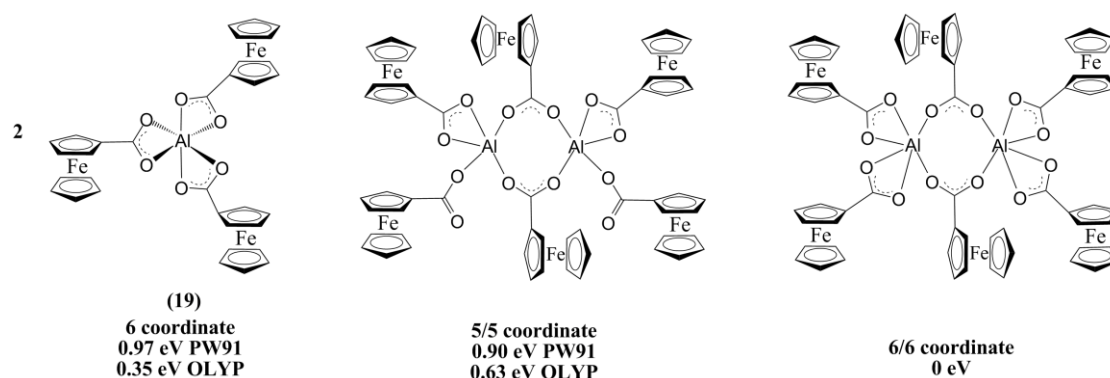


Figure 3.28: The comparison of the total bonding energies of ferrocene-containing monomers and dimers.

The infrared spectra related to the carbonyl stretching of the ferrocene-containing monomer, (19), the 5/5 coordinate dimer and the 6/6 coordinate dimer were calculated and are shown in **Figure 3.29**. The carbonyl stretching frequencies for (19) are summarised in **Table 3.14** and the stretching frequencies of the two dimers are given in **Table 3.15**.

Table 3.14: Calculated carbonyl stretching frequencies of the ferrocene-containing monomer, (19).

Wavenumber (cm ⁻¹)	IR intensity	Assignment
1469.9	142.9	Antisymmetric CO bond stretching
1474.9	706.6	Antisymmetric CO bond stretching
1491.9	396.2	1 symmetric and 2 antisymmetric CO bond stretching
1493.0	623.6	2 symmetric and 1 antisymmetric CO bond stretching
1509.0	166.8	3 symmetric CO bond stretching
1524.3	423.6	Anti symmetric CO bond stretching

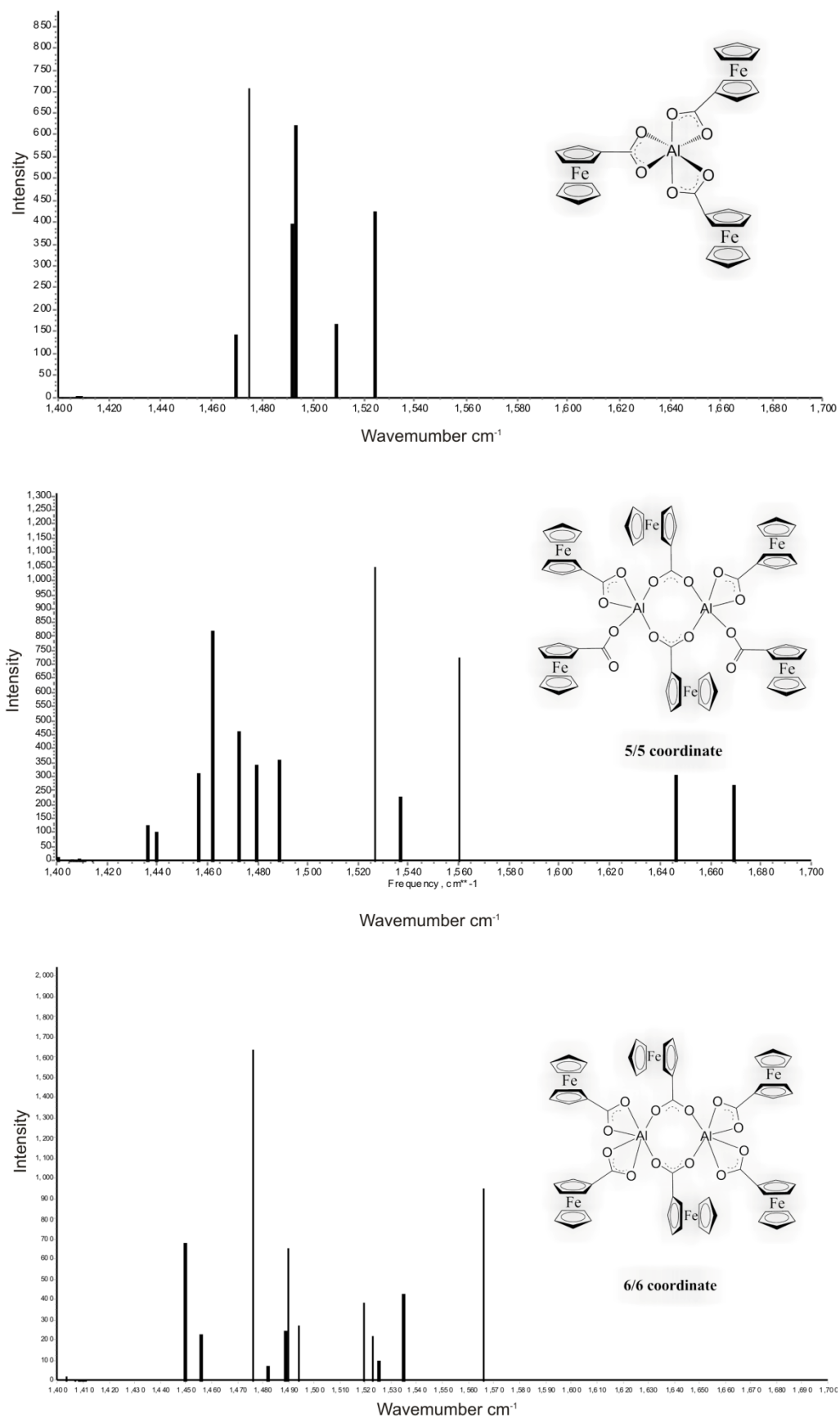
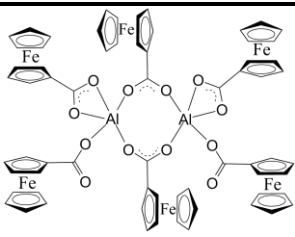
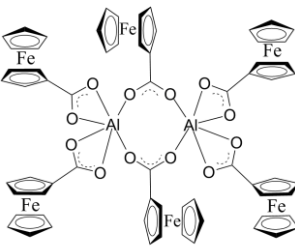


Figure 3.29: The calculated carbonyl infrared spectra of the ferrocene-containing monomer (top), the 5/5 coordinated dimer (middle) and the 6/6 coordinated dimer (bottom).

Table 3.15: Calculated carbonyl stretching frequencies for the 5/5 and 6/6 coordinated ferrocene-containing dimers.

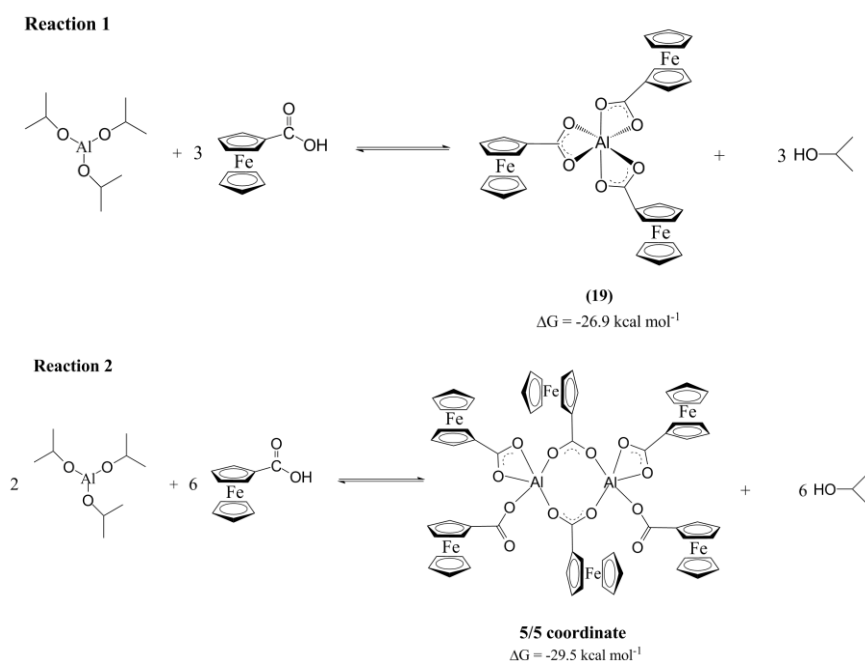
Complex	Symmetric CO bond stretching		Antisymmetric CO bond stretching	
	ν (cm ⁻¹)	IR Intensity	ν (cm ⁻¹)	IR Intensity
 5/5 coordinate	1436.2 ^a	124.6	1479.4	345.8
	1439.8 ^a	104.3	1488.7	360.3
	1456.3	313.1	1526.4	1047.6
	1462.0	824.0	1536.7	227.1
	1472.6	462.2	1560.0	724.1
			1646.4 ^a	304.8
			1669.4 ^a	273.5
 6/6 coordinate	1449.4	685.1	1475.9	1640.1
	1456.0	228.8	1481.8	69.8
			1488.7	247.7
			1489.6	655.2
			1493.9	275.8
			1519.1	384.8
			1522.3	217.0
			1524.3	92.6
			1534.5	423.1
		1565.6	948.6	

a: Stretching frequencies of the monodentate ferrocenecarboxylate ligand.

The ferrocene-containing monomer has three major carbonyl stretching frequencies, 1474.9 cm⁻¹ (antisymmetric), 1493 cm⁻¹ (symmetric and antisymmetric) and 1524.3 cm⁻¹ (antisymmetric). Since there are two major antisymmetric stretching frequencies, there are two differences between symmetric and antisymmetric stretching frequencies ($\Delta\nu$), which are 18.1 cm⁻¹ and 31.3 cm⁻¹. These differences are extremely small as expected where bidentate coordination is involved. The 5/5 coordinated dimer has all three bonding modes. Looking at the stretching of the monodentate ferrocenyl group, the difference between symmetric and antisymmetric stretching frequencies of greatest intensity is 210.4 cm⁻¹ ($\Delta\nu_{\text{mono}} = 1646.4 - 1436$ cm⁻¹). Using 1462 cm⁻¹ as the symmetric stretching frequency and 1526 cm⁻¹ and 1560.0 cm⁻¹ as antisymmetric stretching frequencies, these are the most

intense signals, two $\Delta\nu$'s are produced for the bidentate and bridging carboxylate bridging modes, namely $\Delta\nu_{\text{bid}} = 1526 - 1462 = 64 \text{ cm}^{-1}$ and $\Delta\nu_{\text{brid}} = 1560 - 1462 = 98 \text{ cm}^{-1}$ respectively. Only the most intense bands are used since these will be detected experimentally, whilst smaller intensities will simply occur as signal broadening. In the 6/6 coordinated dimer, using 1449.4 cm^{-1} as the symmetric stretching frequency and 1475.9 cm^{-1} and 1565.6 cm^{-1} as the most intense antisymmetric stretching frequencies produces two $\Delta\nu$'s, namely $\Delta\nu_{\text{bid}} = 1475.9 - 1449.4 = 26.5 \text{ cm}^{-1}$ (bidentate) and $\Delta\nu_{\text{brid}} = 1565.6 - 1449.4 = 116.2 \text{ cm}^{-1}$ (bridging) can be identified. These theoretical results already indicate that $\Delta\nu$ can be used to distinguish between bonding modes (monodentate, bidentate and bridging) encountered in an aluminium carboxylate.

The formation reactions of the 6 coordinated monomer **(19)**, the 5/5 coordinated dimer and the 6/6 coordinated dimer from aluminium tris(isopropoxy) were next investigated quantum mechanically and the free energy of formation ΔG was calculated. According to the Gibbs free energy results, the 6/6 coordinated dimer has the greatest probability (greatest thermodynamic driving force) to be formed (**Table 3.16**) as shown in **Figure 3.30**.



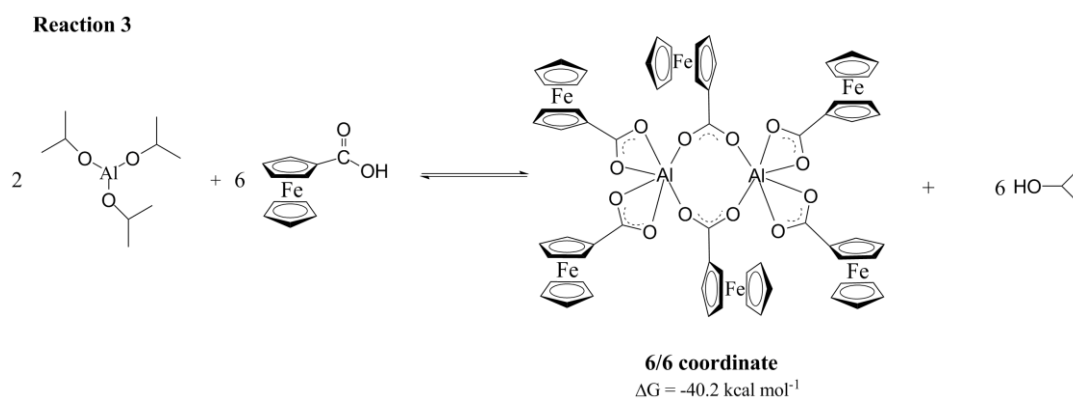


Table 3.16: Calculated internal energy (ΔU), enthalpy (ΔH) and Gibbs free energy (ΔG) for reactions 1 – 3.

Reaction	1	2	3
$\Delta U \text{ (kcal mol}^{-1}\text{)}$	-37.4	-68.1	-82.4
$\Delta H \text{ (kcal mol}^{-1}\text{)}$	-37.4	-68.7	-83.0
$\Delta G \text{ (kcal mol}^{-1}\text{)}$	-26.9	-29.5	-40.2

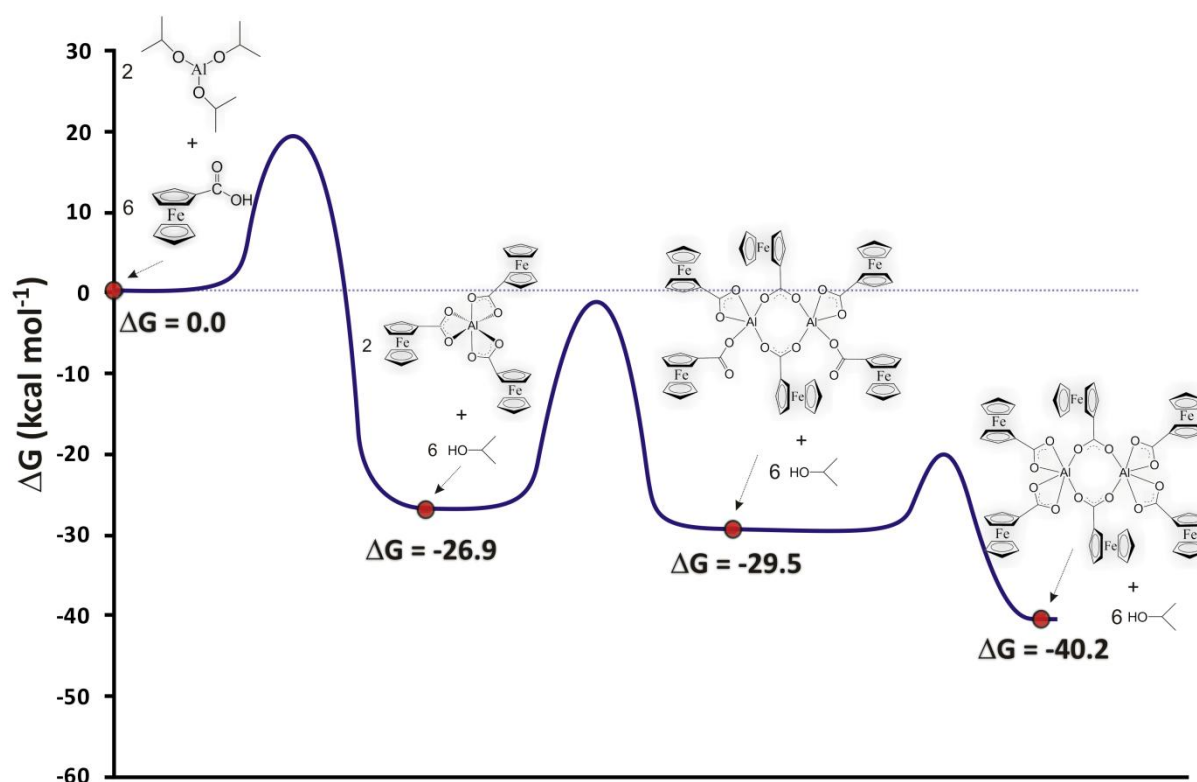


Figure 3.30: Comparison of the Gibbs free energy of the synthetic reactions that will lead to different aluminium carboxylates. Energy barriers are only included for illustrative purposes and were not calculated.

3.3.3.4. Quantum Chemical Computation conclusions

Stable monomeric Al-tricarboxylates adopt a 4-, 5- or 6-coordinate geometry. No 3-coordinate solution was found. The order of stability is:

Least stable – 4-coordinate < 5-coordinate < 6-coordinate – most stable.

Stable dimeric Al-tricarboxylates adopt a 4/5, 5/5, 5/6 or 6/6 coordinate geometry. For ferrocene-containing dimeric Al-tricarboxylates, only the 5/5 and 6/6 coordinate geometry is determined.

The order of stability is (value in brackets represent energy in eV for acetic acid carboxylates of aluminium):

Least stable – 4/5 and 5/5-coordinate (0.7 eV) < 5/6 coordinate (0.3 eV) < 6/6-coordinate (0 eV) – most stable.

The calculated infrared data suggests that the difference between antisymmetric and symmetric carbonyl stretching frequencies, $\Delta\nu$, may be used to indicate the bonding modes encountered in an aluminium carboxylate complex. In particular, it was found that :

- a) $\Delta\nu = 18 - 31 \text{ cm}^{-1}$ suggests a bidentate coordination mode of a carboxylic acid in a monomer.
- b) $\Delta\nu = 64 \text{ cm}^{-1}$ suggests a bidentate coordination mode of the carboxylic acid in a dimeric structure.
- c) $\Delta\nu = 98 \text{ cm}^{-1}$ suggests a bridging coordination mode in a 5/5 coordinated dimeric structure, while 116 cm^{-1} suggests a bridging coordination mode in a 6/6 coordinated dimeric structure.
- d) $\Delta\nu = 210 \text{ cm}^{-1}$ suggests a monodentate coordination mode in a dimeric structure.

The rest of this research project was geared toward establishing whether these theoretical predictions can be confirmed experimentally in aluminium carboxylate complexes.

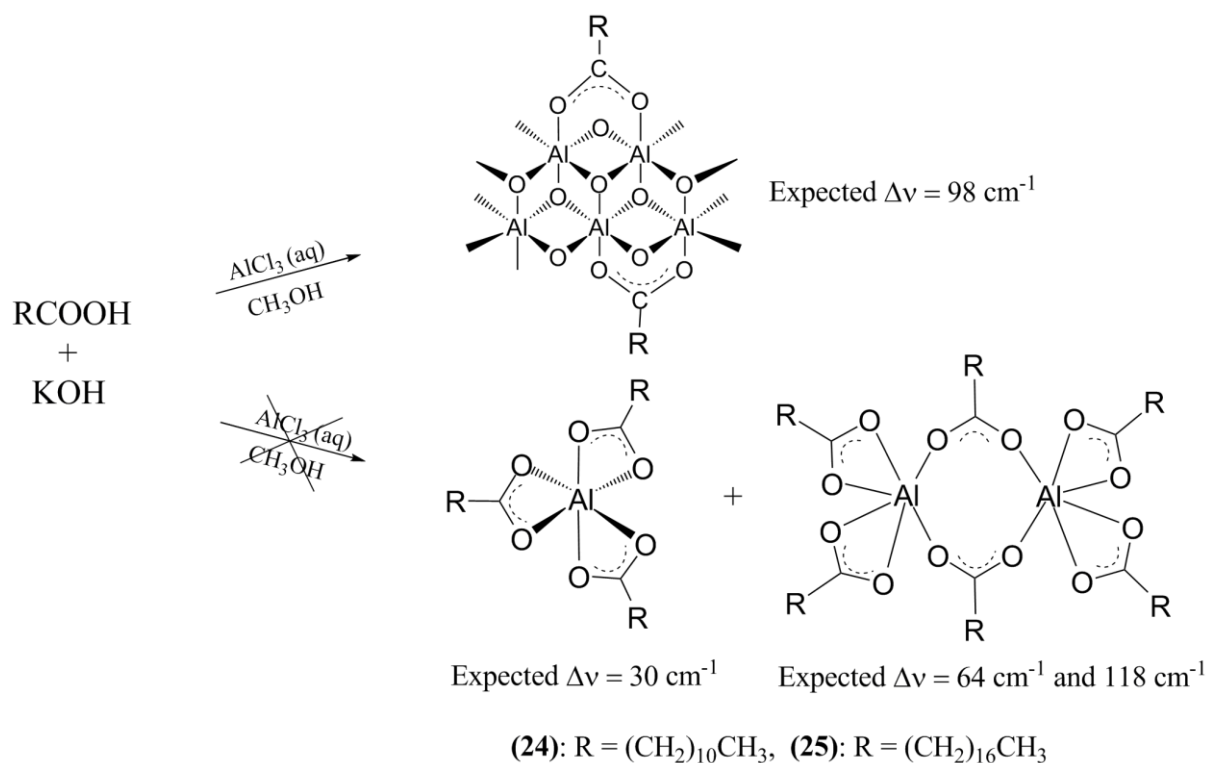
3.3.4. Synthesis and characterisation of aluminium carboxylates

It is reported that a variety of aluminium carboxylates can be synthesised by simply reacting aluminium trichloride or aluminium nitrate with the salt of the appropriate carboxylic acid similar to the preparation of aluminium malonate by Tapparo and co-workers.³⁰ Analogous to these literature reactions, it was then attempted to synthesize long-chained (C_{12} and C_{18}) aluminium carboxylates from the potassium salts of mono-carboxylic acids. The synthetic methodology (**Scheme 3.13**) involved the preparation of the potassium salt of the appropriate carboxylic acid by adding a slight excess 0.5 M potassium hydroxide solution to the melted free carboxylic acid. The potassium salt that is formed is then dried and dissolved in methanol to precipitate any potassium hydroxide, after which the potassium carboxylate is removed and dried. The potassium carboxylate is then redissolved in methanol and added dropwise to aluminium trichloride dissolved in a minimum amount of water.

The resulting products did, however, not resemble aluminium tricarboxylates, lacking solubility in dry organic solvents including carbon tetrachloride, benzene, hexane and THF.^{31, 32} Gel formation was observed in aromatic solvents.

This behaviour accompanied by observed infrared data (**Figure 3.31** and **Figure 3.32**) suggested a resemblance to a class of compounds called carboxylato-alumoxanes.³³

Carboxylato-alumoxanes are three-dimensional cage-like compounds with an aluminium-oxygen core structure similar to that of the mineral boehmite.



Scheme 3.13: The attempted synthesis of aluminium tricarboxylates from the potassium salts of carboxylic acids, leading to the formation of carboxylato-alumoxanes. Structures of carboxylato-alumoxanes are idealised. In practice many O atoms are protonated to give Al-(OH)-Al species. **Figure 3.39**, p. 144 shows two examples of how H atoms may be dispersed in the alumoxane core. Also the Al-O-Al core size can vary between only a few Al-O-Al bridges (as shown above) to many Al-O-Al bridges. (e.g. **Figure 3.34**, p. 134)

The two described reactions resulted not in a monomeric or dimeric aluminium tricarboxylate, but rather in two carboxylato alumoxanes, namely dodecanoato alumoxane **(24)** and octadecanoato alumoxane **(25)**. Infrared spectra of octadecanoic acid, potassium octadecanoato and octadecanoato alumoxane **(25)** are compared in **Figure 3.31**. The free acid shows a clear broad O-H stretching band between 2700 and 2500 cm^{-1} . This broad band disappears upon conversion to the potassium salt.

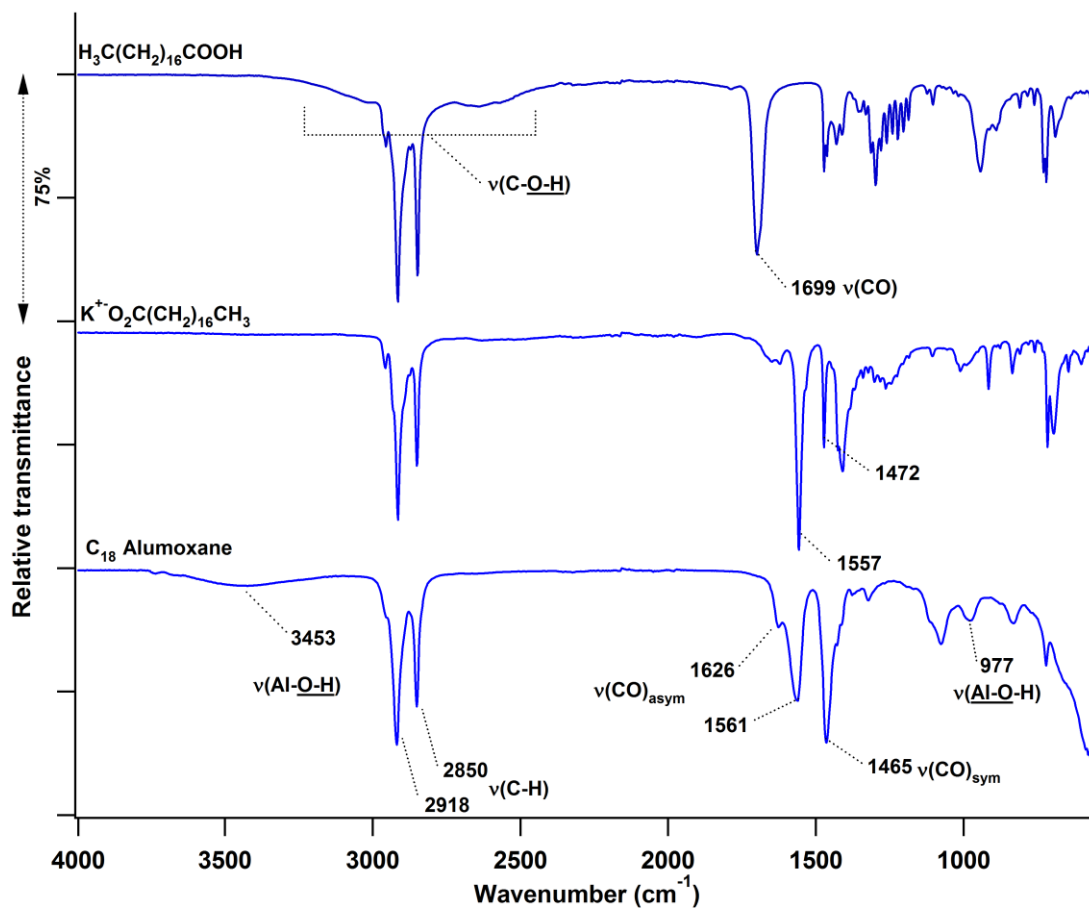


Figure 3.31: The infrared spectra of stearic acid (top), potassium stearate (middle) and octadecanoato alumoxane (**25**) (bottom).

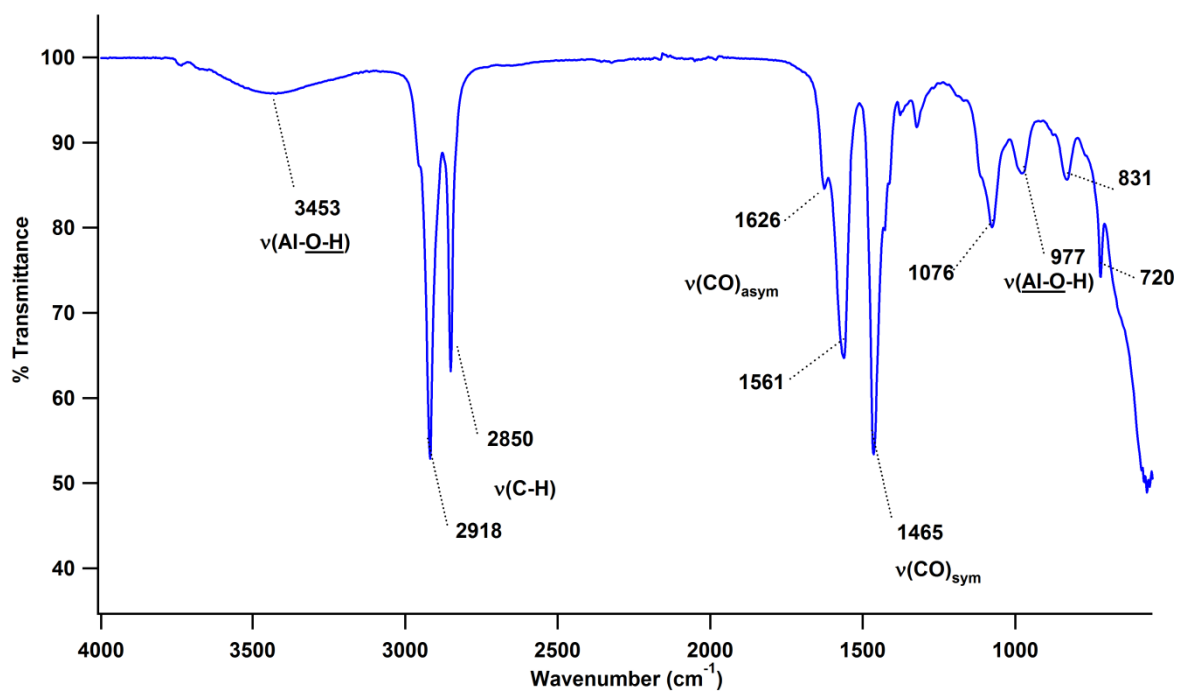


Figure 3.32: The detailed infrared spectrum of octadecanoato alumoxane (**25**).

In the product of the reaction between RCOO^-K^+ and AlCl_3 , proposed to be an alumoxane, there is again a O-H stretching band, but it is shifted to higher wavenumbers and is associated with Al-OH groups within the complex structure of the proposed alumoxane that formed. This also disproves the possibility of the compound being an aluminium tricarboxylate, which would not have Al-OH stretching frequencies at all. A detailed infrared spectrum of octadecanoato alumoxane (**25**) is given in **Figure 3.32**.

The single C=O stretching band in the free acid is replaced by two bands in the potassium salt as well as the proposed alumoxane product, however, the alumoxane also has overlapping stretching frequencies in the carbonyl region. The two major bands in the carbonyl region of (**25**) are the antisymmetric (ν_{asym}) and symmetric (ν_{sym}) C=O stretching bands, respectively at 1561 and 1465 cm^{-1} . The difference between the major antisymmetric and symmetric stretching bands, $\Delta\nu$, is 96 cm^{-1} , corresponding to the computationally predicted $\Delta\nu$ ($\Delta\nu_{\text{bridging}} = 98 \text{ cm}^{-1}$ for ferrocene-containing dimers, p. 125) for bridging coordination. The carbonyl stretching frequencies with smaller intensities (e.g. 1626 cm^{-1}) cannot be assigned unambiguously. The carbonyl band region also corresponds well to what is reported in literature for carboxylato-alumoxanes.³³

For carboxylato-alumoxanes antisymmetric stretching is reported to be between 1590 and 1560 cm^{-1} , whilst symmetric bands are between 1473 and 1464 cm^{-1} . Values in this range are indicative of the aforementioned bridging coordination mode. **Table 3.17** compares the carbonyl stretching bands of the alumoxanes and carboxylato alumoxanes from literature and also gives elemental analysis data for (**24**) and (**25**).

Table 3.17: FTIR data for the carboxylato-alumoxanes synthesised and obtained from literature, and elemental analysis data for the compounds synthesised.

Complexed acids in alumoxanes	Carbonyl stretching frequencies /cm ⁻¹			Elemental analysis / %		
	$\nu_{\text{antisymmetric}}$	$\nu_{\text{symmetric}}$	Δ	C	H	Al
C ₁₂ alumoxane (24)	1586	1464	122	34.34	5.72	4.79
C ₁₈ alumoxane (25)	1561	1465	96	63.11	11.31	5.98
CH ₃ COOH ^a	1586	1466	120	-	-	-
ClCH ₂ COOH ^a	1619	1464	165	-	-	-
CH ₃ CH ₂ COOH ^a	1589	1473	116	-	-	-
CH ₃ CH ₂ CH ₂ COOH ^a	1586	1466	120	-	-	-
C(CH ₃)COOH ^a	1586	1466	120	-	-	-
CH ₃ (CH ₂) ₄ COOH ^a	1587	1465	122	-	-	-
CH ₃ (CH ₂) ₆ COOH ^a	1586	1466	120	-	-	-
CH ₃ (CH ₂) ₁₃ COOH ^a	1587	1466	121	-	-	-

a: From C. C. Landry, N. Pappé, M. R. Manson, A. W. Apblett, A. N. Tyler, A. N. Macinnes and A. R. Barron, *J. Mater. Chem.*, 331, 5 (1995).

When comparing the C₁₈- and C₁₂ alumoxanes (**Figure 3.33**) there is a clear increase in the C-H stretching band intensity from C₁₂ to C₁₈, since there is an increase in carbon atom chain length. This mirrors the same trend as observed in free carboxylic acids (p. 112). The symmetric carbonyl stretching band remains unchanged, whilst the antisymmetric carbonyl stretching band is shifted by 25 cm⁻¹. This leads to $\Delta\nu = 122 \text{ cm}^{-1}$ and 96 cm^{-1} for **24** and **25** respectively.

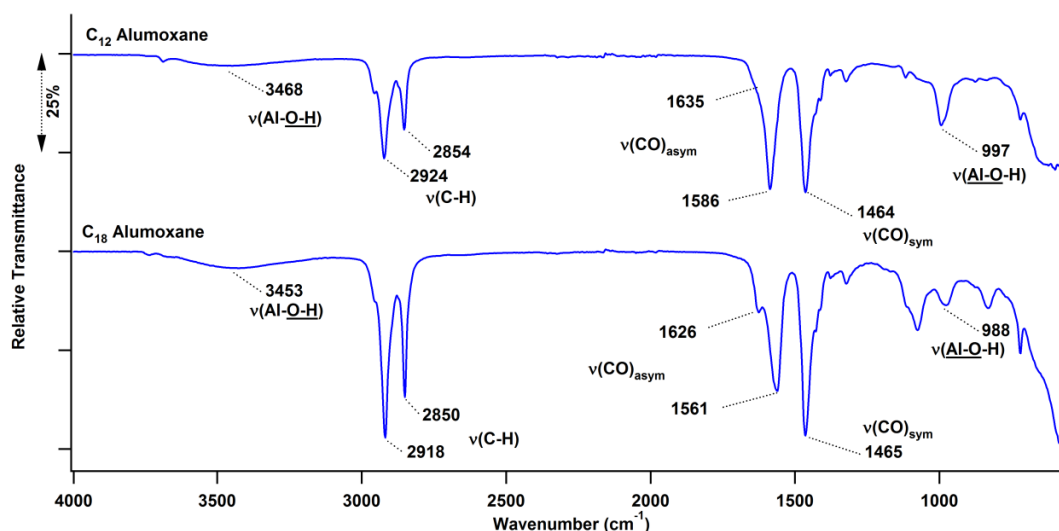


Figure 3.33: Comparison of dodecanoato alumoxane (**24**) and octadecanoato alumoxane (**25**). The Al-O-H band proves the existence of an alumoxane over that of a monomeric or dimeric aluminium tricarboxylate.

The latter value is normally associated with alumoxanes, bearing carboxylates as surface substituents in bridging binding mode (**Figure 3.18** and **Table 3.17**), whilst the former is strongly indicative of a dimeric structure with a penta coordination sphere at each Al-atom. To further aid the structural determination of the carboxylato-alumoxanes, elemental analysis was performed on **(24)** and **(25)**, results are shown in **Table 3.17**. As previously mentioned, carboxylato-alumoxanes are nano-particulate, three-dimensional cage-like compounds with an aluminium-oxygen core structure similar to that of the mineral boehmite. As particles vary in size, different sized core structures arise and the carboxylate ligands are believed to coordinate to the surface of these particles.³³ From the FTIR and elemental analysis data, probable structures of the two carboxylato-alumoxanes were determined (**Figure 3.34**).

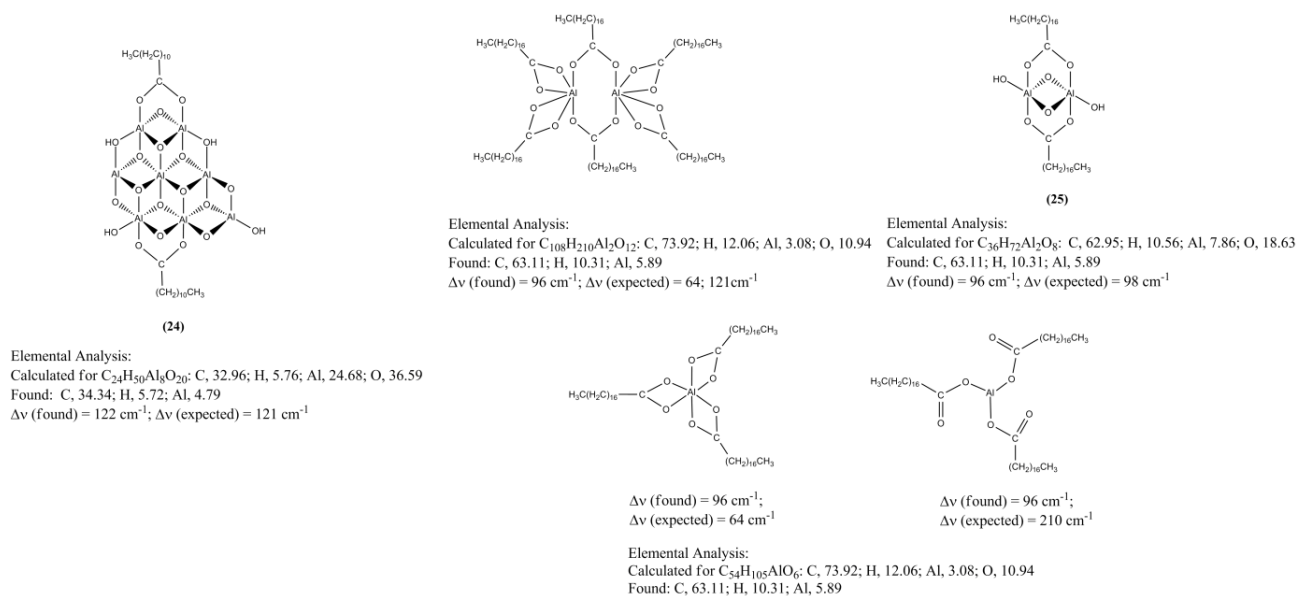


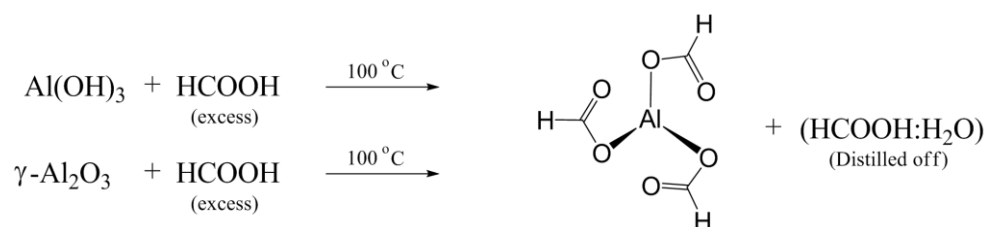
Figure 3.34: The proposed structures of **(24)** and **(25)**, accompanied by theoretical and experimental elemental analysis data.

During elemental analysis, Al-O cores such as those of **(24)** and **(25)** can be converted to stable Al_2O_3 , which cannot be analysed by normal combustion methods and remains

unaccounted for.³⁴ This thus explains the differences between the theoretical (25.74%) and experimental % Al (4.79%) in **Figure 3.34** for **(24)**. Six units of Al_2O_3 in the structure of **(24)** were not observed by elemental analysis and for **(25)** 0.3 units of Al_2O_3 of **(25)** were unaccounted for. The particle core size of **(24)** and **(25)** are proposed on the basis of the conducted elemental analysis, whilst the R-COO coordination modes are concluded to be bridging based on FTIR data. It is important to stress the dimeric nature of **25** by virtue of $\Delta\nu$ (found) = 96 cm^{-1} , as opposed to the polymeric (or oligomeric) nature of **24**. The OH groups in the structures are consistent with the Al-OH signals at 3468 and 3458 cm^{-1} in the IR spectrums of **24** and **25** respectively. Al-O-H bands in the structures of **24** and **25** is evident from the IR signals at 997 and 988 cm^{-1} respectively. In the proposed structures aluminium is six-coordinated, the preferred coordination sphere predicted by the computational study described earlier. Yields for the synthesis of **(24)** and **(25)** were not calculated since the exact structure is not known. It is concluded that the method suggested by Tapparo and co-workers³⁰ as applied to Al-malonato tricarboxylates, cannot be applied as general method to synthesise aluminium tricarboxylates of monocarboxylic acids. The difference between aluminium malonate, tricarboxylates and the present long chain carboxylates is: the malonate complex forms a 6-membered pseudo-aromatic ring between Al and the ligand, having O-Al-O bite angles of 90° , whereas the long chain aliphatic carboxylates of the present study can only form 4-membered pseudo-aromatic rings with expected Al-O-Al bite angles smaller than 70° .

Since the malonate synthetic approach was unsuccessful as a general method for providing aluminium tricarboxylates, a method used by Narayanan and Laine¹⁶ was investigated. This method involves first synthesising aluminium triformate and then displacing the formate ligand with an excess of the desired acid. Accordingly aluminium formate was synthesised

directly from aluminium hydroxide and $\gamma\text{-Al}_2\text{O}_3$ (**Scheme 3.14**). Aluminium hydroxide or gamma aluminium oxide is added to an excess of formic acid. The formic acid – water azeotrope (bp. 101°C) is then distilled off over a period of two to three hours. Water has to be removed, here azeotropically, since aluminium triformate is susceptible to hydrolysis. The remaining solid is then dried under vacuum. The resulting product from this synthesis was highly insoluble suggesting the structure proposed in **Scheme 3.14** and in ref. 16 is not likely.



Scheme 3.14: The synthesis of aluminium triformate from aluminium hydroxide or gamma aluminium oxide. The structure shown for Aluminium triformate is idealized.

The idealised structure of $\gamma\text{-Al}_2\text{O}_3$ is shown in **Figure 3.35**. Considering this structure, carboxylic acids may bond to the surface of $\gamma\text{-Al}_2\text{O}_3$. They may also break the structure apart to form smaller $\gamma\text{-Al}_2\text{O}_3$ fragments with bonded carboxylic acids coordinate to individual Al atoms.

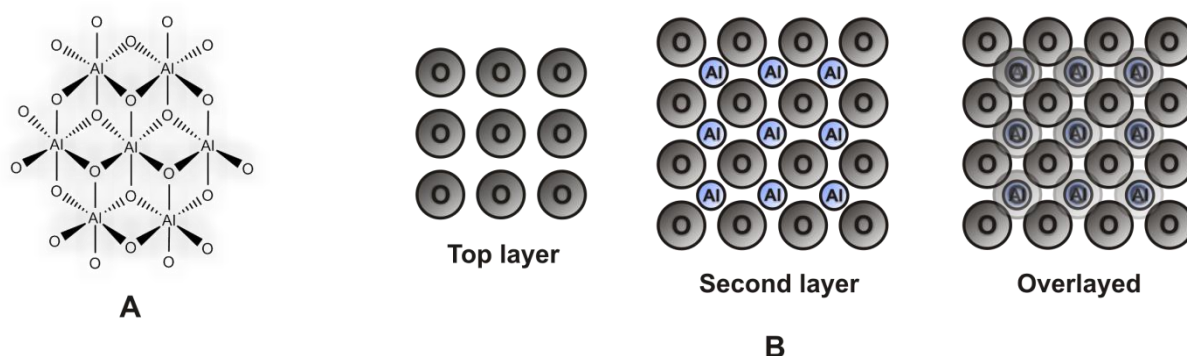


Figure 3.35: The idealised dry surface structure of $\gamma\text{-Al}_2\text{O}_3$ viewed from the side (A) and the top (B). (Adapted from J. B. Peri, *J. Phys. Chem.*, 220, 9 (1965).

Infrared analysis of the synthesised aluminium formate (**Figure 3.36**) shows that the aluminium triformate has O-H stretching bands near 3380 cm^{-1} of much lower intensity than those present in both aluminium hydroxide and formic acid. However, the position of this band at 3380 cm^{-1} is close to the Al-O-H band of alumoxanes observed at 3453 cm^{-1} (**Figure 3.33**, p. 133).

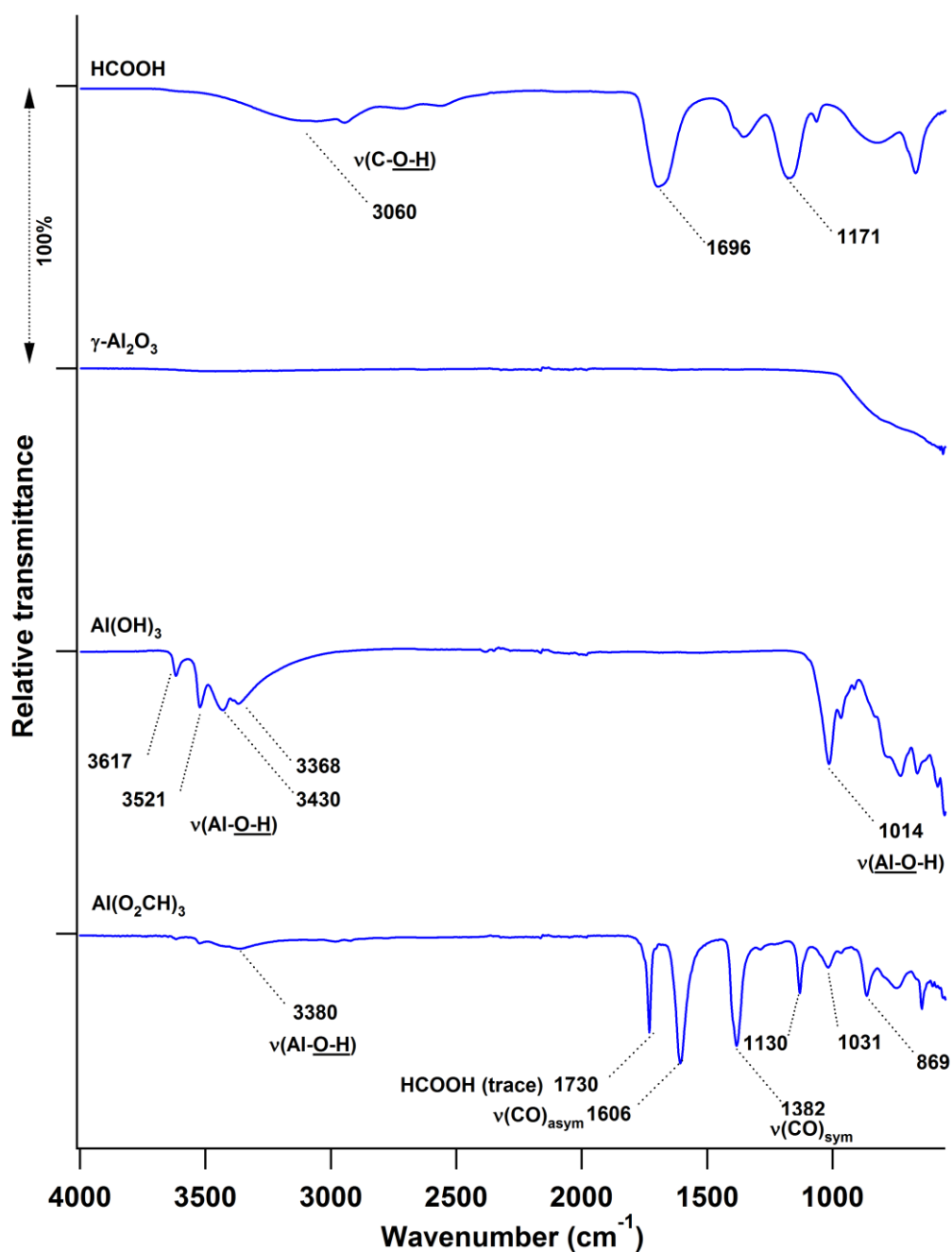


Figure 3.36: Infrared spectra of formic acid (top), gamma aluminium oxide (middle), aluminium trihydroxide and aluminium formate (**19**) (bottom).

The weak intensity of the OH band suggests a more complex molecule than a simple monomeric species. This thus precludes the complex from being aluminium diformate (HO)Al(OOCH)₂ or monoformate (HO)₂Al(OOCH), which would have one or two hydroxide groups respectively, with high intensity FTIR Al-O-H bands. The carbonyl stretching band at 1730 cm⁻¹ of the reaction product is due to traces of formic acid still present in the compound and the intensity of this band decreases further after more intensive solvent removal and drying. Antisymmetric carbonyl stretching occurs at 1606 cm⁻¹, whilst the symmetric band is at 1382 cm⁻¹ ($\Delta\nu = 224 \text{ cm}^{-1}$). These values differ from those observed for carboxylato alumoxanes ($\Delta\nu = 100 - 120 \text{ cm}^{-1}$), but agree closely with a monodentate binding mode of a carboxylic acid in a dimeric structure from the computational results summarised on p. 128. By examining other examples of monodentate coordination of carboxylates to aluminium (**Table 3.18**, p. 138), it is clear that a $\Delta\nu > 200 \text{ cm}^{-1}$ is indicative of monodentate coordination.

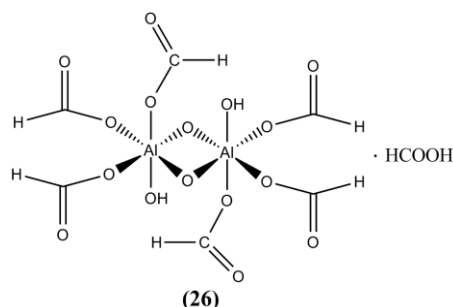
Table 3.18: FTIR data of aluminium complexes from literature showing monodentate carboxylate coordination. For structures see **Table 2.6**, p. 45.

Complex	FTIR $\nu(\text{CO}) / \text{cm}^{-1}$			Ref
	ν_{asym}	ν_{symm}	$\Delta\nu = \nu_{\text{asym}} - \nu_{\text{sym}}$	
Al(CH ₂ CH(OH)COO) ₃	1613	1403	210	35
	1660	1400	260	36
(NH ₄) ₅ [Al(C ₆ H ₄ O ₇) ₂] \cdot 2H ₂ O	1627-1588	1436-1380	> 200	37,38,39
K ₃ [Al(C ₂ O ₄) ₃]	1683	1405	278	40, 41,42,43
K[Al(C ₃ H ₂ O ₄) ₂ (H ₂ O) ₂] \cdot 2H ₂ O	1636	1422	214	44,45

Thus from the above FTIR data for aluminium formate (related to **Figure 3.36**, p. 137), it is clear that the structure of this compound will include a monodentate coordination fragment of formic acid to aluminium and hydroxyl groups will also be present due to the peak at ca. 3360 cm⁻¹. It should also be recalled that the computational results described earlier in this

section indicated that simple 3-coordinate geometry of aluminium carboxylates is unstable (p. 120). Given this fact, the 3-coordinate structure suggested by Narayanan and Laine¹⁶ in **Scheme 3.14**, p. 136, is unlikely to exist. The low intensity of the hydroxyl stretching frequencies excludes the possibility of hydroxyl groups increasing coordination geometry of the 3-coordinate structure to more stable 4-, 5- or 6-coordinate geometries.

All these observations lead us to conclude a dimeric structure for aluminium formate is more likely. Elemental analysis of the formate complex gave an aluminium to carbon ratio of 1:3.5. If the structure is dimeric, this indicates the presence of seven formate ligands, however, the presence of free formic acid, as indicated by FTIR, should also be accounted for. A possible structure satisfying all the described results is shown in **Figure 3.37**.



Elemental Analysis:

Calculated for $C_7H_{10}Al_2O_{18}$: C, 19.28; H, 2.31; Al, 12.37; O, 66.04

Found: C, 19.73; H, 2.38; Al, 12.8

Calculated for $Al(OOCH)_3 \cdot HCOOH$: C, 22.10; H, 2.47; Al, 16.55; O, 58.88

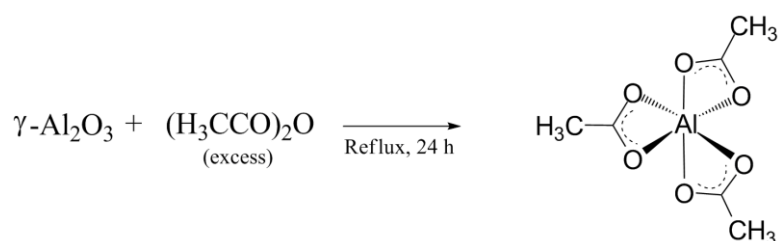
$\Delta\nu$ (found) = 224 cm^{-1} ; $\Delta\nu$ (expected) = 210 cm^{-1}

Figure 3.37: The structure and elemental analysis of aluminium triformate (**26**). Structure (**26**) is considered much more likely than the simple aluminium triformate structure of **Scheme 3.14** that was suggested by Narayanan and Laine.¹⁶

The structure of the dimeric aluminium triformate derivative (**26**) also allows for more extensive Al-O cores, resembling $\gamma\text{-Al}_2\text{O}_3$ fragments, to be formed by allowing bridging through the hydroxyl groups. This is likely, since only a low intensity hydroxyl bands occur in the infrared spectrum of (**26**). In general it is concluded that the synthetic procedure towards aluminium triformate, according to the method of Narayanan and Laine¹⁶, will not

result in a uniquely defined product in repetitive reactions. In some cases a dimeric structure such as **(26)** will result. In other cases, higher homologues with more extended Al-O cores will be the product. Only small reaction differences will result in a large variety of products. These differences will be dictated amongst others by different degrees of wetness of the formic acid.

To further investigate aluminium of short-chained monocarboxylic acids, it was attempted to synthesise aluminium triacetate as in **Scheme 3.15**.



Scheme 3.15: Synthesis of aluminium triacetate. The structure shown for the product is the theoretically expected structure, which is possible according to DFT calculations described on p. 120.

Since one of the key components that appear to prevent tricarboxylato aluminium(III) complex-formation is hydrolysis, acetic anhydride was used rather than normal acetic acid as starting material and solvent for this reaction. Any moisture liberated from the reaction will thus react with acetic anhydride to form dry acetic acid. Trace amounts of moisture are enough to initiate the reaction. The infrared spectrum of the product of the reaction in **Scheme 3.15** is shown in **Figure 3.38**.

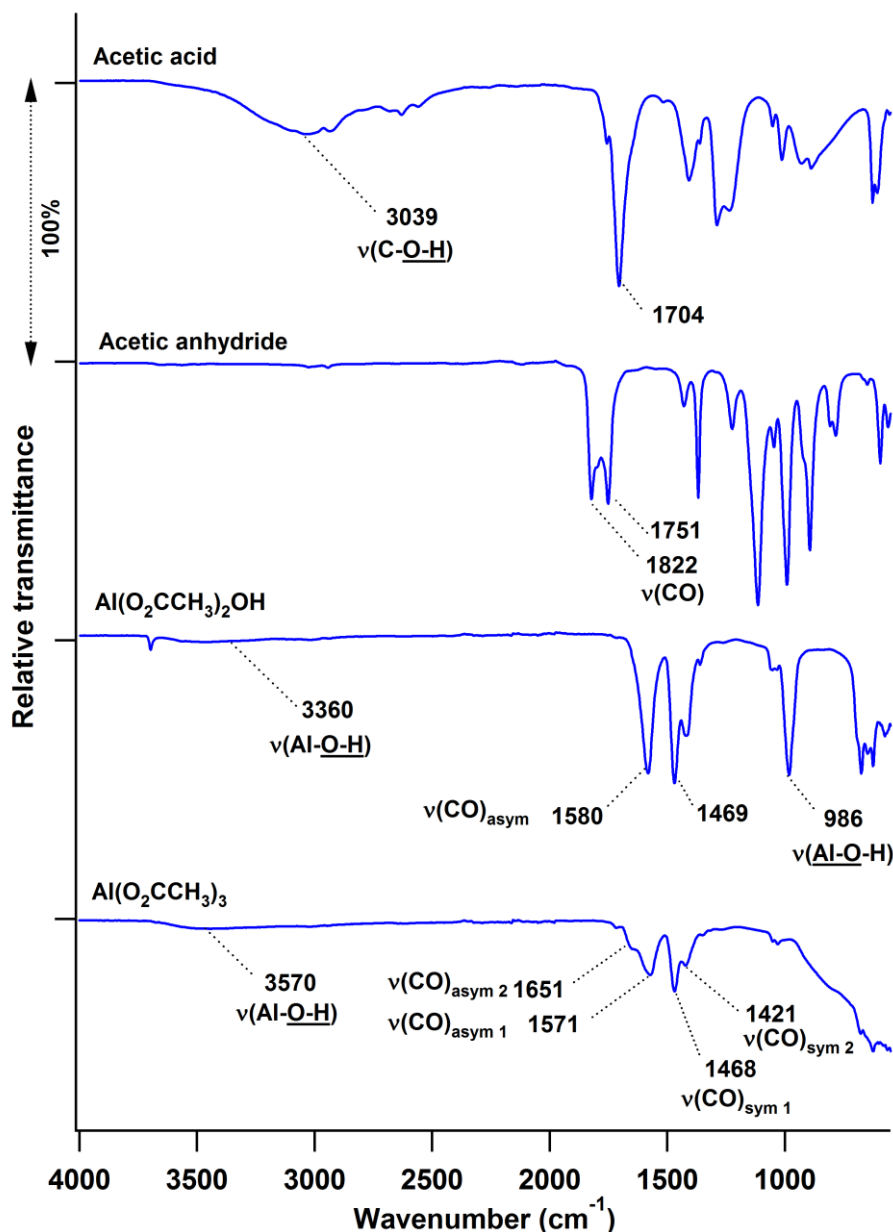


Figure 3.38: Infrared spectra of acetic acid (top), acetic anhydride, commercial aluminium diacetate basic and the synthesised aluminium acetate (bottom).

In the infrared spectra shown in **Figure 3.38**, acetic anhydride does not show the broad O-H stretching band of acetic acid. The synthesised and presumed aluminium triacetate shows antisymmetric carbonyl stretching at 1651 and 1571 cm⁻¹ and symmetric carbonyl stretching at 1468 and 1421 cm⁻¹. This produces two groups of $\Delta\nu$'s, $\Delta\nu_1 = 1651 - 1421 = 230$ cm⁻¹ or $1651 - 1468 = 183$ cm⁻¹ and $\Delta\nu_2 = 1571 - 1468 = 103$ cm⁻¹ or $1571 - 1421 = 150$ cm⁻¹. From

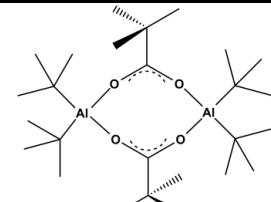
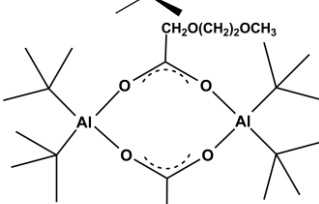
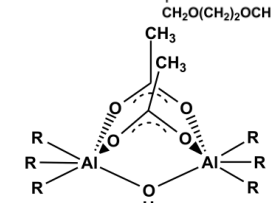
the computational results summarisation on p. 128, this suggests a structure with a simultaneous monodentate carboxylate coordination mode and a bridging carboxylate coordination mode (for $\Delta\nu > 200 \text{ cm}^{-1}$) in a dimeric structure from $\Delta\nu = 103 \text{ cm}^{-1}$. Commercial basic aluminium diacetate, $\text{Al}(\text{O}_2\text{CCH}_3)_2\text{OH}$, shows antisymmetric carbonyl stretching at 1580 cm^{-1} and symmetric stretching at 1469 cm^{-1} . The resulting $\Delta\nu = 111 \text{ cm}^{-1}$ for this complex suggests a dimeric structure with each Al centre being 5-coordinate. Both commercial aluminium diacetate and the presumed aluminium triacetate synthesised here show an Al-OH band at ca. 3500 cm^{-1} .

These results necessitated us to consult literature for proof of the existence of aluminium carboxylato compounds which unquestionably have bridged carboxylato ligands, without alumoxane core structures. Three examples from literature of complexes proven by x-ray crystal structure to have bridging carboxylate coordination, without having alumoxane cores, are given in **Table 3.19**.

The $\Delta\nu$'s for these bridging complexes of **Table 3.19** lie between 100 and 124 cm^{-1} . These values also correspond to carboxylato alumoxanes having bridging coordination (**Table 3.17**, p. 133). It is thus not possible to distinguish between simple bridged dimeric carboxylates and alumoxanes based on $\Delta\nu$ values only. The clear indication of an alumoxane core lies in the presence of an IR Al-O-H band at wave numbers larger than 3450 cm^{-1} . We conclude from all the evidence collected from the target aluminium triacetate complex that the obtained structure must have

- a) monodentate coordinated acetate groups (from $\Delta\nu_1 = 230 > 200 \text{ cm}^{-1}$) and
- b) bridging acetate groups (from $\Delta\nu_1 = 103 \text{ cm}^{-1}$) and
- c) an alumoxane core structure from the Al-O-H band at 3590 cm^{-1} .

Table 3.19: FTIR data of aluminium complexes from literature showing bridging carboxylate coordination.

Structure	FTIR $\nu(\text{CO})$ (cm^{-1})			Ref
	ν_{asym}	ν_{sym}	$\Delta\nu = \nu_{\text{asym}} - \nu_{\text{sym}}$	
	1603	1490	113	28
	1630	1486-1413	>124	28
	1690	1590	100	46

$\text{R} = \text{C}_2\text{H}_5\text{CO}_2\text{CH}_3$

Elemental analysis of the prepared aluminium acetate derivative showed high aluminium content (38%). This would indicate the coordination of the acetate groups on the surface of larger $\gamma\text{-Al}_2\text{O}_3$ cores. According to the FTIR data, some of the acetate groups will be bridging and other monodentate. A structure satisfying both infrared and elemental analysis requirements is shown in **Figure 3.39**. The linear structure of **27** is preferred over the alumoxane structure because of the accurate elemental analysis. Alumoxanes tend to have inaccurate Al and O analyses as per reference 34. The actual core structure of aluminium acetate (**27**) may vary in size from synthesis to synthesis, but the structure in **Figure 3.39** satisfies the elemental analysis results of this particular synthesis. Linkage of several of the fragments in **Figure 3.39** is possible via Al-O bonds, allowing for larger particles to be formed as well.

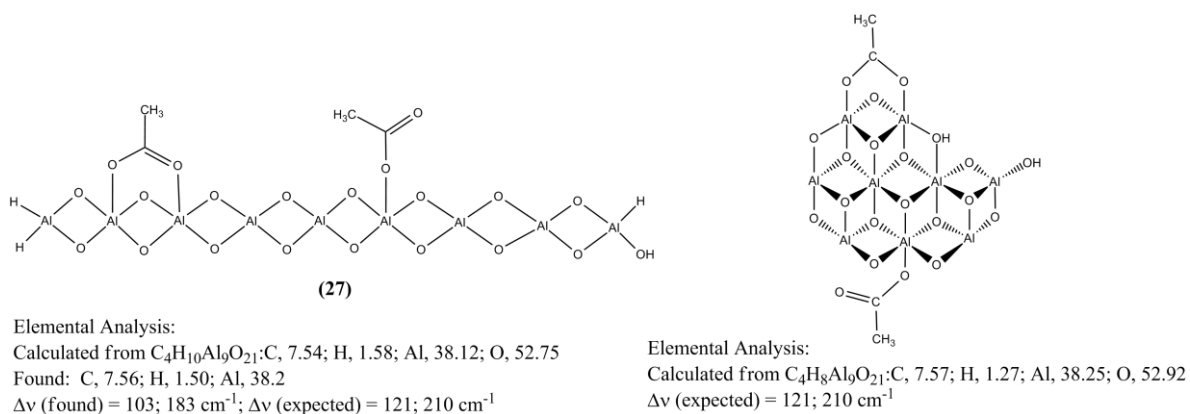


Figure 3.39: Structure and elemental analysis of aluminium acetate (27). Structure (27), unlike the structure in Scheme 3.13 on p. 130, indicates how H-atoms may be part of the alumoxane core. The linear structure is preferred because of the accurate Al elemental analysis, see ref 34.

It is also interesting to note that (27) is susceptible to aqueous hydrolyses. This process is illustrated in Figure 3.40, where (27) was exposed to moisture in the air over a period of several months.

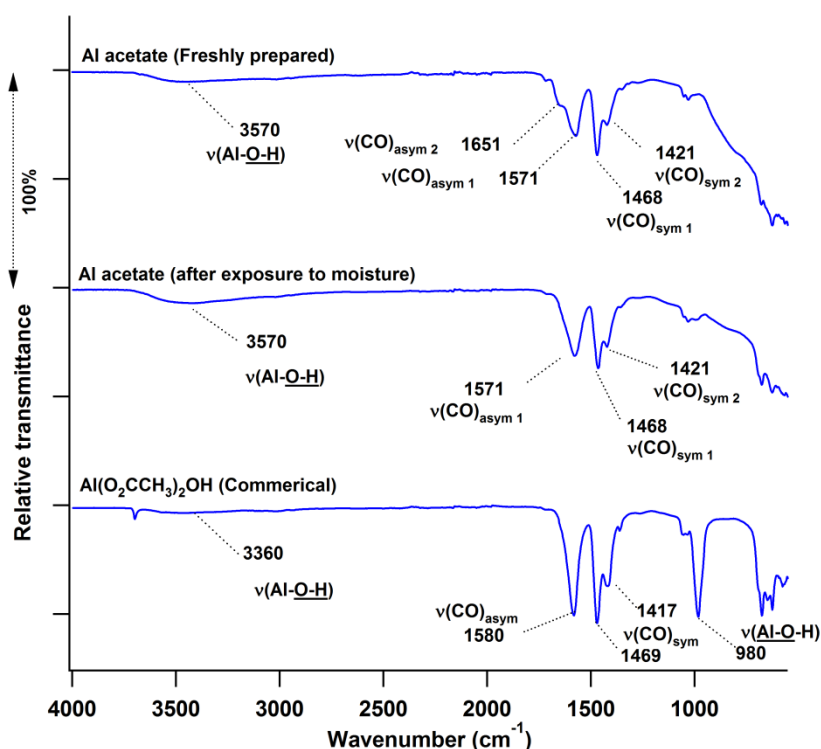


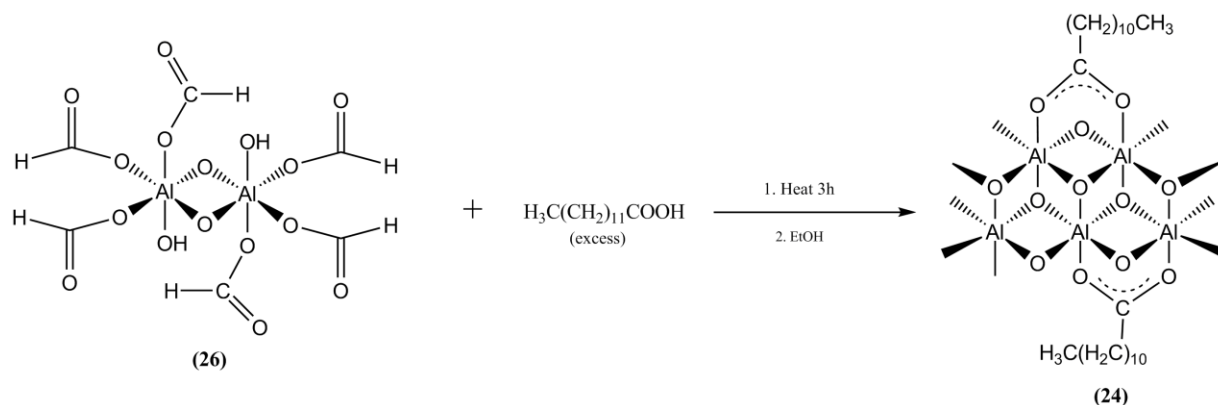
Figure 3.40: The hydrolysis of aluminium acetate. Aluminium acetate (top) is exposed to moisture in the air over a period of several months to produced aluminium diacetate (middle). Note the more intense Al-O-H band compared to the carbonyl peaks Commercial aluminium diacetate is shown at the bottom.

The antisymmetric carbonyl stretching band (**Figure 3.40**) at 1651 cm^{-1} gradually diminishes and only the band at 1571 cm^{-1} increases. The broad O-H stretching band at 3500 cm^{-1} also becomes notable. These bands correspond well to the commercial sample of basic aluminium diacetate. The disappearance of the carbonyl stretching band at 1651 cm^{-1} , which is associated with monodentate coordination, suggests that the monodentate acetate groups are converted to more stable bridging acetate groups. Commercial basic aluminium diacetate is indicated as $\text{Al}(\text{O}_2\text{CCH}_3)_2\text{OH}$, however, infrared data suggest that this is not the true structure of the basic diacetate. A $\Delta\nu$ of 111 cm^{-1} indicates bridging coordination and an Al-O-Al stretching band at 987 cm^{-1} suggests that the real structure has oxygen/hydroxyl bridges between aluminium atoms. The actual structure should resemble that of **(27)**.

We conclude that the synthesis of short chain aluminium tricarboxylates proves to be more difficult in practise than literature seems to suggest. Rigorous exclusion of moisture and oxygen does not prevent Al-O-Al bridge formation. The reason for extensive Al-O-Al bridging observed in these complexes relates directly to using $\gamma\text{-Al}_2\text{O}_3$ as starting material, since Al-O-Al bridging already exists in the core structure of $\gamma\text{-Al}_2\text{O}_3$.

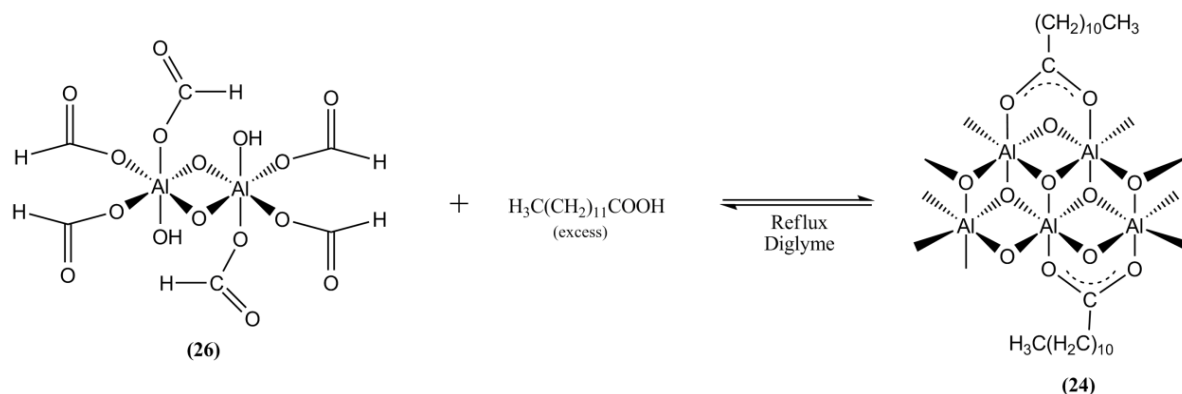
Aluminium formate was also investigated as a synthetic intermediate toward the potential synthesis of longer-chained aluminium carboxylates. Two reactions to potentially prepare long chain aluminium carboxylate complexes were performed using the aluminium formate derivate **(26)** (**Figure 3.37**, p.139) as the starting material. The first reaction (**Scheme 3.16**) involved heating a mixture of dodecanoic acid and the aluminium formate derivate **(26)** until the acid melted. The resulting solid was washed with ether to remove excess acid. The remaining precipitate proved to be unreacted aluminium formate derivate **(26)**. A fine suspension in the ether solution was precipitated with ethanol and was identified as

dodecanoato alumoxane in very low yield (<1%). The alumoxane was identified by virtue of $\Delta\nu$ -values of 121 cm^{-1} (compare **Table 3.17**, p. 133) and an FTIR spectrum identical to that of dodecanoato alumoxane in **Figure 3.33** on p. 133.



Scheme 3.16: The attempted synthesis of aluminium dodecanoate from aluminium formate, leading to the formation of dodecanoato alumoxane.

To try and force the reaction, a second attempt (**Scheme 3.17**) was made using diglyme as high boiling hydrophobic solvent, but this also produced only the corresponding alumoxane in low yield.

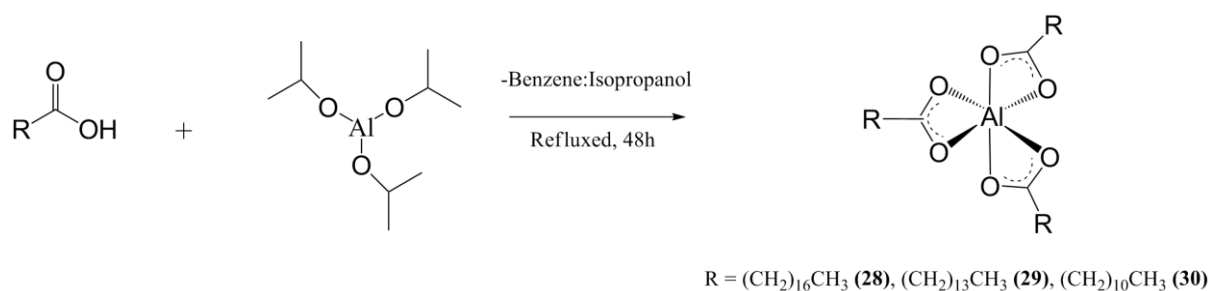


Scheme 3.17: The attempted synthesis of aluminium dodecanoate from aluminium formate using diglyme as solvent.

These two reactions showed that aluminium formate precursors such as (26) can be used to obtain alumoxane derivatives of other carboxylic acids, but pure tricarboxylates cannot be

obtained. The question arises whether this result is necessitated by the use of an inorganic starting material like γ - Al_2O_3 as original aluminium source.

To answer this question, the synthesis of long chained aluminium tricarboxylates was attempted by refluxing aluminium tris(isopropoxide) and the desired acid in dry benzene, whilst removing the liberated isopropanol azeotropically with benzene over time as shown in **Scheme 3.18**.³¹



Scheme 3.18: The synthesis of aluminium tricarboxylates from aluminium tris(isopropoxide). The structures of the tricarboxylates are those theoretically intended, but were not practically obtained.

The aluminium complexes of three long-chained carboxylic acids were synthesised. The acids were dodecanoic acid (C_{12}), pentadecanoic acid (C_{15}) and octadecanoic acid (C_{18}). The aluminium complex of octadecanoic acid is discussed first. Infrared analysis of the intended product, aluminium octadecanoate (**28**) (**Figure 3.41**), showed no broad O-H stretching band. This confirmed that no hydroxide groups were present. By IR comparison, no remnants of unreacted aluminium tris(isopropoxide) or octadecanoic acid could be identified in this product, presumed to be an aluminium trioctadecanoate derivative. An Al-O-Al stretching band is visible at 987 cm^{-1} . The antisymmetric carbonyl stretching band is at 1585 cm^{-1} and the symmetric carbonyl stretching at 1467 cm^{-1} , this gives $\Delta\nu = 118$. The $\Delta\nu$ of 118 cm^{-1} is larger than that observed for bridging coordination in octadecanoato-alumoxane (**25**) dimer having a 5-coordinate coordination shepre to the aluminium centre ($\Delta = 96\text{ cm}^{-1}$).

However, the $\Delta\nu$ value of 118 cm^{-1} still falls within the range for 6-coordinate bridging coordination (**Table 3.17** on p. 133 and **Table 3.19** on p. 143) and is close to the computationally predicted value for bridging coordination in dimeric structures (p. 128). Surprisingly and most excitingly, elemental analysis confirmed a ratio of 3:1 for the C_{18} -carboxylic acid to aluminium. Three possible structures for the aluminium carboxylate are shown in **Figure 3.42**.

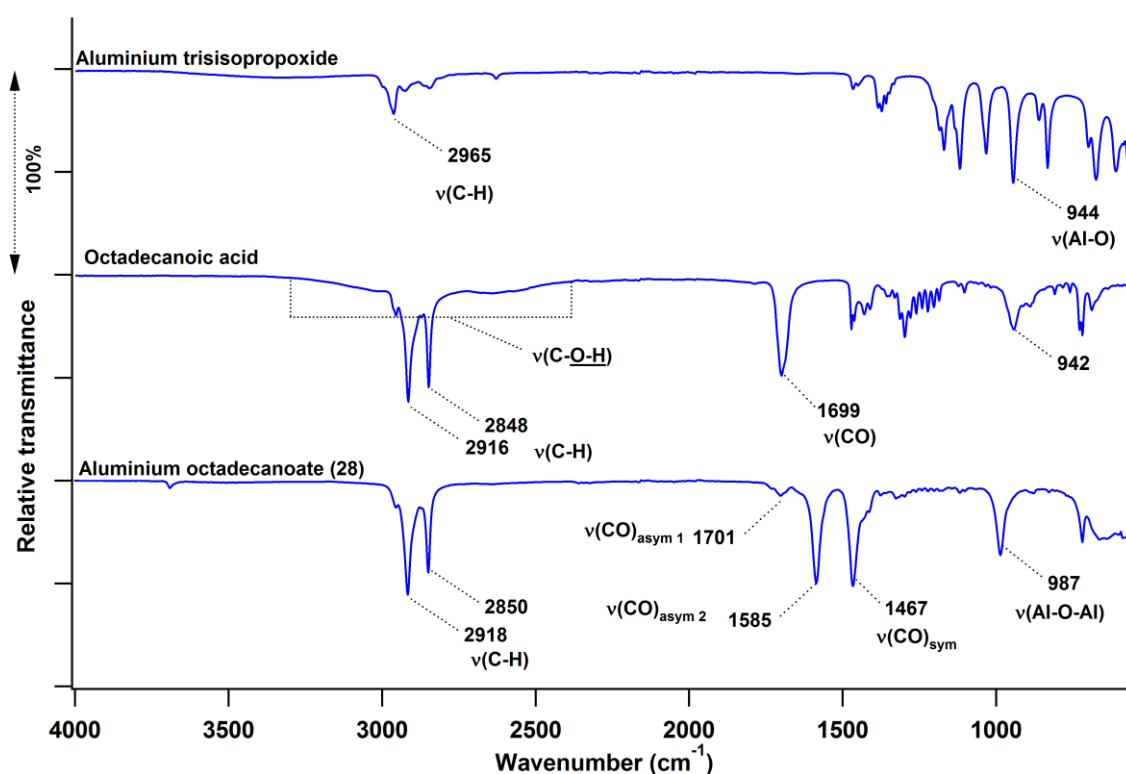


Figure 3.41: Infrared spectra of aluminium trisopropoxide (top), octadecanoic acid (middle) and aluminium trioctadecanoate (bottom).

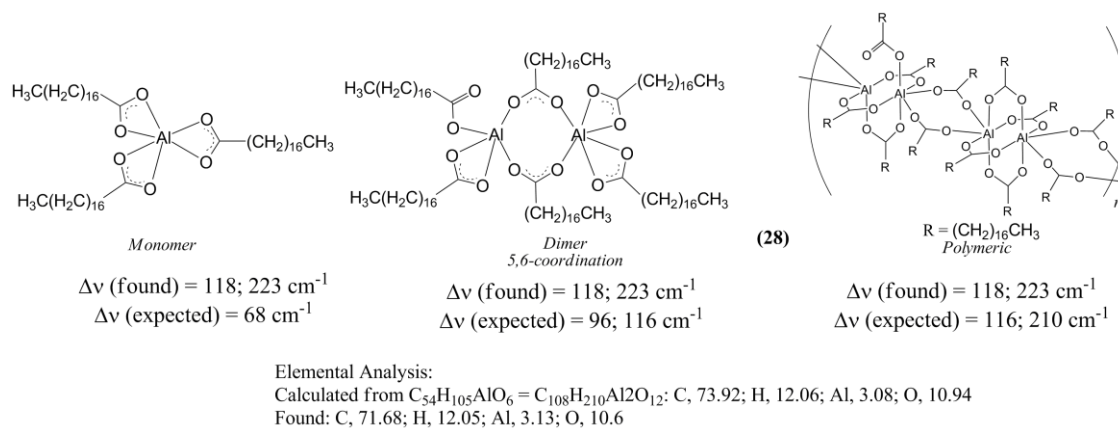


Figure 3.42: The possible structures of aluminium trioctadecanoate, **(28)**, accompanied by elemental analysis data.

The monomeric form in **Figure 3.42** is in agreement with elemental analysis data, however, the carbon content of the sample was slightly lower than predicted (71.68% compared to the calculated value of 73.92%). Infrared data suggest that bridging coordination dominates extensively. This suggests the monomeric form probably does not exist. In all fairness, the author has to point out that significantly different metal-oxygen distances in a coordinated carboxylate fragment can significantly increase $\Delta\nu$. In such cases, only thus far observed unambiguously for tin complexes, $\Delta\nu$ is comparable to that of monodentate coordination (>200).⁴⁷ This may account for the higher $\Delta\nu$ and indicate the monomer as a possible structure but it is not considered likely for the aluminium complexes of the present study. A O-Al-O bite angle of less than 70° would simply not allow a stable bidentate aluminium carboxylate with significantly different Al-O bond lengths. The dimeric or polymeric forms allow for bridging coordination and still satisfy the 3:1 ratio requirement imposed by elemental analysis. The bidentate coordination mode in a dimer is associated with $\Delta\nu$ values of 64 cm^{-1} and a monodentate coordination mode is associated with a $\Delta\nu$ value of 210 cm^{-1} (p. 128). The $\Delta\nu = 64 \text{ cm}^{-1}$ associated with dimer bidentate coordination was not observed, suggesting the dimeric structure of **Figure 3.42** is not a dominant component of the reaction

product. A low intensity peak at 1701 cm^{-1} (not associated with free acid, since no broad OH band is observed) gives a $\Delta\nu$ of 223 cm^{-1} . This does point to a dimeric or higher homologue structure with at least one monodentate coordinated carboxylate. The polymeric structure in **Figure 3.42** satisfies the simultaneous requirement of large amounts of bridging carboxylates, here mostly a paddle wheel structure, and also small monodentate coordinated content. It has no bidentate carboxylato binding modes, which fits in well with the absence the $\Delta\nu = 64\text{ cm}^{-1}$ band pattern. The dimer structure is also disqualified as the dominant species due to the absence of the $\Delta\nu = 64\text{ cm}^{-1}$ band pattern.

Aluminium trioctadecanoate displays somewhat better solubility characteristics than the corresponding alumoxane. The FTIR spectrums of aluminium trioctadecanoate and octadecanoato-alumoxane are compared below (**Figure 3.43**). The first marked difference between the two compounds is the absence of hydroxyl groups in the tricarboxylate. There is also a difference of 24 cm^{-1} in the position of the strongest antisymmetric carbonyl stretching bands.

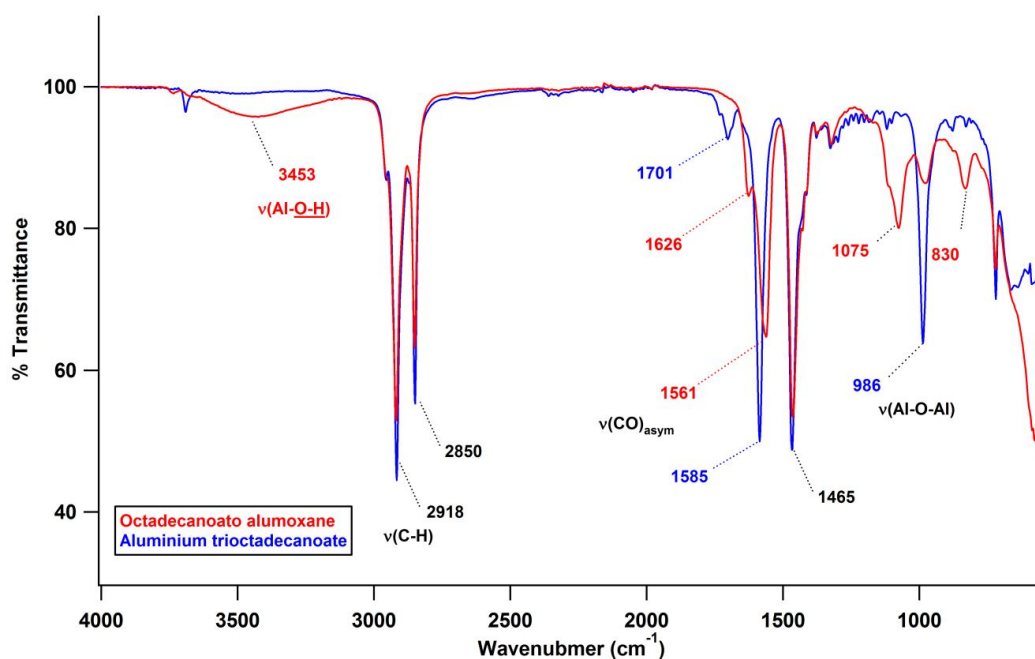


Figure 3.43: Comparison of the C₁₈-tricarboxylate and alumoxane FTIR's.

The next tricarboxylate to be synthesised from aluminium tris(isopropoxide) was aluminium tripentadecanoate (**29**). The FTIR of this complex has two antisymmetric carbonyl stretching bands, $\nu_{\text{asym } 1} = 1641 \text{ cm}^{-1}$ and $\nu_{\text{asym } 2} = 1583 \text{ cm}^{-1}$, and one symmetric stretching band at 1470 cm^{-1} . This gives two $\Delta\nu$'s, i.e. $\Delta\nu_1 = 1641 - 1470 = 171 \text{ cm}^{-1}$ and $\Delta\nu_2 = 1583 - 1470 = 113 \text{ cm}^{-1}$, as shown in **Figure 3.44**. Two carboxylate bonding modes are thus expected. The $\Delta\nu$ of 113 cm^{-1} is associated with bridging coordination. The $\Delta\nu$ of 171 cm^{-1} corresponds either to asymmetric bidentate coordination, having one Al-O distance significantly longer than the other or to a monodentate coordinated carboxylate in a dimeric or higher homologue compound. As described for (**28**) the latter explanation is preferred. The asymmetric bidentate coordination was favoured by Leger and co-workers⁴⁸ (1957) for aluminium, and contrasts this study.

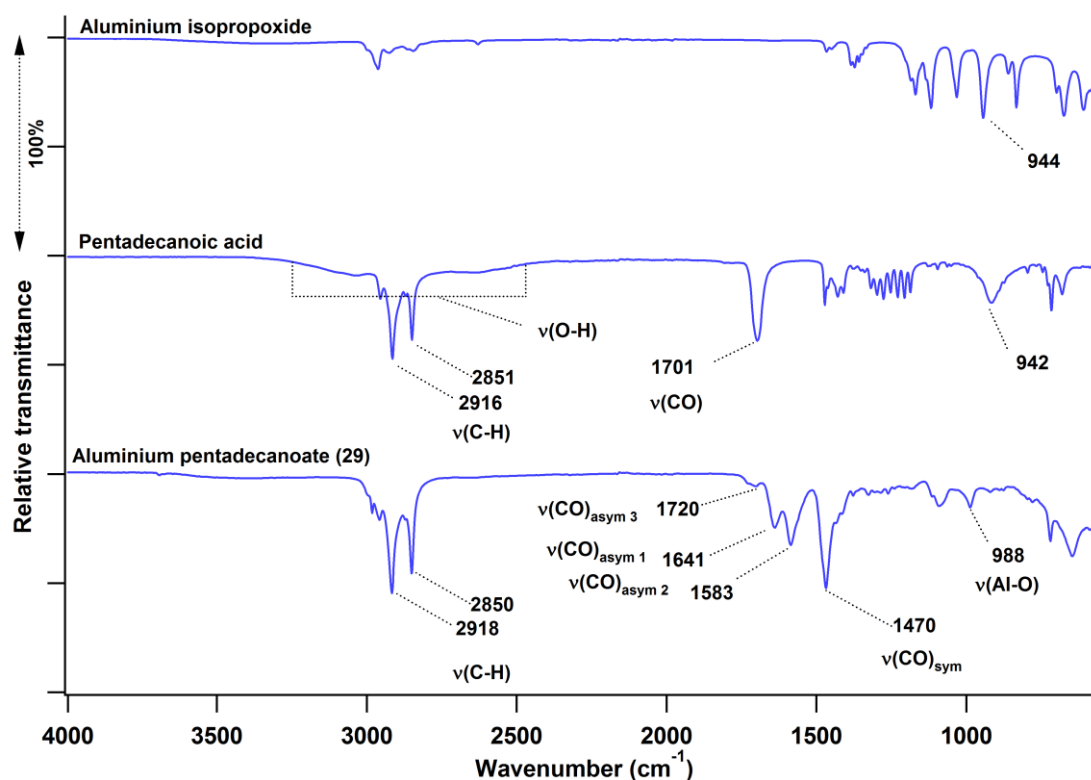


Figure 3.44: Infrared spectra of aluminium isopropoxide (top), pentadecanoic acid (middle) and aluminium tripentadecanoate (bottom).

The absence of the $\Delta\nu = 64 \text{ cm}^{-1}$ in the FTIR of **(29)** pointed to it having no bidentate coordinated carboxylates. This suggested the dimeric structure of **Figure 3.45** is probably not a dominant structure. However, the $\Delta\nu = 113 \text{ cm}^{-1}$ band pattern is associated with 5 or more probably 6 atom aluminium coordination spheres in dimeric or higher homologue structures. The small peak at 1720 cm^{-1} is not associated with free carboxylic acid impurities, because even when the spectrum is greatly enlarged, no broad OH band at 3000 cm^{-1} is observed. This means the 1720 cm^{-1} peak is a third asymmetric band, which leads to $\Delta\nu_3 = 1720 - 1470 = 250 \text{ cm}^{-1}$. Consequently the most likely structure of **(29)** must also have small amounts of monodentate carboxylate coordination. A band of small intensity at 988 cm^{-1} confirms that Al-O-Al bridging does not occur frequently in this compound.

Elemental analysis for **(29)** gave an approximate aluminium to carboxylic acid ratio of 1:3. The calculated elemental analysis differs slightly from the experimentally observed values. Considering the two bonding modes indicated by FTIR, a polymeric structure for **29** as shown in **Figure 3.45** is considered to make up the most important structural entity of the obtained complex.

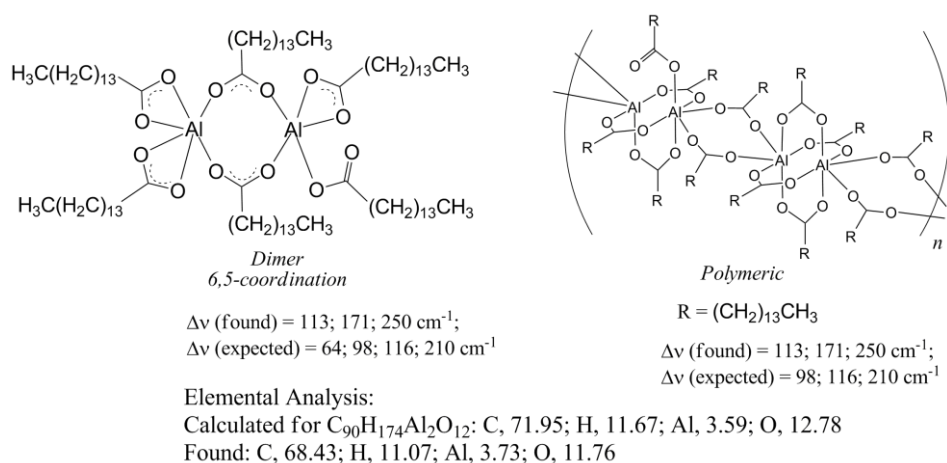


Figure 3.45: FTIR and elemental analysis of aluminium tripentadecanoate **(29)** indicate this complex exist most likely in the polymeric form (right), although small amounts of the dimer (left) cannot be excluded.

The last long-chain carboxylate obtained from aluminium trisopropoxide is aluminium dodecanoate (**30**). This complex has four antisymmetric carbonyl stretching bands at 1708, 1652, 1587 and 1562 cm^{-1} and one symmetric carbonyl stretching band at 1465 cm^{-1} in its FTIR (Figure 3.46). Four $\Delta\nu$'s are thus present, i.e. $\Delta\nu_1 = 1708 - 1465 = 253 \text{ cm}^{-1}$, $\Delta\nu_2 = 1652 - 1465 = 187 \text{ cm}^{-1}$, $\Delta\nu_3 = 1587 - 1465 = 122 \text{ cm}^{-1}$ and $\Delta\nu_4 = 1562 - 1465 = 97 \text{ cm}^{-1}$.

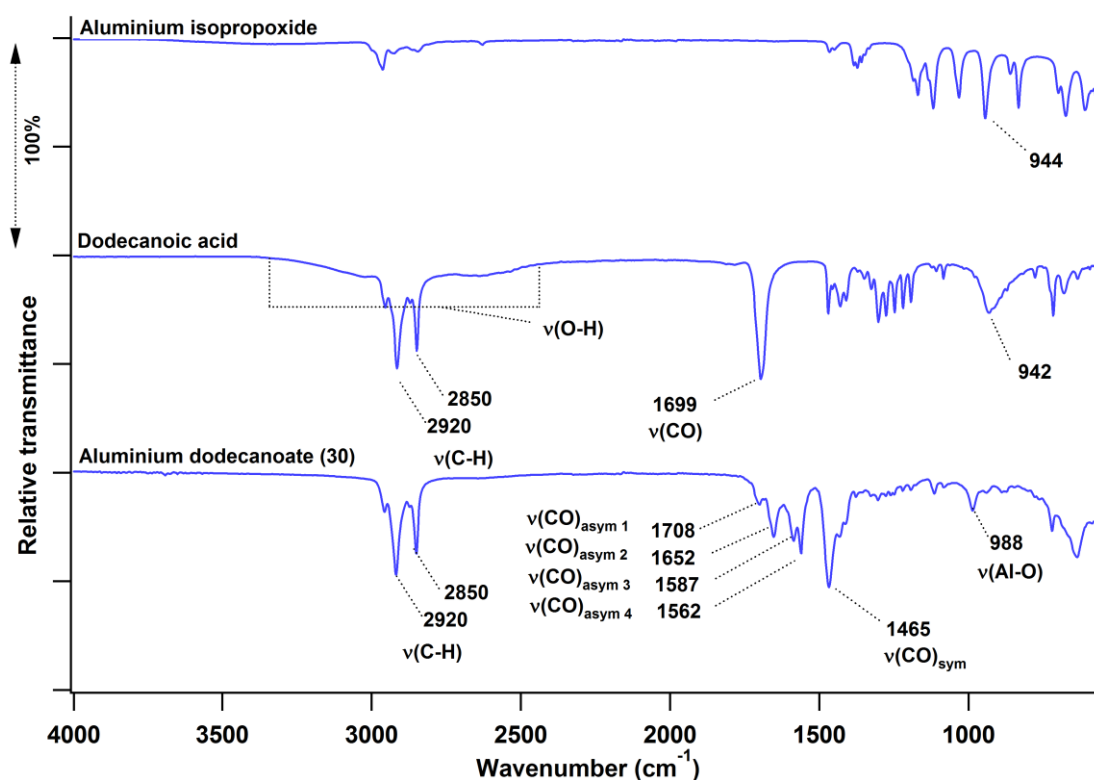
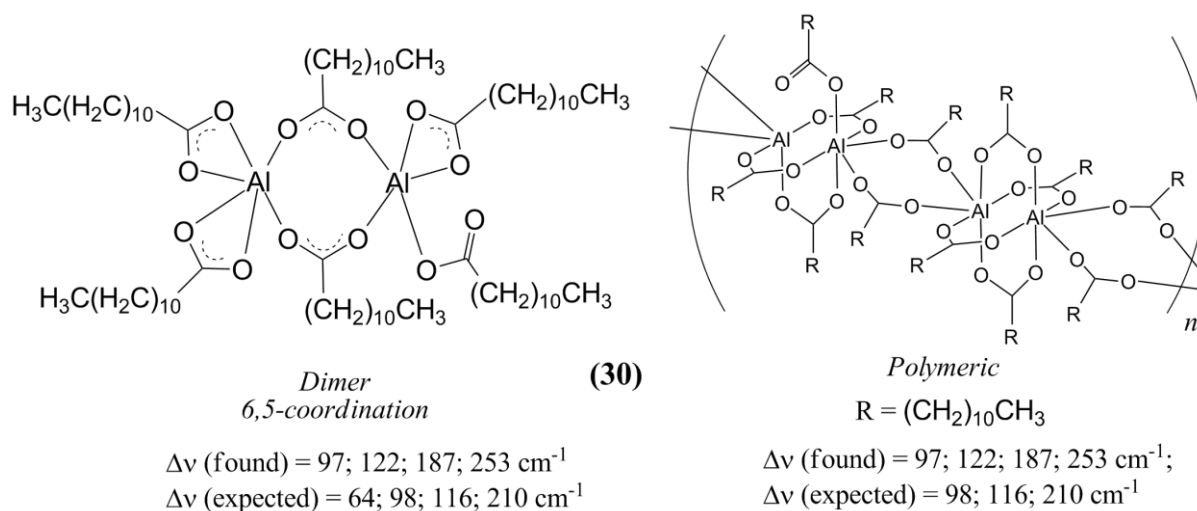


Figure 3.46: Infrared spectra of aluminium isopropoxide (top), dodecanoic acid (middle) and aluminium tridodecanoate (bottom).

The value $\Delta\nu_1 = 253 \text{ cm}^{-1}$ is associated with a monodentate coordinated carboxylato group. As with (**29**), $\Delta\nu_2 = 187 \text{ cm}^{-1}$ probably represents monodentate coordination in a dimer or higher homologue. The $\Delta\nu_3 = 122 \text{ cm}^{-1}$ value is assigned to bridging coordination. The third $\Delta\nu$ (97 cm^{-1}) also falls within the range for bridging coordination especially if 5-coordinate Al atoms are present. In essence, the $\Delta\nu$ values of 122 and 97 cm^{-1} imply that there are two different environments in which bridging groups can lie, a scenario which is possible in the

polymeric structure of **(29)** (**Figure 3.45**). It is important to note that alumoxane formation did not occur since no significant Al-OH band could be detected in the infrared spectrum at ca. 3500 cm^{-1} .

The structure whose theoretical elemental analysis gives the closest approximation of the experimental elemental analysis is shown in **Figure 3.47**.



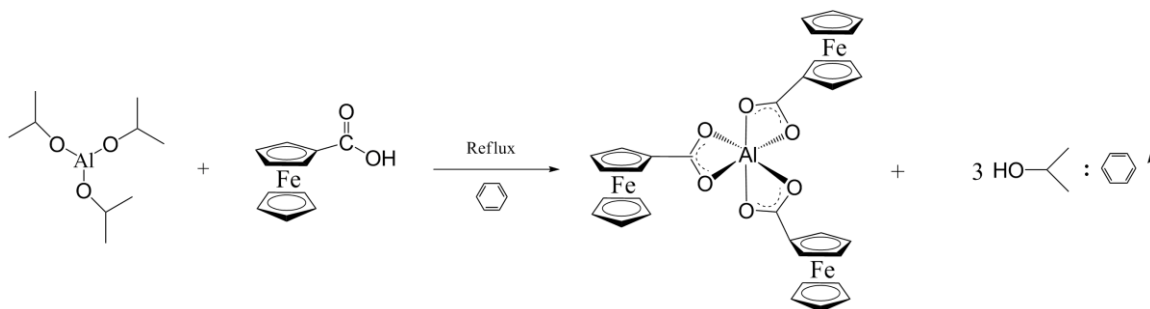
Elemental Analysis:

Calculated for $\text{C}_{72}\text{H}_{138}\text{Al}_2\text{O}_{12}$: C, 69.14; H, 11.20; Al, 4.31; O, 15.35

Found: C, 64.70; H, 10.73; Al, 4.93; O, 13.66

Figure 3.47: Possible structures and elemental analysis of the aluminium complex of dodecanoic acid. The polymeric structure is expected to dominate.

This structure (**Figure 3.47**) shows bidentate coordination and bridging coordination in two different bridging environments in the polymeric derivative. As with **(29)**, the product obtained appears to consist of mixtures of structures closely resembled by those in **Figure 3.47**. To aid in the identification of the aluminium tricarboxylate bonding modes, aluminium ferrocenoate was synthesised as shown in **Scheme 3.19** and the infrared spectrum of the product is shown in **Figure 3.48**.



Scheme 3.19: Synthesis of aluminium triferrocenoate. Structure of the aluminium carboxylate is idealised.

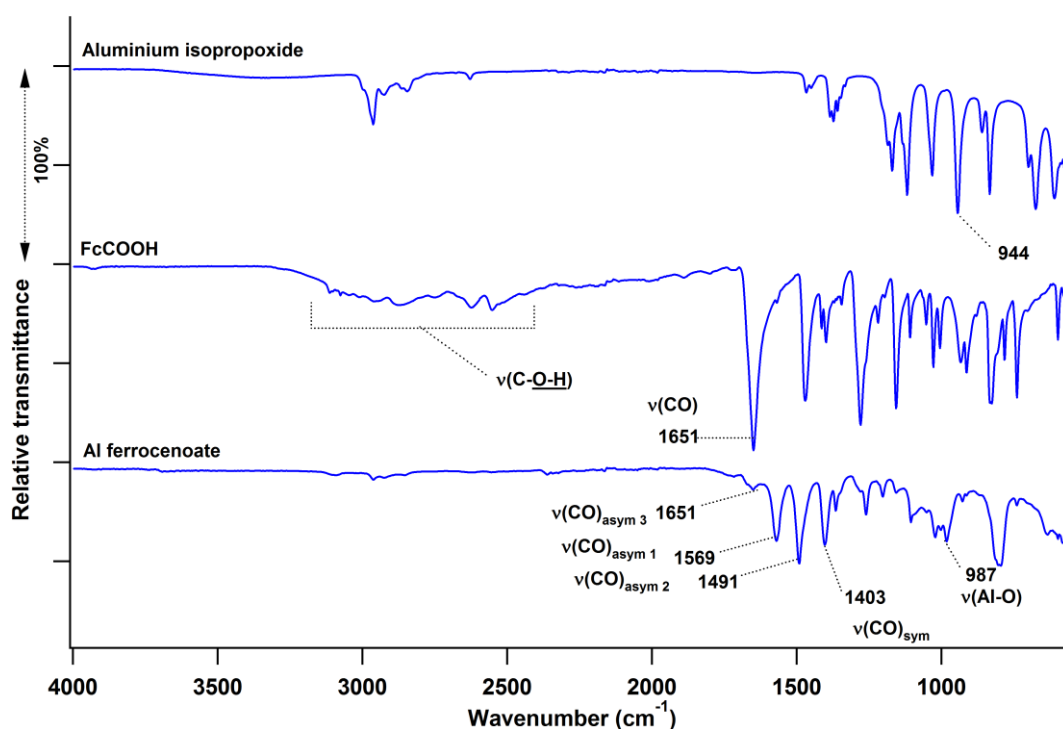


Figure 3.48: Infrared spectra of aluminium isopropoxide (top), ferrocenoic acid (middle) and aluminium ferrocenoate (bottom).

The FTIR spectrum of aluminium ferrocenoate (**Figure 3.48**) does not show a broad O-H stretching band, indicating the absence of OH groups from either FcCOOH or an alumoxane product. Three antisymmetric carbonyl stretching bands at 1569, 1491 and 1651 cm^{-1} , labelled $\nu_{\text{asym } 1}$, $\nu_{\text{asym } 2}$ and $\nu_{\text{asym } 3}$ respectively, are observed, whilst only one symmetric carbonyl stretching band at 1403 cm^{-1} is present. Thus three $\Delta\nu$'s are obtained, i.e. $\Delta\nu_1 = 1569 - 1403 = 166 \text{ cm}^{-1}$, $\Delta\nu_2 = 1491 - 1403 = 88 \text{ cm}^{-1}$ and $\Delta\nu_3 = 1651 - 1403 = 248 \text{ cm}^{-1}$. The

$\Delta\nu$ of 166 cm^{-1} can either be assigned to asymmetric bidentate coordination or more probably a monodentate carboxylate bond. The second $\Delta\nu = 88\text{ cm}^{-1}$ is clearly associated with a bridging coordination mode. The small peak at 1651 cm^{-1} is not associated with free ferrocenoic acid because, even at significant enlargements, there is no trace of OH peaks at ca. $2800 - 3000\text{ cm}^{-1}$. Rather, this peak is associated with a ferrocenoic acid ligated in a monodentate fashion with Al because $\Delta\nu = 1651 - 1403 = 248\text{ cm}^{-1}$ is associated with this bridging mode (p. 128). Elemental analysis of aluminium ferrocenoate suggests an aluminium to iron ratio of 2:3. These results suggest a dimeric or polymeric structure possessing bridged and monodentate carboxylate coordination modes as shown in **Figure 3.49**. The infrared spectrum correlates well to the calculated spectrum of the 5/5 and reasonably well with the 6/6 coordinate aluminium ferrocenoate dimer in the computational investigation in **Figure 3.29**, p. 124 (**Table 3.15**, p. 125).

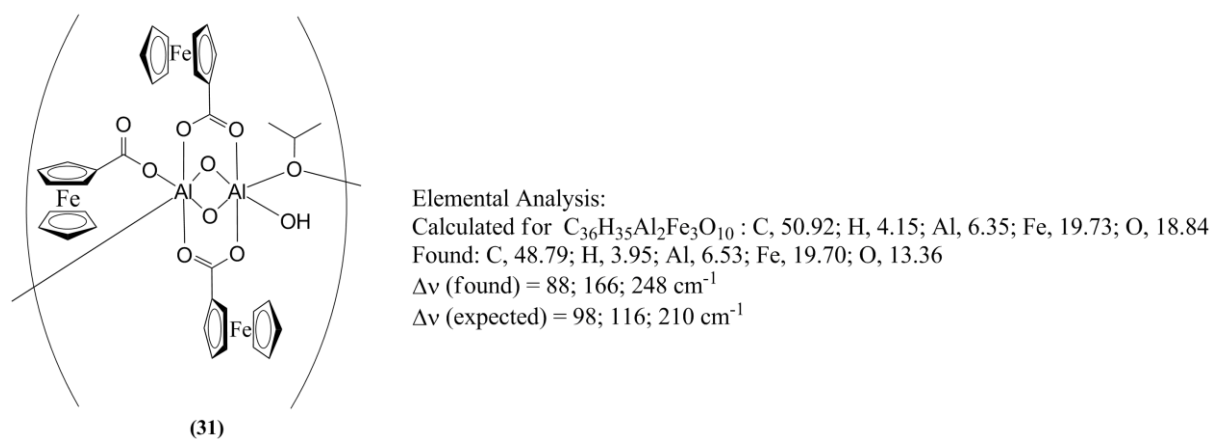


Figure 3.49: A possible structure and elemental analysis of aluminium ferrocenoate complex (31).

3.3.5. Conclusion

The overwhelming impression of this study, in contrast to literature suggestions, is that it is no trivial matter to synthesise simple aluminium tricarboxylates. Rather, dimers, polymers

or even alumoxane derivatives with complicated structures are obtained. In an attempt to predict possible structures and bonding modes of the various types of aluminium carboxylato compounds and carboxylato-alumoxanes, a variety of these compounds were synthesised and characterised. The infrared data for these aluminium carboxylates is summarised in **Table 3.20** below. From this data it is evident that the bonding mode of monocarboxylic acids to aluminium may be predicted by FTIR analysis. In particular, $\Delta\nu = \nu_{\text{Antisymmetric}} - \nu_{\text{Symmetric}}$ indicates the type of coordination which may be monodentate, bidentate or bridging. From the compounds studied here, $88 \leq \Delta\nu \leq 125 \text{ cm}^{-1}$ indicates a bridging coordination mode and $\Delta\nu \geq 200$ indicates monodentate coordination. Symmetrical bidentate coordination is associated with $\Delta\nu = 64 \text{ cm}^{-1}$ but this band pattern is difficult to verify experimentally. Finally, $160 \leq \Delta\nu \leq 190 \text{ cm}^{-1}$ may be indicative of asymmetric bidentate coordination or monodentate coordination. FTIR techniques have thus been developed to quantitatively distinguish between different bonding modes in aluminium carboxylato complexes (Goal 6, Chapter 1).

Table 3.20: Comparison of the carbonyl stretching frequencies and aluminium-oxygen stretching frequencies of the aluminium carboxylate complexes. ($\Delta\nu = \nu_{\text{Antisymmetric}} - \nu_{\text{Symmetric}}$)

Carboxylato-alumoxane	Carbonyl stretching frequencies (cm^{-1})			$\nu(\text{O-Al-O})$ (cm^{-1})
	$\nu_{\text{Antisymmetric}}$	$\nu_{\text{Symmetric}}$	$\Delta\nu$	
C_{12} alumoxane (24)	1586	1464	122	995
C_{18} alumoxane (25)	1626, 1561	1465	96, 161	977
Aluminium formate (26)	1606	1382	224	-
Aluminium acetate (27)	1651, 1571	1468, 1421	230, 103	-
Aluminium dodecanoate (30)	1708, 1652, 1587, 1562	1465	243, 187, 122, 97	988
Aluminium pentadecanoate (29)	1720, 1641, 1583	1470	250, 171, 113	988
Aluminium octadecanoate (28)	1701, 1585	1467	234, 118	986
Aluminium ferrocenoate (31)	1651, 1569, 1491	1403	248, 166, 88	-

This concludes the author's own research. The experimental detail of this research program is given in Chapter 4. Final conclusions and future perspectives are presented in Chapter 5.

- ¹ W. C. du Plessis, W. L. Davis, S. J. Cronje and J. C. Swarts, *Inorg. Chim. Acta*, 97, **314** (2001).
- ² W. C. du Plessis, T. G. Vosloo and J. C. Swarts, *J. Chem. Soc., Dalton Trans.*, 2507, (1998).
- ³ P. Zanello, F. F. de Biani, C. Glidewell, J. Koenig and S. J. Marsh, *Polyhedron*, 1795, **17** (1998).
- ⁴ T. G. Vosloo, *Sintetiese, Kinetiese En Strukturele Aspekte Van B-Diketonkomplekse Met 'n Potensiele Mediese Toepassing*, M. Sc. dissertation, University of the Free State, 1991.
- ⁵ M. B. Smith and J. March in *March's Advanced Organic Chemistry: Reactions, Mechanisms, and Structure*; John Wiley and Sons, New York, 2001, 5th edition, pp. 20 – 36.
- ⁶ F. H. Allen, O. Kennard, D. G. Watson, L. Brammer, A. G. Orpen and R. J. Taylor, *J. Chem. Soc., Perkin Trans.*, S8, **2** (1987).
- ⁷ W. C. Du Plessis, J. J. C. Erasmus, G. J. Lamprecht, J. Conradie, T. S. Cameron, M. A. S. Aquino and J. C. Swarts, *Can. J. Chem.*, 378, **77** (1999).
- ⁸ L. S. von Chrzanowski, M. Lutz and A. L. Spek, *Acta Cryst.*, m3318, **E62** (2006).
- ⁹ L. S. von Chrzanowski, M. Lutz and A. L. Spek, *Acta Cryst.*, m129, **C63** (2007).
- ¹⁰ A. Auger, A. J. Mullera and J. C. Swarts, *Dalton Trans.*, 3593, **33** (2007).
- ¹¹ A. Auger and J. C. Swarts, *Organometallics*, 102, **26** (2007).
- ¹² J. Conradie, T. S. Cameron, M. A. S. Aquino, G. J. Lamprecht and J. C. Swarts, *Inorg. Chim. Acta*, 2530, **358** (2005).
- ¹³ H. J. Gericke, N. L. Barnard and J. C. Swarts, *Unpublished results*.
- ¹⁴ F. Barrière, N. Camire, W. E. Geiger, U. T. Mueller-Westerhoff and R. Sanders, *J. Am. Chem. Soc.*, 7262, **124** (2002).
- ¹⁵ J. C. Swarts, T. G. Vosloo, S. J. Cronje, W. C. du Plessis, C. E. J. van Rensburg, E. Kreft and J. E. Van Lier, Submitted Anticancer Res., 2008.
- ¹⁶ R. Narayanan and R. M. Laine, *J. Mater. Chem.*, 2097, **10** (2000).
- ¹⁷ A. Salifoglou, *Coord. Chem. Rev.*, 297, **228** (2002).
- ¹⁸ K. Nakamoto, *Infrared Spectra of Inorganic and Coordination Compounds*, John Wiley & Sons, p. 197.
- ¹⁹ M. Davies, *Infra-red Spectroscopy and Molecular Structure*, Elsevier Publishing Company, New York, p. 222.
- ²⁰ The ADF program system was obtained from Scientific Computing and Modeling, Amsterdam (<http://www.scm.com/>). For a description of the methods used in ADF, see: G.T. Velde, F.M. Bickelhaupt, E.J. Baerends, C.F. Guerra, S.J.A. van Gisbergen, J.G. Snijders and T.J. Ziegler, *J. Comp. Chem.*, 931, **22** (2001).
- ²¹ J. P. Perdew, J. A. Chevary, S. H. Vosko, K. A. Jackson, M. R. Perderson, D. J. Singh and C. Fiohais, *Phys. Rev.*, 6671, **B46** (1992).
- ²² N. C. Handy and A. Cohen, *J. Mol. Phys.*, 403, **99** (2001).
- ²³ C. Lee, W. Yang and R. G. Parr, *Phys. Rev.*, 785, **B37** (1988).
- ²⁴ B. Miehlich, A. Savin, H. Stoll and H. Preuss, *Chem. Phys. Letters*, 200, **157** (1989).

- ²⁵ *Gaussian 03, Revision C.02*, M. J. Frisch, G. W. Trucks, H. B. Schlegel, G. E. Scuseria, M. A. Robb, J. R. Cheeseman, J. A. Montgomery, T. Vreven, K. N. Kudin, J. C. Burant, J. M. Millam, S. S. Iyengar, J. Tomasi, V. Barone, B. Mennucci, M. Cossi, G. Scalmani, N. Rega, G. A. Petersson, H. Nakatsuji, M. Hada, M. Ehara, K. Toyota, R. Fukuda, J. Hasegawa, M. Ishida, T. Nakajima, Y. Honda, O. Kitao, H. Nakai, M. Klene, X. Li, J. E. Knox, H. P. Hratchian, J. B. Cross, V. Bakken, C. Adamo, J. Jaramillo, R. Gomperts, R. E. Stratmann, O. Yazyev, A. J. Austin, R. Cammi, C. Pomelli, J. W. Ochterski, P. Y. Ayala, K. Morokuma, G. A. Voth, P. Salvador, J. J. Dannenberg, V. G. Zakrzewski, S. Dapprich, A. D. Daniels, M. C. Strain, O. Farkas, D. K. Malick, A. D. Rabuck, K. Raghavachari, J. B. Foresman, J. V. Ortiz, Q. Cui, A. G. Baboul, S. Clifford, J. Cioslowski, B. B. Stefanov, G. Liu, A. Liashenko, P. Piskorz, I. Komaromi, R. L. Martin, D. J. Fox, T. Keith, M. A. Al-Laham, C. Y. Peng, A. Nanayakkara, M. Challacombe, P. M. W. Gill, B. Johnson, W. Chen, M. W. Wong, C. Gonzalez, and J. A. Pople, *Gaussian, Inc., Wallingford CT*, **2004**.
- ²⁶ (a) P. J. Stephens, F. J. Devlin, C. F. Chabalowski and M. J. Frisch, *J. Phys. Chem.*, 11623, **98** (1994) (b) A. Watson, N. C. Handy and A. J. Cohen, *J. Chem. Phys.*, 6475, **119** (2003). (c) R. H. Hertwig and W. Koch, *Chem. Phys. Lett.*, 345, **268** (1997).
- ²⁷ G. A. Zhurko and D. A. Zhurko, *CHEM CRAFT*, Version 1.5 (build 282), 2007.
- ²⁸ C. E. Bethley, C. L. Aitken, C. J. Harlan, Y. Koide, S. G. Bott and A. R. Barron, *Organometallics*, 329, **16** (1997).
- ²⁹ Cambridge Structural Database (CSD), Version 5.27, August 2007 update.
- ³⁰ A. Tapparo, S. L. Heath, P. A. Jordan, G. R. Moore and A. K. Powell, *J. Chem. Soc. Dalton Trans.*, 1601, (1996).
- ³¹ R. C. Mehrotra and A. K. Rai, *Polyhedron*, 1967, **17** (1991).
- ³² A. Gilmour, A. Jobling and S. M. Nelson, *J. Chem. Soc.*, 1972, (1956).
- ³³ C. C. Landry, N. Pappé, M. R. Mason, A.W. Apblett, A. N. Tyler, A. N. MacInnes and A. R. Barron, *J. Mater. Chem.*, 331, **5(2)** (1995).
- ³⁴ Personal communication by C. Maloney from *Canadian Microanalytical Service Ltd*. Quote from the communication: "Our oxygen analysis is performed by initial pyrolysis of the sample * catalyzed thermal degradation of the sample in the absence of oxygen * at around 1150 degrees C. It is optimized to measure 'organic' oxygen * which is to say, oxygen that is part of a substance which will degrade at this temperature. Many metal oxides are stable at these temperatures and the oxygen in them cannot be measured by this method. In the case of your samples, aluminum oxides are extremely thermostable, and it is possible that your structures would 'degrade' into simple aluminum oxides under the analysis conditions described above, and we wouldn't see any oxygen which remained bound to aluminum. In my opinion, this analysis would not be very useful."
- ³⁵ G. G. Bombi, B. Corain, A. A. Sheikh-Osman and G. C. Valle, *Inorg. Chim. Acta*, 79, **171** (1990).
- ³⁶ B. Corain, B. Longato, A. A. Sheikh-Osman, G. G. Bombi and C. Maccà, *J. Chem. Soc. Dalton Trans.*, 169, (1992).
- ³⁷ M. Matzapetakis, M. Kourgiantakis, M. Dakanali, C. P. Raptopoulou, A. Terzis, A. Lakatos, T. Kiss, I. Banyai, L. Iordanidis, T. Mavromoustakos and A. Salifoglou, *Inorg. Chem.*, 1734, **40** (2001).
- ³⁸ P. C. Hidber, T. J. Graule and L. J. Gauckler, *J. Am. Chem. Soc.*, 1857, **79** (1996).
- ³⁹ T. L. Feng, P. L. Gurian, M. D. Healy and A. R. Barron, *Inorg. Chem.*, 408, **29** (1990).
- ⁴⁰ M. K. Wang, J. L. White and S. L. Hem, *Clays Clay Min.*, 65, **31** (1983).
- ⁴¹ A. Salifoglou, *Coord. Chem. Rev.*, 297, **228** (2002).
- ⁴² N. Bulc, L. Golic and J Sifatar, *Acta Cryst.*, 1829, **C40** (1984).
- ⁴³ L. Golic, I. Leban and N. Bulc, *Acta Cryst.*, 44, **C45** (1989).
- ⁴⁴ A. Tapparo, S. L. Heath, P. A. Jordan, G. R. Moore and A. K. Powell, *J. Chem. Soc. Dalton Trans.*, 1601, (1996).
- ⁴⁵ S. B. Johnson, T. H. Yoon, B. D. Kocar and G. E. Brown, *Langmuir*, 4996, **20** (2004).
- ⁴⁶ P. Sobota, M. O. Mustafa, J. Utko and T. Lis, *J. Chem. Soc. Dalton Trans.*, 1809, (1990).

⁴⁷ K. Nakamoto in *Infrared and Raman Spectra of Inorganic and Coordination Compounds Volume B 5th edition*; eds. N. Nakamoto, John Wiley & Sons, New York, 1997, p. 62.

⁴⁸ A. E. Leger, R. L. Haines, C. E. Hubley, J. C. Hyde and H. Sheffer, *Can. J. Chem.*, 799, **35** (1957).

Chapter 4 : Experimental

4.1. Introduction

The materials used in the current research program and the experimental procedures, techniques and reaction conditions that were used, are described in this section.

4.2. Materials

Solid reagents (Merck, Aldrich and Fluka) for synthesis were used without any further purification, these include AlCl_3 (Merck), aluminium isopropoxide (Aldrich) and acetylferrocene (Aldrich). The $\gamma\text{-Al}_2\text{O}_3$ and $\text{Al}(\text{OH})_3$ used in syntheses were industrial samples provided by SASOL. Liquid reagents (Merck and Aldrich) were used without any further purification unless otherwise specified and include ethyl acetate (Merck), ethyl trifluoroacetate (Aldrich) and methyl benzoate (Aldrich). Solvents were dried where specified. Benzene (Aldrich) was distilled and dried over sodium. Double distilled water was used. Column chromatography was performed on Kieselgel 60 (Merck, grain size 0.040 – 0.063 nm).

4.3. Spectroscopic measurements

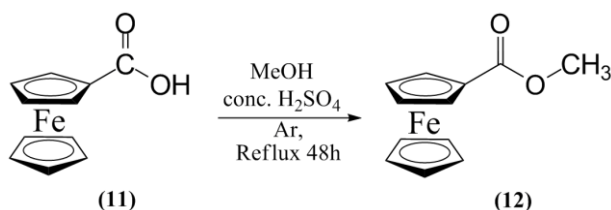
^1H NMR measurements were recorded at 298 K on a Bruker Advance DPX 300 NMR spectrometer. All chemical shifts are reported relative to TMS ($\text{Si}(\text{CH}_3)_4$) at 0.00 ppm. Selected spectra are provided in the appendix.

FTIR measurements were performed on solid samples using a Bruker Tensor 27 IR spectrometer and Pike MIRacle ATR, running OPUS software (V1.1). Melting points were determined on a Olympus BX51 microscope, using a LINKAM TMS 600 hotstage. The given melting points are the onset temperatures of melting.

Elemental analysis was performed by Canadian Microanalytical Service, Ltd.

4.4. Synthesis

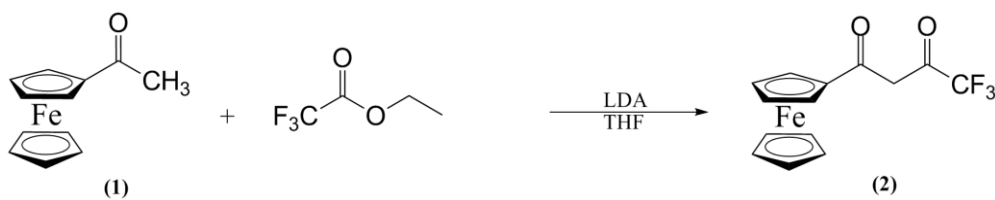
4.4.1. Methylferrocenoate, (12) [Scheme 3.1, p. 63]



Ferrocene carboxylic acid (1.5352 g, 7 mmol) was refluxed in methanol (300 cm³) in the presence of concentrated H₂SO₄ (0.12 cm³, 2.25 mmol) under an Argon atmosphere for 48 hours. Thereafter the cooled mixture was poured onto 200 g ice and extracted with ether (3 x 200 cm³). The ether layer was washed with water (3 x 100 cm³) and 0.1 M NaOH (3 x 100 cm³) and again with water (3 x 100 cm³), dried over anhydrous MgSO₄ and distilled off to give methylferrocenoate (0.9947 g, 75%) as a red crystalline powder. Melting point = 69 °C. ¹H NMR, δ_H (300 MHz, CDCl₃)/ppm: 3.82 (s; 3H; CH₃); 4.23 (s; 5H; C₅H₅); 4.42 (s; 2H; C₅H₄); 4.82 (s; 2H; C₅H₄).

4.4.2. β -diketones

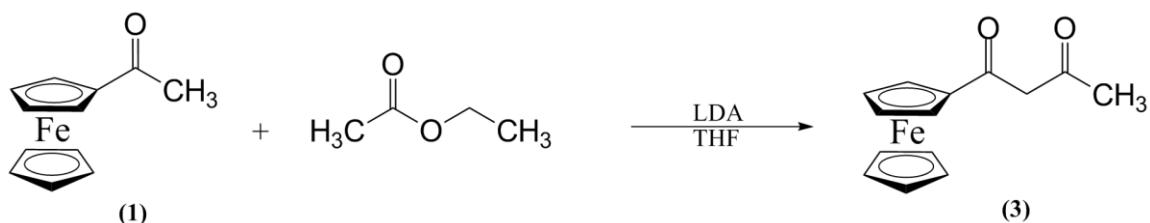
4.4.2.1. 4,4,4-trifluorobutane-1,3-dione, (2) [Scheme 3.2, p. 64]



Schlenk conditions were adhered to. The reaction vessel was flame-dried and degassed with argon for 1 hour and the argon atmosphere was maintained throughout the reaction. Acetylferrocene (0.912 g, 4 mmol) was dissolved in dry THF (8 cm³) to give a dark orange coloured solution. Lithium diisopropylamide (1.8 M solution in heptanes / tetrahydrofuran / ethylbenzene, 2.5 cm³, 4.5 mmol) was added slowly, whereafter the solution was stirred for 20 minutes at room temperature. During this time the colour of the solution changed to orange-red and a precipitate formed. Ethyl trifluoroacetate (0.5680 g, 4 mmol) that was predried over CaCl₂ and distilled^a was added to the reaction mixture and stirred overnight (12 hours). During this time the solution turned homogeneous and dark red but no precipitate formed. Diethyl ether (50 cm³) was added to the reaction mixture, which was then stirred with 1 M HCl (50 cm³) and ice (15 g) for 30 minutes. The layers were separated, the organic layer dried over anhydrous MgSO₄ and the solvent removed under reduced pressure. The residue was separated using column chromatography using hexane:ether, 1:1 (R_f 0.53) to give the clean product as a dark maroon powder (380 mg, 30%). Melting point = 102 °C. ¹H NMR, δ_{H} (600 MHz, CDCl₃, Spectrum 1)/ppm: 4.26 (s; 5H; C₅H₅); 4.70 (t; 2H; C₅H₄); 4.89 (t; 2H; C₅H₄); 6.10 (s; 1H; CH).

^a A better way of drying ethyl trifluoroacetate is given by A. I. Vogel in *Vogel's Textbook of Practical Organic Chemistry* 5th Edition; eds. B. S. Furniss, Pearson Education Limited, Harlow, 1996, p. 409.

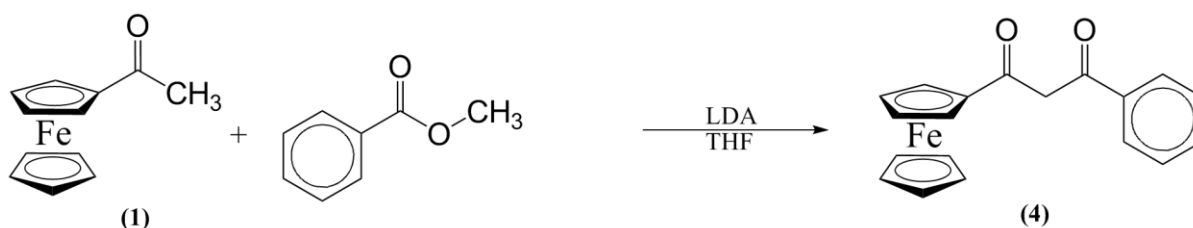
4.4.2.2. 1-ferrocenylbutane-1,3-dione, (3) [Scheme 3.2, p. 64]



Rigorous Schlenk conditions were adhered to. The reaction vessel was flame-dried and degassed with argon for 1 hour and the argon atmosphere was maintained during the reaction period. Acetylferrocene (0.912 g, 4 mmol) was dissolved in a minimum volume of dry THF (5 cm³) and stirred for several minutes. Lithium diisopropylamide (1.8 M solution in heptane / tetrahydrofuran / ethylbenzene, 2.5 cm³, 4.5 mmol) was then added whilst cooling the reaction mixture in an ice bath. The solution was stirred for 20 minutes at room temperature, during which a maroon precipitate formed. Ethyl acetate (0.3520 g, 4 mmol) that was predried over CaCl₂ and distilled,^a was then added and the reaction mixture stirred overnight (14 hours). An orange precipitate formed during this time. The reaction mixture was then added to diethyl ether (50 cm³), the precipitate filtered off and washed with diethyl ether (50 cm³). The precipitate was then added to a mixture of diethyl ether (50 cm³), 1 M HCl (50 cm³) and ice (20 g) and stirred for 30 minutes. The ether layer was washed with water (3 x 50 cm³), dried over anhydrous MgSO₄ and the removed under reduced pressure to give 0.227 g (26%) clean product as a red powder. Melting point = 105 °C. ¹H NMR, δ_H (300 MHz, CDCl₃, Spectrum 2)/ppm: keto isomer (22.1%) 2.34 (s, 3H, CH₃); 3.85 (s, 2H, CH₂); 4.25 (s; 5H; C₅H₅); 4.60 (s; 2H; C₅H₄); 4.80 (s; 2H; C₅H₄); enol isomer (77.9%) 2.11 (s, 3H, CH₃); 4.21 (s, 5H, C₅H₅); 4.52 (s, 2H, C₅H₄); 4.80 (s; 2H; C₅H₄); 5.74 (s, 1H, CH).

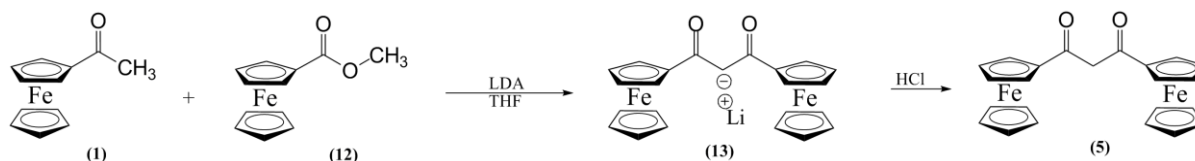
^a A better way of drying ethyl trifluoroacetate is given by A. I. Vogel in *Vogel's Textbook of Practical Organic Chemistry* 5th Edition; eds. B. S. Furniss, Pearson Education Limited, Harlow, 1996, p. 409.

4.4.2.3. Phenylpropane-1,3-dione, (4) [Scheme 3.2, p. 64]

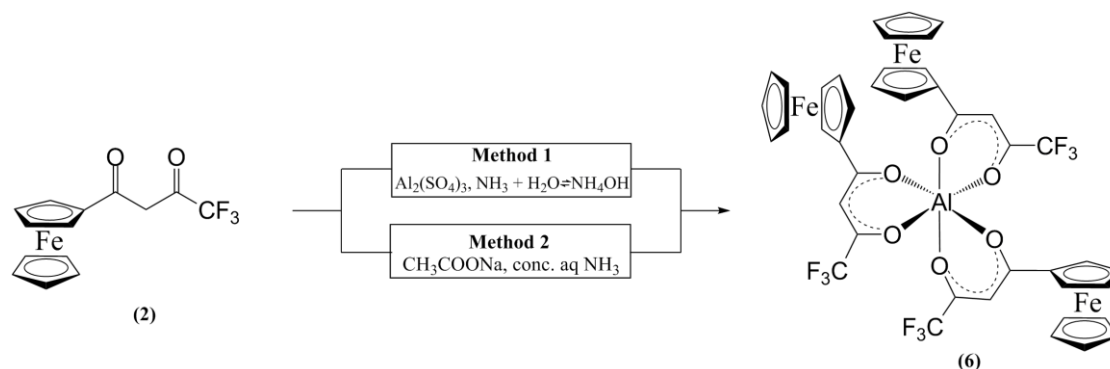


Rigorous Schlenk conditions were adhered to. The reaction vessel was flame-dried and degassed with argon for 1 hour and the argon atmosphere maintained during the reaction. Acetylferrocene (0.912 g, 4 mmol) was dissolved in a minimum volume of dry THF (5 cm³). Lithium diisopropylamide (1.8 M solution in heptanes / tetrahydrofuran / ethylbenzene, 2.5 cm³, 4.5 mmol) was added, whilst cooling the reaction in an ice bath. The solution was then stirred for 20 minutes at room temperature and a maroon precipitate formed. Methyl benzoate (0.544 g, 4 mmol) was added to the reaction mixture, which was then stirred overnight (14 hours). During this time the reaction mixture turned dark orange. The mixture was then poured onto diethyl ether (50 cm³), but no precipitation occurred. The solution was then added to 1 M HCl (50 cm³) and ice (20 g) and stirred for 30 minutes. The ether layer was then washed with water (3 x 50 cm³), dried over anhydrous MgSO₄, filtered and evaporated under reduced pressure. Column chromatography of the residue using hexane : ether, 3:2 (R_f = 0.57) produced 0.326 g (30%) product as a red powder. Melting point = 107 °C. ¹H NMR, δ_H (300 MHz, CDCl₃, Spectrum 3)/ppm: keto isomer (9.9%) 4.10 (s, 2H, CH₂); 4.17 (s, 5H, C₅H₅); 4.38 (s; 2H; C₅H₄); 7.55 - 7.64 (m, 3H, C₆H₅); 8.15 - 8.20 (m, 2H; C₆H₅); enol isomer (91.1%) 4.24 (s; 5H; C₅H₅); 4.58 (t; 2H; C₅H₄); 4.91 (t; 2H; C₅H₄); 6.41 (s; 1H; CH); 7.48 - 7.55 (m; 3H; C₆H₅); 7.87 - 8.02 (m; 2H; C₆H₅).

4.4.2.4. 1,3-diferrocenylpropane-1,3-dione, (5) [Scheme 3.2, p. 64]



Rigorous Schlenk conditions were adhered to. The reaction vessel was flame-dried and degassed with argon for 1 hour and the argon atmosphere was maintained throughout the reaction. Acetylferrocene (0.892 g, 3.9 mmol) was dissolved in a minimum volume of dry THF (5 cm³). Lithium diisopropylamide (1.8 M solution in heptanes / tetrahydrofuran / ethylbenzene, 2.5 cm³, 4.5 mmol) was added to the solution whilst cooling the reaction in an ice bath. The reaction mixture was then stirred at room temperature for 20 minutes during which a maroon precipitate formed. Methyl ferrocenoate (0.954 g, 3.9 mmol) was then added to the solution, which was then stirred overnight (14 hours). The reaction mixture was then added to diethyl ether (50 cm³), an orange precipitate that formed was filtered off, washed with diethyl ether (30 cm³) and air dried. This precipitate (0.532 g, 31%) of **(13)** is stable and can be stored for long periods of time. A portion of the precipitate (0.1 g, 0.22 mmol) was then added to a mixture of diethyl ether (30 cm³), 1 M HCl (20 cm³) and ice (10 g) and stirred for 30 minutes. The ether layer was washed with water (3 x 50 cm³), dried over anhydrous MgSO₄ and then removed under reduced pressure to give 0.084 g (87%) clean product as a red powder. Melting point = 157 °C. ¹H NMR, δ_H (300 MHz, CDCl₃, Spectrum 4)/ppm: keto isomer (37.6%) 4.21 (s; 10H; 2 x C₅H₅); 4.28 (s; 4H; 2 x CH₂); 4.89 (t; 4H; 2 x C₅H₄); 4.95 (t; 4H; 2 x C₅H₄); enol isomer (62.4%) 4.23 (s; 10H; 2 x C₅H₅); 4.54 (t; 4H; 2 x C₅H₄); 4.86 (t; 4H; 2 x C₅H₄); 6.00 (s; 2H; 2 x CH).

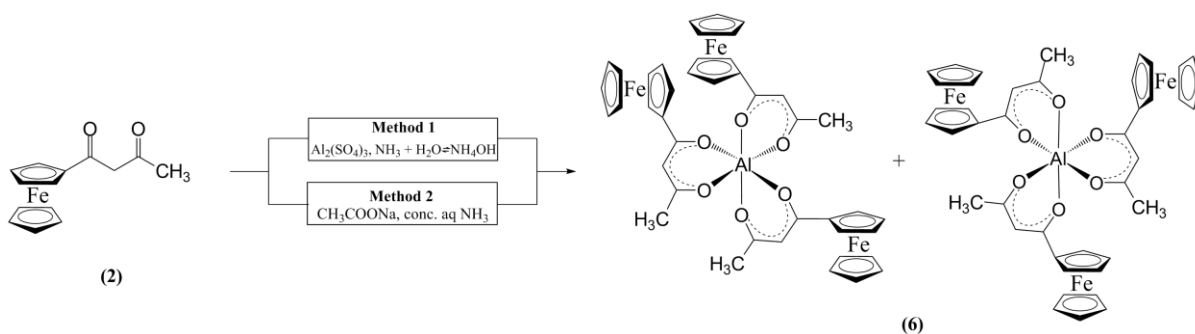
4.4.3. Aluminium β -diketonato complexes4.4.3.1. *Tris(1-ferrocenyl-4,4,4-trifluoroprop-1,3-dionato- κ^2 -O,O') aluminium(III), (6) [Scheme 3.4 and Scheme 3.5, p. 68 and p. 69]***Method 1: Methanol and aqueous NH₃**

A stirred solution of 1-ferrocenyl-4,4,4-trifluoroprop-1,3-dione (0.480 g, 1.48 mmol) and concentrated aqueous ammonia (19 cm³) in methanol (66 cm³) was added dropwise to a solution of aluminium sulphate octadecahydrate (0.327 g, 0.48 mmol) in water (3 cm³). After stirring for 30 minutes a dark maroon precipitate was filtered off and washed with water (3 x 30 cm³). The precipitate was then dissolved in a minimum volume of dichloromethane (ca. 30 cm³) and the resulting solution washed with water (3 x 30 cm³). The organic layer was dried over anhydrous MgSO₄ and evaporated. Chromatography of the residue using acetone:petroleum ether (1.5:8.5) (*R_f* = 0.43) produced 0.168 g (32%) clean product. This compound exists as the *mer*-isomer. Melting point = 187 °C. ¹H NMR, δ_{H} (300 MHz, CDCl₃, Spectrum 5)/ppm: 4.18 (s; 5H; C₅H₅); 4.30 (s; 10H; C₅H₅); 4.65 (m; 7H; fraction of 3 x C₅H₄); 4.92 (m; 5H; C₅H₄); 6.10 (s; 1H; CH); 6.14 (s; 1H; CH); 6.15 (s; 1H; CH).

Method 2: Sodium acetate, methanol and concentrated aqueous ammonia

To a solution of sodium acetate (30 mg, 0.370 mmol) in methanol (40 cm³), 1-ferrocenyl-4,4,4-trifluoroprop-1,3-dione (120 mg, 0.370 mmol) was added whilst stirring at room temperature. This solution was added to aluminium sulphate octadecahydrate (167 mg, 0.25 mmol) in water (2 cm³). Concentrated aqueous ammonia (10 cm³) was added to the solution and the solution left at room temperature overnight. A dark maroon precipitate was filtered off, washed with water (3 x 30 cm³). The solid was then dissolved in a minimum volume of dichloromethane (ca. 10 cm³) and washed with water (3 x 30 cm³). The organic layer was dried over anhydrous MgSO₄ and the solvent removed to give 0.012 g (10%) pure product. Characterization data is given with method 1.

4.4.3.2. Tris(1-ferrocenylbutane-1,3-dionato-κ²-O,O') aluminium(III), (7) [Scheme 3.4 and Scheme 3.5, p. 68 and p. 69]

**Method 1: Methanol and aqueous NH₃**

A solution of 1-ferrocenylbutane-1,3-dione (100 mg, 0.37 mmol) and concentrated aqueous ammonia (5 cm³) in methanol (20 cm³) was added dropwise to a solution of aluminium

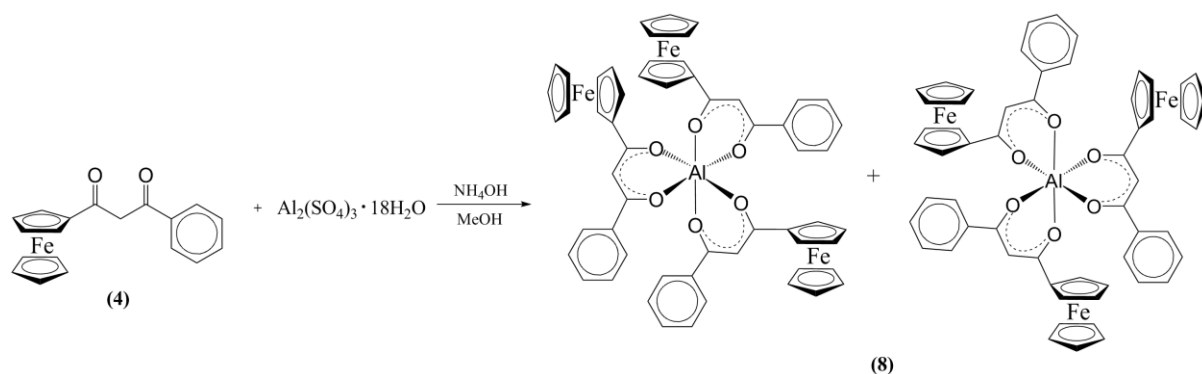
sulphate octadecahydrate (82 mg, 0.123 mmol) in water (2 cm³). After stirring for 2 hours an orange precipitate was filtered off and washed with water (3 x 30 cm³). The precipitate was then dissolved in a minimum volume of dichloromethane (ca. 30 cm³) and the resulting solution washed with water (3 x 30 cm³). The organic layer was dried over anhydrous MgSO₄ and evaporated. The residue was washed with acetone (3 x 10 cm³) and air dried to give 0.063 g (62%) of a mixture of the *mer*- (62%) and *fac*- isomers (38%). No melting was observed, since the compound decomposes above 250 °C. ¹H NMR δ_H (300 MHz, CDCl₃, Spectrum 6)/ppm: *fac*-isomer: 2.10 (s; 9H; 3 x CH₃); 4.22 (m; 15H; 3 x C₅H₅); 4.41 (m; 6H; fraction of 3 x C₅H₄); 4.76 (m; 6H; 3 x C₅H₄); 5.77 (s; 3H; 3 x CH); *mer*-isomer: 2.11 (s; 3H; CH₃); 2.12 (s; 3H; CH₃); 2.17 (s; 3H; CH₃); 4.12 (s; 5H; C₅H₅); 4.22 (s; 5H; C₅H₅); 4.26 (s; 5H; C₅H₅); 4.35 (m; 2H; C₅H₄); 4.38 (m; 4H; C₅H₄); 4.79 (m; 2H; C₅H₄); 4.85 (m; 1H; C₅H₄); 4.87 (m; 1H; C₅H₄); 4.91 (m; 2H; C₅H₄); 5.74 (s; 1H; CH); 5.77 (s; 1H; CH); 5.81 (s; 1H; CH).

Method 2: Sodium acetate, methanol and concentrated aqueous ammonia

To a solution of sodium acetate (30 mg, 0.370 mmol) in methanol (20 cm³), 1-ferrocenyl-1,3-butanedione (100 mg, 0.370 mmol) was added whilst stirring at room temperature. This solution was added to aluminium sulphate octadecahydrate (167 mg, 0.25 mmol) in water (2 cm³) and stirred for 50 minutes. Concentrated aqueous ammonia (10 cm³) was added to the solution and the solution left at room temperature overnight. A small amount of solid [colour orange] was filtered off, washed with water (3 x 10 cm³). The solid was then dissolved in a minimum volume of dichloromethane and washed with water (3 x 30 cm³). The organic layer was dried over anhydrous MgSO₄ and the solvent removed to give 1 mg

(1%) of the *mer*- and *fac*-isomer mixture as in method 1. Characterization data is given in method 1.

4.4.3.3. Tri-(phenylpropane-1,3-dionato- κ^2 -O,O') aluminium (III), (8) [Scheme 3.4 and Scheme 3.5, p. 68 and p. 69]

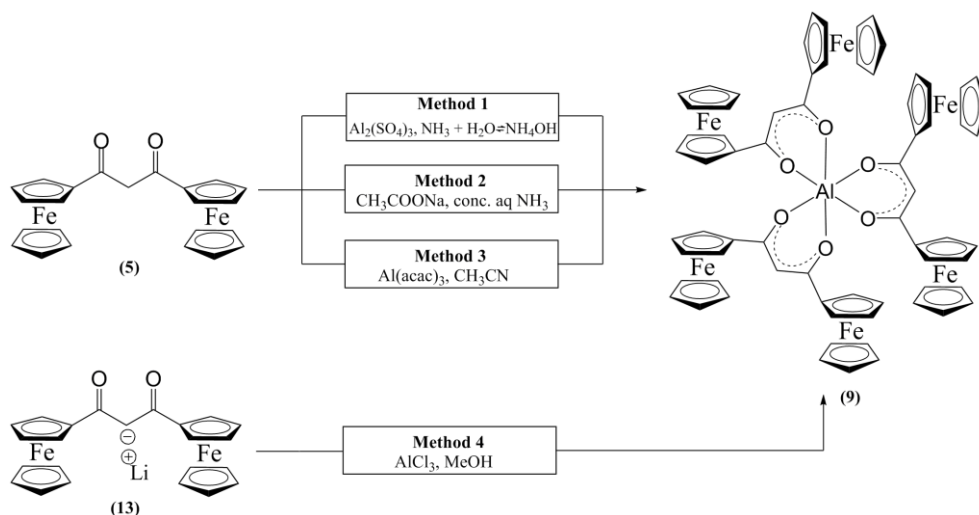


A stirred solution of phenylpropane-1,3-dione (68 mg, 0.246 mmol) and concentrated aqueous ammonia (5 cm³) in methanol (20 cm³) was added dropwise to a solution of aluminium sulphate octadecahydrate (82 mg, 0.123 mmol) in water (2 cm³). After stirring for 4 hours, a red precipitate was filtered off and washed with water (3 x 30 cm³). The precipitate was then dissolved in a minimum volume of dichloromethane and the resulting solution washed with water (3 x 30 cm³). The organic layer was dried over anhydrous MgSO_4 and evaporated. Chromatography of the residue using hexane : diethyl ether (1:1) ($R_f = 0.4$) as eluent produced 35 mg (50%) of a mixture of the *mer*- (75%) and *fac*-isomers (25%). Melting point = 207 °C. ¹H NMR δ_{H} (300 MHz, CDCl_3 , Spectrum 7)/ppm: *fac*-isomer: 4.21 (m; 15H; fraction of 3 x C_5H_5); 4.43 (m; 6H; fraction of 3 x C_5H_4); 5.1 (m; 6H; fraction of 3 x C_5H_4); 6.53 (s; 3H; CH); 7.36 – 7.46 (m; 9H, fraction of 3 x C_6H_5); 8.05 (m, 6H, fraction of C_6H_5); *mer*-isomer: 4.10 (s; 5H; C_5H_5); 4.12 (s; 5H; C_5H_5); 4.17 (s; 5H; C_5H_5); 4.38 (m; 2H; C_5H_4); 4.41 (m; 2H; C_5H_4); 4.43 (m; 2H; C_5H_4); 4.84 (m; 2H; C_5H_4); 4.88 (m; 2H; C_5H_4); 4.91 (m;

2H; C₅H₄); 6.46 (s; 1H; CH); 6.49 (s; 1H; CH); 6.53 (s; 1H; CH); 7.36 – 7.46 (m; 9H, fraction of 3 x C₆H₅); 8.05 (m, 6H, fraction of C₆H₅).

4.4.3.4. *tris(1,3-diferrocenylpropane-1,3-dionato-κ²-O,O')* aluminium(III), (9)

[Scheme 3.4 - Scheme 3.7, pp. 68 - 70]



Method 1: Methanol and aqueous NH₃

A solution of 1,3-diferrocenylpropane-1,3-dione (30 mg, 0.1136 mmol) and concentrated aqueous ammonia (5 cm³) in methanol (20 cm³) was added dropwise to a solution of aluminium sulphate octadecahydrate (25.4 mg, 0.0379 mmol) in water (2 cm³). After stirring for 16 hours an orange suspension formed which was centrifuged. The recovered precipitate was then washed with water (3 x 10 cm³) and acetone (3 x 10 cm³) and air dried to give 8 mg (26%) clean product. No melting was observed, since the compound decomposes above 250 °C. This product was very poorly soluble and no NMR could be obtained. It was proved as the product by electrochemical studies (Section 3.2.5.2, p. 93)

and elemental analysis. Elemental analysis: Calculated for $C_{69}H_{57}AlO_6Fe_6$: C, 61.60; H, 4.35; Al, 2.01; Fe, 24.91; O, 7.14; Found: C, 61.34; H, 4.72; Al, 1.83; Fe, 25.31; O, 6.63.

Method 2: Sodium acetate, methanol and concentrated aqueous ammonia (unsuccessful)

To a solution of 1,3-diferrocenylpropane-1,3-dione (40 mg, 0.091 mmol) in methanol (20 cm³) sodium acetate (8.2 mg, 0.1 mmol) was added whilst stirring at room temperature. This solution was added to aluminium sulphate octadecahydrate (22 mg, 0.033 mmol) in water (2 cm³) and stirred for 1 hour. Concentrated aqueous ammonia (10 cm³) was added to the solution and the solution left at room temperature overnight. No precipitation occurred and 1,3-diferrocenylpropane-1,3-dione was recovered.

Method 3: Aluminium trisacetylacetonate, acetonitrile

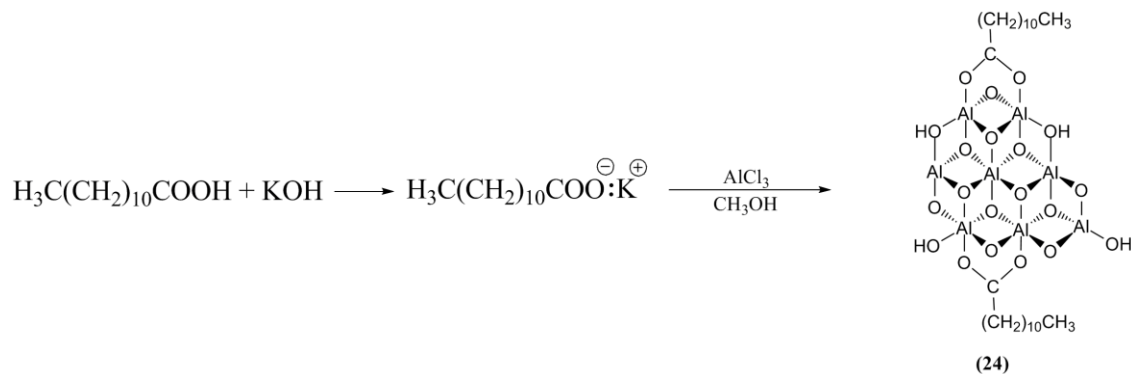
A solution of aluminium trisacetylacetonate (12.3 mg, 0.038 mmol) and 1,3-diferrocenylpropane-1,3-dione (50 mg, 0.114 mmol) in acetonitrile (15 cm³) was refluxed for 3 hours. The solvent was then reduced to ± 2 cm³ and an orange precipitate filtered off and washed with ether (3 x 10 cm³) to give 10.2 mg (7%) clean product.

Method 4: 1,3-diferrocenylpropane-1,3-dionato lithium(I), AlCl₃ and MeOH

A solution of 1,3-diferrocenylpropane-1,3-dionato lithium(I) (100 mg, 0.224 mmol) in methanol (10 cm³) was added dropwise to a solution of AlCl₃ (10 mg, 0.075 mmol) in water (1 cm³). A precipitate [colour orange] was filtered off and washed with water (3 x 10 cm³) and acetone (3 x 10 cm³) and dried in air to give 25 mg (23%) clean product.

4.4.4. Aluminium carboxylate complexes

4.4.4.1. Dodecanoato-alumoxane, (24) [Scheme 3.13, p. 130]

**A. Potassium dodecanoate:**

Potassium hydroxide (0.5 M, ca. 70 cm³) was added dropwise to melted dodecanoic acid (5 g, 25 mmol) at 45 °C whilst stirring, until a clear solution with slight alkaline pH was obtained. The water in the solution was then distilled off under reduced pressure to produce a white solid. Methanol (20 cm³) was then added to the solid. White potassium hydroxide did not dissolve and was filtered off from the solution containing potassium dodecanoate. The methanol was then distilled off under reduced pressure to produce 5.2943 g (89%) potassium dodecanoate. FTIR, $\nu(\text{neat})/\text{cm}^{-1}$: 1558 (CO)_{asym}; 1471 (CO)_{sym}.

B. Dodecanoato-alumoxane

Potassium dodecanoate (2.15 g, 9 mmol) was dissolved in methanol (60 cm³) and added dropwise to a solution of aluminium chloride (400 mg, 3 mmol) in water (0.5 cm³). A beige precipitate was filtered off, washed with methanol and air dried to produce 0.5964 g dodecanoato-alumoxane. No melting up to 450 °C was observed. FTIR, $\nu(\text{neat})$, Spectrum

8)/cm⁻¹: 1635 (CO)_{asym}; 1579 (CO)_{asym}; 1471 (CO)_{sym}. Elemental analysis: Calculated for C₂₄H₄₆Al₈O₁₈: C, 34.38; H, 5.53; Al, 25.74; O, 34.35; Found: C, 34.34; H, 5.72; Al, 4.79. Note: Al cannot be analysed when it exits as Al₂O₃ by the method used, ref. 34, p. 159.

4.4.4.2. Octadecanoato-alumoxane, (25) [Scheme 3.13, p. 130]



A. Potassium octadecanoate:

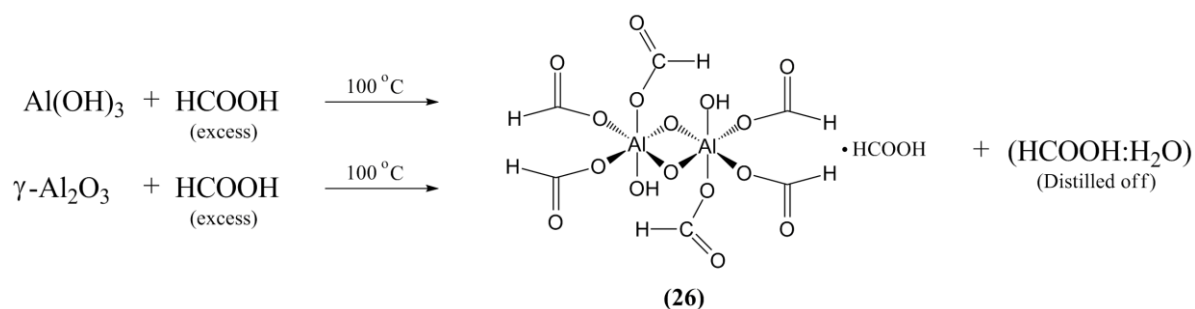
Potassium hydroxide (0.5 M, ca. 70 cm³) was added dropwise to melted stearic acid (3 g, 17.5 mmol) at 70 °C whilst stirring, until a clear solution with alkaline pH was obtained. The water in the solution was then evaporated under reduced pressure to produce a white solid. Methanol (20 cm³) was then added to the solid and white potassium hydroxide did not dissolve and was filtered off. The methanol was then evaporated under reduced pressure to produce 4.876 g (86%) potassium stearate. FTIR, $\nu(\text{neat})/\text{cm}^{-1}$: 1559 (CO)_{asym}; 1477 (CO)_{sym}.

B. Octadecanoato-alumoxane

Potassium stearate (0.9677 g, 3 mmol) was dissolved in methanol (20 cm³) and added dropwise to a solution of aluminium chloride (133 mg, 1 mmol) in water (0.5 cm³). A beige precipitate was filtered off, washed with methanol and air dried to produce 0.2467 g octadecanoato-alumoxane. No melting up to 450 °C was observed. FTIR, $\nu(\text{neat, Spectrum}$

9)/cm⁻¹: 1626 (CO)_{asym}; 1559 (CO)_{asym}; 1461 (CO)_{sym}. Elemental analysis: Calculated for C₃₆H₇₀Al₂O₈: C, 63.13; H, 10.30; Al, 7.88; O, 18.69; Found: C, 63.11; H, 10.31; Al, 5.89. Note: Al cannot be analysed when it exits as Al₂O₃ by the method used, ref. 34, p. 159.

4.4.4.3. Aluminium formate, (26) [Scheme 3.14, p. 136]



A. From Al(OH)₃

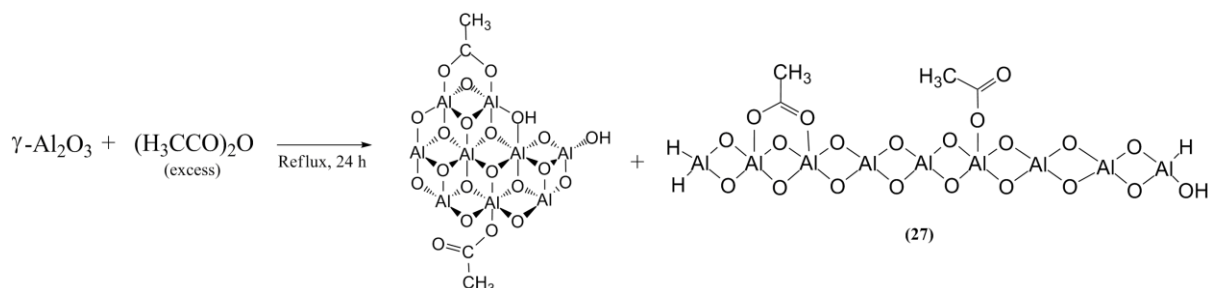
Aluminium hydroxide (gibbsite) (10 g, 0.128 mol) was added to formic acid (100 cm³, 2.65 mol). The mixture was heated to 100 °C and 80 cm³ formic acid was distilled off over a period of 2 – 3 hours whilst stirring. A white solid was filtered off from the remaining formic acid, washed with acetone and distilled under reduced pressure at 100 °C over 4 hours to give 9.4907 g (34%) aluminium formate. No melting up to 450 °C was observed. FTIR, ν(neat, Spectrum 10)/cm⁻¹: 1610 (CO)_{asym}; 1377 (CO)_{sym}.

B. From γ-Al₂O₃

The same experimental procedure as in **A** above was used except for Al(OH)₃ being replaced by γ-Al₂O₃ (10 g, 0.098 mol). The yield of aluminium triformate was 16.5 g (38.6%). FTIR,

$\nu(\text{neat, Spectrum 10})/\text{cm}^{-1}$: 1606 (CO)_{asym}; 1382 (CO)_{sym}. Elemental analysis: Calculated for C₇H₁₀Al₂O₁₈: C, 19.28; H, 2.31; Al, 12.37; O, 66.04; Found: C, 19.73; H, 2.38; Al, 12.80.

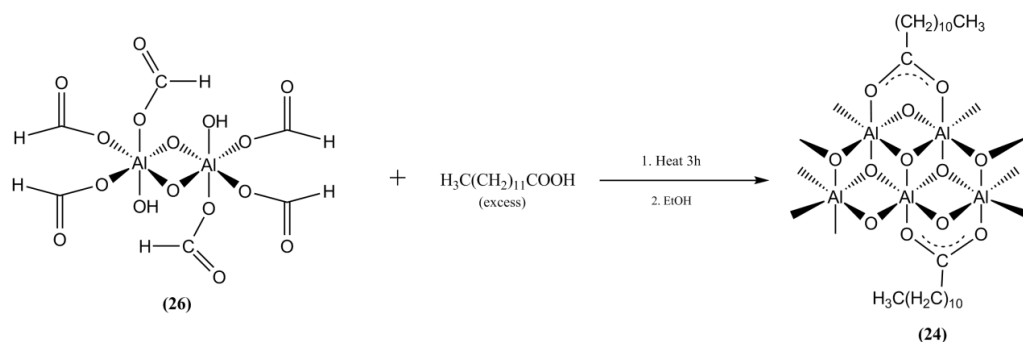
4.4.4.4. Aluminium acetate, (27) [Scheme 3.15, p. 140]



Gamma aluminium oxide (10 g, 98 mmol) was refluxed in acetic anhydride (100 cm³) for 24 hours. A white solid was filtered off, washed with acetone and air dried for 3 hours to give 11.297 g aluminium acetate. No melting up to 450 °C was observed. FTIR, $\nu(\text{neat, Spectrum 11})/\text{cm}^{-1}$: 1651 (CO)_{asym}; 1571 (CO)_{asym}; 1468 (CO)_{sym}; 1421 (CO)_{sym}. Elemental analysis: Calculated for linear structure: C₄H₁₀Al₉O₂₁: C, 7.54; H, 1.58; Al, 38.12; O, 52.75; Alumoxane: C₄H₈Al₉O₂₁: C, 7.57; H, 1.27; Al, 38.25; O, 52.92; Found: C, 7.56; H, 1.50; Al, 38.2.

4.4.4.5. Dodecanoato-alumoxane (24) from aluminium formate [Scheme 3.16, p. 146]

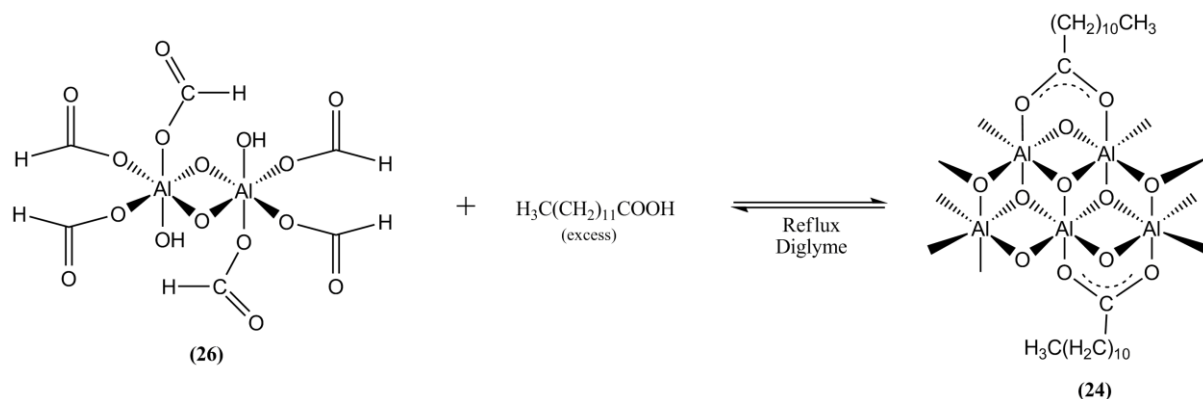
(Low temperature route)



A mixture of dodecanoic acid (3.70 g, 18.5 mmol) and aluminium formate (1 g, 2.29 mmol) was heated to 46 °C, where the acid melted. The reaction mixture was stirred for 24 hours, after which it was allowed to cool and pulverised with diethyl ether (40 cm³). The finely dispersed reaction mixture was then filtered. Dodecanoato-alumoxane was precipitated in very low yield (<1%, 50 mg) from the filtrate by the addition of ethanol (20 cm³). Characterisation is given for dodecanoato-alumoxane in 4.4.4.1 on p. 174.

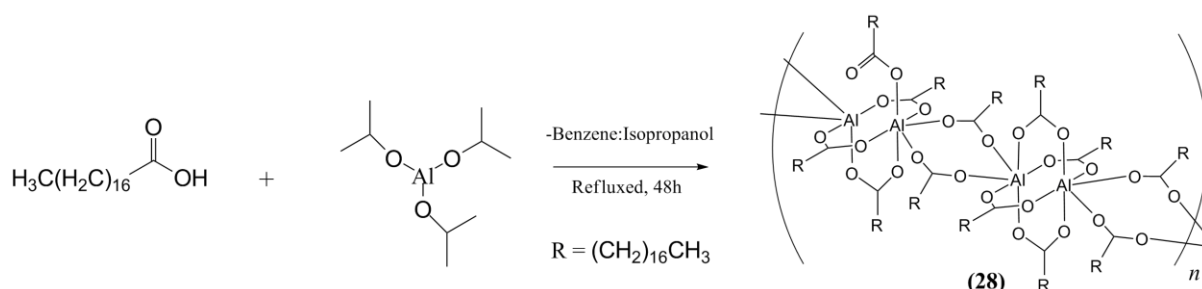
4.4.4.6. Dodecanoato-alumoxane (24) from aluminium formate [Scheme 3.17, p. 146]

(High temperature route)



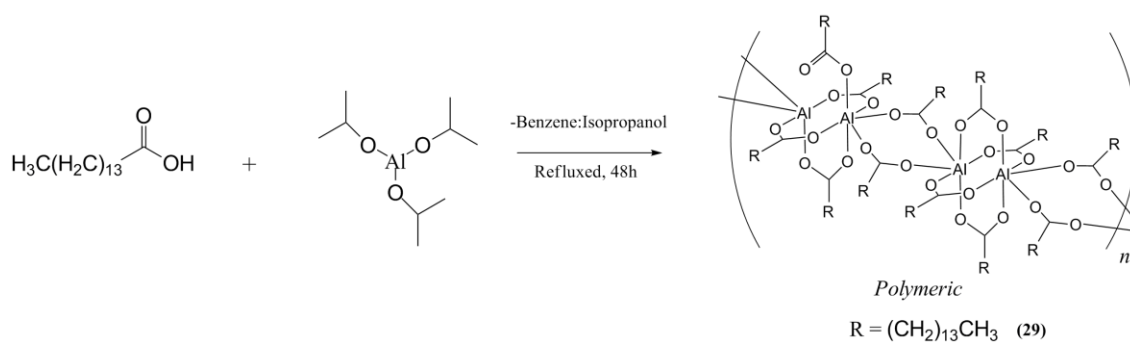
Dodecanoic acid (3.71 g, 18.5 mmol) and aluminium formate (1.1 g, 2.52 mmol) was refluxed in diglyme (boiling point = 162 °C) for 24 hours. After which it was allowed to cool and pulverised with diethyl ether (40 cm³). The finely dispersed reaction mixture was then filtered. Dodecanoato-alumoxane was precipitated in very low yield (<1%, 46 mg) from the filtrate by the addition of ethanol (20 cm³). Characterisation is given for dodecanoato-alumoxane in 4.4.4.1 on p. 174.

4.4.4.7. Octadecanoato aluminium(III) (28) [Scheme 3.18, p. 147]



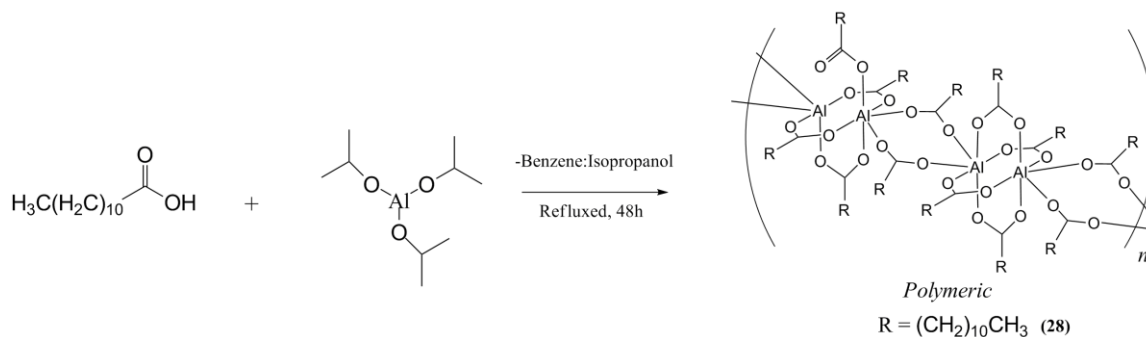
Aluminium isopropoxide (0.75g, 3.67 mmol) and stearic acid (3.132 g, 11 mmol) were dissolved in dry benzene (80 cm³). The mixture was refluxed for 48 hours, whilst a distillate (71 – 74 °C) was periodically collected, until no more isopropanol could be detected by refractive index measurements (see 4.4.4.11). An insoluble product was filtered off and washed with dry acetone to yield 1.81 g aluminium tristearate. The exact yield was not calculated due to the exact structure not being known. Melting point = 137 °C (onset of melting). FTIR, $\nu(\text{neat, Spectrum } 12)/\text{cm}^{-1}$: 1701 (CO)_{asym}; 1585 (CO)_{asym}; 1467 (CO)_{sym}. Elemental analysis: Calculated for C₁₀₈H₂₁₀Al₂O₁₂: C, 73.92; H, 12.06; Al, 3.08; O, 10.94; Found: C, 71.68; H, 12.05; Al, 3.13; O, 10.6.

4.4.4.8. Pentadecanoato aluminium(III) (29) [Scheme 3.18, p. 147]



Remark: The structure of the product is more likely a mixture of the polymeric and dimeric structures shown on p. 152. Aluminium isopropoxide (2.67 g, 11 mmol) and pentadecanoic acid (0.75 g, 11 mmol) were dissolved in dry benzene (80 cm³). The mixture was refluxed for 48 hours, whilst a distillate (71 – 74 °C) was periodically collected, until no more isopropanol could be detected by refractive index measurements (see 4.4.4.11). An insoluble product was filtered off and washed with dry acetone to yield 2.12 g aluminium tripentadecanoate. The exact yield was not calculated due to the exact structure being unknown. Melting point = 121 °C (onset of melting). FTIR, $\nu(\text{neat, Spectrum 13})/\text{cm}^{-1}$: 1720 (CO)_{asym}; 1641 (CO)_{asym}; 1583 (CO)_{asym}; 1470 (CO)_{sym}. Elemental analysis: Calculated for C₉₀H₁₇₄Al₂O₁₂: C, 71.95; H, 11.67; Al, 3.59; O, 12.78; Found: C, 68.43; H, 11.07; Al, 3.73; O, 11.76.

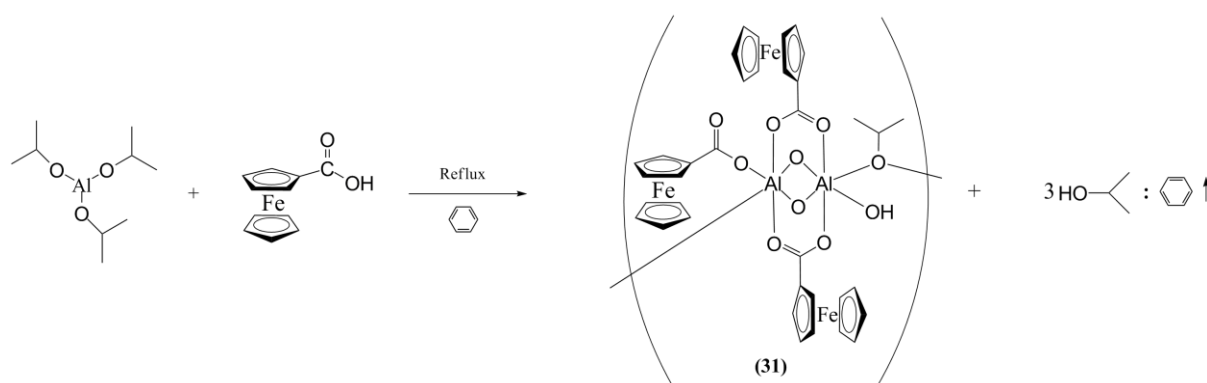
4.4.4.9. Dodecanoato aluminium(III) (30) [Scheme 3.18, p. 147]



Remark: The structure of the product is more likely a mixture of the polymeric and dimeric structures shown on p. 154. Aluminium isopropoxide (0.373 g, 1.83 mmol) and dodecanoic acid (2.21g, 11 mmol) were dissolved in dry benzene (80 cm³). The mixture was refluxed for 48 hours, whilst a distillate (71 – 74 °C) was periodically collected, until no more isopropanol could be detected by refractive index measurements (see 4.4.4.11). An insoluble product was filtered off and washed with dry acetone to yield 1.8 g aluminium pentadecanoate. The exact yield was not calculated due to the exact structure being unknown. Melting point =

167 °C (onset of melting). FTIR, $\nu(\text{neat, Spectrum 14})/\text{cm}^{-1}$: 1708 (CO)_{asym}; 1652 (CO)_{asym}; 1587 (CO)_{asym}; 1562 (CO)_{asym}; 1465 (CO)_{sym}. Elemental analysis: Calculated for C₇₂H₁₃₈Al₂O₁₂: C, 69.14; H, 11.20; Al, 4.31; O, 15.35; Found: C, 64.70; H, 10.73; Al, 4.93; O, 13.66.

4.4.4.10. Ferrocenoato Aluminium(III)(31) [Scheme 3.19, p.155]



Aluminium isopropoxide (0.1192g, 0.5821 mmol) and FcCOOH (0.4017 g, 1.75 mmol) were dissolved in dry benzene (80 cm³). The mixture was refluxed for 48 hours, whilst a distillate (71 – 74 °C) was periodically collected, until no more isopropanol could be detected by refractive index measurements (see 4.4.4.11). An insoluble product was filtered off and washed with dry acetone to yield 0.20 g aluminium ferrocenoate (69%). No melting was observed up to 450 °C. FTIR, $\nu(\text{neat, Spectrum 13})/\text{cm}^{-1}$: 1651 (CO)_{asym}; 1569 (CO)_{asym}; 1491 (CO)_{asym}; 1403 (CO)_{sym}. Elemental analysis: Calculated for C₄₇H₄₃Al₂Fe₄O₉: C, 54.85; H, 4.21; Al, 5.24; Fe, 21.70; O, 13.99; Found: C, 48.79; H, 3.95; Al, 6.53; Fe, 19.70; O, 13.36.

4.4.4.11. Refractive index determination of isopropanol

During the synthesis of **(28)** - **(31)** an azeotropic mixture of benzene and isopropanol was removed by distillation. The refractive index of pure, dry benzene (1.5018) was obtained at 25 °C.

The refractive index of periodically collected distillate was obtained at 25 °C. The reaction was allowed to proceed until the distillate had a refractive index of pure benzene (1.5018).

4.5. Electrochemistry

Cyclic voltammetry, square wave voltammetry and linear sweep voltammetry was conducted using a BAS 100 B/W voltammograph. A three-electrode configuration was used. A Vicor-tipped, in-house constructed Ag/AgCl reference electrode immersed in an acetonitrile Luggin capillary bridged by a second capillary containing CH₂Cl₂ to minimize potential drift (over potentials). The AgCl-coated silver wire was prepared by anodic electrolysis of the wire in a 1 M HCl solution using a potential of 1.5 V and a 20 μA current for a period of 30 seconds. A glassy carbon working electrode and Pt auxiliary electrode was used.

Spectrochemical grade CH₂Cl₂ (Aldrich) was used as solvent in a 4 cm³ cell. Tetrabutylammonium tetrakis(pentafluorophenyl)borate, [NBu₄][B(C₆F₅)₄], was used as supporting electrolyte in a concentration of 0.1 M. The supporting electrolyte was also present within the Luggin capillary. β-diketonato aluminium concentrations were 0.5 mmol

dm⁻³. Analyses were performed at ambient temperatures and under nitrogen. Decamethyl ferrocene (Fc*) was used as an internal standard but all potential values are reported against ferrocene at 0 mV. Decamethyl ferrocene has a potential of -610 mV versus free ferrocene. Data were exported to Microsoft Excel for manipulation and diagram preparation.

4.6. Single crystal X-ray crystallography of Al(FcCOCHCOF₃)₃

The author thanks Dr. F.J. Muller for solving this crystal structure.

A red plate-like crystal of Al(FcCOCHCOF₃)₃ with approximate dimensions 0.575 × 0.094 × 0.06 mm³ was mounted on a glass fibre and used for the X-ray crystallographic analysis. The X-ray intensity data were measured on a Bruker X8 Apex II 4K CCD area detector diffractometer equipped with a graphite monochromator and Mo-K α fine-focus sealed tube ($k = 0.71073 \text{ \AA}$) operated at 1.5 KW power (50 KV, 30 mA). The detector was placed at a distance of 3.75 cm from the crystal. Crystal temperature during the data collection was kept constant at 100(2)K using an Oxford 700 series cryostream cooler.

The initial unit cell and data collection were achieved by the Apex2 software utilizing COSMO for optimum collection of more than a hemisphere of reciprocal space. A total of 862 frames were collected with a scan width of 0.5 in φ and ω , and an exposure time of 250 s frame⁻¹. The frames were integrated using a narrow frame integration algorithm and reduced with the Bruker SAINTPlus and XPREP **software** packages respectively. Analysis of the data showed no significant decay during the data collection. Data were corrected for

absorption effects using the multi-scan technique SADABS. The structure was solved by the direct methods package SIR97 and refined using the WinGX software package incorporating SHELXL. The aromatic protons were placed in geometrically idealized positions (C–H = 0.95 Å) and constrained to ride on their parent atoms with $U_{\text{iso}}(\text{H}) = 1.2 U_{\text{eq}}(\text{C})$. Non-hydrogen atoms were refined with anisotropic displacement parameters. Atomic scattering factors were taken from the International Tables for Crystallography Volume C. The molecular plot was drawn using the DIAMOND program with a 50% thermal envelope probability for non-hydrogen atoms. Hydrogen atoms were drawn as arbitrary sized spheres with a radius of 0.135Å°.

4.7. Cytotoxic determinations

The author thanks Prof. C.E.J. van Rensburg from Department of Pharmacology, University of Pretoria, for performing cytotoxic measurements.

4.7.1. Sample preparation

The samples were dissolved in dimethyl sulphoxide (DMSO) to produce stock solutions with concentrations of 20 mmol dm⁻³, followed by dilution in the appropriate growth medium supplemented with fetal calf serum (FCS). Giving final DMSO concentrations of less than 0.5% and drug concentrations of 10 – 50 µmol dm⁻³.

4.7.2. Cell cultures

The human cervix epitheloid cancer cell line, HeLa (ATCC CCL-2) (American Type Culture Collection, Manassas, Virginia, USA), was grown as a mono layer culture using MEM. The growth media was kept at 37°C under 5% CO₂ and fortified with 10% FCS and 1% penicillin and streptomycin. Mononuclear leukocytes were prepared from whole blood collected from healthy donors by density centrifugation on Histopaque-1077 (Sigma-Aldrich, St Louis, Missouri, USA) cushions at 400 g for 25 minutes at room temperature. The lymphocyte band was washed and the cells were resuspended in RPMI 1640 supplemented with 10% FCS. Cells were seeded at 500 cells/well in 96 well microtiter plates in a final volume of 200 µl of growth medium, in the presence or absence of different concentrations of experimental drugs. Appropriate control systems were included. After seven days of incubation at 37°C, cell survival was measured by means of the colorimetric 3-(4,5-dimethylthiazol-2-yl)-diphenyltetrazodium bromide (MTT) assay (8, 22, 23). Wells without cells and wells without drugs were included as controls.

Chapter 5 : Summary and future perspectives

5.1. Introduction

In this chapter, the main results of the current research project will be highlighted, summarised and the implications thereof considered.

5.2. Summary of results

Ferrocene-containing β -diketonato ligands, $\text{FcCOCH}_2\text{COR}$ with $\text{R} = \text{CF}_3$ (**2**), CH_3 (**3**), C_6H_5 (**4**) and $\text{Fc} = \text{ferrocenyl}$ (**5**), were successfully synthesised (yields 22 – 31%) and coordinated to aluminium(III). This expanded the only known ferrocene-containing β -diketonato aluminium(III) compound, $\text{Al}(\text{FcCOCHCOF}_3)_3$, to a series, $\text{Al}(\text{FcCOCHCOR})_3$, with substituents R spanning a range of electronegativities from 1.87 (Fc), 2.21 (Ph) and 2.34 (CH_3) to 3.01 (CF_3). ^1H NMR studies indicated that these compounds can occur as two isomers, the *mer*- and *fac*-isomers. $\text{Al}(\text{FcCOCHCOF}_3)_3$, however, occurred as only the *mer*-isomer, the structure of which was determined by single crystal x-ray crystallography. $\text{Al}(\text{FcCOCHCOF}_3)_3$ crystallised in a $\text{P2}_1\text{2}_1\text{2}_1$ space group with $Z = 4$ molecules in the unit cell and an R -value of 0.0887. The octahedral arrangement of the ferrocene-containing β -diketonato ligands around aluminium(III) was confirmed and bond lengths (average Al-O bond length is 1.881 Å) suggested good communication between the iron atoms of the three ferrocenyl-moieties is possible through the Al core atom.

That good communication between the Fe atoms of the ferrocenyl groups do exist was proved and quantified by an electrochemical study. Strikingly, all six of the Fc/Fc⁺ couples of Al(FcCOCHCOFc)₃ could be resolved with formal reduction potentials of E^{o'} = 33, 123, 304, 432, 583 and 741 mV. The formal reduction potentials for the CF₃ complex was E^{o'} = 280, 403 and 533 mV, whilst E^{o'} = 86, 202 and 293 mV for the CH₃ complex and E^{o'} = 100, 207 and 298 mV for the C₆H₅ complex. The largest formal reduction potential was observed for the sixth oxidation of Al(FcCOCHCOFc)₃ with E^{o'} = 741 mV versus Fc/Fc⁺. For each complex a linear relationship between the sum of the electronegativities ($\sum \chi_R = 3\chi_R + 3\chi_{Fc}$) of the six substituents (two on each FcCOCHCOR ligand) and the formal reduction of the Fc/Fc⁺ couples of each complex was obtained. Barring the last 4 oxidations of Al(FcCOCHCOFc)₃ these could be unified in a linear relationship between $\sum \chi_R$ and E^{o'} of all the ferrocene-related redox processes for all the compounds of $E^{o'} = 91.525 \sum \chi_R - 1019$. Basic electrostatic calculations were used to conclude that electrochemical communication occurred through bonds and not through-space.

From cytotoxicity studies it was concluded that aluminium has an inhibiting effect on ferrocenyl cytotoxicity. Low solubility in biological media is a major drawback in cytotoxic studies of the present series of aluminium complexes. Only the Al(FcCOCHCOF₃)₃ complex could effectively be studied. This complex had an IC₅₀ value of 10.58 μM and is 12 times less cytotoxic than cisplatin. It differentiated between cancer and healthy cells with a ratio of 4.7 (IC₅₀ = 50 μM for stimulated lymphocytes).

The study of ferrocene-containing β-diketonato aluminium(III) complexes formed a crucial foundation for the study of aluminium carboxylates. From the β-diketonato complexes the monomeric octahedral AlO₆-core was shown to be preferred by aluminium(III). Six-

membered ring formation was the only observed coordination sphere observed in $\text{Al}(\text{FcCOCHCOR})_3$ complexes. No dimers or higher homologues were identified and the solubility of $\text{Al}(\text{FcCOCHCOR})_3$ compounds in organic solvents were fairly high.

In contrast aluminium carboxylates are very sluggish to form monomeric four-membered bidentate coordinated rings with Al^{3+} . Monodentate coordination may be observed, but alumoxane structures bearing bridging carboxylate bonding to Al centres, held together by μ -oxygen bridges dominate. Dimerisation or polymerisation frequently occurs and solubility is severely hampered by the presence of Al_2O_3 cores in many of the alumoxane products of reactions between Al_2O_3 and carboxylic acids.

An initial computational investigation of aluminium carboxylates proved invaluable in the structural predictions from FTIR spectroscopy of the aluminium carboxylates investigated in this study. It was shown from the computational study that bidentate coordination of carboxylic acids to monomeric aluminium centres is possible but unlikely due to high molecular energy content. The energy content of a monodentate monomeric tricarboxylate is infinite, indicating this structural entity does not exist. In contrast, dimeric structures with the coordination sphere around each aluminium atom being four, five or six are very likely. Energetically, the coordination spheres of $5_{\text{Al}(1)}/5_{\text{Al}(2)}$ or $6_{\text{Al}(1)}/6_{\text{Al}(2)}$ are the preferred coordination of these dimeric complexes.

An FTIR analysis of freshly synthesised aluminium carboxylates indicated that bridging carboxylate coordination is the prevalent bonding mode in most aluminium carboxylates. Carboxylato-alumoxanes are preferentially formed in oxygen and moisture rich environments. The aluminium source used in the synthesis of aluminium carboxylates has a significant impact on structure of the aluminium carboxylates formed. The core of the

aluminium source is likely to be retained within the structure of the aluminium carboxylate. When using an organic aluminium source, like aluminium *tris*-isopropoxide, it is possible to synthesise aluminium carboxylates, void of an alumoxane having a 1:3 ratio of aluminium to carboxylic acid (indicated by elemental analysis). However, obtaining a true tricarboxylate is difficult as dimeric and polymeric structures occur frequently. In contrast, if γ -Al₂O₃ is used as the aluminium source, or if oxygen or moisture gains only slight access to the reaction mixture, carboxylato-alumoxanes are the dominant product.

FTIR characterisation showed that the separation between symmetric and antisymmetric carbonyl stretching bands ($\Delta\nu = \nu_{\text{antisymmetric}} - \nu_{\text{symmetric}}$) can be used as an initial indication of the bonding mode of a carboxylic acid to aluminium. The monodentate carboxylate coordination mode is associated with $\Delta\nu \geq 200 \text{ cm}^{-1}$. Bridging coordination modes are associated with $80 \leq \Delta\nu \leq 125 \text{ cm}^{-1}$. Symmetric bidentate coordination is associated with $\Delta\nu = 60 - 70 \text{ cm}^{-1}$, but the IR band pattern resulting in this $\Delta\nu$ value is difficult to verify experimentally.

5.3. Future prospects

The current research project can be expanded in several key areas.

The synthesis of mixed ferrocene-containing β -diketonato aluminium complexes will allow further investigation of the electrochemical communication between ferrocenyl and/or other redox active moieties like osmocenyl or tetrathiofulvanyl, substituted as side groups on the β -diketonato ligand. Such a study will give more detail on the effect of electronegativity of the side groups on formal reduction potential. Expanding on the basic

electrostatic calculations performed here, a detailed computational study will indicate whether ferrocene-related oxidations in $\text{Al}(\text{FcCOCHCOCF}_3)_3$ and other related complexes occur in a specific order or randomly.

Mixed ligand complexes, containing alkoxide and β -diketonato ligands may be synthesised and they may improve bio-solubility and anti-cancer ability. A kinetic study of ligand substitution of complexes of the type $\text{Al}(\text{FcCOHCO}_R)_3$ with other ligands will show if this process is constructed of three individual, but consecutive steps of different rates, or if these substitution patterns occur randomly at the same rate.

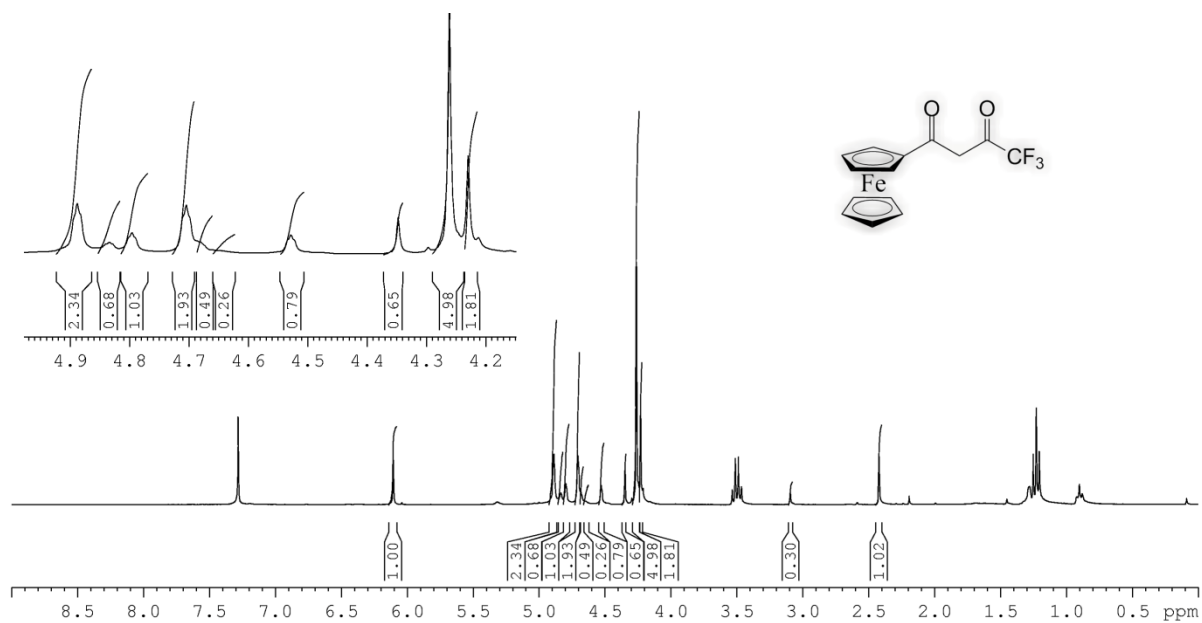
As mentioned previously the insolubility of the current aluminium carboxylates hamper characterisation. Finding and developing effective solid state characterisation techniques, such as Magic Angle Spinning ^{27}Al NMR and XAFS, will greatly expand on what is currently known on aluminium carboxylates. Other techniques, if available, that can be considered to gather information on the microscopic structure of these carboxylates include nanoscale Auger spectroscopy (nanoSAM) and X-ray photon spectroscopy (XPS).

Methods of preparing and isolating target mono-coordinated aluminium carboxylate complexes need to be developed, as well as synthetic routes to unique monomeric aluminium tricarboxylates possessing bidentate coordination. This probably will require the use of strongly donating and highly sterically restricted carboxylic acids.

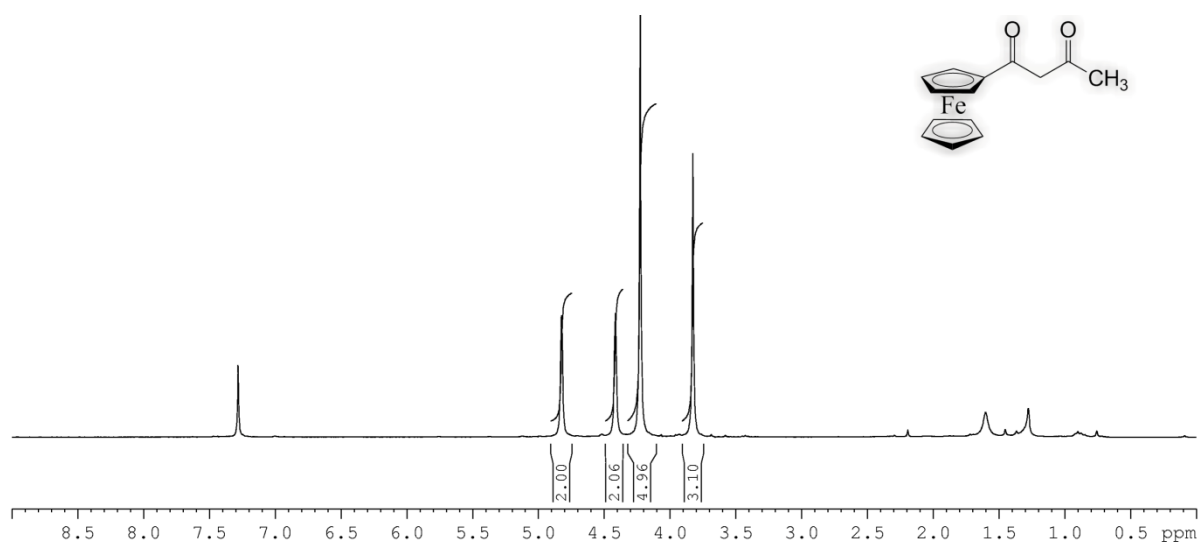
Appendix

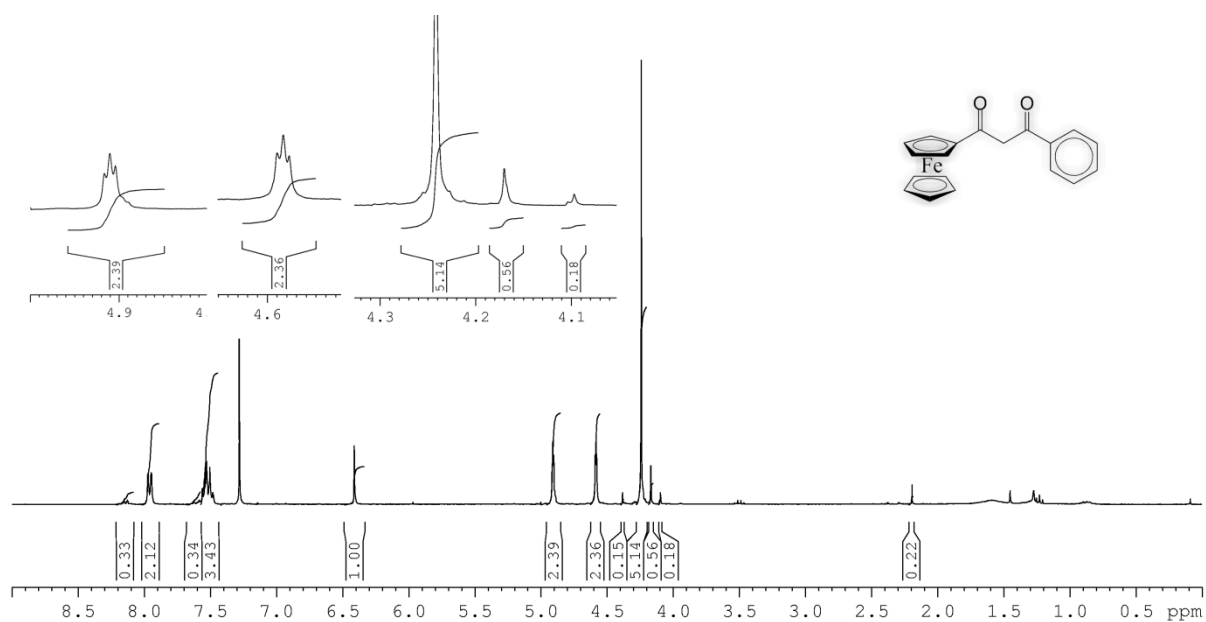
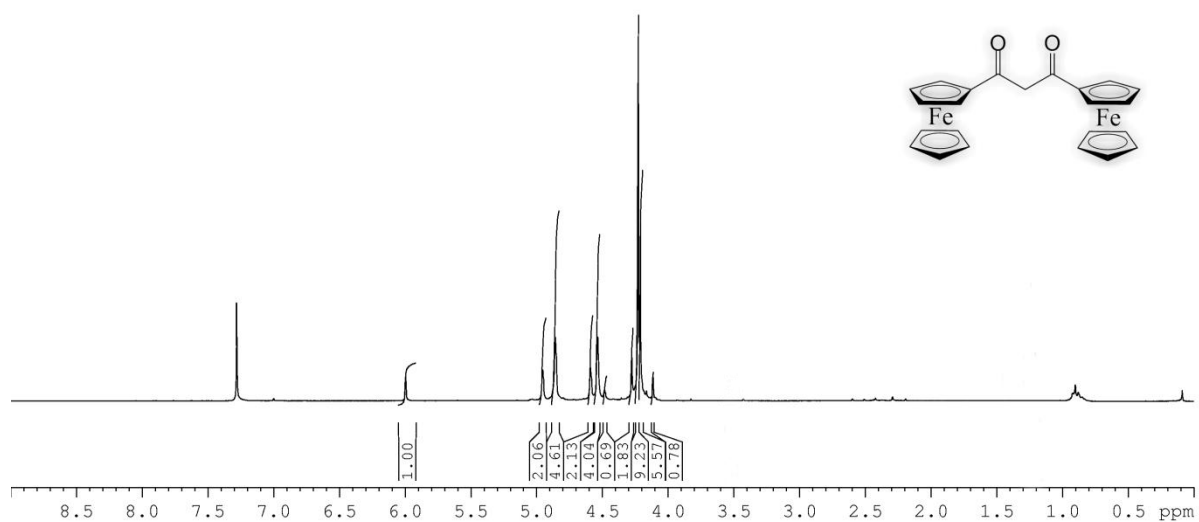
NMR spectra

Spectrum 1: 4,4,4-trifluorobutane-1,3-dione, (2) [Scheme 3.2, p. 64]

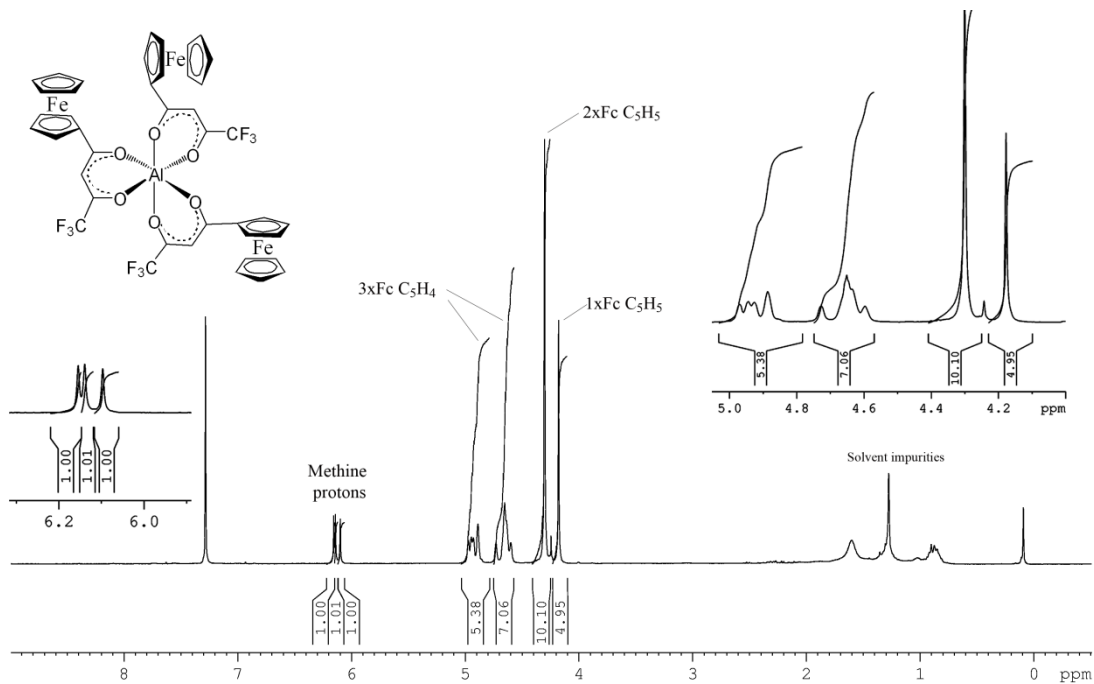


Spectrum 2: 1-ferrocenylbutane-1,3-dione, (3) [Scheme 3.2, p. 64]



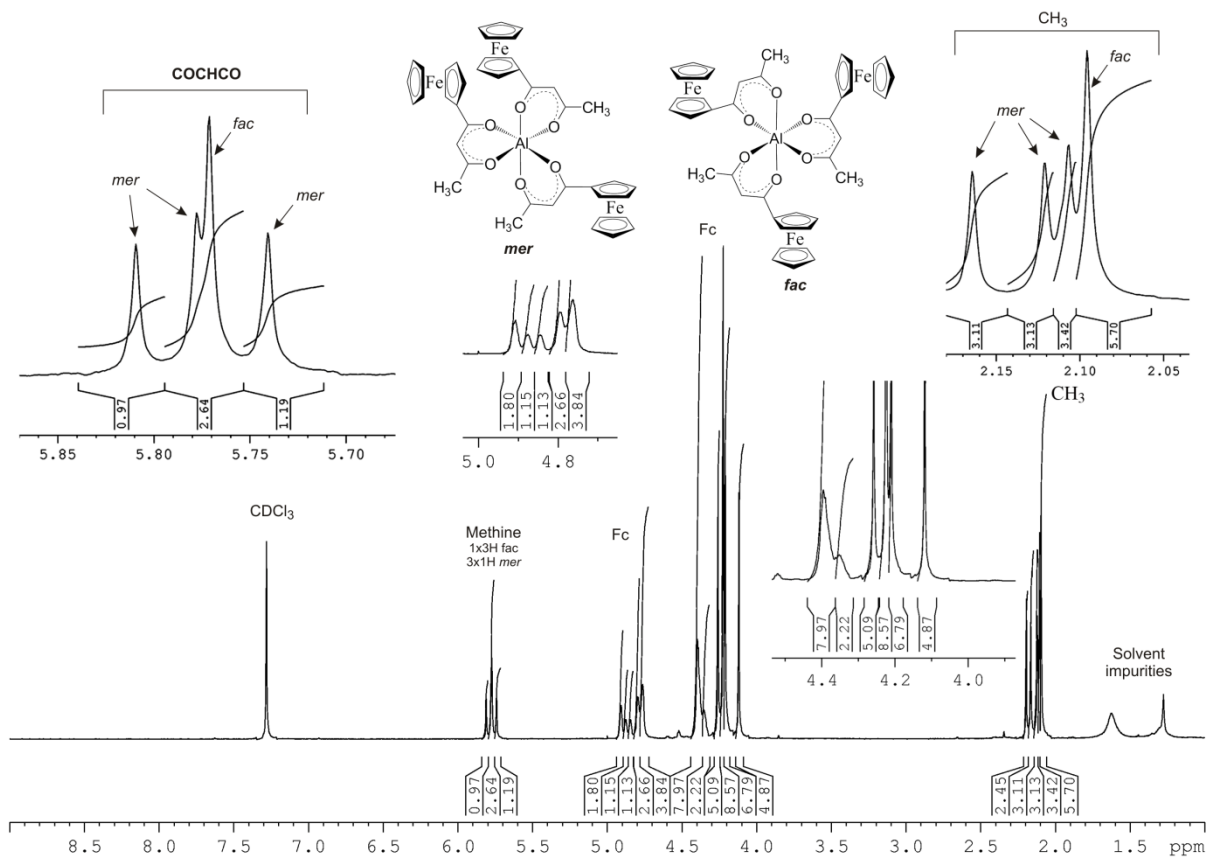
Spectrum 3: Phenylpropane-1,3-dione, (4) [Scheme 3.2, p. 64]**Spectrum 4: 1,3-diferrocenylpropane-1,3-dione, (5) [Scheme 3.2, p. 64]**

Spectrum 5: Tris(1-ferrocenyl-4,4,4-trifluoroprop-1,3-dionato- κ^2 -O,O') aluminium(III), (6) [Scheme 3.4 and Scheme 3.5, p. 68 and p. 69]

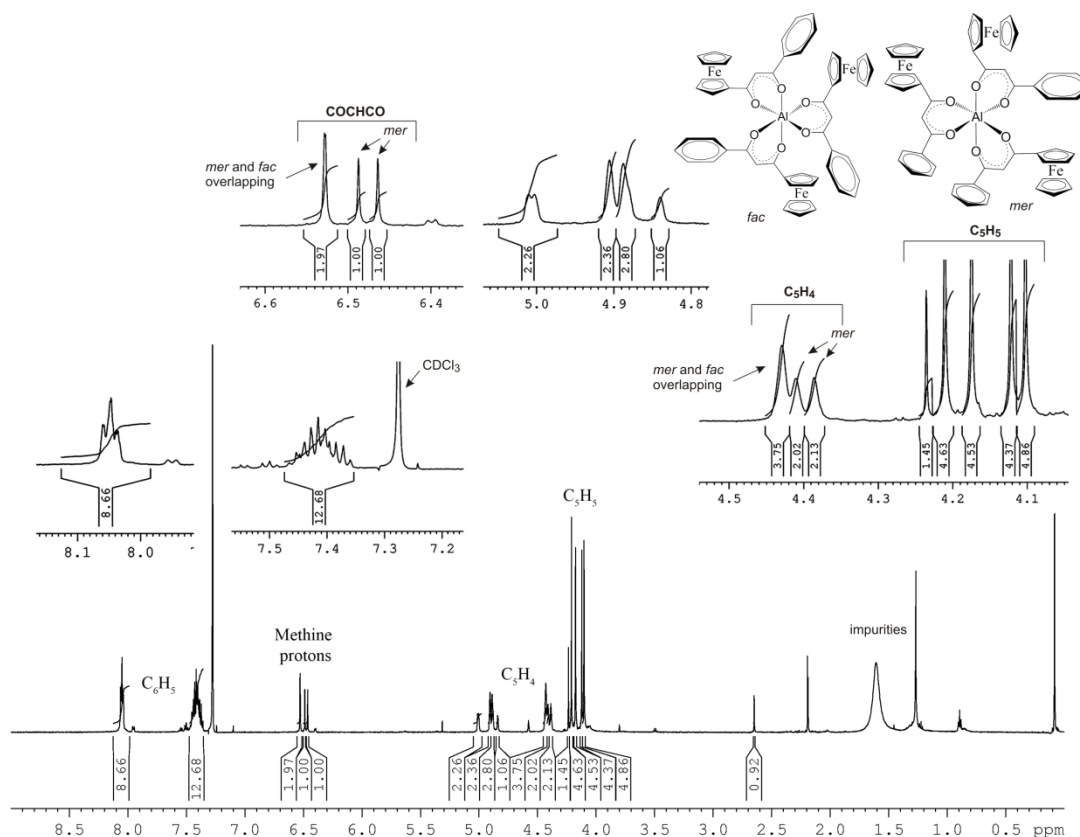


Spectrum 6: Tris(1-ferrocenyl-1,3-butanedionato-O,O') aluminium(III), (7)

[Scheme 3.4 and Scheme 3.5, p. 68 and p. 69]

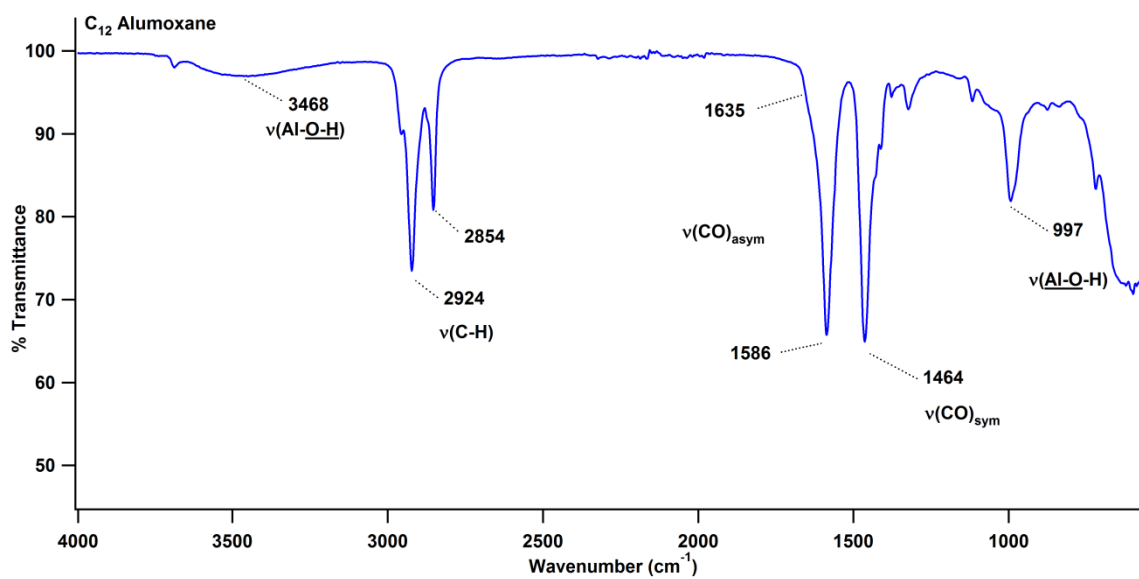


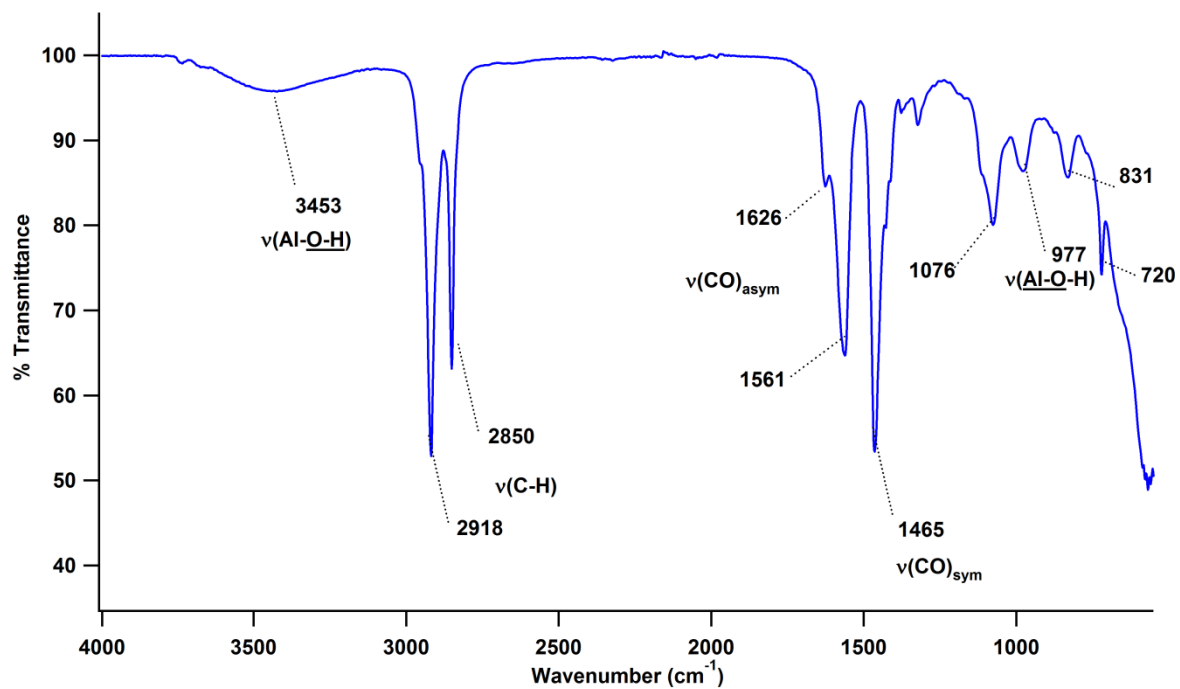
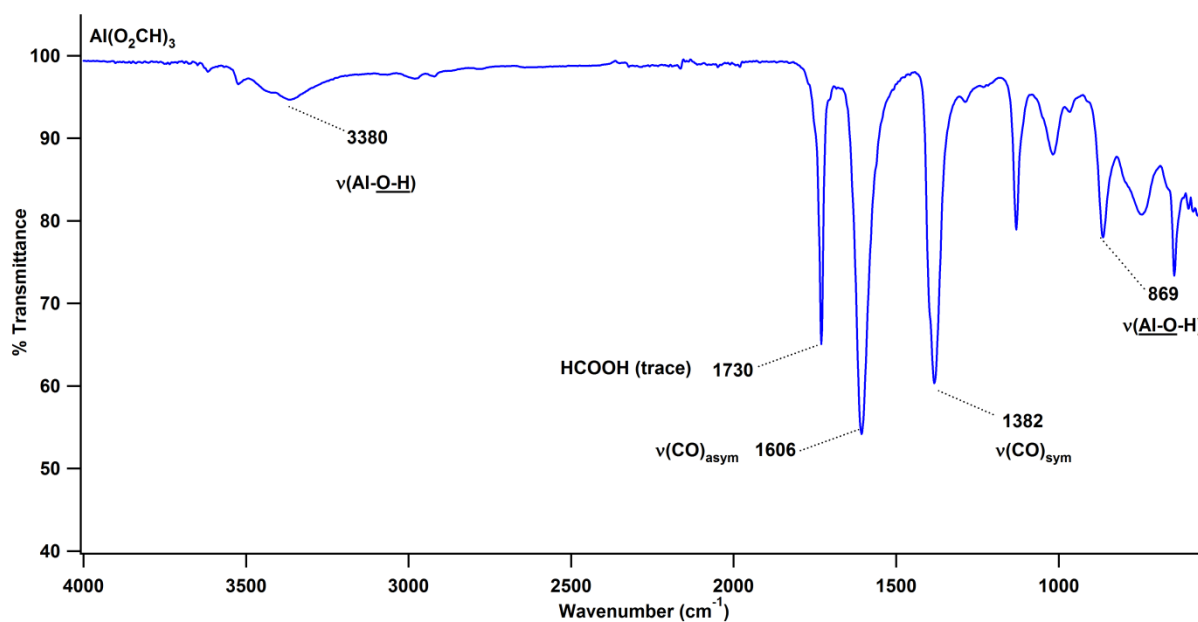
Spectrum 7: Tri-(phenylpropane-1,3-dionato-O,O') aluminium (III), (8) [Scheme 3.4 and Scheme 3.5, p. 68 and p. 69]

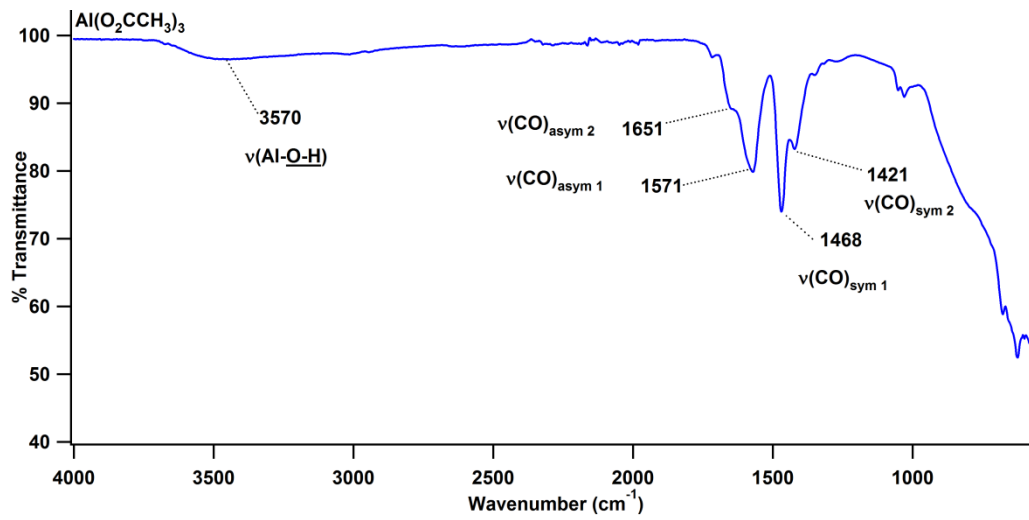
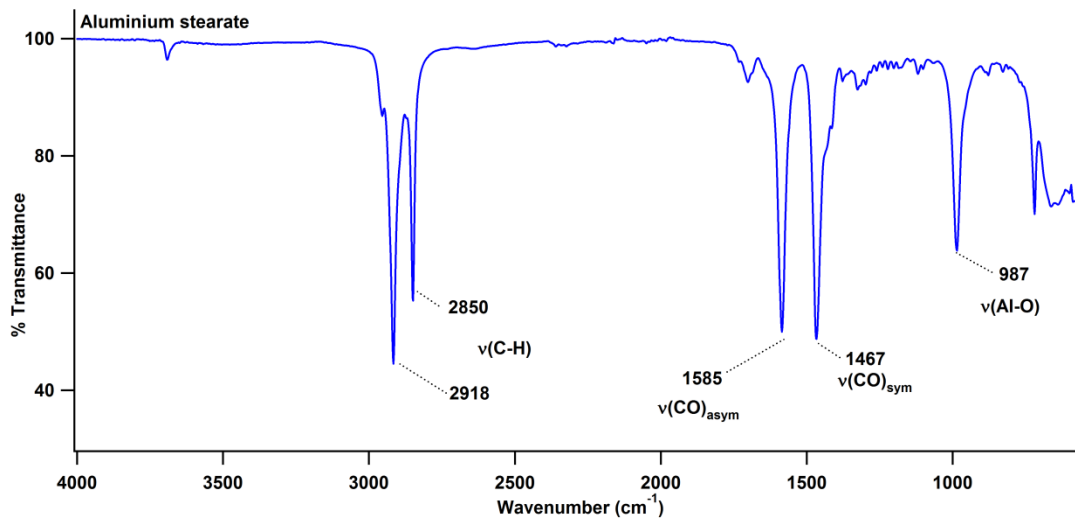
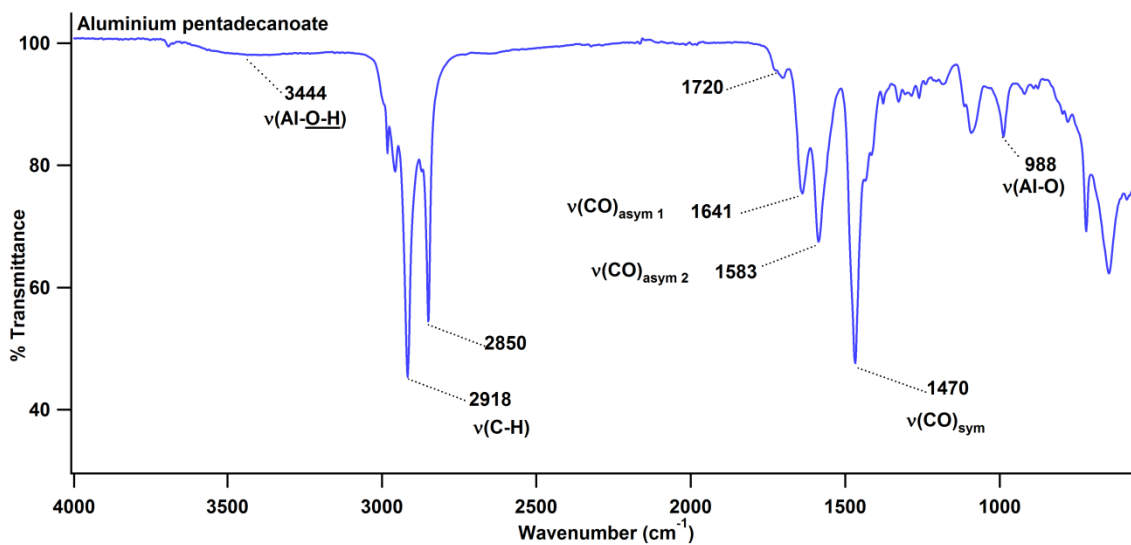


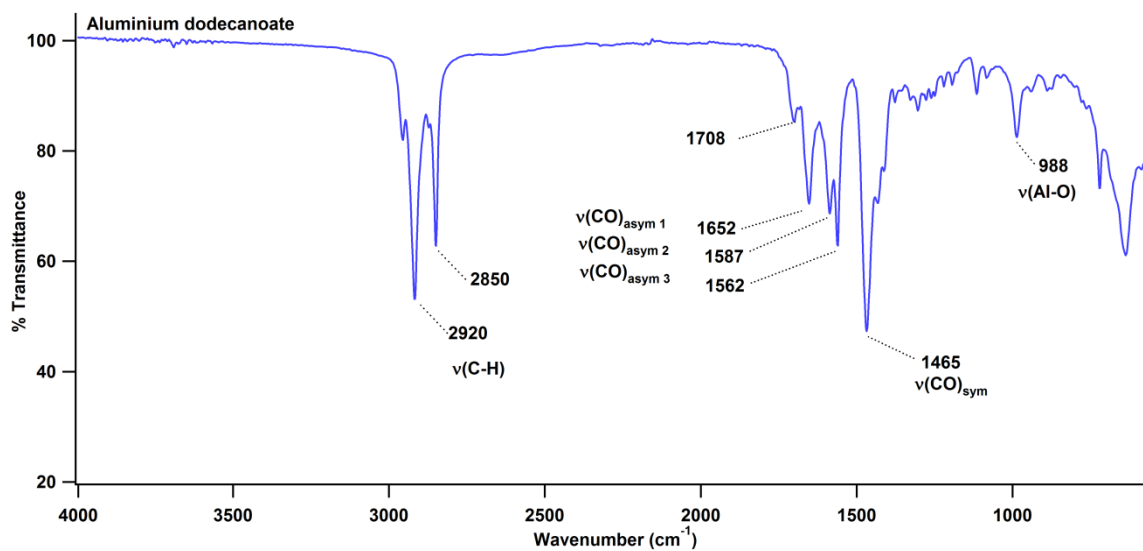
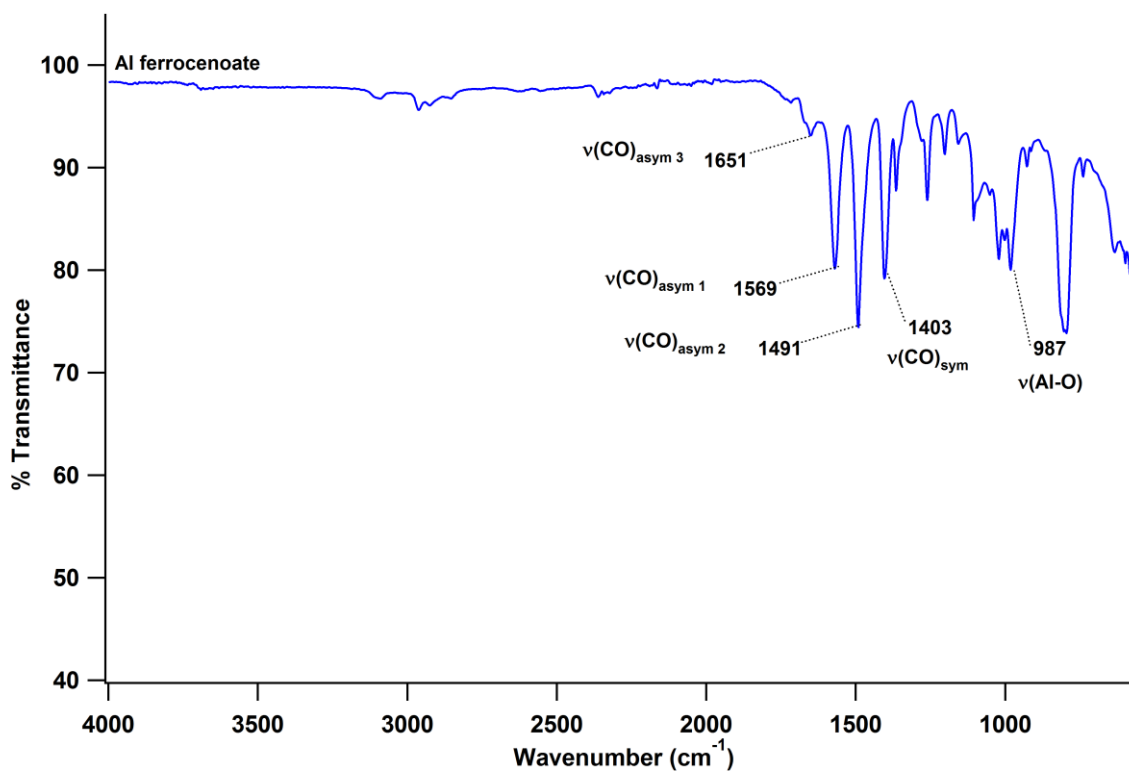
Infrared spectra

Spectrum 8: Dodecanoato-alumoxane, (24) [Scheme 3.13, p. 130]



Spectrum 9: Octadecanoato-alumoxane, (25) [Scheme 3.13, p. 130]**Spectrum 10: Aluminium formate, (26) [Scheme 3.14, p. 136]**

Spectrum 11: Aluminium acetate, (27) [Scheme 3.15, p. 140]**Spectrum 12: Octadecanoato aluminium(III) (28) [Scheme 3.18, p. 147]****Spectrum 13: Pentadecanoato aluminium(III) (29) [Scheme 3.18, p. 147]**

Spectrum 14: Dodecanoato aluminium(III) (30) [Scheme 3.18, p. 147]**Spectrum 15: Ferrocenoato Aluminium(III) (31) [Scheme 3.19, p.155]**

Crystallographic data for Al(FcCOCHCOF₃)₃

Table A1: The bond lengths (Å) of Al(FcCOCHCOF₃)₃.

Bond	Length (Å)	Bond	Length (Å)	Bond	Length (Å)	Bond	Length (Å)
Al-O(5)	1.859(4)	C(14)-H(14)	0.9500	C(31)-C(32)	1.444(6)	C(009)-C(010)	1.526(8)
Al-O(4)	1.868(3)	C(15)-H(15)	0.9500	C(32)-C(33)	1.415(7)	C(010)-C(011)	1.357(7)
Al-O(3)	1.871(3)	C(21)-C(22)	1.359(8)	C(32)-H(32)	0.9500	C(011)-C(012)	1.411(7)
Al-O(2)	1.890(3)	C(21)-C(25)	1.403(8)	C(33)-C(34)	1.430(7)	C(011)-H(011)	0.9500
Al-O(1)	1.890(3)	C(21)-H(21)	0.9500	C(33)-H(33)	0.9500	C(012)-C(51)	1.468(7)
Al-O(6)	1.905(3)	C(22)-C(23)	1.416(9)	C(34)-C(35)	1.404(7)	C(51)-C(55)	1.405(7)
O(1)-C(004)	1.271(6)	C(22)-H(22)	0.9500	C(34)-H(34)	0.9500	C(51)-C(52)	1.419(8)
O(2)-C(002)	1.286(6)	C(23)-C(24)	1.410(8)	C(35)-H(35)	0.9500	C(52)-C(53)	1.415(7)
F(1)-C(001)	1.324(6)	C(23)-H(23)	0.9500	C(41)-C(45)	1.397(8)	C(52)-H(52)	0.9500
F(2)-C(001)	1.336(6)	C(24)-C(25)	1.429(8)	C(41)-C(42)	1.441(9)	C(53)-C(54)	1.382(8)
F(3)-C(001)	1.351(6)	C(24)-H(24)	0.9500	C(41)-H(41)	0.9500	C(53)-H(53)	0.9500
C(001)-C(002)	1.517(7)	C(25)-H(25)	0.9500	C(42)-C(43)	1.423(9)	C(54)-C(55)	1.400(7)
C(002)-C(003)	1.374(7)	O(3)-C(006)	1.276(6)	C(42)-H(42)	0.9500	C(54)-H(54)	0.9500
C(003)-C(004)	1.406(7)	O(4)-C(008)	1.282(5)	C(43)-C(44)	1.414(8)	C(55)-H(55)	0.9500
C(003)-H(003)	0.9500	F(4)-C(005)	1.325(6)	C(43)-H(43)	0.9500	C(61)-C(62)	1.390(8)
C(004)-C(11)	1.449(7)	F(5)-C(005)	1.354(6)	C(44)-C(45)	1.406(8)	C(61)-C(65)	1.426(10)
C(11)-C(15)	1.423(7)	F(6)-C(005)	1.325(6)	C(44)-H(44)	0.9500	C(61)-H(61)	0.9500
C(11)-C(12)	1.441(7)	C(005)-C(006)	1.517(7)	C(45)-H(45)	0.9500	C(62)-C(63)	1.417(10)
C(12)-C(13)	1.408(7)	C(006)-C(007)	1.342(7)	O(5)-C(010)	1.289(6)	C(62)-H(62)	0.9500
C(12)-H(12)	0.9500	C(007)-C(008)	1.446(6)	O(6)-C(012)	1.274(6)	C(63)-C(64)	1.415(10)
C(13)-C(14)	1.403(7)	C(007)-H(007)	0.9500	F(7)-C(009)	1.324(7)	C(63)-H(63)	0.9500
C(13)-H(13)	0.9500	C(008)-C(31)	1.424(6)	F(8)-C(009)	1.330(8)	C(64)-C(65)	1.445(9)
C(14)-C(15)	1.396(7)	C(31)-C(35)	1.444(6)	F(9)-C(009)	1.300(7)	C(64)-H(64)	0.9500
						C(65)-H(65)	0.9500

Table A2: Bond angles (°) of Al(FcCOCHCOF₃)₃.

Atoms	Angle (°)	Atoms	Angle (°)	Atoms	Angle (°)
O(5)-Al-O(4)	91.10(16)	C(23)-C(22)-H(22)	126.1	C(45)-C(44)-H(44)	126.1
O(5)-Al-O(3)	92.11(16)	C(24)-C(23)-C(22)	108.1(5)	C(43)-C(44)-H(44)	126.1
O(4)-Al-O(3)	91.68(15)	C(24)-C(23)-H(23)	125.9	C(41)-C(45)-C(44)	108.8(5)
O(5)-Al-O(2)	176.56(16)	C(22)-C(23)-H(23)	125.9	C(41)-C(45)-H(45)	125.6
O(4)-Al-O(2)	88.42(15)	C(23)-C(24)-C(25)	107.1(5)	C(44)-C(45)-H(45)	125.6
O(3)-Al-O(2)	91.31(15)	C(23)-C(24)-H(24)	126.5	C(010)-O(5)-Al	126.3(3)
O(5)-Al-O(1)	88.98(16)	C(25)-C(24)-H(24)	126.5	C(012)-O(6)-Al	127.8(3)
O(4)-Al-O(1)	179.21(17)	C(21)-C(25)-C(24)	106.5(5)	F(9)-C(009)-F(7)	106.9(6)
O(3)-Al-O(1)	89.10(16)	C(21)-C(25)-H(25)	126.8	F(9)-C(009)-F(8)	110.1(5)
O(2)-Al-O(1)	91.46(15)	C(24)-C(25)-H(25)	126.8	F(7)-C(009)-F(8)	105.4(5)

Appendix

O(5)-AI-O(6)	90.69(14)	C(006)-O(3)-AI	123.5(3)	F(9)-C(009)-C(010)	114.5(5)
O(4)-AI-O(6)	88.97(15)	C(008)-O(4)-AI	130.3(3)	F(7)-C(009)-C(010)	110.7(5)
O(3)-AI-O(6)	177.12(16)	F(4)-C(005)-F(6)	106.4(5)	F(8)-C(009)-C(010)	108.8(6)
O(2)-AI-O(6)	85.90(15)	F(4)-C(005)-F(5)	105.4(4)	O(5)-C(010)-C(011)	126.9(5)
O(1)-AI-O(6)	90.24(15)	F(6)-C(005)-F(5)	106.8(4)	O(5)-C(010)-C(009)	114.7(4)
C(004)-O(1)-AI	130.2(3)	F(4)-C(005)-C(006)	112.6(4)	C(011)-C(010)-C(009)	118.3(5)
C(002)-O(2)-AI	122.7(3)	F(6)-C(005)-C(006)	112.3(4)	C(010)-C(011)-C(012)	121.6(5)
F(1)-C(001)-F(2)	108.8(4)	F(5)-C(005)-C(006)	112.8(5)	C(010)-C(011)-H(011)	119.2
F(1)-C(001)-F(3)	105.0(4)	O(3)-C(006)-C(007)	128.7(4)	C(012)-C(011)-H(011)	119.2
F(2)-C(001)-F(3)	106.2(4)	O(3)-C(006)-C(005)	110.8(4)	O(6)-C(012)-C(011)	123.0(4)
F(1)-C(001)-C(002)	113.6(4)	C(007)-C(006)-C(005)	120.4(4)	O(6)-C(012)-C(51)	115.1(5)
F(2)-C(001)-C(002)	112.5(4)	C(006)-C(007)-C(008)	122.0(4)	C(011)-C(012)-C(51)	121.8(5)
F(3)-C(001)-C(002)	110.2(4)	C(006)-C(007)-H(007)	119	C(55)-C(51)-C(52)	107.6(4)
O(2)-C(002)-C(003)	128.6(5)	C(008)-C(007)-H(007)	119	C(55)-C(51)-C(012)	125.6(5)
O(2)-C(002)-C(001)	111.7(4)	O(4)-C(008)-C(31)	117.8(4)	C(52)-C(51)-C(012)	126.5(5)
C(003)-C(002)-C(001)	119.7(5)	O(4)-C(008)-C(007)	119.9(4)	C(53)-C(52)-C(51)	107.0(5)
C(002)-C(003)-C(004)	122.1(5)	C(31)-C(008)-C(007)	122.3(4)	C(53)-C(52)-H(52)	126.5
C(002)-C(003)-H(003)	118.9	C(008)-C(31)-C(35)	124.3(4)	C(51)-C(52)-H(52)	126.5
C(004)-C(003)-H(003)	118.9	C(008)-C(31)-C(32)	128.8(4)	C(54)-C(53)-C(52)	108.6(5)
O(1)-C(004)-C(003)	121.3(5)	C(35)-C(31)-C(32)	106.6(4)	C(54)-C(53)-H(53)	125.7
O(1)-C(004)-C(11)	118.8(4)	C(33)-C(32)-C(31)	108.5(4)	C(52)-C(53)-H(53)	125.7
C(003)-C(004)-C(11)	120.0(5)	C(33)-C(32)-H(32)	125.7	C(53)-C(54)-C(55)	108.5(5)
C(15)-C(11)-C(12)	107.3(4)	C(31)-C(32)-H(32)	125.7	C(53)-C(54)-H(54)	125.7
C(15)-C(11)-C(004)	127.6(4)	C(32)-C(33)-C(34)	107.6(4)	C(55)-C(54)-H(54)	125.7
C(12)-C(11)-C(004)	124.6(4)	C(32)-C(33)-H(33)	126.2	C(54)-C(55)-C(51)	108.2(5)
C(13)-C(12)-C(11)	106.2(4)	C(34)-C(33)-H(33)	126.2	C(54)-C(55)-H(55)	125.9
C(13)-C(12)-H(12)	126.9	C(35)-C(34)-C(33)	109.1(4)	C(51)-C(55)-H(55)	125.9
C(11)-C(12)-H(12)	126.9	C(35)-C(34)-H(34)	125.4	C(62)-C(61)-C(65)	108.4(6)
C(14)-C(13)-C(12)	110.0(4)	C(33)-C(34)-H(34)	125.4	C(62)-C(61)-H(61)	125.8
C(14)-C(13)-H(13)	125	C(34)-C(35)-C(31)	108.1(4)	C(65)-C(61)-H(61)	125.8
C(12)-C(13)-H(13)	125	C(34)-C(35)-H(35)	125.9	C(61)-C(62)-C(63)	108.8(7)
C(15)-C(14)-C(13)	107.6(4)	C(31)-C(35)-H(35)	125.9	C(61)-C(62)-H(62)	125.6
C(15)-C(14)-H(14)	126.2	C(45)-C(41)-C(42)	108.4(6)	C(63)-C(62)-H(62)	125.6
C(13)-C(14)-H(14)	126.2	C(45)-C(41)-H(41)	125.8	C(64)-C(63)-C(62)	108.6(6)
C(14)-C(15)-C(11)	108.8(4)	C(42)-C(41)-H(41)	125.8	C(64)-C(63)-H(63)	125.7
C(14)-C(15)-H(15)	125.6	C(43)-C(42)-C(41)	106.2(5)	C(62)-C(63)-H(63)	125.7
C(11)-C(15)-H(15)	125.6	C(43)-C(42)-H(42)	126.9	C(63)-C(64)-C(65)	106.7(6)
C(22)-C(21)-C(25)	110.5(6)	C(41)-C(42)-H(42)	126.9	C(63)-C(64)-H(64)	126.7
C(22)-C(21)-H(21)	124.8	C(44)-C(43)-C(42)	108.7(5)	C(65)-C(64)-H(64)	126.7
C(25)-C(21)-H(21)	124.8	C(44)-C(43)-H(43)	125.6	C(61)-C(65)-C(64)	107.6(6)

Appendix

C(21)-C(22)-C(23)	107.8(6)	C(42)-C(43)-H(43)	125.6	C(61)-C(65)-H(65)	126.2
C(21)-C(22)-H(22)	126.1	C(45)-C(44)-C(43)	107.8(5)	C(64)-C(65)-H(65)	126.2

Table A3: Torsion angles ($^{\circ}$) for Al(FcCOCHCOF₃)₃.

Atoms	Torsion ($^{\circ}$)	Atoms	Torsion ($^{\circ}$)
O(5)-Al-O(1)-C(004)	161.4(4)	Al-O(4)-C(008)-C(31)	174.1(3)
O(4)-Al-O(1)-C(004)	66(13)	Al-O(4)-C(008)-C(007)	-4.5(6)
O(3)-Al-O(1)-C(004)	-106.5(4)	C(006)-C(007)-C(008)-O(4)	-6.9(7)
O(2)-Al-O(1)-C(004)	-15.2(4)	C(006)-C(007)-C(008)-C(31)	174.5(4)
O(6)-Al-O(1)-C(004)	70.7(4)	O(4)-C(008)-C(31)-C(35)	4.3(6)
O(5)-Al-O(2)-C(002)	-77(3)	C(007)-C(008)-C(31)-C(35)	-177.0(4)
O(4)-Al-O(2)-C(002)	-158.9(4)	O(4)-C(008)-C(31)-C(32)	177.1(4)
O(3)-Al-O(2)-C(002)	109.5(4)	C(007)-C(008)-C(31)-C(32)	-4.3(7)
O(1)-Al-O(2)-C(002)	20.3(4)	C(008)-C(31)-C(32)-C(33)	-174.3(4)
O(6)-Al-O(2)-C(002)	-69.8(4)	C(35)-C(31)-C(32)-C(33)	-0.5(5)
Al-O(2)-C(002)-C(003)	-17.6(7)	C(31)-C(32)-C(33)-C(34)	0.2(5)
Al-O(2)-C(002)-C(001)	163.6(3)	C(32)-C(33)-C(34)-C(35)	0.2(5)
F(1)-C(001)-C(002)-O(2)	178.4(4)	C(33)-C(34)-C(35)-C(31)	-0.6(5)
F(2)-C(001)-C(002)-O(2)	54.2(5)	C(008)-C(31)-C(35)-C(34)	174.8(4)
F(3)-C(001)-C(002)-O(2)	-64.1(5)	C(32)-C(31)-C(35)-C(34)	0.7(5)
F(1)-C(001)-C(002)-C(003)	-0.6(7)	C(45)-C(41)-C(42)-C(43)	0.2(6)
F(2)-C(001)-C(002)-C(003)	-124.8(5)	C(41)-C(42)-C(43)-C(44)	-0.9(6)
F(3)-C(001)-C(002)-C(003)	116.9(5)	C(42)-C(43)-C(44)-C(45)	1.2(6)
O(2)-C(002)-C(003)-C(004)	0.6(8)	C(42)-C(41)-C(45)-C(44)	0.6(6)
C(001)-C(002)-C(003)-C(004)	179.4(4)	C(43)-C(44)-C(45)-C(41)	-1.1(6)
Al-O(1)-C(004)-C(003)	4.3(6)	O(4)-Al-O(5)-C(010)	107.3(4)
Al-O(1)-C(004)-C(11)	-176.6(3)	O(3)-Al-O(5)-C(010)	-161.0(4)
C(002)-C(003)-C(004)-O(1)	6.9(7)	O(2)-Al-O(5)-C(010)	25(3)
C(002)-C(003)-C(004)-C(11)	-172.2(4)	O(1)-Al-O(5)-C(010)	-71.9(4)
O(1)-C(004)-C(11)-C(15)	-179.0(4)	O(6)-Al-O(5)-C(010)	18.3(4)
C(003)-C(004)-C(11)-C(15)	0.0(7)	O(5)-Al-O(6)-C(012)	-19.7(4)
O(1)-C(004)-C(11)-C(12)	-8.2(7)	O(4)-Al-O(6)-C(012)	-110.7(4)
C(003)-C(004)-C(11)-C(12)	170.9(4)	O(3)-Al-O(6)-C(012)	146(3)
C(15)-C(11)-C(12)-C(13)	0.6(5)	O(2)-Al-O(6)-C(012)	160.8(4)
C(004)-C(11)-C(12)-C(13)	-171.8(4)	O(1)-Al-O(6)-C(012)	69.3(4)
C(11)-C(12)-C(13)-C(14)	0.4(6)	Al-O(5)-C(010)-C(011)	-10.1(9)
C(12)-C(13)-C(14)-C(15)	-1.3(6)	Al-O(5)-C(010)-C(009)	171.3(4)
C(13)-C(14)-C(15)-C(11)	1.6(5)	F(9)-C(009)-C(010)-O(5)	-167.7(6)
C(12)-C(11)-C(15)-C(14)	-1.4(5)	F(7)-C(009)-C(010)-O(5)	-46.8(8)
C(004)-C(11)-C(15)-C(14)	170.7(4)	F(8)-C(009)-C(010)-O(5)	68.6(6)
C(25)-C(21)-C(22)-C(23)	1.7(6)	F(9)-C(009)-C(010)-C(011)	13.6(9)
C(21)-C(22)-C(23)-C(24)	-1.3(6)	F(7)-C(009)-C(010)-C(011)	134.5(6)
C(22)-C(23)-C(24)-C(25)	0.4(6)	F(8)-C(009)-C(010)-C(011)	-110.1(6)
C(22)-C(21)-C(25)-C(24)	-1.5(6)	O(5)-C(010)-C(011)-C(012)	-5.1(10)
C(23)-C(24)-C(25)-C(21)	0.6(6)	C(009)-C(010)-C(011)-C(012)	173.4(6)

Appendix

O(5)-Al-O(3)-C(006)	-112.5(4)	Al-O(6)-C(012)-C(011)	11.9(7)
O(4)-Al-O(3)-C(006)	-21.3(4)	Al-O(6)-C(012)-C(51)	-169.0(3)
O(2)-Al-O(3)-C(006)	67.1(4)	C(010)-C(011)-C(012)-O(6)	4.1(9)
O(1)-Al-O(3)-C(006)	158.6(4)	C(010)-C(011)-C(012)-C(51)	-174.9(6)
O(6)-Al-O(3)-C(006)	82(3)	O(6)-C(012)-C(51)-C(55)	12.5(8)
O(5)-Al-O(4)-C(008)	107.8(4)	C(011)-C(012)-C(51)-C(55)	-168.5(5)
O(3)-Al-O(4)-C(008)	15.6(4)	O(6)-C(012)-C(51)-C(52)	-173.9(5)
O(2)-Al-O(4)-C(008)	-75.6(4)	C(011)-C(012)-C(51)-C(52)	5.1(9)
O(1)-Al-O(4)-C(008)	-157(13)	C(55)-C(51)-C(52)-C(53)	-1.5(7)
O(6)-Al-O(4)-C(008)	-161.6(4)	C(012)-C(51)-C(52)-C(53)	-176.0(5)
Al-O(3)-C(006)-C(007)	18.3(7)	C(51)-C(52)-C(53)-C(54)	2.7(7)
Al-O(3)-C(006)-C(005)	-165.5(3)	C(52)-C(53)-C(54)-C(55)	-2.9(7)
F(4)-C(005)-C(006)-O(3)	51.3(6)	C(53)-C(54)-C(55)-C(51)	1.9(7)
F(6)-C(005)-C(006)-O(3)	-68.8(6)	C(52)-C(51)-C(55)-C(54)	-0.2(6)
F(5)-C(005)-C(006)-O(3)	170.4(4)	C(012)-C(51)-C(55)-C(54)	174.4(5)
F(4)-C(005)-C(006)-C(007)	-132.2(5)	C(65)-C(61)-C(62)-C(63)	0.2(8)
F(6)-C(005)-C(006)-C(007)	107.7(6)	C(61)-C(62)-C(63)-C(64)	-0.2(9)
F(5)-C(005)-C(006)-C(007)	-13.1(6)	C(62)-C(63)-C(64)-C(65)	0.2(8)
O(3)-C(006)-C(007)-C(008)	-0.7(8)	C(62)-C(61)-C(65)-C(64)	-0.1(7)
C(005)-C(006)-C(007)-C(008)	-176.6(4)	C(63)-C(64)-C(65)-C(61)	-0.1(7)

Table A4: Atomic coordinates ($\times 10^4$) and equivalent isotropic displacement parameters ($\text{\AA}^2 \times 10^3$). U(eq) is defined as one third of the trace of the orthogonalized U^{ij} tensor.

Atom	x	y	z	U(eq)	Atom	x	y	z	U(eq)
Al	3482(1)	9779(1)	3545(1)	30(1)	Fe(2)	1472(1)	7301(1)	4114(1)	26(1)
O(1)	3809(3)	10714(2)	3501(2)	34(1)	C(31)	2427(4)	7776(2)	3383(2)	25(1)
O(2)	4291(3)	9635(2)	2731(2)	31(1)	C(32)	1588(4)	7259(2)	3129(2)	30(1)
F(1)	6692(4)	10163(2)	1660(2)	62(1)	C(33)	1963(5)	6633(3)	3397(2)	35(1)
F(2)	5143(3)	9460(2)	1480(1)	47(1)	C(34)	3031(4)	6754(3)	3820(2)	34(1)
F(3)	6620(3)	9240(2)	2181(2)	51(1)	C(35)	3316(4)	7445(2)	3819(2)	26(1)
C(001)	5878(5)	9740(3)	1940(3)	38(1)	C(41)	378(6)	7993(3)	4595(3)	50(2)
C(002)	5092(5)	10057(3)	2483(2)	32(1)	C(42)	-406(5)	7446(4)	4361(3)	61(2)
C(003)	5279(5)	10722(2)	2641(2)	35(1)	C(43)	82(6)	6852(3)	4661(3)	53(2)
C(004)	4570(5)	11043(3)	3135(2)	32(1)	C(44)	1142(5)	7028(3)	5058(2)	42(1)
Fe(1)	3581(1)	12368(1)	2693(1)	31(1)	C(45)	1303(5)	7730(3)	5019(2)	45(1)
C(11)	4686(4)	11764(2)	3228(2)	28(1)	O(5)	2778(3)	9905(2)	4369(2)	36(1)
C(12)	3880(5)	12157(3)	3654(2)	36(1)	O(6)	5138(3)	9634(2)	3917(2)	28(1)
C(13)	4187(5)	12836(2)	3532(2)	34(1)	F(7)	1660(3)	10661(2)	5311(2)	75(1)
C(14)	5138(5)	12878(3)	3048(2)	33(1)	F(8)	1929(4)	9674(3)	5669(2)	86(1)
C(15)	5463(4)	12221(2)	2869(2)	30(1)	F(9)	3178(3)	10483(3)	5969(2)	115(2)
C(21)	2443(6)	11788(3)	2117(3)	48(2)	C(009)	2560(5)	10223(4)	5480(3)	58(2)
C(22)	1713(5)	12198(3)	2497(3)	53(2)	C(010)	3402(5)	10044(3)	4895(2)	42(1)
C(23)	2038(5)	12872(3)	2344(3)	51(2)	C(011)	4696(5)	10033(3)	4978(3)	47(2)
C(24)	3013(6)	12861(3)	1867(3)	47(1)	C(012)	5529(4)	9806(3)	4482(2)	34(1)
C(25)	3277(5)	12170(3)	1726(3)	46(1)	Fe(3)	8124(1)	10542(1)	4516(1)	40(1)
O(3)	1895(3)	9925(2)	3138(2)	36(1)	C(51)	6920(5)	9741(3)	4586(3)	39(1)
O(4)	3182(3)	8853(2)	3593(2)	34(1)	C(52)	7586(5)	9838(3)	5182(3)	48(2)
F(4)	648(3)	10262(2)	2037(2)	54(1)	C(53)	8913(5)	9769(3)	5046(3)	43(1)
F(5)	-333(3)	9320(2)	2013(2)	56(1)	C(54)	9063(5)	9664(3)	4384(3)	41(1)

Appendix

F(6)	-717(3)	10038(2)	2775(2)	77(1)	C(55)	7842(5)	9632(3)	4097(3)	39(1)
C(005)	219(5)	9774(3)	2419(3)	41(1)	C(61)	7112(7)	11409(3)	4300(3)	66(2)
C(006)	1274(4)	9468(2)	2836(2)	29(1)	C(62)	7774(7)	11487(3)	4884(3)	69(2)
C(007)	1407(4)	8797(3)	2876(2)	32(1)	C(63)	9104(7)	11390(3)	4766(4)	63(2)
C(008)	2354(4)	8486(2)	3295(2)	27(1)	C(64)	9280(6)	11247(3)	4096(4)	63(2)
					C(65)	8019(7)	11259(3)	3800(3)	59(2)

Table A5: Anisotropic displacement parameters ($\text{\AA}^2 \times 10^3$) for $\text{Al}(\text{FcCOCHCOCF}_3)_3$. The anisotropic displacement factor exponent takes the form: $-2\pi^2 [h^2 a^{*2} U^{11} + \dots + 2 h k a^* b^* U^{12}]$

Atom	U₁₁	U₂₂	U₃₃	U₂₃	U₁₃	U₁₂
Al	29(1)	29(1)	31(1)	7(1)	-9(1)	-6(1)
O(1)	36(2)	32(2)	34(2)	8(1)	-2(2)	-9(1)
O(2)	43(2)	22(2)	26(2)	5(1)	-4(2)	-10(2)
F(1)	90(3)	40(2)	55(2)	-11(2)	37(2)	-13(2)
F(2)	71(2)	32(2)	38(2)	-3(1)	-10(2)	2(2)
F(3)	49(2)	33(2)	72(2)	0(2)	-4(2)	6(2)
C(001)	44(3)	23(3)	47(3)	8(2)	2(2)	-5(2)
C(002)	37(3)	31(3)	27(2)	1(2)	-6(2)	-2(2)
C(003)	41(3)	31(3)	32(3)	8(2)	-2(2)	-3(2)
C(004)	32(3)	34(3)	30(2)	5(2)	-13(2)	3(2)
Fe(1)	31(1)	28(1)	33(1)	2(1)	-7(1)	3(1)
C(11)	27(2)	22(2)	34(2)	0(2)	-10(2)	1(2)
C(12)	38(3)	41(3)	30(2)	4(2)	0(2)	-1(2)
C(13)	49(3)	21(3)	33(3)	1(2)	1(2)	4(2)
C(14)	33(3)	32(3)	35(3)	4(2)	-4(2)	-3(2)
C(15)	33(2)	25(3)	31(2)	3(2)	-4(2)	-1(2)
C(21)	48(3)	38(3)	58(4)	4(3)	-26(3)	-5(3)
C(22)	36(3)	65(4)	59(4)	12(3)	-19(3)	-2(3)
C(23)	40(3)	50(4)	62(4)	-2(3)	-26(3)	16(3)
C(24)	51(3)	49(4)	41(3)	16(3)	-17(3)	-7(3)
C(25)	47(3)	55(4)	36(3)	-2(2)	-18(3)	3(3)
O(3)	35(2)	35(2)	39(2)	7(2)	-12(2)	-8(2)
O(4)	27(2)	34(2)	40(2)	9(2)	-12(2)	-11(1)
F(4)	59(2)	53(2)	49(2)	19(2)	-20(2)	-11(2)
F(5)	52(2)	57(2)	58(2)	14(2)	-30(2)	-8(2)
F(6)	50(2)	126(4)	54(2)	12(2)	4(2)	39(2)
C(005)	39(3)	46(3)	39(3)	9(3)	-3(2)	-7(3)
C(006)	31(2)	33(3)	23(2)	9(2)	1(2)	-2(2)
C(007)	23(2)	45(3)	29(2)	5(2)	-6(2)	-13(2)
C(008)	22(2)	34(3)	24(2)	4(2)	4(2)	-3(2)
Fe(2)	21(1)	30(1)	27(1)	5(1)	2(1)	-1(1)
C(31)	27(2)	29(3)	20(2)	3(2)	6(2)	-5(2)
C(32)	28(2)	37(3)	24(2)	-5(2)	-4(2)	-5(2)
C(33)	36(3)	25(3)	44(3)	-2(2)	3(2)	-7(2)
C(34)	26(2)	33(3)	43(3)	5(2)	2(2)	6(2)

Appendix

C(35)	24(2)	28(2)	26(2)	-1(2)	3(2)	0(2)
C(41)	56(4)	54(4)	41(3)	13(3)	29(3)	25(3)
C(42)	23(3)	127(7)	34(3)	5(3)	7(2)	9(3)
C(43)	47(3)	53(4)	58(4)	-6(3)	28(3)	-23(3)
C(44)	41(3)	59(4)	25(3)	15(2)	7(2)	7(3)
C(45)	39(3)	65(4)	33(3)	-4(3)	10(2)	3(3)
O(5)	26(2)	43(2)	39(2)	12(2)	-7(2)	-5(2)
O(6)	22(2)	32(2)	29(2)	6(1)	-2(1)	-7(1)
F(7)	44(2)	114(3)	66(2)	-9(2)	5(2)	21(2)
F(8)	49(2)	133(4)	75(3)	36(3)	27(2)	11(2)
F(9)	41(2)	263(7)	42(2)	-45(3)	-5(2)	24(3)
C(009)	30(3)	106(6)	38(3)	17(4)	2(3)	7(3)
C(010)	25(3)	62(4)	39(3)	8(2)	8(2)	-1(3)
C(011)	30(3)	77(4)	33(3)	10(3)	-3(2)	-5(3)
C(012)	25(2)	46(3)	32(3)	14(2)	4(2)	-4(2)
Fe(3)	31(1)	45(1)	45(1)	4(1)	-13(1)	0(1)
C(51)	31(2)	44(3)	41(3)	8(2)	5(2)	4(2)
C(52)	25(3)	79(5)	39(3)	11(3)	-4(2)	4(3)
C(53)	25(3)	58(4)	47(3)	17(3)	-5(2)	1(2)
C(54)	29(2)	44(3)	48(3)	14(3)	2(2)	-1(2)
C(55)	43(3)	44(3)	29(2)	9(2)	-2(2)	-2(2)
C(61)	83(5)	44(4)	72(5)	-10(3)	-45(4)	9(4)
C(62)	79(5)	63(5)	64(4)	-21(4)	-37(4)	27(4)
C(63)	61(4)	40(4)	89(5)	-13(3)	-35(4)	-3(3)
C(64)	50(4)	46(4)	94(5)	12(4)	-1(4)	-9(3)
C(65)	80(5)	35(3)	62(4)	15(3)	-20(4)	-12(3)

Table A6: Hydrogen coordinates ($\times 10^4$) and isotropic displacement parameters ($\text{\AA}^2 \times 10^3$.)

Atom	x	y	z	U(eq)
H(003)	5908	10973	2409	42
H(12)	3264	11992	3957	43
H(13)	3806	13211	3746	41
H(14)	5495	13280	2874	40
H(15)	6098	12100	2557	35
H(21)	2396	11310	2117	57
H(22)	1094	12058	2810	64
H(23)	1663	13264	2530	61
H(24)	3418	13241	1675	56
H(25)	3896	12001	1427	55
H(007)	861	8518	2621	38
H(32)	900	7328	2831	36
H(33)	1575	6208	3312	42
H(34)	3476	6420	4063	41
H(35)	3978	7658	4062	31

Appendix

H(41)	283	8454	4481	60
H(42)	-1108	7476	4066	74
H(43)	-250	6410	4604	63
H(44)	1653	6727	5306	50
H(45)	1938	7984	5243	55
H(011)	5050	10181	5381	56
H(52)	7212	9933	5595	57
H(53)	9588	9791	5357	52
H(54)	9859	9621	4161	49
H(55)	7669	9550	3649	46
H(61)	6208	11449	4244	80
H(62)	7397	11588	5295	82
H(63)	9766	11418	5084	76
H(64)	10073	11160	3882	76
H(65)	7829	11181	3353	71

Table A7: Hydrogen bonds (Å) for Al(FcCOCHCOF₃)₃.

D-H...A	d(D-H)	d(H...A)	d(D...A)
C(003)-H(003)...F(1)	0.95	2.37	2.727(6)
C(007)-H(007)...F(5)	0.95	2.37	2.736(5)
C(011)-H(011)...F(9)	0.95	2.37	2.724(7)
C(52)-H(52)...F(1)#1	0.95	2.47	3.122(6)
C(53)-H(53)...F(8)#2	0.95	2.53	3.392(6)
C(63)-H(63)...F(7)#2	0.95	2.52	3.228(8)